CONTROLLED RADICAL POLYMERIZATION: TOWARDS INDUSTRIALLY RELEVANT CONDITIONS

By

Kevin Andrew Payne

A thesis submitted to the Department of Chemical Engineering

In conformity with the requirements for the

Degree of Doctor of Philosophy

Queen's University

Kingston, Ontario, Canada

September, 2015

Abstract

Reversible deactivation radical polymerization (RDRP), also known as controlled radical polymerization (CRP), has been a significant area of polymer research for more than 20 years, allowing the facile synthesis of complex macromolecules previously unattainable by conventional free radical polymerization (FRP). However, industrial adoption of RDRP has been minimal largely due to the significant economic barrier to commercialization, with complex synthesis of the mediating agents required and the necessary post polymerization processing to recover the mediating agent. In an effort to overcome this obstacle to industrial adoption, the mediating agent concentration can be significantly reduced, such as the copper level in activator regenerated by electron transfer atom transfer radical polymerization (ARGET ATRP), or the mediating agent can be incorporated into the polymer as in nitroxide-mediated polymerization (NMP), where no post polymerization processing is required other than removal of residual monomer. This thesis presents a study of these two chemistries towards industrially relevant conditions.

To build upon recent developments of continuous ARGET ATRP, a systematic batch study is conducted to pursue decreased copper levels in the generation of short chain acrylic and methacrylic polymers of interest to the coatings industry. The limitations to reducing copper levels are understood with the development of a kinetic model, with the improved understanding of the ARGET ATRP system suggesting that a reduction in copper loading must be accompanied by an increase in reducing agent loading in order to maintain an appreciable polymerization rate.

Alternatively, NMP does not require a reduction in mediating nitroxide level as it reversibly terminates the polymer chain end, and may present a smaller barrier to commercialization. Indeed, certain nitroxides are currently produced at pilot scale. However, limited research has been conducted into continuous operation which is commonly used in industry to improve productivity. A batch NMP study at elevated temperatures demonstrates the effectiveness of a novel alkoxyamine to mediate the polymerization of styrene and butyl acrylate under industrially relevant conditions. A kinetic study is developed to

understand the novel system, and the polymerization is implemented in a continuous stirred-tank reactor (CSTR), the first demonstration of NMP in an existing industrial process.

Co-Authorship

The bulk of the research in this thesis was conducted independently under the supervision of Dr. Michael Cunningham and Dr. Robin Hutchinson at Queen's University. The material presented in Chapters 3, 4, 5, and 6 have been accepted and published in a variety of peer-reviewed journals as detailed later on in the thesis.

The majority of the kinetic modeling work in Chapter 4 and 5 was conducted at the Laboratory for Chemical Technology in Ghent, Belgium with the help of Dr. Dagmar D'hooge and Dr. Paul Van Steenberge, who also assisted in the editing of the manuscript and subsequent publication.

The novel alkoxyamine used in the batch NMP study in Chapter 6 was synthesized by Dr. Peter Nesvadba of BASF Schweiz AG in Basel, Switzerland, who assisted with the preparation of the manuscript along with Dr. Jon Debling of BASF Corp. in Wyandotte.

The adaptation of NMP with the same alkoxyamine to a CSTR in Chapter 7 was done in collaboration with Dr. Jon Debling at BASF Corp. in Wyandotte.

Acknowledgements

First and foremost, I am grateful for the encouragement of my supervisors, Dr. Michael Cunningham and Dr. Robin Hutchinson. Their advice and guidance have helped me to develop into the researcher I am today, and I appreciate the opportunities they have given me over the last 5 years.

I would like to thank Dr. Guy B. Marin and Dr. Marie-Françoise Reyniers for the opportunity to work in the Laboratory for Chemical Technology at Ghent University as part of my PhD studies. I am especially grateful to the fruitful collaboration with Dr. Dagmar R. D'hooge and Dr. Paul Van Steenberge. It was a great research opportunity, and I was fortunate to make some good friends to help me explore a few of the beautiful cities of Belgium and appreciate the wonderful world of Belgian beer.

I would like to thank Dr. Jon Debling for the opportunity to work at BASF Corp. in Wyandotte, Michigan as part of my PhD studies. I am grateful for the valuable experience which strengthened my thesis with the ability to see my project from a different perspective. I would also like to give an honorable mention to Mr. Robert Brunnelson, with whom it was a pleasure to work, and I appreciate all of your patience in helping me as I reached the conclusion of my research.

I would also like to thank all of my friends and colleagues at Queen's University over the years for helping me get through this, the next round is on me. I would also like to thank hip hop for keeping me sane during the many hours spent in the lab and in front of a computer.

Finally, to my family and loved ones who supported me through all of the highs and lows of this experience, I cannot thank you enough. My sister for being the optimist I need in my life, supporting me while nearby on campus and far away in England, I hope you are as proud of me as I am of you. My mother, ever supportive and proud of my endeavors, and the strongest woman I will ever meet. I owe you more than words can describe, and I appreciate that you tolerate my explanation of my work as long as it is under 10 seconds. My late father, my idol and my mentor, I wish you could have seen me through all of this, yet somehow you knew I would get here. I hope I still make you proud, this thesis is dedicated to you.

Table of Contents

List of Figures

List of Tables

List of Schemes

Nomenclature

AA	acrylic acid
AGET	activator generated by electron transfer
ARGET	activator regenerated by electron transfer
ATRP	atom transfer radical polymerization
BA	butyl acrylate
BMA	butyl methacrylate
bpy	bipyridine
CLD	chain length distribution
C/LRP	controlled/living radical polymerization
CSA	camphorsulfonic acid
CSTR	continuous stirred-tank reactor
CuBr	copper (I) bromide
$CuBr_2$	copper (II) bromide
CuCl	copper (I) chloride
$Cu^{I}X/L$	ATRP activator
$Cu^{II}X_2/L$	ATRP deactivator
$Đ$	dispersity (formerly polydispersity index, PDI)
DEPN (or SG1)	N-*tert*-butyl-N-[1-diethylphosphono-(2,2-dimethylpropyl)] nitroxide
DCF	dead chain fraction
DCM	dichloromethane
DMF	N,N-dimethylformamide
DP_n	degree of polymerization
DVB	divinyl benzene
eATRP	electrochemically mediated ATRP
EBiB	ethyl 2-bromoisobutyrate
EGF	end group functionality

EMA	ethyl methacrylate
ESI-MS	electrospray ionization - mass spectrometry
f_{init}	initiator efficiency
FPT	freeze-pump-thaw
FRP	conventional free radical polymerization
GC-FID	gas chromatography - flame ionization detector
GPC	gel permeation chromatography
ICAR	initiators for continuous activator regeneration
k_a	activation rate coefficient
K_{ATRP}	ATRP equilibrium constant ($=k_a/k_{da}$)
k_{da}	deactivation rate coefficient
kMC	kinetic Monte Carlo
k_p	propagation rate coefficient
k_{r1}	first reduction rate coefficient
k_{r2}	second reduction rate coefficient
k_t	termination rate coefficient
k_{tc}	termination by combination rate coefficient
k_{td}	termination by disproportionation rate coefficient
L	catalyst complex ligand
L_2	reducing agent complex ligand
LPV	low pressure/vacuum
M	monomer
MA	methyl acrylate
MAA	methacrylic acid
MALDI-TOF	matrix-assisted laser desorption/ionization time of flight
Me_6TREN	tris[2-(dimethylamino)ethyl]amine
MMA	methyl methacrylate
MMD	molar mass distribution

M_n	number-average molar mass
M_w	weight-average molar mass
MW	molecular weight
NMP	nitroxide-mediated polymerization
NMR	nuclear magnetic resonance
photoRDRP	photochemically mediated RDRP
PMDETA	N,N,N′,N″,N″-pentamethyldiethylenetriamine
ppm	parts per million
Pr	Predici®
PRE	persistent radical effect
PS	polystyrene
R_iX	halogen-capped polymer
R_oX	alkyl halide initiator
R-Y	alkoxyamine
R_n-Y	macroalkoxyamine
R•	active radical species
RAFT	reversible addition-fragmentation chain transfer
RAFT-CLD-T	RAFT - chain length dependent termination
RDRP	reversible deactivation radical polymerization
SARA	supplemental activator and reducing agent
SEC	size exclusion chromatography
SET-LRP	single electron transfer-living radical polymerization
$Sn(EH)_2$	tin (II) 2-ethylhexanoate
τ	mean residence time
TBPA	*tert*-butyl peroxyacetate
TCL	target chain length
TEMPO	2,2,6,6-tetramethyl-1-piperidinyloxy
THF	tetrahydrofuran

TIPNO	2,2,5-trimethyl-4-phenyl-3-azahexane-3-oxyl
TPMA	tris[(2-peridyl)methyl]amine
x_n	number-average chain length
X	halogen/end group functionality
Y•	stable free nitroxide
λ_{max}	wavelength of maximum absorbance

Subscripts

i	chain length of first polymer species
j	chain length of second polymer species
o	initial condition or initiator species

Chapter 1

Introduction

Reversible deactivation radical polymerization (RDRP), also known as controlled radical polymerization (CRP), has continued to be an intensely researched area, due to the possibility to tailor macromolecules using a wide range of monomers under relatively mild conditions.[1-3] The major chemistries under the umbrella of RDRP include reversible addition-fragmentation chain transfer (RAFT), atom transfer radical polymerization (ATRP), and nitroxide-mediated polymerization (NMP). The increasing complexity of molecules being synthesized is far beyond what is accessible to conventional free radical polymerization (FRP), with a wealth of innovative applications from improved dispersants in coatings to polymers for controlled-release drug therapies. Despite the multitude of potential applications and accompanying publications, there are limited examples of RDRP in industry. The main reason for this lack of industrial adoption is the economic barrier to commercialization for RDRP, as the mediating compounds required often involve a complex synthesis, and in some cases require removal from the final polymer due to toxicity or discoloration concerns.[4]

Progress has been made to reduce the amount of copper metal complexes required for ATRP, with the development of activator regenerated by electron transfer (ARGET) and supplemental activator and reducing agent (SARA) ATRP, as will be discussed in Chapter 2. Nitroxides and RAFT agents are incorporated into the polymer and as such do not require post polymerization processing, however thio-based RAFT agents are less desirable in an industrial process, while nitroxides have been used in only a few commercial products. Further details regarding RDRP in industry will be provided in Chapter 2.

Industrial adoption of RDRP would be accelerated by the development of a continuous process for this technology to increase efficiency and throughput compared to batch processes. Currently, limited continuous processes have been developed experimentally, with a number of

theoretical studies demonstrating the possibility of moving RDRP towards industrially relevant conditions.

1.1 Thesis Objectives

RDRP allows for the synthesis of polymers with controlled composition and architecture. Automotive coatings have moved toward high temperature semi-batch operation to produce lower molecular weight polymers (<5,000 g mol^{-1}) in an effort to reduce solvent loadings in response to more strict environmental regulations. RDRP provides a facile method to synthesize low molecular weight polymers with tailored functional groups. In addition, the low polymer dispersity leads to inherently lower viscosities than conventional FRP, enabling further decreases in solvent content. As such, the experimental work in this thesis focuses on the synthesis of well-controlled low molecular weight polymers, while conducting a thorough investigation of the reaction conditions in order to minimize the economic barriers to commercialization for ATRP and NMP. To aid in the investigation, kinetic modeling is utilized to explain experimental results while guiding further optimization of the conditions. Finally, a kinetic model can be used to help the transfer of the technology from batch to continuous operation. The primary goals of the study are:

1. Gain understanding of the limitations of reducing the level of copper metal complex required in ARGET ATRP
2. Develop a kinetic model for ARGET ATRP to provide insight into experimental results and guide optimization at reduced copper levels
3. Explore the possibility of NMP at elevated temperatures using currently available nitroxides
4. Gain a thorough understanding of a novel alkoxyamine with increased thermal stability, and explore its effectiveness as a mediating agent at elevated temperatures

5. Investigate the transfer of NMP technology from batch to continuous stirred tank reactor
6. Develop a kinetic model to obtain first estimates of the NMP activation/deactivation kinetics for the novel alkoxyamine and to represent and interpret batch and continuous data collected in this study

1.2 Thesis Outline

This thesis is presented in manuscript format, with the main results sandwiched between perspectives of the field at the beginning and end of this thesis. Chapter 2 covers the relevant background and literature review, presenting the major factors influencing polymerization rate and control for ATRP and NMP, previous developments in block copolymer synthesis, and an overview of the kinetic models that were currently available.

Chapter 3 summarizes the systematic experimental study of the ARGET ATRP of butyl methacrylate (BMA) and butyl acrylate (BA) conducted in an effort to reduce copper levels and therefore lower the economic barrier to industrial adoption.[5] Copper levels are decreased along with changes in monomer type, initiator loading (or target chain length), and reducing agent loading. The study outlines the limitations of reducing copper loadings while generating low molecular weight polymers (<5,000 g mol^{-1}) and maintaining an acceptable polymerization rate. The experimental results from the homopolymerization study of BMA are then explained using a kinetic model in Chapter 4.[6] Distinct parameter estimates for the initiator and polymeric activation and deactivation are required to capture the experimentally observed behavior. The significant decrease in the polymerization rate with copper loading is attributed to a decrease in the ratio of activator to deactivator, and is only recovered with a significant increase in the reducing agent loading.

The kinetic model is further expanded to represent BA homopolymerization, along with the copolymerization of BMA and BA in Chapter 5.[7] Improved initiator efficiency for BA

compared to BMA is attributed to a difference in the activation/deactivation kinetics of the two monomers. The model is then used to develop a semi-batch feeding strategy for reducing agent, as an improvement over the significant excess required to increase the polymerization rate at low copper loadings in batch. Ultimately, it is shown that any decrease in copper loading must be accompanied by an increase in reducing agent loading in order to maintain an acceptable polymerization rate.

Given the inevitable post polymerization processing of ATRP, the research focus shifted to NMP as a more promising RDRP chemistry. As the nitroxide is incorporated in the polymer, there is no need for additional polymer processing. In addition, stable nitroxide can be an effective mediating agent at the high temperatures currently employed in industrial continuous reactors which take advantage of increased polymerization rates and require smaller reaction volumes to obtain high throughput. A commercially available nitroxide 2,2,6,6-tetramethyl-1-piperidinyloxy (TEMPO) is first investigated at elevated temperatures, with results summarized in Appendix B. The limited stability of the nitroxide at industrially relevant conditions leads to the use of a novel alkoxyamine; as discussed in Chapter 6, the novel alkoxyamine is used to effectively mediate styrene and butyl acrylate polymerizations up to 200 °C.[8] A range of temperatures and alkoxyamine loadings (target chain lengths) is studied, with the experimental results effectively represented by a kinetic model, outlined in Chapter 7. The kinetic model is also applied to a continuous process, which helps to explain the experimental results obtained from a continuous stirred-tank reactor (CSTR), the first known implementation of NMP in a CSTR.

Finally, the conclusions are discussed in Chapter 8 along with the latest developments in RDRP from the literature. Future work based on the experimental results is suggested, along with a perspective on the future outlook of RDRP in a commercially viable process.

1.3 References

(1) Hill, M. R.; Carmean, R. N.; Sumerlin, B. S. *Macromolecules* **2015**, *48*, 5459–5469.

(2) Matyjaszewski, K. *Macromolecules* **2012**, *45*, 4015–4039.

(3) Nicolas, J.; Guillaneuf, Y.; Lefay, C.; Bertin, D.; Gigmes, D.; Charleux, B. *Prog. Polym. Sci.* **2013**, *38*, 63–235.

(4) Destarac, M. *Macromol. React. Eng.* **2010**, *4*, 165–179.

(5) Payne, K. A.; Cunningham, M. F.; Hutchinson, R. A. In *Progress in Controlled Radical Polymerization: Mechanisms and Techniques*; Matyjaszewski, K.; Sumerlin, B. S.; Tsarevsky, N. V., Eds.; ACS Symposium Series, American Chemical Society: Washington, DC, 2012; pp. 183–202.

(6) Payne, K. A.; D'hooge, D. R.; Van Steenberge, P. H. M.; Reyniers, M.-F.; Cunningham, M. F.; Hutchinson, R. A.; Marin, G. B. *Macromolecules* **2013**, *46*, 3828–3840.

(7) Payne, K. A.; Van Steenberge, P. H. M.; D'hooge, D. R.; Reyniers, M.-F.; Marin, G. B.; Hutchinson, R. A.; Cunningham, M. F. *Polym. Int.* **2014**, *63*, 848–857.

(8) Payne, K. A.; Nesvadba, P.; Debling, J.; Cunningham, M. F.; Hutchinson, R. A. *ACS Macro Lett.* **2015**, *4*, 280–283.

Chapter 2

Literature Review

2.1 Activator ReGenerated by Electron Transfer Atom Transfer Radical Polymerization

ATRP was developed by the Matyjaszewski group in the early 1990s as a method to produce polymers of controlled topology and composition from various monomers.[1,2] ATRP is a form of reversible deactivation radical polymerization (RDRP) in which the polymerization is mediated by a metal/ligand complex (most commonly copper) that has n and $n+1$ oxidation states. As shown in Scheme 2.1, the activator species ($Cu^{I}X/L$, where L = ligand) abstracts the halide from the alkyl halide initiator (R_oX) through homolytic bond cleavage, creating the propagating radical (R•) and the deactivator species ($Cu^{II}X_2/L$). This forward reaction is known as activation, with rate coefficient k_a, with the reverse reaction commonly known as deactivation (k_{da}). The deactivation rate coefficient is several orders of magnitude higher than the activation rate coefficient, so that the majority of the polymer chains are in the "capped" or dormant state. As a result, the radical concentration is maintained at a low level, allowing only a few monomer units to propagate while minimizing reactions such as irreversible termination and backbiting, leading to a linear increase in number-average molar mass (M_n) with conversion and a low polymer dispersity ($Đ$).

A well-controlled and living system exhibits a narrow polymer molar mass distribution (MMD) with preserved end group functionality (EGF, X). Unfortunately, for normal ATRP there is the accumulation of the Cu^{II} species due to loss of radicals by termination, and by oxidation of Cu^{I} by impurities such as oxygen. Thus, an elevated initial Cu^{I} level is required to prevent the premature decrease of polymerization rate, often approaching one catalyst species per chain. The copper must then be removed from the polymer product once the reaction is complete as it produces significant discoloration.

To remedy the problem of high Cu loadings, various low Cu chemistries were developed as modifications of the original ATRP mechanism, including Initiators for Continuous Activator Regeneration (ICAR), Activator Generated by Electron Transfer (AGET), Supplemental Activator and Reducing Agent (SARA), and Activator ReGenerated by Electron Transfer (ARGET).[3–7] Of particular interest to this study is ARGET ATRP (Scheme 2.1), for which a reducing agent is used to continuously (re)generate the activator species from deactivator. As a result, Cu levels can be reduced to ppm levels with respect to monomer, while using the oxidatively stable deactivator species at the beginning of the polymerization, thus eliminating the need for stringent reaction conditions and even allowing the polymerization to be conducted in the presence of air.[8,9]

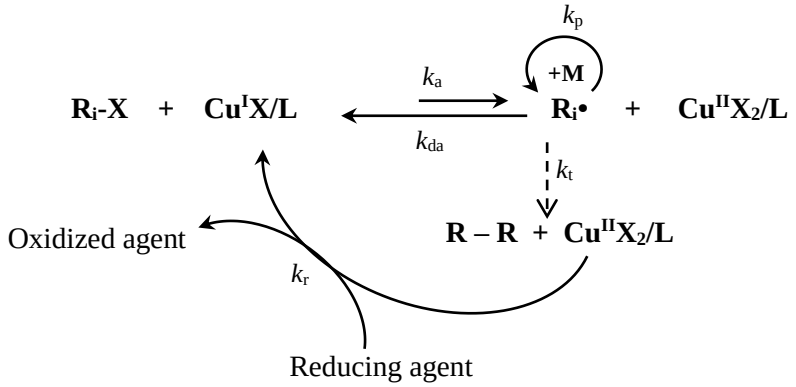

Scheme 2.1: Mechanism of ARGET ATRP; in normal ATRP initially only ATRP initiator (R_oX), monomer (M) and activator (Cu^IX/L) are present (where L = ligand), whereas in ARGET ATRP there is initially only ATRP initiator, monomer and deactivator ($Cu^{II}X_2/L$) with an excess of reducing agent to (re)generate the activator; $k_{a,da,p,t,r}$: rate coefficient for activation, deactivation, propagation, termination, and reduction, respectively.[1,6,10]

In the original work, ARGET ATRP was used to successfully control the polymerization of styrene, butyl acrylate (BA), and methyl methacrylate (MMA) with the use of a Food and Drug Administration (FDA) approved reducing agent tin (II) 2-ethylhexanoate ($Sn(EH)_2$) and ATRP catalysts $CuCl_2$ or $CuBr_2$ with tris[(2-peridyl)methyl]amine (TPMA) or tris[2-(dimethylamino)ethyl]amine (Me_6TREN) as ligand.[3,5,6]

2.1.1 Factors Affecting ATRP

A significant number of studies have been conducted in order to understand the mechanisms and improve the control and kinetics of ATRP. In particular, the structures of the alkyl halide initiator and the ligand used to complex with Cu have been investigated for their effect on the activation rate coefficient in the absence of monomer.[11–16] A summary of these studies can be seen in Figure 2.1 and Figure 2.2.

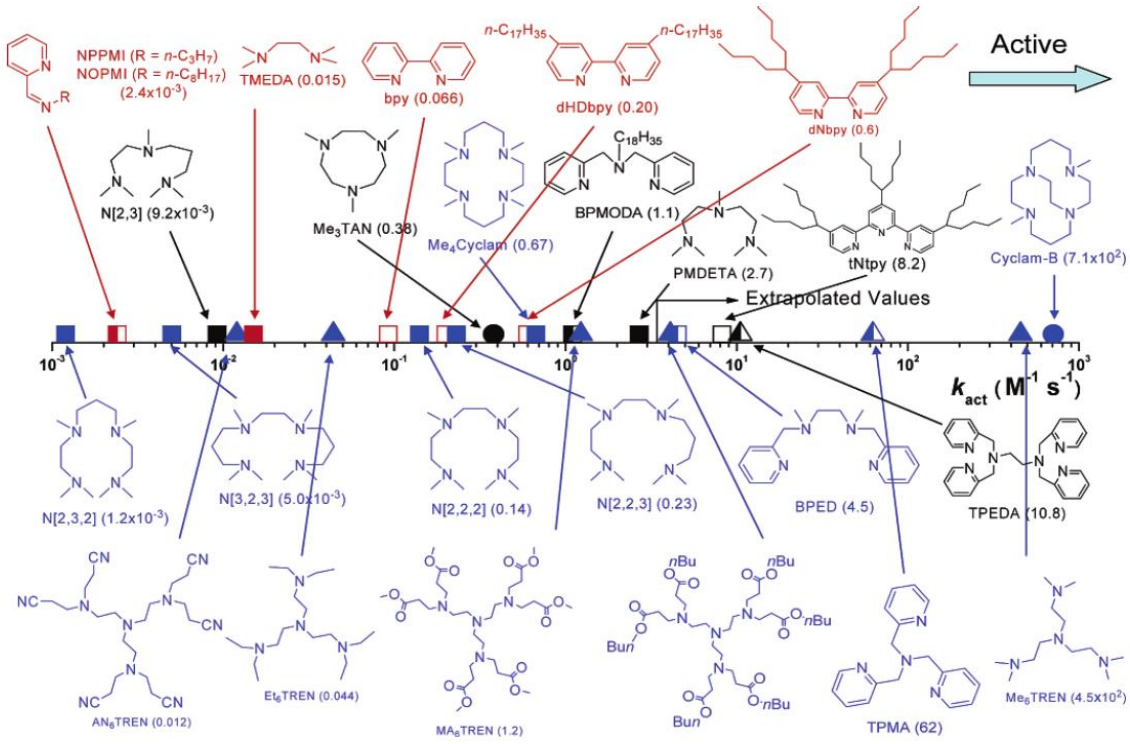

Figure 2.1: Activation rate coefficients (k_a) for various ligands (Y) in the presence of EBiB and $Cu^{I}Y$ at 35 °C in acetonitrile. Reprinted with permission from Tang *et al.*[11] Copyright 2006 American Chemical Society.

The ligand structure was found to be an important factor on the activation rate coefficient with the following general trend: tetradentate (cyclic-bridged) > tetradentate (branched) > tetradentate (cyclic)>tridentate>tetradentate (linear)>bidentate ligands. Also important is the nature of the nitrogen atoms, with pyridines being more active than aliphatic amines and imines being the

least active.[11] One study used a substituted TPMA complex with significantly increased activation kinetics.[17]

The ligand to Cu ratio was found to be influential in minimizing the side reactions with the Cu complex, especially at low Cu levels where the duty of each Cu complex is significantly increased, which has led to the use of excess ligand in most experimental procedures.[18,19] Some amine-based ligands have also been known to act as reducing agents.[20] However, developments were made to utilize stoichiometric amounts of ligand and Cu and still maintain good control and kinetics of the ARGET ATRP system using the more active ligand TPMA in a variety of solvents, thus mitigating the economic impact of the Cu complex.[21] Another active ligand, Me_6TREN, was found to have difficulty complexing with $CuBr_2$ in certain solvents and is required in excess. As such, TPMA is a preferred ligand for optimizing the ARGET ATRP process.

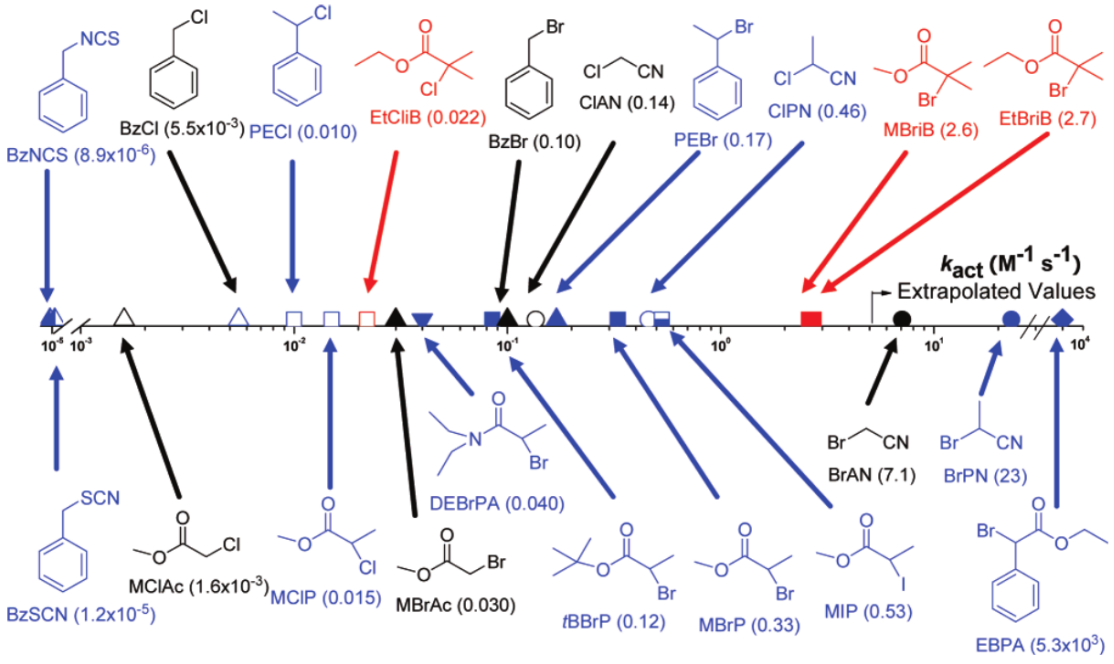

Figure 2.2: Activation rate coefficients (k_a) for various alkyl halide initiators in the presence of Cu^IX/PMDETA (X = Cl or Br) at 35 °C in acetonitrile. Reprinted with permission from Tang *et al.*.[15] Copyright 2007 American Chemical Society.

With N,N,N′,N′,N″-pentamethyl-diethylenetriamine (PMDETA) as ligand, initiator activity was found to increase with increased stability of the corresponding radical after halogen transfer such that tertiary alkyl halides were more active initiators. Additionally, the leaving group was found to lead to increased activity with the following trend: NCS (SCN) << Cl < Br ≤ I.[15] In addition to its relatively higher activation rate coefficient, ethyl 2-bromoisobutyrate (EtBriB or EBiB) has been shown to be a structural analogue for MMA with high initiator efficiency, and was therefore chosen for the polymerization of butyl methacrylate (BMA) in this study.

Other studies have looked into the effect of solvent, monomer, ligand to Cu ratio, and reaction temperature and pressure on the kinetics of the ATRP system.[18,22–26] It was found that the monomer can impact the activation/deactivation kinetics by coordinating with the Cu complex, while a more polar solvent can significantly increase the equilibrium constant K_{ATRP}.[24,26,27] Anisole was chosen as solvent due to the previous work of Chan *et al*. to reduce ligand requirements to stoichiometric levels, with faster polymerization rates found in anisole than benzonitrile and comparable rates with toluene, while exhibiting good control of the M_n and $Đ$.[21] As can be expected, an increase in temperature or a significant increase in pressure leads to an increase in the activation rate coefficient.[22,28]

2.1.2 Copolymerization using ARGET ATRP

In order to increase the value of polymer products, copolymerizations are conducted to incorporate the attractive properties of two or more monomers into a single polymer chain. By doing so, polymer properties such as the rheology, glass transition temperature, and melting point, can be tuned while incorporating various functional groups or altering the degree of branching. With free radical polymerization, only random copolymers can be produced from a comonomer solution. With the development of various RDRP techniques, the polymer architecture can be tuned to produce a wide range of polymer products with various topologies and compositions. Due to the

low radical concentration and slow evolution of M_n, monomer units can be added to the propagating chain in a tailored fashion, such that block, gradient, and random copolymers may be formed. Another benefit that arises from acrylate/methacrylate copolymerization is an increase in initiator efficiency with an increase in acrylate content, as shown for BA with MMA at low Cu levels.[29]

The order of monomer addition must be considered in order to effectively synthesize block copolymers with ATRP. The relative propagation rate coefficients of the two monomers must be considered with respect to their activation/deactivation kinetics to ensure efficient reinitiation of the first block and to maintain control of the polymer dispersity. It has been shown that if the monomer with the larger propagation rate coefficient is used as the macroinitiator, then a bromine end group on the polymer and CuCl as activator should be used to promote halogen exchange and effectively initiate the polymerization.[29–32] Without the promotion of halogen exchange to overcome the stability of the dormant species in the polymerization, initiation efficiency will be considerably lowered, leading to high polymer dispersities and decreased production of desirable block copolymers.

2.1.3 Kinetic Modeling

In order to acquire further understanding of polymerization processes and the mechanisms involved, kinetic models have been developed using a variety of methods, the most common of which is the Predici® software package.[33,34] Kinetic parameters that have been measured in the literature are incorporated into the model, with optimization algorithms in the package available to estimate any remaining unknown coefficients. The influence of diffusion-controlled rate coefficients (including chain length dependent termination) on RDRP systems has also been explored through simulation.[35–38] The kinetic models can be utilized to predict the measured experimental data such as conversion, M_n, and EGF, as well as predicting difficult to measure quantities and concentrations of various species in the reaction. Using insights gained from

simulation, kinetic modeling can be a powerful tool to aid experimentation and the scale-up of a polymerization process.

ARGET ATRP has not been extensively modeled in the literature, with only one kinetic model recently published by Li *et al.* to represent the original experimental work of Jakubowski *et al.*.[3,5,39] This kinetic model was able to represent the data using FRP rate coefficients from the literature and estimated ATRP rate coefficients. The model assumed identical intrinsic activation/deactivation rate coefficients for polymeric and initiator species, and a constant apparent termination rate coefficient. The model, which also neglected side reactions such as backbiting and chain transfer, was used to explore the effect of varying ATRP rate coefficients such as the equilibrium constant ($K_{ATRP} = k_a/k_{da}$) and the apparent reducing rate coefficient (k_r) to demonstrate the impact of utilizing Cu catalysts and reducing agents of different activity. The findings from the model suggested that increasing the reducing rate coefficient would lead to an increase in the monomer conversion and a decrease in EGF, with no significant impact on the MMD. Meanwhile, an increase in the ATRP equilibrium constant was shown to lead to loss of control of the polymerization while having a negligible impact on the conversion profile.[39]

The difficulty in modeling ATRP systems arises from the catalyst complex and the variety of influences on the activation/deactivation rate coefficients, as mentioned above. As the activation rate is influenced by choice of monomer, solvent, ligand, temperature, pressure and nature of the halide in the Cu complex, the studies in the literature have only looked at comparisons of a few of these parameters for a single system.[12,15,18,22,23,40-42] As a result, many parameters must be extrapolated for different systems using a combination of the trends that have been observed in the literature.

2.1.4 Continuous ATRP

Limited attempts have been made to develop a continuous process for the ATRP technology, with theoretical studies conducted in the literature indicating a clear interest in developing ATRP towards an industrial process.[43-45] According to Matyjaszewski, one success has been the commercial production of polymers using ATRP technology by Kaneka.[46] However, a major barrier to continuous operation is the limited solubility of the copper complex in the monomer/solvent for conventional ATRP, which requires higher copper levels. In addition, the need to remove the catalyst from the polymer poses a major problem during scale-up, with various strategies attempted including solid-supported catalyst; however, there is a significant economic barrier coupled with a short reactor lifetime.[47-49] Semi-batch operation, which is often used industrially to facilitate good temperature control and control over polymer composition, has been attempted.[50-52] The most common continuous reactor configurations are tubular and continuous stirred-tank reactors (CSTRs) as they allow for continuous operation with high throughput. Tubular reactors provide excellent temperature control due to the high surface-to-volume ratio, as well as the capability to control the microstructure (block copolymers, for example) by adding feed streams along the reactor. However, tubular reactors are vulnerable to being plugged, while CSTRs are less prone to fouling. As a result, CSTRs tend to be a more economical method of producing the same material for extended periods once steady state has been reached. Tubular reactors have been used to generate homo and block copolymers with good control using normal ATRP as well as SARA ATRP,[53-59] while ARGET ATRP and SARA ATRP (or SET-LRP) have been conducted in a CSTR.[51,60] As would be expected, a tubular reactor produces polymer with a lower polymer dispersity than a CSTR due to the residence time distribution being much narrower; the tubular reactor exhibits similar behavior to that of the batch polymerization due to nearly plug flow behaviour.[45,51,53,56,59] Due to the long lifetime of the polymer chains, the residence time distribution will lead to significant broadening of the MMD in a CSTR. It should be noted that a narrow MMD

is not the only measure of EGF, and this has been demonstrated with the batch chain extension of polymer produced in a CSTR.[54] If a narrow MMD is desirable, as with batch RDRP, then it is predicted that multiple CSTRs in series will result in a tighter residence time distribution and therefore a lowering of the polymer dispersity with increasing tank number.[43,61-63]

2.2 Nitroxide-Mediated Polymerization

The first mention of nitroxide-mediated polymerization (NMP) was by the group of Solomon and coworkers, whose seminal work with the use of 2,2,6,6-tetramethylpiperidinyl-1-oxy (TEMPO) based alkoxyamines led to further development by Georges *et al.* to produce polystyrene (PS) resins with narrow MMDs using TEMPO as mediating agent.[64-67] Originally, a bimolecular system comprised of a conventional thermal initiator and a stable free nitroxide was used to initiate the polymerization. With a unimolecular system, an alkoxyamine undergoes homolytic bond cleavage to generate the initiating radical and the mediating nitroxide on a stoichiometric basis.[64,68,69] As with other RDRP methods, the general mechanism for NMP involves the reversible trapping of the propagating radical (R•) by the stable free nitroxide (Y•) to produce the dormant species or (macro)alkoxyamine (R_n-Y), as shown in Scheme 2.2. Initially the radical concentration increases until bimolecular termination may occur, producing the persistent radical (Y•) which is unable to self-terminate. As the nitroxide concentration increases, the equilibrium is shifted towards the dormant macroalkoxyamine, thus limiting the radical concentration. The forward activation (decomposition) reaction is significantly lower than the reverse deactivation (cross-coupling) reaction such that the radical species concentration is small, facilitating control over the polymerization due to the suppression of termination and other side reactions.

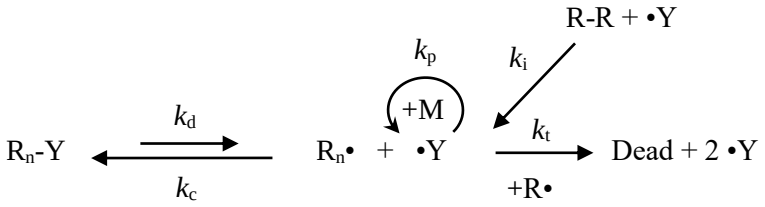

Scheme 2.2: Simplified mechanisms for nitroxide-mediated polymerization involving the use of a conventional thermal initiator (R-R) and stable free nitroxide (Y•) or alkoxyamine (R_n-Y) to produce polymers with controlled architecture and preserved end group functionality (EGF, Y); $k_{d,c,p,i,t}$ are the rate coefficients for dissociation, cross-coupling, propagation, initiation, and termination, respectively.[70]

Following the initial TEMPO work, the control and kinetics of the styrene homopolymerization were subsequently investigated in depth. It was found that an excess of nitroxide present in the polymerization led to improved control over the M_n and a slower polymerization rate, with the original study using a ratio of nitroxide to initiator = 1.3.[67,71,72]

The polymerization of styrene in the presence of TEMPO was limited to ~140 °C due to the significant loss of TEMPO to decomposition and disproportionation at 120 °C.[73-78] Although the use of TEMPO and derivatives to mediate styrene was extensively studied,[69,79,80] the inability to mediate other monomers without any additional styrene was a serious limitation to further development of NMP.

2.2.1 Expansion to Different Monomers

The inability for TEMPO to mediate monomers other than styrene was circumvented with the development of other nitroxides, beginning with TEMPO derivatives and leading to 2,2,5-trimethyl-4-phenyl-3-azahexane-3-oxyl (TIPNO)[81] and N-*tert*-butyl-N-[1-diethylphosphono-(2,2-dimethylpropyl)] nitroxide (DEPN or SG1).[82,83] This led to the inspiration for a diversity of nitroxides and alkoxyamines, allowing the first successful NMP of MMA,[84,85] BA,[86] and acrylic

acid (AA),[87] among other monomers. The synthesis of novel nitroxides or alkoxyamines is not the focus of this thesis, however a summary of the different synthetic routes and their products can be seen in the review paper of Nicolas *et al.* and the references contained therein.[70] To summarize, the main influences on the activation/deactivation kinetics are the steric and polar effects, as illustrated in Scheme 2.3, where bulky substituents can increase C-ON bond homolysis while increased polarity in the nitroxide can benefit the cross-coupling reaction.[88] Also, the penultimate unit on the polymer chain has been shown to impact both reactions, with a significant effect on the cross-coupling reaction.[89,90]

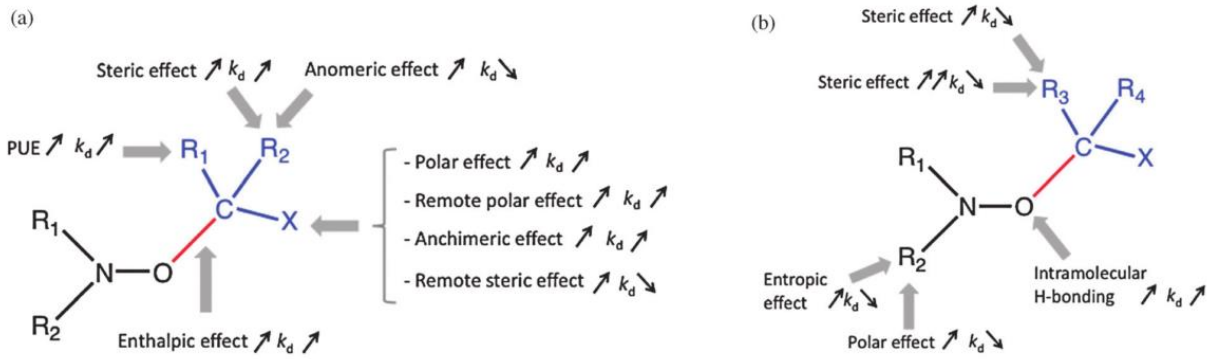

Scheme 2.3: Effect of various groups on the C-ON bond homolysis in the (a) alkyl and (b) nitroxyl fragments. Reproduced from Bertin *et al.*[88] with permission of The Royal Society of Chemistry.

Polymer chemists have had a difficult time in the pursuit of a mediating agent for the homopolymerizations of BA and MMA, due to the initial requirement of excess nitroxide to successfully mediate BA, and the need to minimize H-transfer to the nitroxide during the polymerization of MMA.[84,91,92] The polymerization of BA was achieved with promising results when camphorsulfonic acid (CSA) or ascorbic acid was added to reduce the concentration of free nitroxide in the system, as acrylate systems are more sensitive to excess free nitroxide, which is not consumed by the autopolymerization exhibited by styrene.[72,81,91,93,94] For MMA, the alkoxyamine

would need to minimize H-transfer by maintaining a low equilibrium constant in order to achieve good control and livingness up to an appreciable conversion, a result achieved through copolymerization with styrene or acrylonitrile and by the synthesis of alkoxyamines that have a low dissociation temperature due to long-range polar effects.[84,85,95,96] With AA, the acid group had been observed to undergo side reactions with the nitroxide; however this was overcome with the use of SG1, which also helps to offset the high propagation rate of AA with the low activation/deactivation kinetics of SG1.[80,87]

These factors have made it difficult to pursue the industrial application of NMP, as there is the need to tailor the alkoxyamine/nitroxide to the reaction conditions. Despite this, NMP shows promise over other RDRP techniques, as no polymer purification other than removal of unreacted monomer is required. Indeed, commercial pigment dispersants have been developed by CIBA using various nitroxides.[97] In addition, Arkema has developed SG1 and the SG1-based alkoxyamine BlocBuilder MA, which have progressed towards commercialization, with production of BlocBuilder MA at an industrial scale.[98,99]

2.2.2 Block Copolymers

Block copolymers are one of the polymer architectures afforded by RDRP which are unattainable by conventional FRP, as the preservation of EGF facilitates further chain extension when the first monomer is consumed and a second monomer is added.[100] With the polymer chains that are terminated by the nitroxide, post polymerization modification can add increased functionality to the polymer chain end or act as the junction between the polymer blocks.[101] For example, block copolymers have been made with styrene, MMA, BMA, BA and ethyl methacrylate (EMA) to name a few.[83,102,103] In addition, amphiphilic block copolymers have been made with methacrylic acid (MAA) and styrene.[104] It was found as a general concept that, for copolymerization to be successful, the first monomer must be significantly more active than the

second monomer, with residual initial monomer available throughout the polymerization.[105] This order in the sequence of monomers has been shown to be crucial in preparing block copolymers as well in order to maintain adequate activation/deactivation kinetics for a controlled polymerization.[106]

It is not enough to prepare block copolymers without also conducting proper characterization to ensure the quality of their syntheses. Of course ^{1}H NMR is effective in determining the polymer composition, however the most common techniques used to ensure the correct architecture and EGF are matrix-assisted laser desorption/ionization time of flight (MALDI-TOF) or electrospray ionization - mass spectrometry (ESI-MS).[107-113] ESI-MS has been shown to be the most promising when determining the chain-end structure, while caution must be used during analysis with MALDI-TOF to avoid fragmentation of the nitroxide. However, MALDI-TOF tends to be consistent in the determination of M_n, with results comparable to size exclusion chromatography (SEC), while ESI-MS underestimates average molar masses.[108]

2.2.3 Kinetic Modeling of NMP

In order to gain further understanding of the NMP technique, kinetic modeling studies were undertaken to aid in the development of novel nitroxides and alkoxyamines. The first study looked at the polymerization of styrene with TEMPO, using the model to estimate the activation/deactivation kinetics of the system.[114] Further studies then looked into optimization of the nitroxide and rate enhancement in the polystyrene system.[115-120] After an abundance of experimental trials were conducted to pursue different nitroxides with different monomers, further modeling efforts helped to understand the mechanisms and kinetics that are most important for the success of NMP with various monomers.[85,89,90,92,121] Expanding on these studies, simulations were conducted to evaluate the impact of side reactions in NMP and whether diffusion has a significant influence on the kinetic parameters.[122-127]

There have also been models developed to represent copolymerization systems, as it would be beneficial to better understand the mechanisms and to optimize the process towards an industrially attractive application of these higher value polymers. Models have been developed to investigate the copolymerization of styrene with BA, BMA, MMA and divinyl benzene (DVB).[121,125,128-132] The modeling studies have led to general guidelines such as which monomer should be used first in the synthesis of block copolymers, and the feeding strategies required to produce suitable gradient copolymers. The knowledge gained from these modeling studies is essential for further development of NMP towards commercialization, and for the design of novel mediating agents to achieve the optimal activation/deactivation kinetics required to effectively control the polymerization of various monomers and create attractive polymer products with precision. As the kinetic models become increasingly comprehensive, they may be utilized for the eventual scale-up to industrially relevant conditions.

2.2.4 Continuous NMP

As with ATRP, the development of a continuous process for NMP has been limited at an industrial scale. Meanwhile, academic interest in continuous processes strongly supports the desire to successfully scale up the NMP technology. Semi-batch operation of an NMP was proven to be feasible by testing a variety of initiating systems, with a significant loss of chains during the initiation of the polymerization leading to difficulty in balancing an increased polymerization rate with control.[52] The semi-batch polymerization of styrene and BA by NMP has been conducted with kinetic modeling suggesting that the loss of chains in the system was due to the bimolecular initiation system, as 4-hydroxy-TEMPO irreversibly terminates the initiating radicals from *tert*-butyl peroxyacetate (TBPA).[133] The NMP of styrene and further block copolymers has been conducted under bulk and miniemulsion conditions in a tubular reactor, with good agreement with batch experimental results.[134,135] A theoretical study focused on the reactor design and temperature

profile in the NMcoP of styrene and α-methyl-styrene, although only semi-batch and tubular reactor designs were considered, neglecting a CSTR configuration.[136] In fact, experimental studies with RDRP and CSTRs have been limited to ATRP (as mentioned above) and RAFT, which has even been implemented in a train of CSTRs to produce homopolymers and block copolymers under miniemulsion conditions.[61,62] Despite the attractiveness of a continuous NMP process, only theoretical studies of NMP in a CSTR are currently available in the literature.[137-139]

2.3 References

(1) Wang, J.-S.; Matyjaszewski, K. *Macromolecules* **1995**, *28*, 7901–7910.

(2) Wang, J.-S.; Matyjaszewski, K. *J. Am. Chem. Soc.* **1995**, *117*, 5614–5615.

(3) Jakubowski, W.; Matyjaszewski, K. *Angew. Chem.* **2006**, *45*, 4482–4486.

(4) Jakubowski, W.; Matyjaszewski, K. *Macromolecules* **2005**, *38*, 4139–4146.

(5) Jakubowski, W.; Min, K.; Matyjaszewski, K. *Macromolecules* **2006**, *39*, 39–45.

(6) Matyjaszewski, K.; Jakubowski, W.; Min, K.; Tang, W.; Huang, J.; Braunecker, W. A.; Tsarevsky, N. V. *Proc. Natl. Acad. Sci. U.S.A.* **2006**, *103*, 15309–15314.

(7) Percec, V.; Popov, A. V.; Ramirez-Castillo, E.; Monteiro, M. J.; Barboiu, B.; Weichold, O.; Asandei, A. D.; Mitchell, C. M. *J. Am. Chem. Soc.* **2002**, *124*, 4940–4941.

(8) Matyjaszewski, K.; Dong, H.; Jakubowski, W.; Pietrasik, J.; Kusumo, A. *Langmuir* **2007**, *23*, 4528–4531.

(9) Min, K.; Jakubowski, W.; Matyjaszewski, K. *Macromol. Rapid Commun.* **2006**, *27*, 594–598.

(10) Jakubowski, W.; Kirci-Denizli, B.; Gil, R. R.; Matyjaszewski, K. *Macromol. Chem. Phys.* **2008**, *209*, 32–39.

(11) Tang, W.; Matyjaszewski, K. *Macromolecules* **2006**, *39*, 4953–4959.

(12) Kwak, Y.; Matyjaszewski, K. *Macromolecules* **2008**, *41*, 6627–6635.

(13) Tang, W.; Kwak, Y.; Braunecker, W.; Tsarevsky, N. V.; Coote, M. L.; Matyjaszewski, K. *J. Am. Chem. Soc.* **2008**, *130*, 10702–10713.

(14) Goto, A.; Fukuda, T. *Macromol. Rapid Commun.* **1999**, *20*, 633–636.

(15) Tang, W.; Matyjaszewski, K. *Macromolecules* **2007**, *40*, 1858–1863.

(16) Tang, W.; Tsarevsky, N. V.; Matyjaszewski, K. *J. Am. Chem. Soc.* **2006**, *128*, 1598–1604.

(17) Schröder, K.; Mathers, R. T.; Buback, J.; Konkolewicz, D.; Magenau, A. J. D.; Matyjaszewski, K. *ACS Macro Lett.* **2012**, *1*, 1037–1040.

(18) Nanda, A. K.; Matyjaszewski, K. *Macromolecules* **2003**, *36*, 1487–1493.

(19) Kwak, Y.; Magenau, A. J. D.; Matyjaszewski, K. *Macromolecules* **2011**, *44*, 811–819.

(20) Kwak, Y.; Matyjaszewski, K. *Polym. Int.* **2009**, *58*, 242–247.

(21) Chan, N.; Cunningham, M. F.; Hutchinson, R. A. *Macromol. Chem. Phys.* **2008**, *209*, 1797–1805.

(22) Morick, J.; Buback, M.; Matyjaszewski, K. *Macromol. Chem. Phys.* **2012**, *213*, 2287–2292.

(23) Tang, W.; Nanda, A. K.; Matyjaszewski, K. *Macromol. Chem. Phys.* **2005**, *206*, 1171–1177.

(24) Braunecker, W. A.; Tsarevsky, N. V.; Pintauer, T.; Gil, R. R.; Matyjaszewski, K. *Macromolecules* **2005**, *38*, 4081–4088.

(25) Chambard, G.; Klumperman, B.; German, A. L. *Macromolecules* **2000**, *33*, 4417–4421.

(26) Horn, M.; Matyjaszewski, K. *Macromolecules* **2013**, *46*, 3350–3357.

(27) Braunecker, W. A.; Tsarevsky, N. V.; Gennaro, A.; Matyjaszewski, K. *Macromolecules* **2009**, *42*, 6348–6360.

(28) Seeliger, F.; Matyjaszewski, K. *Macromolecules* **2009**, *42*, 6050–6055.

(29) Mueller, L.; Jakubowski, W.; Tang, W.; Matyjaszewski, K. *Macromolecules* **2007**, *40*, 6464–6472.

(30) Shipp, D. A.; Wang, J.-L.; Matyjaszewski, K. *Macromolecules* **1998**, *31*, 8005–8008.

(31) Matyjaszewski, K.; Shipp, D. A.; McMurtry, G. P.; Gaynor, S. G.; Pakula, T. *J. Polym. Sci., Part A Polym. Chem.* **2000**, *38*, 2023–2031.

(32) Tsarevsky, N. V.; Sarbu, T.; Go, B.; Matyjaszewski, K.; Göbelt, B. *Macromolecules* **2002**, *35*, 6142–6148.

(33) Wulkow, M. *Macromol. Theory Simul.* **1996**, *5*, 393–416.

(34) Wulkow, M. *Macromol. React. Eng.* **2008**, *2*, 461–494.

(35) Fierens, S. K.; D'hooge, D. R.; Van Steenberge, P. H. M.; Reyniers, M.-F.; Marin, G. B. *Polymers* **2015**, *7*, 655-679.

(36) Hernández-Ortiz, J. C., Vivaldo-Lima, E., Dubé, M. A. and Penlidis, A. *Macromol. Theory Simul*. **2014**, *23*: 429–441.

(37) Rabea, A. M.; Zhu, S. *Polymers* **2015**, *7*, 819-835.

(38) D'hooge, D. R.; Reyniers, M.-F.; Marin, G. B. *Macromol. React. Eng.* **2013**, *7*, 362-379.

(39) Li, X.; Wang, W.-J.; Li, B.-G.; Zhu, S. *Macromol. React. Eng.* **2011**, *5*, 467–478.

(40) Schroeder, H.; Buback, J.; Schrooten, J.; Buback, M.; Matyjaszewski, K. *Macromol. Theory Simul.* **2014**, *23*, 279–287.

(41) Toloza Porras, C.; D'hooge, D. R.; Van Steenberge, P. H. M.; Reyniers, M.-F.; Marin, G. B. *Macromol. React. Eng.* **2013**, *7*, 311–326.

(42) Buback, M.; Morick, J. *Macromol. Chem. Phys.* **2010**, *211*, 2154–2161.

(43) Zhang, M.; Ray, W. H. *J. Appl. Polym. Sci.* **2002**, *86*, 1630–1662.

(44) Zhang, M.; Ray, W. H. *J. Appl. Polym. Sci.* **2002**, *86*, 1047–1056.

(45) Wang, W.; Zhou, Y.-N.; Luo, Z.-H. *Macromol. React. Eng.* **2015**, n/a – n/a.

(46) Matyjaszewski, K.; Spanswick, J. *Mater. Today* **2005**, *8*, 26–33.

(47) Shen, Y.; Tang, H.; Ding, S. *Prog. Polym. Sci.* **2004**, *29*, 1053–1078.

(48) Shen, Y.; Zhu, S.; Pelton, R. *Macromol. Rapid Commun.* **2000**, *21*, 956–959.

(49) Shen, Y.; Zhu, S. *AIChE J.* **2002**, *48*, 2609–2619.

(50) Fu, Y.; Cunningham, M. F.; Hutchinson, R. A. *Macromol. Symp.* **2007**, *259*, 151–163.

(51) Chan, N.; Cunningham, M. F.; Hutchinson, R. A. *Macromol. React. Eng.* **2010**, *4*, 369–380.

(52) Wang, Y.; Hutchinson, R. A.; Cunningham, M. F. *Macromol. Mater. Eng.* **2005**, *290*, 230–241.

(53) Noda, T.; Grice, A. J.; Levere, M. E.; Haddleton, D. M. *Eur. Polym. J.* **2007**, *43*, 2321–2330.

(54) Chan, N.; Cunningham, M. F.; Hutchinson, R. A. *J. Polym. Sci., Part A Polym. Chem.* **2013**, *51*, 3081-3096.

(55) Chan, N.; Boutti, S.; Cunningham, M. F.; Hutchinson, R. A. *Macromol. React. Eng.* **2009**, *3*, 222–231.

(56) Burns, J. A.; Houben, C.; Anastasaki, A.; Waldron, C.; Lapkin, A. A.; Haddleton, D. M. *Polym. Chem.* **2013**, *4*, 4809-4813.

(57) Rosenfeld, C.; Serra, C. A.; Brochon, C.; Hadziioannou, G. *Chem. Eng. Sci.* **2007**, *62*, 5245–5250.

(58) Parida, D.; Serra, C. A.; Garg, D. K.; Hoarau, Y.; Muller, R.; Bouquey, M. *Macromol. React. Eng.* **2014**, *8*, 597–603.

(59) Müller, M.; Cunningham, M. F.; Hutchinson, R. A. *Macromol. React. Eng.* **2008**, *2*, 31–36.

(60) Chan, N.; Meuldijk, J.; Cunningham, M. F.; Hutchinson, R. A. *Ind. Eng. Chem. Res.* **2013**, *52*, 11931–11942.

(61) Smulders, W. W.; Jones, C. W.; Schork, F. J. *AIChE J.* **2005**, *51*, 1009–1021.

(62) Smulders, W. W.; Jones, C. W.; Schork, F. J. *Macromolecules* **2004**, *37*, 9345–9354.

(63) Schork, F. J.; Smulders, W. W. *J. Appl. Polym. Sci.* **2004**, *92*, 539–542.

(64) Solomon, D. H.; Rizzardo, E.; Cacioli, P. Polymerization Process and Polymers Produced Thereby. US 4581429, 1986.

(65) Moad, G.; Solomon, D. H. *The Chemistry of Free Radical Polymerization*; Elsevier Science: Oxford, 1995; Vol. 42.

(66) Solomon, D. H. *J. Polym. Sci., Part A Polym. Chem.* **2005**, *43*, 5748–5764.

(67) Georges, M. K.; Veregin, R. P. N.; Kazmaier, P. M.; Hamer, G. K. *Macromolecules* **1993**, *26*, 2987–2988.

(68) Hawker, C. J.; Barclay, G. G.; Orellana, A.; Dao, J.; Devonport, W. *Macromolecules* **1996**, *29*, 5245–5254.

(69) Hawker, C. J. *J. Am. Chem. Soc.* **1994**, *116*, 11185–11186.

(70) Nicolas, J.; Guillaneuf, Y.; Lefay, C.; Bertin, D.; Gigmes, D.; Charleux, B. *Prog. Polym. Sci.* **2013**, *38*, 63–235.

(71) Dollin, M.; Szkurhan, A. R.; Georges, M. K. *J. Polym. Sci., Part A Polym. Chem.* **2007**, *45*, 5487–5493.

(72) Georges, M. K.; Veregin, R. P. N.; Kazmaier, P. M.; Hamer, G. K.; Saban, M. *Macromolecules* **1994**, *27*, 7228–7229.

(73) Nilsen, A.; Braslau, R. *J. Polym. Sci., Part A Polym. Chem.* **2006**, *44*, 697–717.

(74) Ingold, K. U.; Adamic, K.; Bowman, D. F.; Gillan, T. *J. Am. Chem. Soc.* **1971**, *93*, 902–908.

(75) Bowman, D. F.; Gillan, T.; Ingold, K. U. *J. Am. Chem. Soc.* **1971**, *93*, 6555–6561.

(76) Bowman, D. F.; Brokenshire, J. L.; Gillan, T.; Ingold, K. U. *J. Am. Chem. Soc.* **1971**, *93*, 6551–6555.

(77) Goto, A.; Kwak, Y.; Yoshikawa, C.; Tsujii, Y.; Sugiura, Y.; Fukuda, T. *Macromolecules* **2002**, *35*, 3520–3525.

(78) Ananchenko, G. S.; Fischer, H. *J. Polym. Sci., Part A Polym. Chem.* **2001**, *39*, 3604–3621.

(79) Devonport, W.; Michalak, L. M.; Malmström, E.; Mate, M.; Kurdi, B.; Hawker, C. J.; Barclay, G. G.; Sinta, R. *Macromolecules* **1997**, *30*, 1929–1934.

(80) Odell, P. G.; Veregin, R. P. N.; Michalak, L. M.; Brousmiche, D.; Georges, M. K. *Macromolecules* **1995**, *28*, 8453–8455.

(81) Benoit, D.; Chaplinski, V.; Braslau, R.; Hawker, C. J. *J. Am. Chem. Soc.* **1999**, *121*, 3904–3920.

(82) Le Mercier, C.; Lutz, J.-F.; Marque, S. R. A.; Le Moigne, F.; Tordo, P.; Lacroix-Desmazes, P.; Boutevin, B.; Couturier, J.-L.; Guerret, O.; Martschke, R.; Sobek, J.; Fischer, H. In *Controlled/Living Radical Polymerization*; ACS Symposium Series, American Chemical Society: Washington, DC, 2000; pp. 108–122.

(83) Benoit, D.; Grimaldi, S.; Robin, S.; Finet, J.-P.; Tordo, P.; Gnanou, Y. *J. Am. Chem. Soc.* **2000**, *122*, 5929–5939.

(84) Guillaneuf, Y.; Gigmes, D.; Marque, S. R. A.; Astolfi, P.; Greci, L.; Tordo, P.; Bertin, D. *Macromolecules* **2007**, *40*, 3108–3114.

(85) Greene, A. C.; Grubbs, R. B. *Macromolecules* **2009**, *42*, 4388–4390.

(86) Studer, A.; Harms, K.; Knoop, C. A.; Müller, C.; Schulte, T. *Macromolecules* **2004**, *37*, 27–34.

(87) Couvreur, L.; Lefay, C.; Belleney, J.; Charleux, B.; Guerret, O.; Magnet, S. *Macromolecules* **2003**, *36*, 8260–8267.

(88) Bertin, D.; Gigmes, D.; Marque, S. R. A.; Tordo, P. *Chem. Soc. Rev.* **2011**, *40*, 2189–2198.

(89) Bertin, D.; Dufils, P.-E.; Durand, I.; Gigmes, D.; Giovanetti, B.; Guillaneuf, Y.; Marque, S. R. A.; Phan, T. N. T.; Tordo, P. *Macromol. Chem. Phys.* **2008**, *209*, 220–224.

(90) Guillaneuf, Y.; Gigmes, D.; Marque, S. R. A.; Tordo, P.; Bertin, D. *Macromol. Chem. Phys.* **2006**, *207*, 1278–1288.

(91) Georges, M. K.; Lukkarila, J. L.; Szkurhan, A. R. *Macromolecules* **2004**, *37*, 1297–1303.

(92) Chauvin, F.; Dufils, P.-E.; Gigmes, D.; Guillaneuf, Y.; Marque, S. R. A.; Tordo, P.; Bertin, D. *Macromolecules* **2006**, *39*, 5238–5250.

(93) Keoshkerian, B.; Georges, M. K.; Quinlan, M.; Veregin, R. P. N.; Goodbrand, B. *Macromolecules* **1998**, *31*, 7559–7561.

(94) Le Du, Y.; Binet, L.; Hémery, P.; Marx, L. *J. Polym. Sci., Part A Polym. Chem.* **2012**, *50*, 2871–2877.

(95) Charleux, B.; Nicolas, J.; Guerret, O. *Macromolecules* **2005**, *38*, 5485–5492.

(96) Nicolas, J.; Brusseau, S.; Charleux, B. *J. Polym. Sci., Part A Polym. Chem.* **2010**, *48*, 34–47.

(97) Auschra, C.; Eckstein, E.; Knischka, R.; Nesvadba, P. *Asia Pac. Coat. J.* **2003**, *16*, 20–23.

(98) Gerard, P.; Inoubli, R.; Magnet, S. *Abstr. Pap. Am. Chem. Soc.* **2008**, *236*, POLY 611.

(99) Gigmes, D.; Vinas, J.; Chagneux, N.; Lefay, C.; Phan, T. N. T.; Trimaille, T.; Dufils, P.-E.; Guillaneuf, Y.; Carrot, G.; Boué, F.; Bertin, D. In *Controlled/Living Radical Polymerization: Progress in RAFT, DT, NMP & OMRP*; ACS Symposium Series, American Chemical Society: Washington, DC, 2009; pp. 245–262.

(100) Hawker, C. J.; Bosman, A. W.; Harth, E. *Chem. Rev.* **2001**, *101*, 3661–3688.

(101) Guillaneuf, Y.; Dufils, P.-E.; Autissier, L.; Rollet, M.; Gigmes, D.; Bertin, D. *Macromolecules* **2010**, *43*, 91–100.

(102) Yousi, Z.; Jian, L.; Rongchuan, Z.; Jianliang, Y.; Lizong, D.; Lansun, Z. *Macromolecules* **2000**, *33*, 4745–4749.

(103) Butz, S.; Baethge, H.; Schmidt-Naake, G. *Macromol. Rapid Commun.* **1997**, *18*, 1049–1055.

(104) Dire, C.; Charleux, B.; Magnet, S.; Couvreur, L. *Macromolecules* **2007**, *40*, 1897–1903.

(105) Zaremski, M. Y.; Plutalova, A. V.; Lachinov, M. B.; Golubev, V. B. *Macromolecules* **2000**, *33*, 4365–4372.

(106) Ruzette, A.-V.; Tencé-Girault, S.; Leibler, L.; Chauvin, F.; Bertin, D.; Guerret, O.; Gérard, P. *Macromolecules* **2006**, *39*, 5804–5814.

(107) Perrin, L.; Phan, T. N. T.; Querelle, S.; Deratani, A.; Bertin, D. *Macromolecules* **2008**, *41*, 6942–6951.

(108) Ladavière, C.; Lacroix-Desmazes, P.; Delolme, F. *Macromolecules* **2009**, *42*, 70–84.

(109) Mazarin, M.; Phan, T. N. T.; Charles, L. *Rapid Commun. Mass Spectrom.* **2008**, *22*, 3776–3782.

(110) Wienhöfer, I. C.; Luftmann, H.; Studer, A. *Macromolecules* **2011**, *44*, 2510–2523.

(111) Dempwolf, W.; Flakus, S.; Schmidt-Naake, G. *Macromol. Symp.* **2009**, *275-276*, 166–172.

(112) Hoogenboom, R.; Zorn, A.-M.; Keul, H.; Barner-Kowollik, C.; Moeller, M. *Polym. Chem.* **2012**, *3*, 335.

(113) Kim, K.; Hasneen, A.; Paik, H.; Chang, T. *Polymer* **2013**, *54*, 6133–6139.

(114) Greszta, D.; Matyjaszewski, K. *Macromolecules* **1996**, *29*, 7661–7670.

(115) He, J.; Li, L.; Yang, Y. *Macromol. Theory Simul.* **2000**, *9*, 463–468.

(116) Souaille, M.; Fischer, H. *Macromolecules* **2002**, *35*, 248–261.

(117) Souaille, M.; Fischer, H. *Macromolecules* **2000**, *33*, 7378–7394.

(118) Bentein, L.; D'hooge, D. R.; Reyniers, M.-F.; Marin, G. B. *Macromol. Theory Simul.* **2011**, *20*, 238–265.

(119) Gigmes, D.; Bertin, D.; Lefay, C.; Guillaneuf, Y. *Macromol. Theory Simul.* **2009**, *18*, 402–419.

(120) Toloza Porras, C.; D'hooge, D. R.; Reyniers, M.-F.; Marin, G. B. *Macromol. Theory Simul.* **2013**, *22*, 136–149.

(121) Nicolas, J.; Mueller, L.; Dire, C.; Matyjaszewski, K.; Charleux, B. *Macromolecules* **2009**, *42*, 4470–4478.

(122) Faliks, A.; Yetter, R. A.; Floudas, C. A.; Wei, Y.; Rabitz, H. *Polymer* **2001**, *42*, 2061–2065.

(123) Roa-Luna, M.; Nabifar, A.; McManus, N. T.; Vivaldo-Lima, E.; Lona, L. M. F.; Penlidis, A. *J. Appl. Polym. Sci.* **2008**, *109*, 3665–3678.

(124) Diaz-Camacho, F.; Lopez-Morales, S.; Vivaldo-Lima, E.; Saldívar-Guerra, E.; Vera-Graziano, R.; Alexandrova, L. *Polym. Bull.* **2004**, *52*, 339–347.

(125) Hernández-Ortiz, J. C.; Vivaldo-Lima, E.; Lona, L. M. F.; McManus, N. T.; Penlidis, A. *Macromol. React. Eng.* **2009**, *3*, 288–311.

(126) Bertin, D.; Chauvin, F.; Marque, S. R. A.; Tordo, P. *Macromolecules* **2002**, *35*, 3790–3791.

(127) Gryn'ova, G.; Lin, C. Y.; Coote, M. L. *Polym. Chem.* **2013**, *4*, 3744-3754.

(128) Wang, L.; Broadbelt, L. J. *Macromolecules* **2009**, *42*, 7961–7968.

(129) Kavitha, A. A.; Singha, N. K. *Macromolecules* **2010**, *43*, 3193–3205.

(130) Wang, L.; Broadbelt, L. J. *Macromolecules* **2009**, *42*, 8118–8128.

(131) Wang, L.; Broadbelt, L. J. *Macromolecules* **2010**, *43*, 2228–2235.

(132) Hlalele, L.; Klumperman, B. *Macromolecules* **2011**, *44*, 6683–6690.

(133) Fu, Y.; Cunningham, M. F.; Hutchinson, R. A. *Macromol. React. Eng.* **2007**, *1*, 243–252.

(134) Enright, T. E.; Cunningham, M. F.; Keoshkerian, B. *Macromol. Rapid Commun.* **2005**, *26*, 221–225.

(135) Enright, T. E.; Cunningham, M. F.; Keoshkerian, B. *Macromol. React. Eng.* **2010**, *4*, 186–196.

(136) Fortunatti, C.; Sarmoria, C.; Brandolin, A.; Asteasuain, M. *Macromol. React. Eng.* **2014**, *8*, 260–281.

(137) Farkas, E.; Meszéna, Z. G. *Period. Polytech. Chem.* **2010**, *54*, 15-25.

(138) Lemos, T.; Melo, P. A.; Pinto, J. C. *Macromol. React. Eng.* **2015**, *9*, 259-270.

(139) Lemoine-Nava, R.; Flores-Tlacuahuac, A.; Saldívar-Guerra, E. *Chem. Eng. Sci.* **2006**, *61*, 370–387.

Chapter 3

ARGET ATRP of BMA and BA: Exploring Limitations at Low Copper Levels

Preface

It can be seen from the literature review that ARGET ATRP is capable of increased polymerization rates with lower levels of copper and ligand than conventional ATRP. This can be helpful in improving the economic viability of this chemistry. Reduced ligand reduces cost and the amount of copper that must be removed. A systematic batch experimental study was conducted to decrease the copper loading in this system while still maintaining acceptable polymerization rates and control for the polymerization of butyl methacrylate (BMA) and butyl acrylate (BA). The results demonstrate the limitations of reducing copper levels with different monomers, different target chain lengths (initiator concentrations), and different reducing agent loadings. The work in this chapter has been published as a chapter in the peer-reviewed ACS Symposium Series eBook: Progress in Controlled Radical Polymerization: Mechanisms and Techniques, Chapter 12.

Abstract

Batch ARGET ATRP of butyl methacrylate (BMA) and butyl acrylate (BA) was systematically investigated over a range of initiator, catalyst, and reducing agent loadings to produce material with a target molecular weight of 5,000 g mol^{-1}. Reducing copper catalyst loading to 36 ppm with respect to monomer (800 chains per Cu) in the BMA system, however, led to a significant decrease in reaction rate and initiator efficiency. Reaction rate was recovered with a large excess of reducing agent, with some loss of livingness. Similar trends were observed for BA polymerization, but initiator efficiencies were significantly higher than found with BMA. Thus, achieving reasonable rates of reaction while maintaining control of livingness at low catalyst levels requires a trade-off between catalyst and reducing agent loadings.

3.1 Introduction

Atom Transfer Radical Polymerization (ATRP) is a form of Controlled/Living Radical Polymerization (CRP/LRP) in which the polymerization is mediated by a metal that has n and n+1 oxidation states. The reaction mechanism with the most common catalyst choice, copper, is shown in Scheme 3.1. The forward activation reaction with rate coefficient k_{act} creates the radical as Cu^{I} is oxidized to Cu^{II}, with the rate coefficient for the reverse deactivation reaction (k_{deact}) several orders of magnitude greater than k_{act} such that the radical typically adds only a few monomer units before deactivating.[1-6] A well-controlled and living system exhibits a narrow polymer molar mass distribution (MMD) with minimal termination such that the entire MMD shifts to higher values with increasing conversion. The concern for normal ATRP is the accumulation of the Cu^{II} species due to loss of radicals by termination, and by oxidation of Cu^{I} by impurities such as oxygen. The resulting reduction in polymerization rate necessitates operation with an elevated Cu level approaching one catalyst species per chain. The copper must then be removed from the polymer product once the reaction is complete as it produces discoloration.

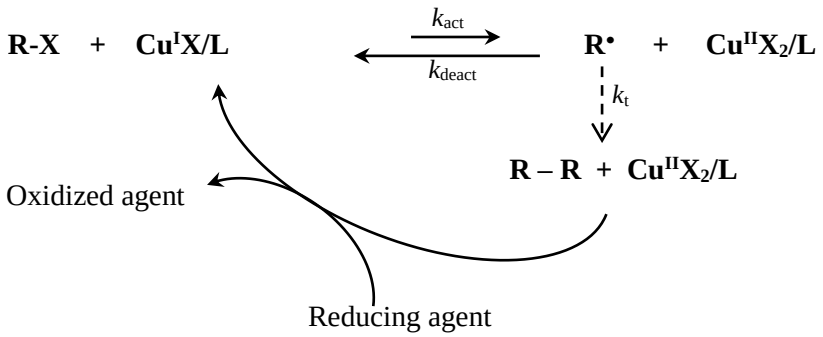

Scheme 3.1: Mechanism for ARGET ATRP. The Cu^{I} activator is constantly regenerated from Cu^{II} by the reducing agent.

Matyjaszewski *et al*. have recently developed a modified version of ATRP known as ARGET, for "activators regenerated by electron transfer", through which catalyst concentration can be lowered to parts per million (ppm) levels with respect to monomer while still maintaining a reasonable reaction rate and control. The technique employs the more oxidatively stable and easier to handle Cu^{II} species as a starting material, along with an excess of an additional reagent which reduces deactivator (whose concentration has built up due to termination) to regenerate Cu^{I} activating species, as seen in Scheme 3.1.[7,8]

The rate expression for the ATRP system, which also holds for ARGET ATRP, is written as

$$R_p = k_p[M][R-X]\frac{k_{act}[Cu^{I}X/L]}{k_{deact}[Cu^{II}X_2/L]} \qquad \textbf{Equation 3-1}$$

where $K_{ATRP} = k_{act}/k_{deact}$ is the ATRP equilibrium constant, k_p is the propagation rate coefficient of the monomer, [M] is monomer concentration, [R-X] is the concentration of dormant chains, $[Cu^{I}]$ and $[Cu^{II}]$ are the concentration of activator and deactivator species present in the system with (pseudo) halide X and ligand L.[8] Usually, as most chains are in the dormant state at any instant in time, [R-X] is approximated by $[R\text{-}X]_o$, the amount of alkyl halide initiator added to the system.

The polymer dispersity (*Đ*) may be estimated by Equation 3-2.

$$Đ = \frac{Mw}{Mn} = 1 + \frac{1}{DP_{nT}} + \left(\frac{[R-X]_o k_p}{k_{deact}[Cu^{II}X_2/L]}\right)\left(\frac{2}{x} - 1\right) \qquad \textbf{Equation 3-2}$$

where *x* is polymer conversion, M_n and Mw are the number-average and weight-average polymer molar masses, respectively, and DP_{nT} is the target chain length. The latter quantity is given by $[M]_o/[R\text{-}X]_o$, the ratio of the initial molar concentrations of monomer and initiator, respectively.[8] The target molar mass (M_{nT}) at full conversion can be calculated by Equation 3-3.

$$Mn_T = \frac{m_{monomer}}{\eta_{init}} \qquad \textbf{Equation 3-3}$$

where $m_{monomer}$ is the mass of monomer and η_{init} is the number of moles of initiator added to the reactor. The initiator efficiency (f_{init}) is estimated by Equation 3-4.

$$f_{init} = \frac{Mn_T}{Mn_{exp}} \cdot x \qquad \textbf{Equation 3-4}$$

where $M_{n,exp}$ is the number-average molar mass obtained from size exclusion chromatography (SEC).

Recently, Zhong *et al*.[9] have derived a relationship to estimate dead chain fraction (DCF), under the assumption that the radical concentration does not change significantly.

$$DCF = \frac{[T]}{f_{init}[R-X]_o} = \frac{2DP_{nT}k_t\left(ln(1-x)\right)^2}{f_{init}[M]_o k_p^2 t} \qquad \textbf{Equation 3-5}$$

where [T] is the concentration of terminated chains, $[R\text{-}X]_o$ is the number of chains (initiator) added to the system, k_t is the termination rate constant and t is the reaction time.[9] We have modified Equation 3-5 by adding an initiator efficiency factor, f_{init}, to correct for deviation from quantitative initiation. This equation shows that DCF increases with increasing conversion and target chain length, and decreases with reduced reaction rate (longer t to reach the same value of x).

Previous work in low Cu ARGET ATRP has been performed for target chain lengths of 100-200 units with molar concentrations of Cu as low as ~2 ppm with respect to monomer. The number of polymer molecules being mediated per catalyst molecule is often 100,[8,10,11] although studies at over 1000 chains per Cu have been reported.[7,12,13] This previous work finds that an increase in the number of chains mediated per Cu complex results in longer reaction times, sometimes requiring over 20 h to achieve a conversion greater than 40%. Termination as well as transfer can be minimized by limiting the targeted chain length, as these reactions increase in proportion to chain length and conversion.[14] Zhong *et al*. suggested that the combination of higher DP_{nT} and lower conversion should give fewer dead chains when targeting a desired chain length

and still achieving a reasonable polymerization rate.[9] However, this strategy requires additional separation of unconverted monomer and higher Cu levels from the polymer.

The purpose of this experimental study is to determine practical operating regimes for the ARGET ATRP system in a batch reactor. For industry to consider adoption of ARGET ATRP chemistry, the system must include limited reaction time with minimal copper levels to be competitive with conventional free radical polymerization (FRP) processes. The reaction conditions investigated include changes in monomer type, chain length (initiator loading), the initial concentrations of catalyst, reducing agent, and initiator, as well as the ratios of the catalyst to reducing agent and initiator to catalyst/reducing agent. In this work, the catalyst concentration was lowered to 34-37 ppm on a molar basis relative to monomer. Unless otherwise stated, the target molecular weight for each reaction was 5,000 g mol^{-1}, while the solvent content was 30 wt%; the short chain length and high polymer content are applicable to the coatings industry.[15,16] Thus, the reactions are run with as many as 800 chains per Cu complex, with typical reaction times of 6 h. Loss of control and termination at higher monomer conversion are problems that are particularly apparent in this type of system (low DP_{nT} and large number of chains), and as such are a major hindrance in the ability to lower catalyst levels.

3.2 Experimental

3.2.1 Materials

Butyl methacrylate (BMA; 99%, Aldrich), butyl acrylate (BA; 99%, Aldrich), copper (II) bromide ($CuBr_2$, 99% Aldrich), anisole (99%, Aldrich), ethyl 2-bromoisobutyrate (EBiB; 98%, Aldrich), and tin (II) 2-ethylhexanoate ($Sn(EH)_2$, 95%, Aldrich) were used as received.

3.2.2 Procedure

All polymerizations were carried out under batch conditions in a 100 mL two-neck round-bottom flask in a thermostated oil bath with a condenser to prevent loss of solvent or monomer.

The catalyst [Cu(II)TPMABr]Br was synthesized according to the literature[17] and dissolved in 10 g of anisole by sonication for 20 min. [TPMA]:[Cu(II)] was kept at a 1:1 molar ratio for all reactions. 35 g of monomer was mixed with the catalyst and anisole in a round-bottom flask. The mixture was purged under nitrogen and stirred at 250 rpm for 40 min before heating to the desired reaction temperature. The initiator ethyl 2-bromoisobutyrate (EBiB) was dissolved in 2.5 g of anisole and injected into the round-bottom flask using a degassed syringe. After approximately 10 min, the reducing agent, tin (II) 2-ethylhexanoate ($Sn(EH)_2$), which was dissolved in 2.5 g of anisole and purged with nitrogen, was injected, marking the beginning of the reaction. Samples were taken with a deoxygenated syringe at various times throughout the reaction, with polymerizations assumed to stop upon exposure to air.

3.2.3 Analytical Methods

Conversion was calculated by gravimetry and molecular weight was measured by size exclusion chromatography (SEC) using a Waters 2960 separation module with Styragel packed columns HR 0.5, HR 1, HR 3, HR 4, and HR 5E (Waters Division Millipore) coupled with a refractive index detector operating at 40 °C. THF was used as eluent and the flow rate was set to 1.0 mL min^{-1}. The detector was calibrated with eight narrow polystyrene standards, ranging from 347 to 355000 g mol^{-1}. The molecular weights of poly(BMA), and poly(BA) samples were obtained by universal calibration using known Mark-Houwink parameters for polystyrene ($K = 11.4x10^{-5}$ dL g^{-1}, $a = 0.716$),[18] poly(BMA) ($K = 14.8x10^{-5}$ dL g^{-1}, $a = 0.664$),[18] and poly(BA) ($K = 7.4x10^{-5}$ dL g^{-1}, $a = 0.750$).[19]

3.3 Results and Discussion

3.3.1 Initiator Loading

Butyl methacrylate (BMA) was polymerized at 70 °C, with the target polymer molecular weight (MW) altered by changing the [M]:[R-X] ratio, thus changing the number of chains in the

system and also the number of chains that each catalyst molecule has to initiate and regulate. The catalyst and reducing agent loadings were adjusted in this set of initial experiments to ensure a constant molar ratio relative to initiator of [R-X]:[Cu]:[Sn] = 1:0.01:0.1. A summary of the results, which compare well with those previously published for a target chain length of 200,[12] is presented in Table 3.1. The target MWs corresponding to [BMA]:[R-X] ratios of 400:1, 100:1, 70:1, and 35:1 are 56,800 g mol^{-1}, 14,200 g mol^{-1}, 10,000 g mol^{-1} and 5,000 g mol^{-1}, respectively. Note that all tabulated results are for the final sample in each reaction, and that the added Cu levels are presented on a molar basis with respect to initial monomer content (ppm or μmol mol^{-1}).

Table 3.1: Batch ARGET ATRP of BMA at 70 °C with 30 wt% anisole and

Initial Ratio [M]:[R-X]:[Cu]:[Sn]	Cu (ppm)[a]	Time (min)	Conversion	$M_{n,exp}$ (g mol^{-1})	Initiator Efficiency
400:1:0.01:0.1	28	360	0.43	36200	0.64
200:1:0.01:0.1[b]	50	300	0.59	18500	0.64
100:1:0.01:0.1	100	360	0.95	18529	0.72
70:1:0.01:0.1	143	300	0.96	13156	0.73
35:1:0.01:0.1	285	120	0.87	6954	0.62

[a]Cu level reported as a molar ratio with respect to initial monomer concentration. [b]Previously reported[12]

The experimental profiles are plotted in Figure 3.1. The increased initiator concentration that results from lowering the target chain length leads to an increased polymerization rate (Figure 3.1a), as expected from Equation 3-1. M_n increased linearly with conversion (Figure 3.1b), and $Đ$ was <1.3 for all cases (Figure 3.1c). What is most noteworthy is the apparent increase in initiator efficiency that occurs with reaction time (Figure 3.1d), as estimated from polymer M_n values by Equation 3-4. Efficiencies are less than unity in all cases, and indicate that the activation of R-X is slow and not complete. This situation is most obvious at the lowest Cu levels (<30 ppm, DP_{nT} =

400), for which the reduced initiator efficiency as well as the reduced $[R\text{-}X]_o$ value contributes to the lower rate of polymerization.

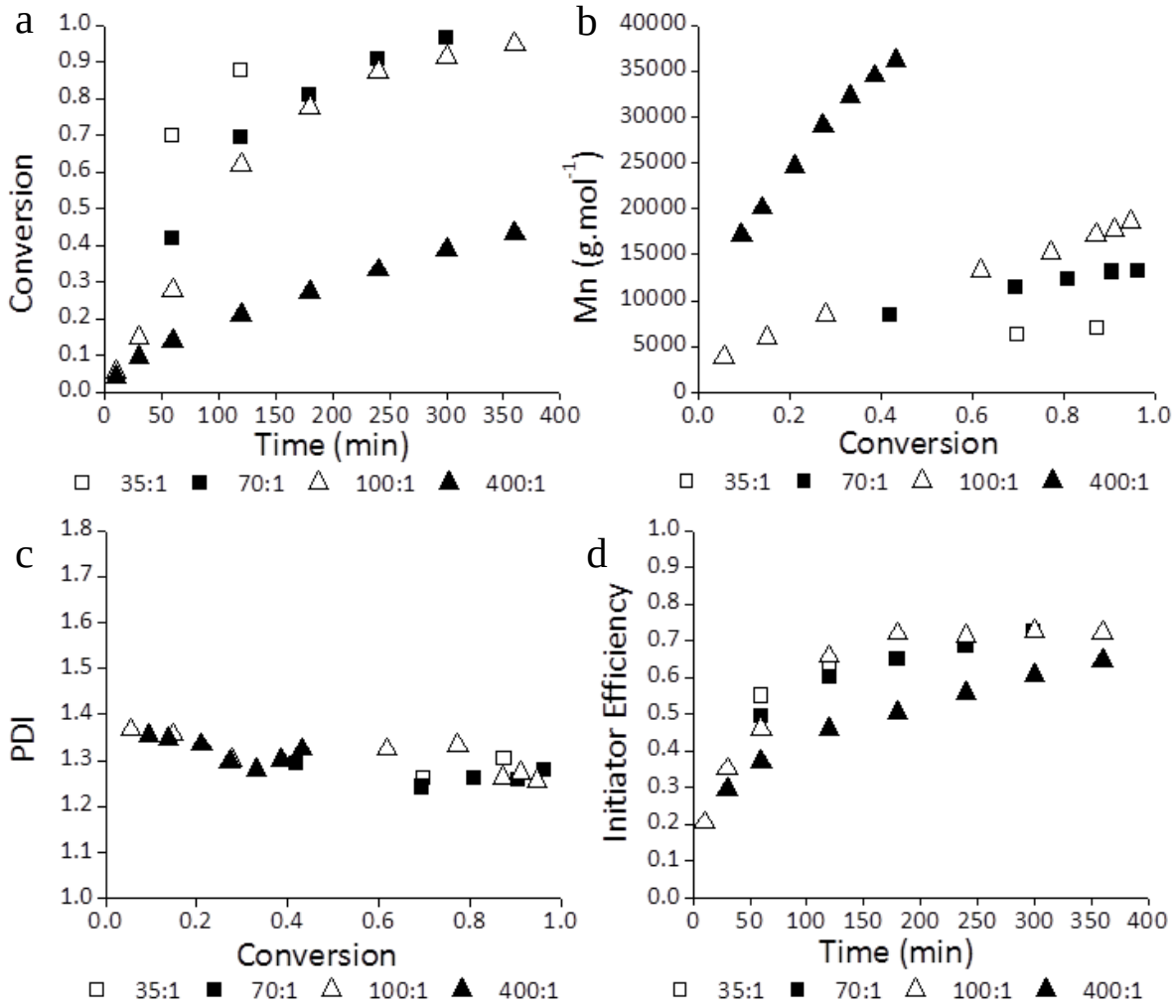

Figure 3.1: Batch ARGET ATRP of BMA with varying initiator loading at 70 °C: (a) monomer conversion versus time; (b) number-average molecular weight (M_n) and (c) polydispersity index (PDI or $Đ$) as a function of conversion; (d) initiator efficiency versus time. Legend shows initial molar ratios of [M]:[R-X], with [R-X]:[Cu]:[Sn] = 1:0.01:0.1.

The polymer MMDs for the BMA polymerizations with target chain lengths of 70 and 400 are shown in Figure 3.2; both systems have a similar $Đ$ (Figure 3.1c) despite the difference in DP_{nT}.

The MMDs exhibit a low MW tail which remains visible even at increased reaction times. This tail may be the result of termination of low MW chains early in the batch, or may be an indication of slow initiation in the system. The latter explanation is consistent with the initiator efficiencies shown in Figure 3.1d. As the decrease in DP_{nT} (and resulting increase in rate) was achieved by a simultaneous increase in initiator and copper levels, the effect of varying copper level at constant DP_{nT} was examined in the next set of experiments.

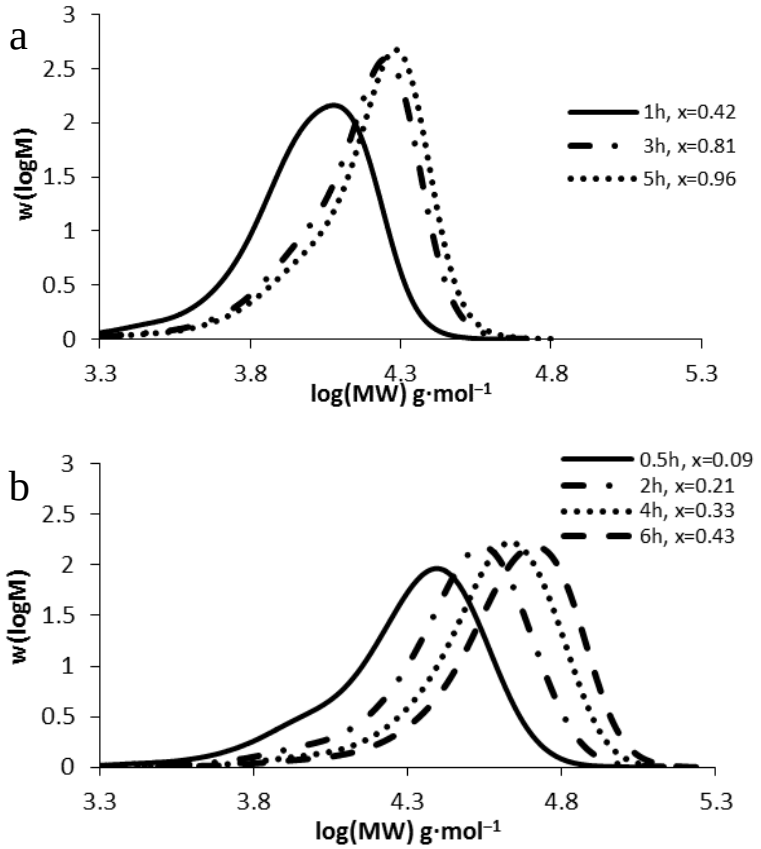

Figure 3.2: MMDs of pBMA produced by batch ARGET ATRP AT 70 °C, sampled hourly to confirm living nature of polymerization: (a) [M]:[R-X]:[Cu]:[Sn]=70:1:0.01:0.1; (b) [M]:[R-X]:[Cu]:[Sn]=400:1:0.01:0.1.

3.3.2 Effect of Decreased Catalyst and Reducing Agent Loading

To measure the effect of decreased catalyst level, the amounts of Cu and reducing agent were kept at a constant molar ratio of [Cu(II)TPMABr$_2$]:[Sn(EH)$_2$] = 1:10 while reducing the catalyst loading from 285 to 36 ppm at constant monomer and initiator levels. The ratio of catalyst to number of chains was therefore decreased from one Cu per 100 chains to one Cu per 800 chains, assuming 100% initiator efficiency, while maintaining a target chain length of 35 (M_{nT} = 5,000 g mol^{-1}). A summary of the experiments is presented in Table 3.2 and plotted as Figure 3.3.

Table 3.2: Batch ARGET ATRP of BMA with varying catalyst levels and 30 wt% anisole at 70 °C with M_{nT} = 5,000 g mol^{-1}, maintaining [Cu]:[Sn] at 1:10.

Initial Ratio [M]:[R-X]:[Cu]:[Sn]	Cu (ppm)	Time (min)	Conversion	$M_{n,exp}$ (g mol^{-1})	Initiator Efficiency
35:1:0.01:0.1	285	120	0.88	6954	0.62
35:1:0.005:0.05	145	360	0.88	8726	0.50
35:1:0.005:0.05	145	360	0.85	8707	0.48
35:1:0.0025:0.025	72	300	0.69	7863	0.44
35:1:0.00125:0.0125	36	360	0.44	8778	0.25

Assuming that a constant ratio of catalyst to reducing agent preserves a similar Cu^{I}/Cu^{II} ratio across varying catalyst levels, there should not be a decrease in reaction rate with lower catalyst concentrations (Equation 3-1). However, it is clear from the monomer conversion profiles (Figure 3.3a) that the polymerization rate decreases significantly with decreasing catalyst concentration, as has been seen previously in other ARGET systems with higher M_{nT}.[8,12,20] The experimental M_n values are well above the target chain length (Figure 3.3b), with the difference becoming greater as the Cu level is decreased from 285 ppm to 36 ppm. The estimated decrease in initiator efficiency (Figure 3.3d) matches the trends seen in the conversion profiles, suggesting that the decrease in effective chain concentration causes the decrease in the reaction rate. The polymer MMDs (Figure 3.4) have an observable high MW shoulder as well as a significant short chain

population at the reduced copper level of 36 ppm (Figure 3.4b), indicating the gradual loss of control and difficulty with uniform initiation, respectively. Estimates of catalyst equilibrium at various initial copper loadings will be discussed in a later section.

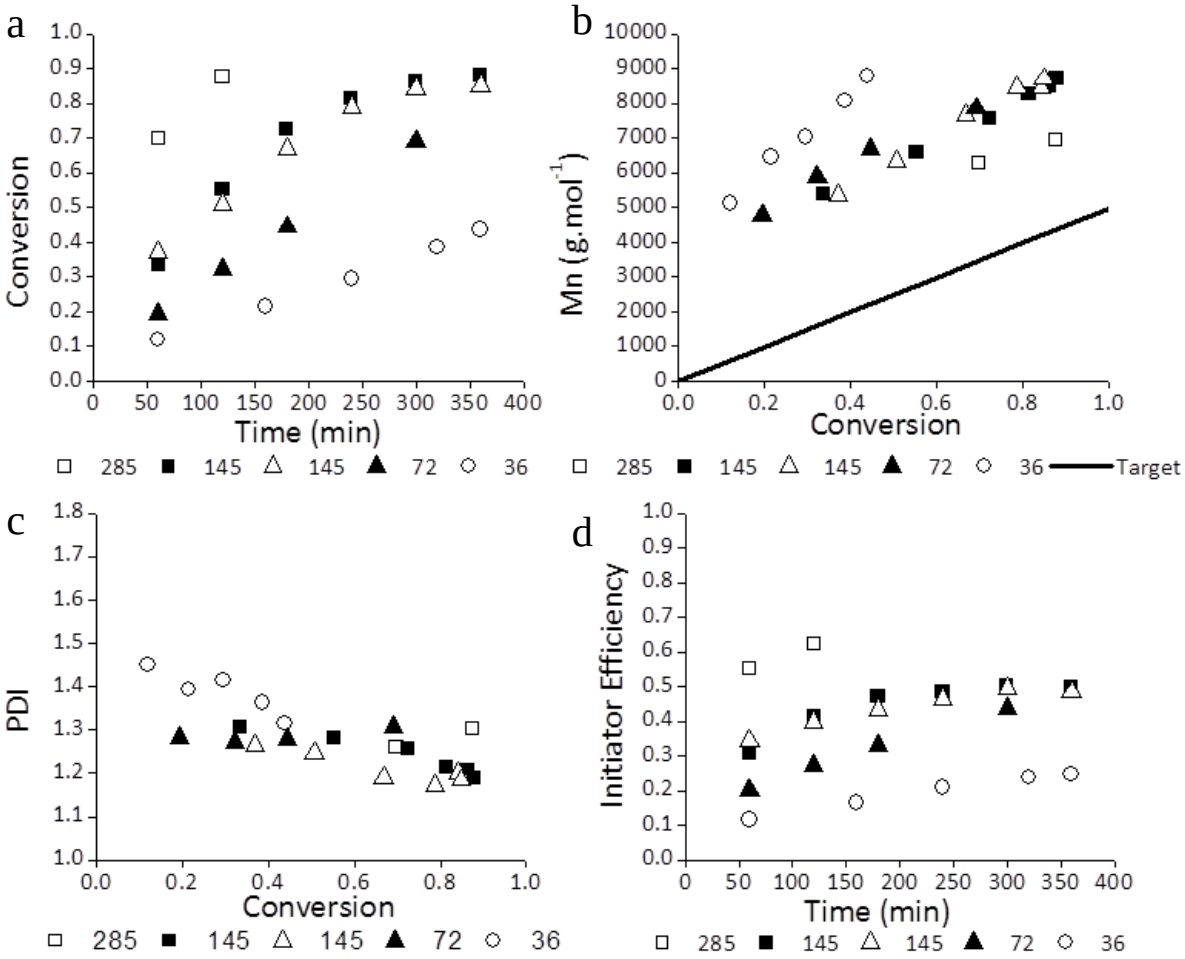

Figure 3.3: Batch ARGET ATRP of BMA with decreasing catalyst loading for target M_n = 5,000 g mol^{-1} at 70 °C (see Table 3.2): (a) monomer conversion versus time; (b) number-average molecular weight (M_n) and (c) polydispersity index (PDI or $Đ$) as a function of conversion; (d) initiator efficiency versus time. The Cu level (ppm) in the legend is presented on a molar basis with respect to monomer.

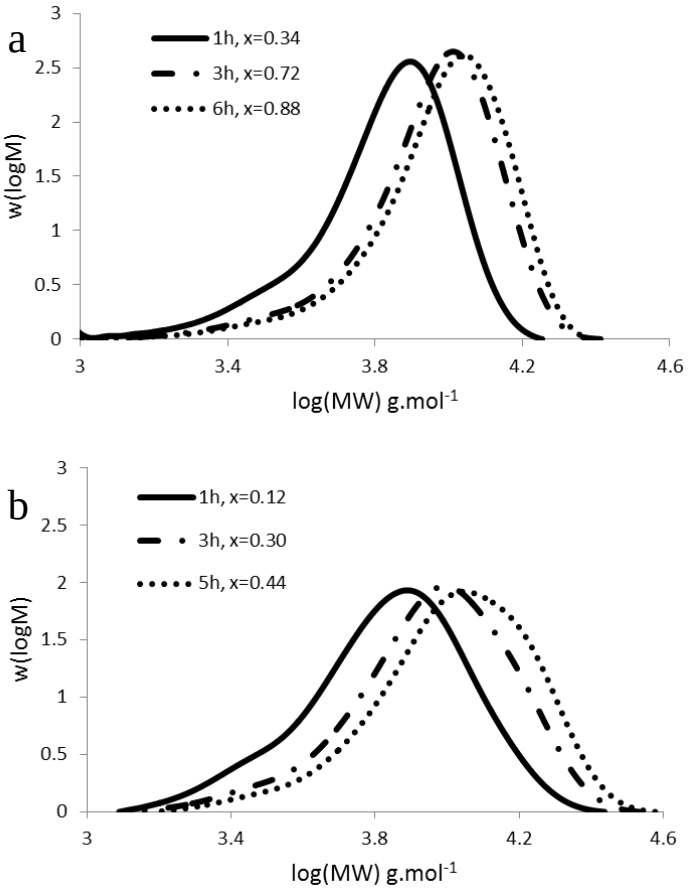

Figure 3.4: MMDs of pBMA produced by batch ARGET ATRP at 70 °C, sampled hourly to confirm living nature of polymerization. Copper concentration of (a) 145 ppm and (b) 36 ppm on a molar basis with respect to monomer.

3.3.3 Effect of Varying Catalyst and Reducing Agent Loading

The first set of BMA experiments indicated that a reasonable polymerization rate and MW control could be maintained while lowering the target MW of the polymer to 5,000 g mol^{-1}. However, the copper levels were increased proportionally with [R-X], such that the experiment had a Cu level of 285 ppm relative to monomer. As the Cu level was reduced from 285 to 36 ppm at a constant [Cu]:[Sn] ratio of 1:10 (Table 3.2), there was a significant decrease in polymerization rate and initiator efficiency. Thus, the next investigation was to determine the effect of increasing the

reducing agent ($Sn(EH)_2$) loading while keeping a constant ratio of [M]:[R-X]:[Cu]. The experiments are summarized in Table 3.3 with the results presented in Figure 3.5. The initiator efficiency was also plotted with respect to conversion, as shown in Figure 3.6.

Table 3.3: Batch ARGET ATRP of BMA at 70 °C with varying reducing agent levels and 30 wt% anisole with a constant molar ratio of [M]:[R-X]:[Cu] = 35:1:0.00125. M_{nT} is constant at 5,000 g mol^{-1}.

Initial Ratio [Cu]:[Sn]	Cu (ppm)	Time (min)	Conversion	$M_{n,exp}$ (g mol^{-1})	Initiator Efficiency
1:10	36	360	0.44	8778	0.25
1:20	36	360	0.45	8915	0.26
1:40	34	300	0.45	8473	0.26
1:100	37	360	0.94	11237	0.42

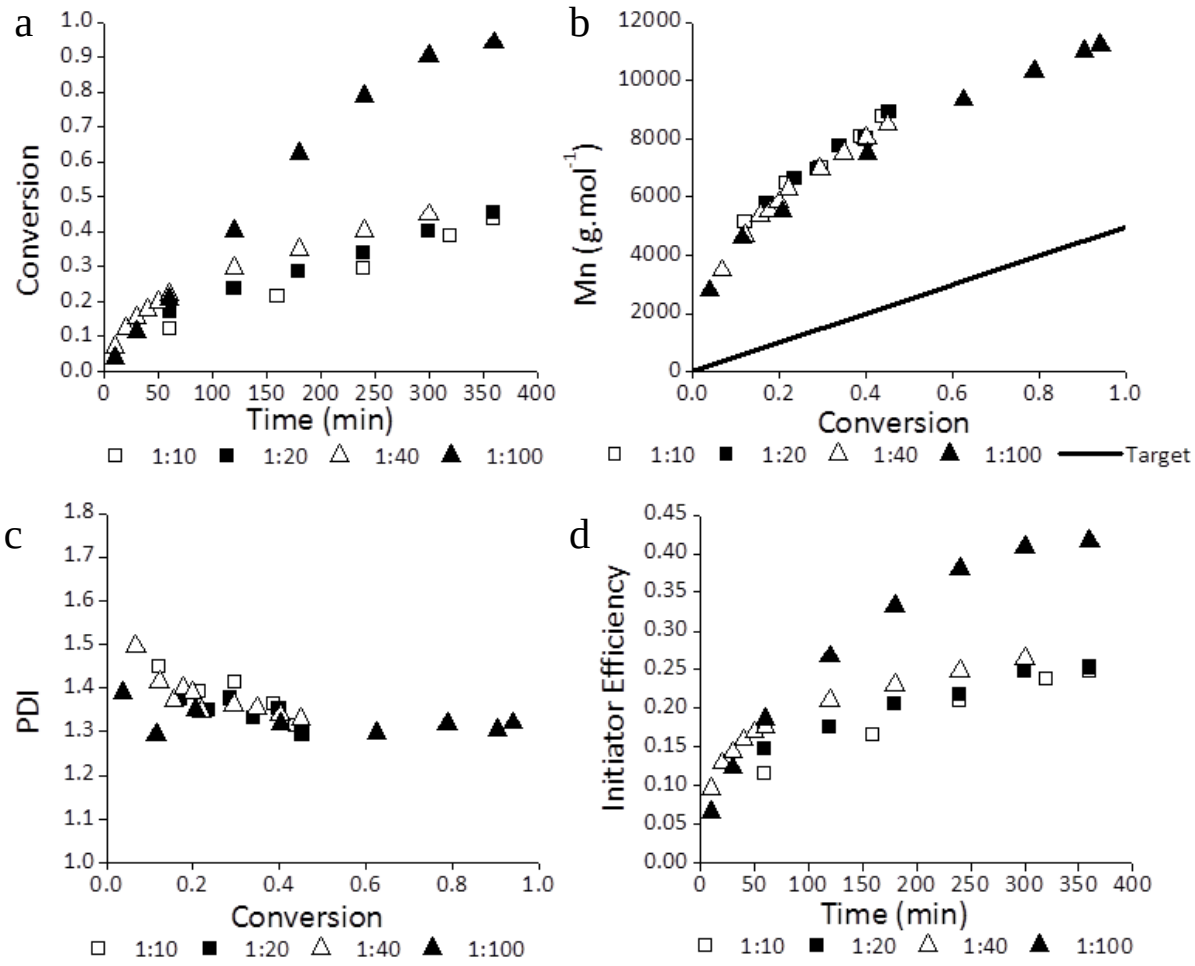

Figure 3.5: Batch ARGET ATRP of BMA with 36 ppm Cu and varying reducing agent level at 70 °C: (a) monomer conversion versus time, (b) number-average molecular weight (M_n) and (c) polydispersity index (PDI or $Đ$) as a function of conversion; (d) initiator efficiency versus time. Molar [Cu]:[Sn] ratios are presented in the legend, with [M]:[R-X]:[Cu] = 35:1:0.00125.

The results shown earlier (Figure 3.3) demonstrated that reducing the Cu level from 145 to 36 ppm while maintaining a [Cu]:[Sn] ratio of 1:10 led to a marked reduction in polymerization rate and initiator efficiency, with almost 88% conversion seen at the higher Cu level and approximately 44% conversion at the lower Cu level. Increasing the reducing agent loading at 36

ppm Cu has minimal impact on the reaction rate until a Cu:Sn ratio of 1:100 is reached, at which point a large increase in polymerization rate, especially after 2 h, was observed (Figure 3.5a). This increase was also found in previous studies for systems where the chain to Cu ratio is lower.[20-22] A methyl acrylate conversion of 93% was achieved in 3.3 h versus 87% in 5 h when the reducing agent (ascorbic acid) to catalyst ratio was lowered from 100:1 to 10:1 for a system with 100 chains per Cu complex.[20] Using $Sn(EH)_2$ at 90 °C with 200 chains per Cu complex, 97% versus 87% conversion of BMA was achieved in 6 h when the [Sn]:[Cu] ratio was changed from 40:1 to 10:1.[21] The effect of reducing agent on BMA conversion profiles is much larger for our system with 800 chains per Cu complex. According to Equation 3-1, the decreased polymerization rates found at decreased Cu levels may result from a lower $[Cu^I]/[Cu^{II}]$ ratio in the system, an effect partially remedied with a large excess of reducing agent. Note that the M_n profiles (Figure 3.5b) are similar for all experiments in this set; however apparent initiator efficiency (number of chains) continues to rise for $x>0.5$ with [Sn]:[Cu] at the 100:1 ratio (Figure 3.5d and Figure 3.6). The combination of low Cu levels and a high number of chains per Cu complex requires that higher levels of reducing agent be used. Thus, the same rates and M_n values (initiator efficiencies) are achieved with 36 ppm Cu and 3560 ppm Sn as with 145 ppm Cu and 1450 ppm Sn.

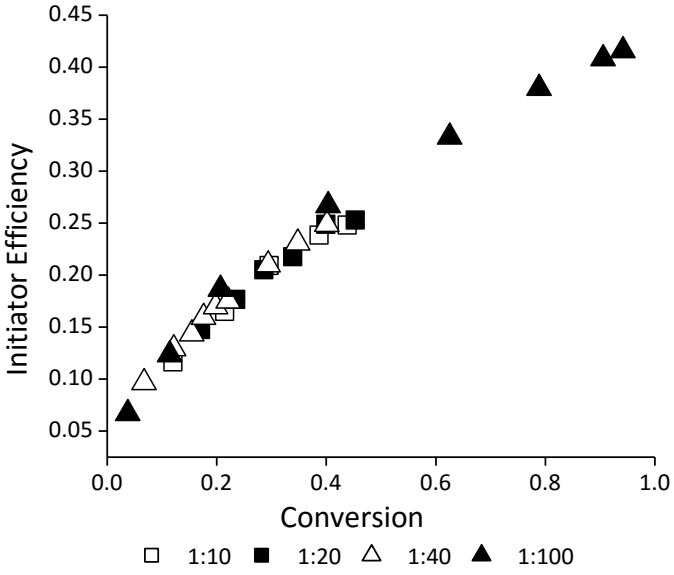

Figure 3.6: Initiator efficiency versus conversion for batch ARGET ATRP of BMA with 36 ppm Cu and varying reducing agent level at 70 °C. Molar ratios in the legend are presented as [Cu]:[Sn] with [M]:[R-X]:[Cu] = 35:1:0.00125.

It is also interesting to examine the polymer MMDs produced with the highest level of reducing agent (Figure 3.7). Once again, a tail on the low MW side of the MMD is observed, consistent with the slow activation of initiator indicated by initiator efficiency. However, the polymer MMD is broader (*Đ* of 1.3) when compared to that obtained with 145 ppm Cu (Figure 3.4a, *Đ* of 1.2). Thus, the abundance of reducing agent, while effectively increasing the rate of monomer conversion, also results in a less controlled polymerization. The increased Cu level of 145 ppm allows for more chains to be activated and mediated with good control compared to the low Cu case (36 ppm) with an increased reducing agent concentration.

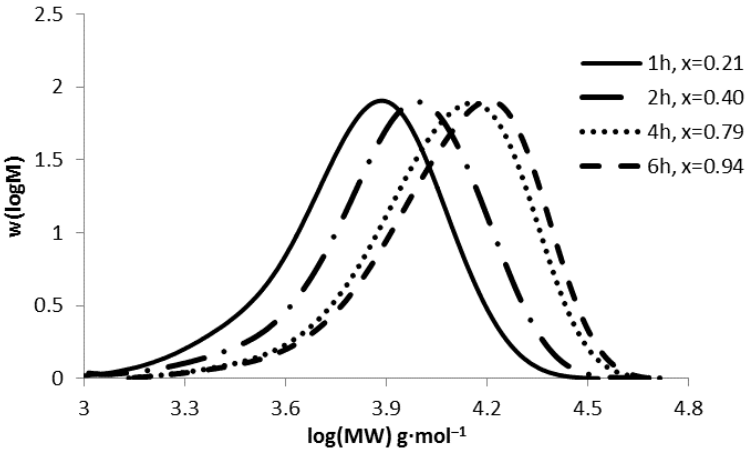

Figure 3.7: MMDs of pBMA produced by batch ARGET ATRP at 70 °C, sampled hourly to confirm living nature of polymerization. [M]:[R-X]:[Cu]:[Sn] = 35:1:0.00125:0.125.

To estimate the combined impact of varying reducing agent and catalyst loadings for the experiments with DP_{nT} = 35, the initial rates of polymerization were also compared. By rearranging the simplified rate equation, $R_p = k_p[M][R\cdot]$, the radical concentration was determined by dividing the slope of the kinetic plot by the propagation rate constant. The catalyst ratio was then determined using Equation 3-6.

$$f_{init}\frac{[Cu^I]}{[Cu^{II}]} = \frac{[R\cdot]}{K_{ATRP}[R-X]_o} \qquad \textbf{Equation 3-6}$$

This method assumes a constant radical concentration, an assumption that is verified by linearity in the kinetic plot of ln[1/(1-*x*)] vs time. As seen in Figure 3.8, there is some deviation from linearity observed at longer times.

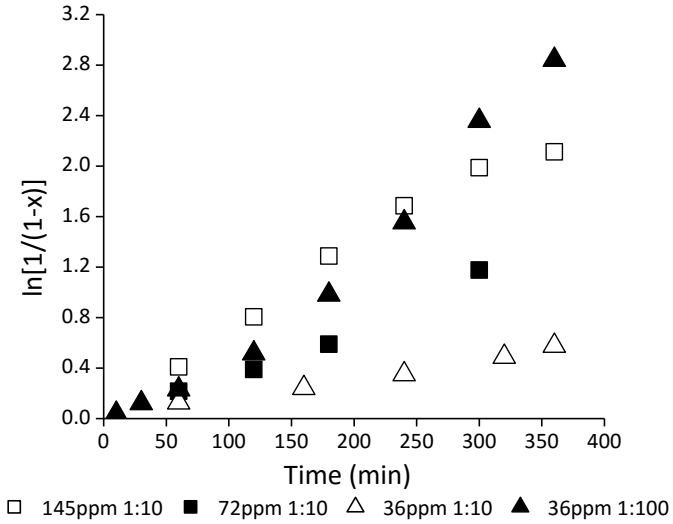

Figure 3.8: Kinetic plot of batch ARGET ATRP of BMA at 70 °C with varying Cu and reducing agent levels. Cu concentration presented on a molar basis with respect to monomer. Molar ratios in the legend are presented as [Cu]:[Sn] with [M]:[R-X] = 35:1.

For the reaction with 36 ppm Cu and a Cu:Sn ratio of 1:100, the upward curvature is consistent with an increasing number of chains in the system, while the reaction with 145 ppm Cu has a slight downward curvature, which is consistent with a buildup of Cu^{II} in the system. Nonetheless, the expected linear relationship is observed up to 3 h, allowing the use of Equation 3-6 to estimate the product of $[Cu^{I}]/[Cu^{II}]$ and initiator efficiency from the initial concentration of initiator and an estimate of $K_{ATRP} = 2.88 \times 10^{-5}$ extrapolated from the literature.[23-25] Results are shown in Figure 3.9. The two highest reducing agent concentrations (1424 and 3654 ppm) at the lowest copper loading of 36 ppm have an increased value of ($f_{init}[Cu^{I}]/[Cu^{II}]$) compared to the lower Sn loadings. However, the highest level of reducing agent is required to match the increased reaction rate found at the higher copper loading of 145 ppm. This result suggests that there is not enough reducing agent present to continuously reduce Cu^{II} to Cu^{I} if the low Cu level (36 ppm) must regulate a large number of chains (800:1, assuming 100% initiator efficiency). There is a definite trade-off

between the amount of reducing agent and the amount of copper necessary to maintain good control and a reasonable polymerization rate.

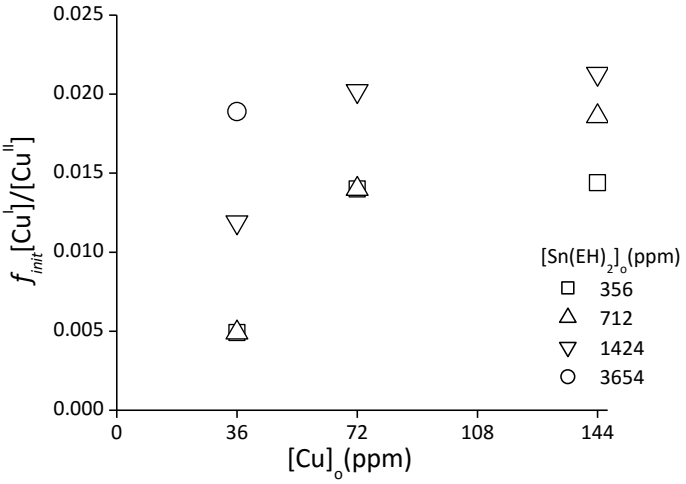

Figure 3.9: ARGET ATRP catalyst ratios at various initial copper and reducing agent loadings at 70 °C under batch conditions, as estimated from initial rates of polymerization. Concentrations are molar ratios with respect to monomer. [M]:[R-X] = 35:1 for all cases.

3.3.4 Comparison of BMA and BA

Butyl acrylate (BA) has a higher k_p value than BMA and therefore is expected to exhibit a higher polymerization rate. The comparison of BA to BMA was conducted at 90 °C, in order to achieve higher rates of monomer conversion than those found at 70 °C for BMA with low Cu levels; results are summarized in Table 3.4 and shown in Figure 3.10. The chain length was changed from DPn = 35 for BMA to DPn = 39 for BA in order to maintain a target MW of 5,000 g mol^{-1}. The experiments at the higher Cu level were conducted at a Cu:Sn ratio of 1:10, while those at the lower Cu level were run at the ratio of 1:40.

Table 3.4: Batch ARGET ATRP of BMA and BA with varying catalyst levels and 30 wt% anisole at 90 °C. M_{nT} was constant at 5,000 g mol^{-1}.

Initial Ratio [M]:[R-X]:[Cu]:[Sn]	Monomer	Cu (ppm)	Conversion at 360 min	$M_{n,exp}$ (g mol^{-1})	Initiator Efficiency
35:1:0.005:0.05	BMA	145	0.72	6452	0.55
39:1:0.005:0.05	BA	130	0.88	5561	0.79
35:1:0.00125:0.05	BMA	35	0.80	10331	0.39
39:1:0.00125:0.05	BA	34	0.86	5491	0.78

As expected, there is an increase in the polymerization rate from BMA to BA (Figure 3.10a), although the profiles level off at close to the same conversion for the two systems. The increased polymerization rate is markedly greater at 35 ppm Cu than at 145 ppm Cu. There is also a significant increase in the initiator efficiency for BA compared to BMA (Figure 3.10d). A constant initiator efficiency of 0.7-0.8 for BA is found at both Cu levels, compared to the slow increase over time observed for BMA; the efficiency for BMA also exhibits a significant increase as Cu is increased from 35 to 145 ppm. Due to the higher initiator efficiency, the $M_{n,exp}$ values for poly(BA) are much closer to the target value of 5,000 g mol^{-1} (Figure 3.10b). The polymer MMD for BA at 130 ppm Cu (Figure 3.11) does not have the low MW tail seen with BMA in Figure 3.4; however, a pronounced low MW tail is seen for the 34 ppm Cu BA experiment, a finding also reflected in the slightly higher value of $Đ$ (Figure 3.10c).

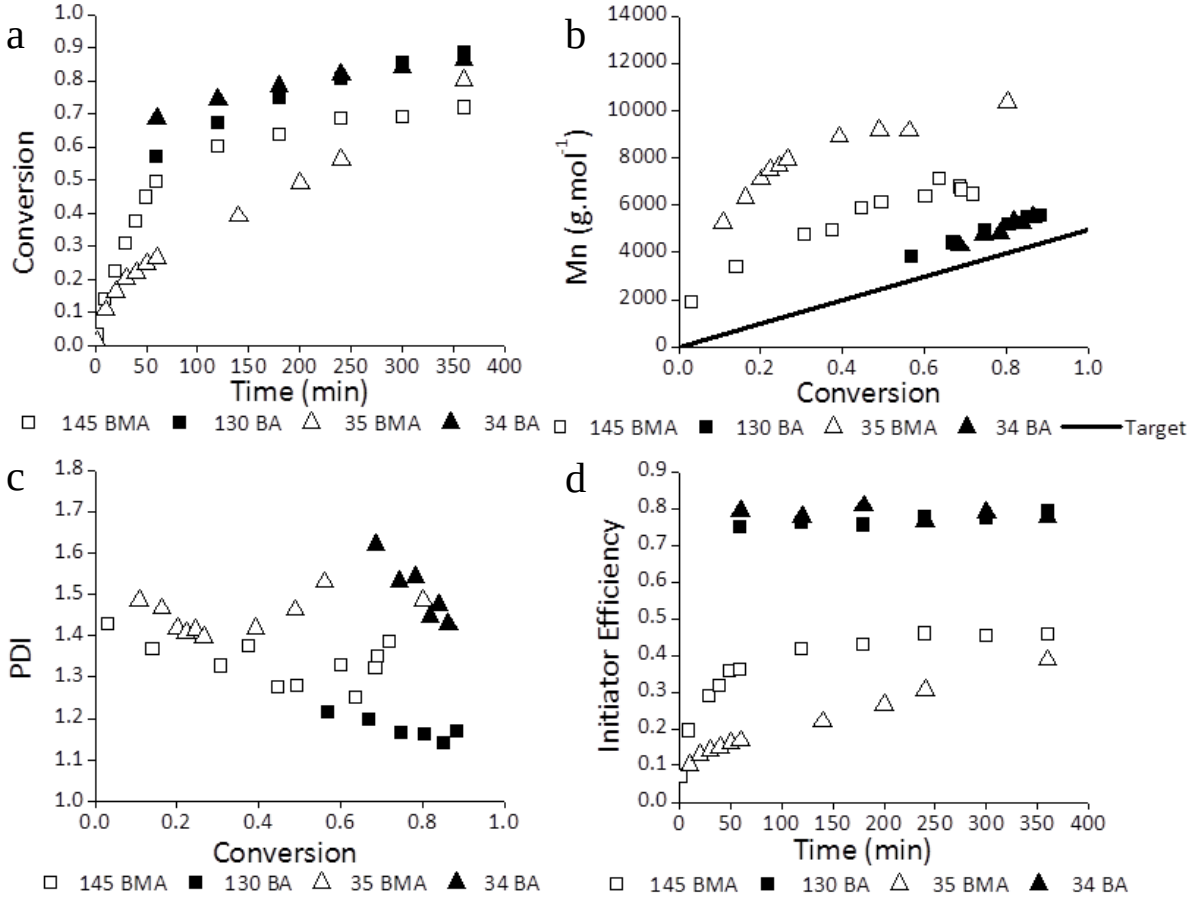

Figure 3.10: Batch ARGET ATRP of BMA and BA at 90 °C: (a) monomer conversion versus time, (b) number-average molecular weight (M_n) and (c) polydispersity index (PDI or *Đ*) as a function of conversion; (d) initiator efficiency versus time. Legend shows ppm Cu levels for experiments with BMA (open symbols) and BA (closed symbols); see Table 3.4 for further experimental details.

This comparison indicates that EBiB is activated earlier in the BA system, as opposed to throughout the reaction for the BMA system. The increased efficiency with BA has been reported in the literature,[10] although another comparison of methyl acrylate and methyl methacrylate suggests that acrylate binds more strongly to Cu^I than methacrylate and hinders the rate of polymerization.[26,27] To minimize side reactions with the catalyst complex, excess ligand has been

recommended.[7,10] Increasing the ratio of [TPMA]:[Cu^{II}] from 1:1 to 6:1 had a negligible effect on the conversion and initiator efficiency profiles for our system (results not shown), indicating monomer coordination is not a major contributor to the difference in rate.

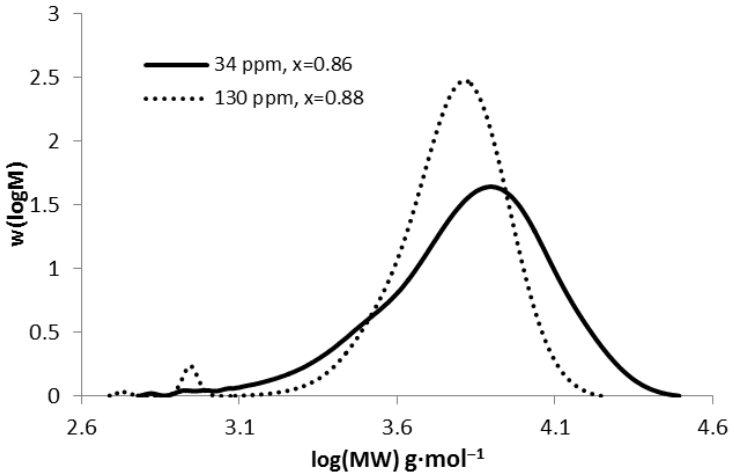

Figure 3.11: MMDs of pBA (final samples) produced by batch ARGET ATRP at 90 °C. Cu concentration specified on a molar basis with monomer. [M]:[R-X]:[Sn] = 39:1:0.05.

As shown in Figure 3.12a and summarized in Table 3.5, varying the amount of reducing agent added to the BA system with 36 ppm Cu has a lesser effect on polymerization rate and initiator efficiency compared to BMA polymerizations. The largest effect is observable at the initial stages of the polymerization. Rates level off quickly, as do the estimated efficiency values at 0.7-0.8, independent of the amount of added Sn (Figure 3.12d). The increased polymerization rate observed at short times with higher Sn levels is most likely caused by a shift in the [Cu^{I}]:[Cu^{II}] ratio, as well as the faster activation of initiator. The data indicate an upper limit to the achievable initiator efficiency that is unaltered by copper or reducing agent levels. In all cases the initial $Đ$ is high (>1.6) and decreases to 1.4 as the reaction proceeds to near full conversion (Figure 3.12c). The slower initiation observed with the 1:10 Cu:Sn ratio leads to an appreciable low MW tail; even with Cu:Sn at 1:40, a low MW tail is observed in the MMD of poly(BA) produced at a Cu level of

34 ppm (Figure 3.11). While increasing the concentration of reducing agent still has a clear effect on BA polymerization rate for these low Cu experiments, the impact is smaller than observed for BMA polymerization, in agreement with a previous comparison in literature conducted with a higher M_{nT}.[12]

Table 3.5: Batch ARGET ATRP of BA with varying reducing agent levels at 90 °C with 30 wt% anisole. Molar ratio of [M]:[R-X]:[Cu] = 39:1:0.00125 is constant in all cases.

Initial Ratio [Cu]:[Sn]	Cu (ppm)	Time (min)	Conversion	$M_{n,exp}$ (g mol^{-1})	Initiator Efficiency
1:10	31	240	0.68	4721	0.72
1:20	34	240	0.70	4646	0.75
1:40	34	360	0.86	5491	0.78
1:100	39	360	0.99	6572	0.75

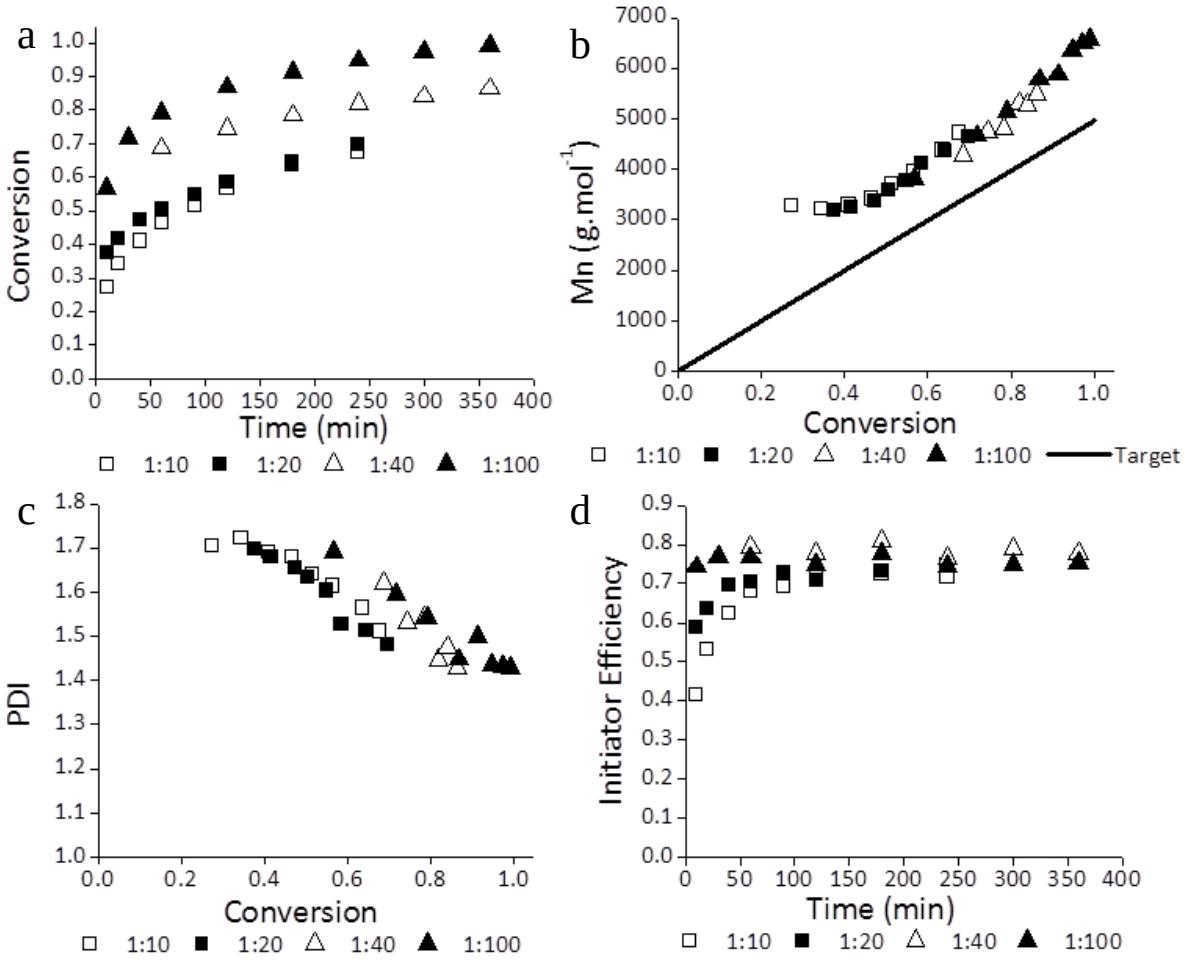

Figure 3.12: Batch ARGET ATRP of BA with varying reducing agent levels at 90 °C and 36 ppm Cu: (a) monomer conversion versus time, (b) number-average molecular weight (M_n) and (c) polydispersity index (PDI or $Đ$) as a function of conversion; (d) initiator efficiency versus time. Molar ratios in the legend presented as [Cu]:[Sn] with [M]:[R-X]:[Cu] = 39:1:0.00125.

3.4 Conclusions

A systematic study investigating the impact of reaction conditions on the rate of monomer conversion and polymer MW has been conducted for ARGET ATRP with low Cu concentrations. Decreasing the DP_{nT} value by increasing initiator concentration while keeping the Cu to initiator

level constant led to an expected increase in rate. However, initiator efficiency was observed to increase slowly throughout the reaction, indicating chain formation was not instantaneous. The Cu level was then decreased to 36 ppm relative to monomer for M_{nT} = 5,000 g mol^{-1} such that there were 800 chains to be mediated by each Cu complex assuming 100% initiator efficiency. Under these conditions, the decrease in Cu concentration caused a significant decrease in polymerization rate and estimated initiator efficiency. At this low Cu level, the amount of reducing agent had to be subsequently increased, with only a large excess having an impact on polymerization rate and initiator efficiency. A definite trade-off between catalyst level and reducing agent level is evident, with 1:100 [Cu]:[Sn] resulting in high conversion in 6 h at 36 ppm Cu, comparable to a polymerization conducted with 145 ppm Cu and 1:10 [Cu]:[Sn].

The initiator efficiency for BA increased rapidly to an essentially constant level of 0.7-0.8, a value consistently higher than the steadily increasing efficiency observed for BMA polymerization with 36 ppm Cu. Increasing the concentration of reducing agent in the BA system had a smaller impact on polymerization rate and initiator efficiency than found for BMA. However, the poly(BA) produced had higher $Đ$ values than found for BMA with $Đ$ lowering with conversion to a final value of 1.3-1.4.

Recently, the first model of ARGET ATRP examining the effect of reducing agent on polymerization rate has been published.[13] The data presented here summarize a systematic study of the combined effects of Cu and Sn concentrations, information that will be essential to improve understanding and aid further model development. Studies are also underway to explore the effect of temperature and monomer composition (copolymerization) on initiator efficiency and rate under low Cu conditions.

3.5 References

(1) Wang, J.-S.; Matyjaszewski, K. *J. Am. Chem. Soc*. **1995**, *117*, 5614-5615.

(2) Matyjaszewski, K.; Xia, J. *Chem. Rev*. **2001**, *101*, 2921-2990.

(3) Wang, J.-S.; Matyjaszewski, K. *Macromolecules* **1995**, *28*, 7901-7910.

(4) Grimaud, T.; Matyjaszewski, K. *Macromolecules* **1997**, *30*, 2216-2218.

(5) Percec, V.; Barboiu, B. *Macromolecules* **1995**, *28*, 7970-7972.

(6) Wang, J.-L.; Grimaud, T.; Matyjaszewski, K. *Macromolecules* **1997**, *30*, 6507-6512.

(7) Jakubowski, W.; Min, K.; Matyjaszewski, K. *Macromolecules* **2006**, *39*, 39-45.

(8) Matyjaszewski, K.; Jakubowski, W.; Min, K.; Tang, W.; Huang, J.; Braunecker, W. A.; Tsarevsky, N. V. *Proc. Natl. Acad. Sci. U.S.A.* **2006**, *103*, 15309-15314.

(9) Zhong, M.; Matyjaszewski, K. *Macromolecules* **2011**, *44*, 2668-2677.

(10) Jakubowski, W.; Matyjaszewski, K. *Angew. Chem*. **2006**, *118*, 4594-4598.

(11) Mueller, L.; Matyjaszewski, K. *Macromol. React. Eng*. **2010**, *4*, 180-185.

(12) Chan, N.; Cunningham, M. F.; Hutchinson, R. A. *Macromol. Chem. Phys*. **2008**, *209*, 1797-1805.

(13) Li, X.; Wang, W.-J.; Li, B.-G.; Zhu, S. *Macromol. React. Eng*. **2011**, *5*, 467-478.

(14) Matyjaszewski, K. *Macromolecules* **1998**, *31*, 4710-4717.

(15) Chan, N.; Cunningham, M. F.; Hutchinson, R. A. *Macromol. React. Eng*. **2010**, *4*, 369-380.

(16) Destarac, M. *Macromol. React. Eng*. **2010**, *4*, 165-179.

(17) Britovsek, G. J. P.; England, J.; White, A. J. P. *Inorg. Chem*. **2005**, *44*, 8125-8134.

(18) Hutchinson, R. A.; Beuermann, S.; Paquet, D. A.; McMinn, J. H. *Macromolecules* **1997**, *30*, 3490-3493.

(19) Penzel, E.; Goetz, N. *Die Angew. Makromol. Chem*. **1990**, *178*, 191-200.

(20) Min, K.; Gao, H.; Matyjaszewski, K. *Macromolecules* **2007**, *40*, 1789-1791.

(21) Chan, N.; Boutti, S.; Cunningham, M. F.; Hutchinson, R. A. *Macromol. React. Eng*. **2009**, *3*, 222-231.

(22) Matyjaszewski, K.; Dong, H.; Jakubowski, W.; Pietrasik, J.; Kusumo, A. *Langmuir* **2007**, *23*, 4528-4531.

(23) Seeliger, F.; Matyjaszewski, K. *Macromolecules* **2009**, *42*, 6050-6055.

(24) Tang, W.; Tsarevsky, N. V.; Matyjaszewski, K. *J. Am. Chem. Soc*. **2006**, *128*, 1598-1604.

(25) Tang, W.; Matyjaszewski, K. *Macromolecules* **2007**, *40*, 1858-1863.

(26) Braunecker, W. A.; Tsarevsky, N. V.; Pintauer, T.; Gil, R. R.; Matyjaszewski, K. *Macromolecules* **2005**, *38*, 4081-4088.

(27) Braunecker, W. A.; Pintauer, T.; Tsarevsky, N. V.; Kickelbick, G. *J. Organomet. Chem*. **2005**, *690*, 916-924.

Chapter 4

ARGET ATRP of Butyl Methacrylate: Utilizing Kinetic Modeling to Understand Experimental Trends

Preface

To help understand the limitations of reducing copper levels, a kinetic model was developed in collaboration with Prof. Dr. Ir. Dagmar D'hooge and Dr. Ir. Paul Van Steenberge during my 4 month visit to the Laboratory for Chemical Technology at Ghent University. A kinetic model can be very useful in predicting the concentrations of species that are difficult to measure *in situ*, for example, the variation in Cu^{I} and Cu^{II} species throughout the polymerization. The model was developed with the kinetic Monte Carlo method from Ghent University, and a comparison was made with the commercially available Predici® software. The model demonstrates the need to incorporate slow activation of the initiator species in order to effectively model the experimental results. The model also shows the necessity for a second reduction step, as has been suggested in the first findings of ARGET and AGET ATRP. The model provides an understanding as to why the polymerization is limited at the copper level used experimentally, as the copper equilibrium is less favourable for such a large number of chains per copper mediating species. The coupling of the slow initiation with the low copper levels leads to the experimentally-observed low initiation efficiency, which limits the ability to achieve desired target chain-lengths. The work in this section has been published as a full paper in Macromolecules (2013, vol. 46, 3828-3840). Supporting Information can be found in Appendix A.

Abstract

A comprehensive kinetic Monte Carlo (kMC) model is used to interpret and better understand the results of a systematic experimental investigation of activators regenerated by electron transfer atom transfer radical polymerization (ARGET ATRP) of butyl methacrylate (BMA) using $Sn(EH)_2$ as reducing agent, ethyl 2-bromoisobutyrate (EBiB) as ATRP initiator, and $CuBr_2$/TPMA (TPMA: tris[(2-pyridyl)methyl]amine) as deactivator. The model demonstrates the importance of slow initiation, with distinct activation and deactivation rate coefficients for the initiator and polymeric species required to match the experimental data. In addition, the model incorporates a second reduction step for the reducing agent and accounts for diffusional limitations on chain-length-dependent termination. The effect of temperature on the slow ATRP initiation is limited, and a sufficiently high initial reducing agent concentration is crucial to obtain a high conversion, although achieved at the expense of decreased end group functionality.

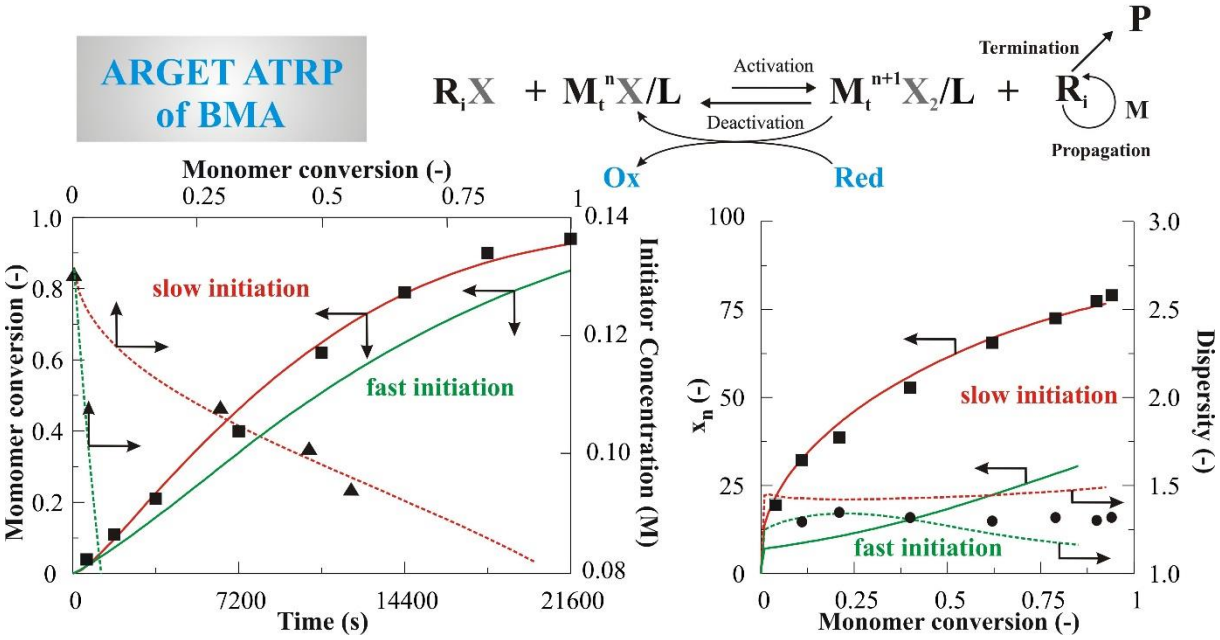

4.1 Introduction

Atom transfer radical polymerization (ATRP) is a type of controlled/living radical polymerization (C/LRP) which allows the polymerization of various monomers to create polymers of controlled composition and architecture with low dispersities (*Đ*) and high livingness. As shown in Scheme 4.1a, these features are achieved by the addition of a transition metal complex (most commonly Cu based) to the reaction medium, which allows for fast deactivation of growing radicals (k_{da}) relative to their formation through activation (k_a), i.e., in a controlled ATRP process the radical concentration is low, and termination events are well-suppressed.

Ideally, only a few monomer units add to the polymeric radical R_i (*i*: chain length) before deactivation returns the chain to a dormant or "capped" state R_iX, and thus a high end group functionality (EGF; X) is preserved. Moreover, at complete monomer consumption ideally every polymer chain has a length equal to the initial molar ratio of monomer to ATRP initiator ($[M]_o$:$[R_oX]_o$), which is also known as the targeted chain length (TCL).[1–6] Note that the transition metal complex in Scheme 4.1a can be considered as a polymerization catalyst, which changes oxidation states when activation/deactivation takes place. The lower and higher oxidation state forms are respectively referred to as the activator (Cu^IX/L) and deactivator ($Cu^{II}X_2$/L).

In early studies, one Cu^I molecule per ATRP initiator molecule (R_oX) was used to achieve sufficiently high polymerization rates, specifically to mitigate the tendency of the decreasing polymerization rate with time as the Cu^{II} species accumulate due to inevitable termination reactions, a phenomenon referred to as the persistent radical effect (PRE).[7] However, in practice high Cu levels (> ~5000 parts per million (ppm) with respect to monomer on a molar basis) should be avoided since they pose a health and economic barrier to the industrial adoption of ATRP, in addition to the unwanted discoloration of the final polymer product.[8] Therefore, recent research has shifted to the development of modified ATRP techniques in which a low catalyst amount is utilized

(<300 ppm), and no Cu^{I} species are initially present to allow for simple handling of the starting materials.[9–19]

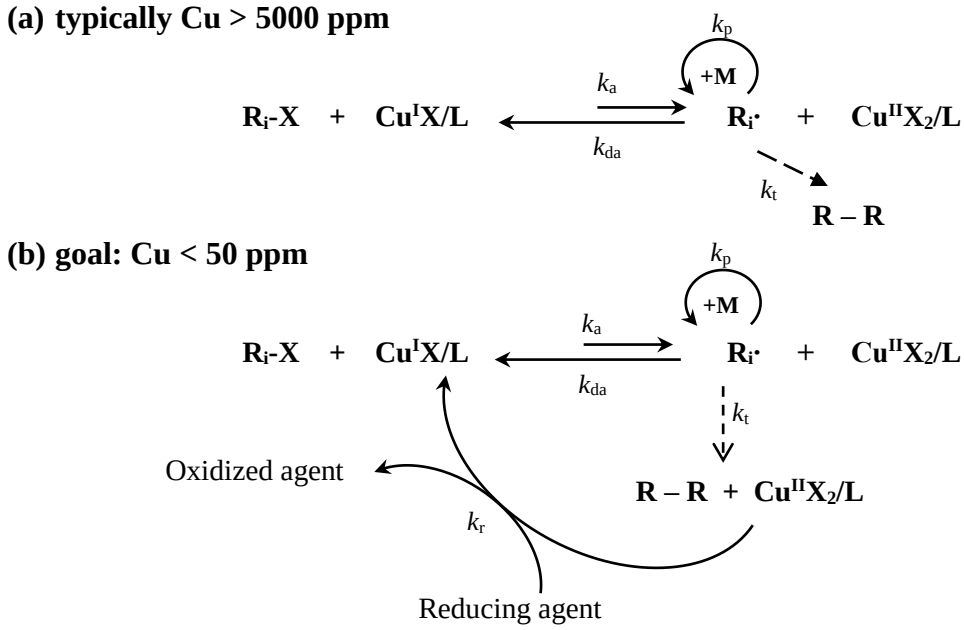

Scheme 4.1: Principle of (a) normal ATRP and (b) ARGET ATRP[a]

[a]In normal ATRP initially only ATRP initiator (R_oX), monomer (M) and activator ($Cu^{I}X/L$) are present (where L = ligand), whereas in ARGET ATRP there is initially only ATRP initiator, monomer and deactivator ($Cu^{II}X_2/L$) with an excess of reducing agent to (re)generate the activator; $k_{a,da,p,t,r}$: rate coefficient for activation, deactivation, propagation, termination, and reduction, respectively.[9,20]

One of the most promising modified ATRP techniques is activators regenerated by electron transfer (ARGET) ATRP, by which the Cu level can be reduced well below 300 ppm.[9,10,18,21–24] The principle of this technique is given in Scheme 4.1b. Here activator is continuously (re)generated via added reducing agent species and thus the normal ATRP process is maintained. It should however be stressed that only at sufficiently low Cu levels (~50 ppm[24]) and for polymerization rates comparable to those of current industrial radical polymerization processes the ARGET ATRP

system may be attractive to industry, necessitating the optimization with respect to polymerization conditions and starting compounds.

Originally, Jakubowski *et al.*[21,22] showed that the Cu level in ARGET ATRP can be reduced to very low ppm levels while using the oxidatively stable deactivator species as a starting compound. They demonstrated the ability to successfully control the polymerization of styrene, butyl acrylate and methyl methacrylate below 50 ppm Cu with the use of a Food and Drug Administration (FDA) approved reducing agent tin (II) 2-ethylhexanoate ($Sn(EH)_2$) and ATRP catalysts $CuCl_2$ or $CuBr_2$ ligated with tris[(2-pyridyl)methyl]amine (TPMA) or tris[2-(dimethylamino)ethyl]amine (Me_6TREN).[21,22,9] On the basis of the experimental data of the previous authors, Li *et al.*[23] highlighted the importance of the value of the equilibrium coefficient of the ATRP catalyst K_{ATRP} (k_a/k_{da}) and the reduction rate coefficient (k_r) for a controlled ARGET ATRP up to complete conversion. They showed that a significant increase in the equilibrium coefficient results in higher simulated *Đ*s and a significantly increased number-average chain length (x_n) and lower EGF, with minimal impact on the conversion profile. The significant increase in reducing rate coefficient, on the other hand, was shown to lead to a significant increase in the polymerization rate and a pronounced decrease in EGF, with negligible impact on x_n and *Đ*.[23]

Very recently, Payne *et al.*[18] conducted a systematic isothermal (70 °C) experimental study for the ARGET ATRP of butyl methacrylate (BMA) in anisole using $Sn(EH)_2$ as reducing agent, ethyl 2-bromoisobutyrate (EBiB) as ATRP initiator, and $CuBr_2$/TPMA as deactivator. In this study, the effect of various reaction conditions, such as TCL (35-400) and Cu level (35-285 ppm), was investigated to determine the potential limitations while reducing the Cu level towards an industrially attractive process. The experimental data indicated in particular that for a TCL of 35 at low Cu levels of ~35 ppm, the polymerization rate and ATRP initiator efficiency are both significantly reduced, in agreement with literature reports on related systems.[9,25–27] Under such conditions (TCL=35), the actual number of polymeric species being mediated per Cu complex is

much lower than the value of 800 expected for 100% ATRP initiator efficiency. On the other hand, a large increase in the initial $Sn(EH)_2$ concentration was shown to be able to significantly increase both the conversion and ATRP initiator efficiency, in agreement with the simulation results of Li *et al.*.[23]

It can be expected that this low ATRP initiator efficiency for BMA can be attributed to slow ATRP initiation. For example, Nanda and Matyjaszewski[28] reported that the intrinsic activation rate coefficient for H-MMA-Br (MMA: methyl methacrylate) is ca. 10 times smaller than for H-MMA-MMA-Br using CuBr/bpy (bpy: bipyridine) as ATRP catalyst, clearly indicating that a very pronounced difference in reactivity for activation can be expected between ATRP initiator and dormant polymeric species in methacrylate ATRP due to a steric strain effect. In addition, this slow activation has been confirmed by ab initio calculations of the homolytic bond dissociation energy of the R-X bond in model compounds representative for initiator and dormant polymer molecules.[29–31]

In this work, kinetic modeling and additional experimental data are used to assess the importance of this slow ATRP initiation as a function of polymerization temperature, Cu level and TCL. The kinetic Monte Carlo (kMC) method[32–34] is selected for the description of the polymerization characteristics while accounting for the possible influence of diffusional limitations on termination. The simulation results are benchmarked with the commercially available Predici® software package.[35] The kMC approach is selected since it is more suited for a detailed kinetic study of related copolymerization systems, as envisaged in the near future.

It is shown that the number-average chain length profile can only be described by considering distinct ATRP initiator and macromonomer intrinsic activation and deactivation rate coefficients, thereby confirming the role of slow ATRP initiation in this system, while the conversion profile is best simulated including two consecutive reduction steps. Diffusional limitations on termination are shown to result mainly in rate acceleration and improved livingness.

4.2 Experimental

4.2.1 Materials

Butyl methacrylate (BMA; 99%, Aldrich), copper (II) bromide ($CuBr_2$; 99% Aldrich), anisole (99%, Aldrich), ethyl 2-bromoisobutyrate (EBiB; 98%, Aldrich), and tin (II) 2-ethylhexanoate ($Sn(EH)_2$; 95%, Aldrich), dichloromethane (DCM; 99,8%; anhydrous Aldrich), and N,N-dimethylformamide (DMF; 99,8%; anhydrous Aldrich) were used as received. The ligand tris[(2-pyridyl)methyl]amine (TPMA) was synthesized according to the literature.[36,37]

4.2.2 Batch ARGET ATRP of BMA

In this work, additional experimental data are reported with respect to the previous experimental study of Payne *et al.*[18] to study the ARGET ATRP of BMA initiated by EBiB with $CuBr_2$/TPMA as deactivator and $Sn(EH)_2$ as reducing agent under a broader range of polymerization conditions. All studied polymerization conditions are summarized in Table 4.1. During all experiments there were homogenous reaction solutions, an indication that solubility limits for the complexes do not need to be considered in the kinetic modeling study. For the Cu complexes, this can be directly understood based on the very low (ppm) amounts present.

Table 4.1: Experimental conditions for batch isothermal ARGET ATRP of BMA in anisole; targeted chain length TCL given as molar ratio of $[M]_o$:$[R_oX]_o$[a]

Experiment	Reactant	Amount (g)	Molar Ratio $[Reactant]_o/[R_oX]_o$
	BMA	35	35
1	EBiB	1.3717	1
(70 °C)	(Cu^{II}TPMABr)Br	0.0181	0.005
	$Sn(EH)_2$	0.1424	0.05
	BMA	35	35
2	EBiB	1.3717	1
(70 °C)	(Cu^{II}TPMABr)Br	0.0045	0.00125
	$Sn(EH)_2$	0.0356	0.0125
	BMA	35	35
3	EBiB	1.3717	1
(70 °C)	(Cu^{II}TPMABr)Br	0.0045	0.00125
	$Sn(EH)_2$	0.356	0.125
	BMA	35	50
4	EBiB	0.9602	1
(70 °C)	(Cu^{II}TPMABr)Br	0.0032	0.00125
	$Sn(EH)_2$	0.2493	0.125
	BMA	35	400
5	EBiB	0.1200	1
(70 °C)	(Cu^{II}TPMABr)Br	0.0032	0.01
	$Sn(EH)_2$	0.0249	0.1
	BMA	35	35
6	EBiB	1.3717	1
(90 °C)	(Cu^{II}TPMABr)Br	0.0045	0.00125
	$Sn(EH)_2$	0.0356	0.0125
	BMA	35	35
7	EBiB	1.3717	1
(90 °C)	(Cu^{II}TPMABr)Br	0.0045	0.00125
	$Sn(EH)_2$	0.356	0.125

[a]Anisole solvent content is 30 %w/w with respect to monomer in all cases; Experiment 1-3, and 5: taken from Payne *et al*.[18]

4.2.3 Analytical Methods

The analytical methods for the measurement of the conversion and control over chain length are the same as those used in the original study.[18] For the measurement of the chain length distribution (CLD) and in particular the dispersity (*Đ*) via size exclusion chromatography (SEC) a certain unavoidable experimental error (~5-10%) exists.

In this study, gas chromatography (GC) was further used for the experimental determination of the ATRP initiator conversion. A trace-GC ultra-Gas Chromatograph equipped with an AS3000 autosampler, flame ionization detector (FID) detector and a CP Wax 52 CB 30m capillary column was employed. The injector and detector temperature were 275 °C. Helium (flow rate: 30 mL/min) was used as carrier gas and a stepwise temperature program was set as follows: 50 °C for 3 min, followed by a heating ramp of 10 °C/min until a temperature of 110 °C was reached. DMF was used as internal standard and DCM as solvent to prepare the samples.

4.3 Kinetic Model

The kinetic Monte Carlo (kMC) technique is used to simulate the conversion profile and control over chain length and livingness as a function of conversion for the ARGET ATRP of BMA using EBiB as ATRP initiator, $CuBr_2$/TPMA as deactivator, and $Sn(EH)_2$ as reducing agent. For more computational details, the reader is referred to Van Steenberge *et al.*,[32] in which a detailed description of the technique is provided, and this technique is applied to the normal ATRP of acrylates, methacrylates, and styrene.

Table 4.2 presents the set of reactions that are included in the simulations. Besides the typical free radical polymerization reactions, such as propagation and termination, ATRP specific reactions such as activation and deactivation are considered. Chain transfer reactions to monomer and solvent are neglected based on results from previous kinetic modeling studies.[38] In particular, a first and second reduction step are included for the reducing agent species based on literature

data, where Jakubowski *et al.*[39] reported the highly favourable reduction of two deactivator molecules by one $Sn(EH)_2$ molecule. This reduction process is also shown in Scheme 4.2.

$$\mathbf{Sn^{II}(EH)_2 + Cu^{II}TPMABr_2} \xrightarrow{k_{r1}} \mathbf{Sn^{III}(EH)_2Br + Cu^{I}TPMABr}$$
$$\mathbf{Sn^{III}(EH)_2Br + Cu^{II}TPMABr_2} \xrightarrow[k_{r2}]{} \mathbf{Sn^{IV}(EH)_2Br_2 + Cu^{I}TPMABr}$$

Scheme 4.2: Two-step reduction process for reducing agent $Sn(EH)_2$, with one molecule of $Sn(EH)_2$ leading to the reduction of two deactivator molecules.

Table 4.2: Reactions and Arrhenius parameters for the simulation of ARGET ATRP of BMA using EBiB as ATRP initiator, $Cu^{II}X_2$/L as deactivator and $Sn^{II}L_2$ as reducing agent where X=Br, L = TPMA and L_2 = $(EH)_2$; Subscript "o" relates to ATRP initiator.

			A ($L\ mol^{-1}\ s^{-1}$)	E_a ($J\ mol^{-1}$)	Value at 70 °C	Ref.
ATRP activation/deactivation						
R_o-X + $Cu^{I}X$/L	$\xrightarrow{k_{a,o}}$	R_o• + $Cu^{II}X_2$/L	5.38×10^4	2.77×10^4	3.25	*a*
R_iX + $Cu^{I}X$/L	$\xrightarrow{k_{a}}$	R_i• + $Cu^{II}X_2$/L	3.99×10^6	2.77×10^4	2.40×10^2	40,41
R_o• + $Cu^{II}X_2$/L	$\xrightarrow{k_{da,o}}$	R_o-X + $Cu^{I}X$/L	3.94×10^8	7.98×10^3	2.40×10^7	*a*
R_i• + $Cu^{II}X_2$/L	$\xrightarrow{k_{da}}$	R_iX + $Cu^{I}X$/L	1.97×10^8	7.98×10^3	1.20×10^7	*a*
Propagation						
R_o• + M	$\xrightarrow{k_{p,o}}$	R_1•	3.80×10^6	2.29×10^4	1.23×10^3	42
R_i• + M	$\xrightarrow{k_{p}}$	R_{i+1}•	3.80×10^6	2.29×10^4	1.23×10^3	42
Reduction						
$Cu^{II}X_2$/L + $Sn^{II}L_2$	$\xrightarrow{k_{r1}}$	$Cu^{I}X$/L + $Sn^{III}L_2X$	5.55×10^1	1.49×10^4	0.30	*a*
$Cu^{II}X_2$/L + $Sn^{III}L_2X$	$\xrightarrow{k_{r2}}$	$Cu^{I}X$/L + $Sn^{IV}L_2X_2$	1.87×10^2	1.49×10^4	1.00	*a*
Irreversible Termination*b*						
R_o• + R_o•	$\xrightarrow{k_{t,11}^{app}}$	R_o-R_o				
R_i• + R_o•	$\xrightarrow{k_{t,i1}^{app}}$	P_i + P_0				
R_i• + R_j•	$\xrightarrow{k_{tc,ij}^{app}}$	P_{i+j}				
R_i• + R_j•	$\xrightarrow{k_{td,ij}^{app}}$	P_i + P_j				

*a*This work. *b*For termination: fraction of termination by disproportionation is 0.9; apparent termination rate coefficients are used based on RAFT-CLD-T measurements with MMA (composite k_t model; Equation 4-1 to Equation 4-8, where $\alpha_s = 0.65$, $\alpha_l = 0.15$, and $i_{SL} = 100$);[43–46] for termination between macroradicals with chain length of one and ATRP initiator radicals at zero conversion a value of 1.1×10^9 L mol^{-1} s^{-1} is used (also denoted $k_{t,11}^{app}$).[47]

For each reaction, the intrinsic temperature dependency is accounted for via an Arrhenius equation. For the non-ARGET specific reaction steps, literature data are directly used,[42,43,48]

whereas for the other reactions, these parameters are assessed based on experimental and literature data according to the following procedure. First, $k_{a,o}$ and k_a are calculated at 70 °C using the Arrhenius expression developed for EBiB and CuBr/PMDETA (PMDETA: N,N,N′,N″,N″-pentamethyldiethylenetriamine) and the relative activation rate coefficients for CuBr/TPMA and CuBr/PMDETA.[40,41] As a first guess at this temperature, $K_{ATRP(,o)}$ is set equal to 2×10^{-5} as reported by Buback and Morick[48] and the reduction rate coefficients are set to 0.3 L mol^{-1} s^{-1} as proposed by Li *et al.* as a first approximation.[23] Subsequently, the macromolecular activation and deactivation kinetic parameters are varied systematically and independently in order to match the experimental average chain length data and calculated ATRP initiator efficiency data at 70 °C. Once these data are well described, the reducing rate coefficients are altered to effectively simulate the experimental conversion profile, with the activation energies of both reduction steps assumed to be equal due to lack of data in the literature. The parameters are finally optimized in order to match the complete set of experimental conditions in Table 4.1. Using the Table 4.2 parameters, an equilibrium coefficient of 4.39 10^{-8} is calculated for EBiB at 22 °C, a value two orders of magnitude lower than that measured by Tang et al. in acetonitrile in the absence of monomer and thus polymerization.[49] Hence, the experiments and kMC simulations in this work indicate an important solvent effect, also reported by others.[50,51] A high deactivation rate coefficient, which leads to a low equilibrium coefficient, is necessary to explain the experimentally observed slow initiation under polymerization conditions.

In the kMC procedure, the termination behavior is described through a population-weighted apparent rate coefficient of which the terminating radicals are randomly selected taking into account their individual concentration and apparent termination reactivity. The individual (chain length dependent) apparent termination rate coefficients ($k_{t,ij}^{app}$; i, j: chain length) are calculated as a function of conversion (x) via a composite k_t model while considering a correction factor for the solvent:[52,53]

$$\text{for } i < i_{\text{gel}} \text{ and } i < i_{\text{SL}}: k_{\text{t,ii}}^{\text{app}} = k_{\text{t,11}}^{\text{app}} i^{-\alpha_{\text{s}}} \quad \textbf{Equation 4-1}$$

$$\text{for } i < i_{\text{gel}} \text{ and } i \geq i_{\text{SL}}: k_{\text{t,ii}}^{\text{app}} = k_{\text{t,11}}^{\text{app}} i_{\text{SL}}^{\alpha_{\text{l}}-\alpha_{\text{s}}} i^{-\alpha_{\text{l}}} \quad \textbf{Equation 4-2}$$

$$\text{for } i \geq i_{\text{gel}} \text{ and } i < i_{\text{SL}}: k_{\text{t,ii}}^{\text{app}} = k_{\text{t,11}}^{\text{app}} i_{\text{gel}}^{\alpha_{\text{gel}}-\alpha_{\text{s}}} i^{-\alpha_{\text{gel}}} \quad \textbf{Equation 4-3}$$

$$\text{for } i \geq i_{\text{gel}} \text{ and } i < i_{\text{SL}}: k_{\text{t,ii}}^{\text{app}} = k_{\text{t,11}}^{\text{app}} i_{\text{SL}}^{\alpha_{\text{l}}-\alpha_{\text{s}}} i_{\text{gel}}^{\alpha_{\text{gel}}-\alpha_{\text{l}}} i^{-\alpha_{\text{gel}}} \quad \textbf{Equation 4-4}$$

$$k_{\text{t,ij}}^{\text{app}} = \sqrt{k_{\text{t,ii}}^{\text{app}} k_{\text{t,jj}}^{\text{app}}} \quad \textbf{Equation 4-5}$$

$$i_{\text{gel}} = 0.53 w_{\text{p}}^{-2.5} \quad \textbf{Equation 4-6}$$

$$\alpha_{\text{gel}} = 1.66 w_{\text{p}} - 0.06 \quad \textbf{Equation 4-7}$$

$$w_{\text{p}} = \frac{x m_{\text{monomer,o}}}{m_{\text{monomer,o}} + m_{\text{solvent,o}}} \quad \textbf{Equation 4-8}$$

where x is the conversion, i_{gel} the characteristic chain length at the onset of the gel regime, α_{s} the short chain power law exponent in dilute solution, α_{l} the long chain power law exponent in dilute solution, i_{SL} the dilute solution crossover chain length when power laws for termination change from short to long chains, α_{gel} the power law exponent for termination in the gel regime, with w_{p} the mass fraction of polymer in the solution, and $m_{\text{monomer/solvent,o}}$ the initial mass of monomer/solvent added.[52,53]

Unfortunately, for BMA radical polymerization the only data available relate solely to low conversions.[44] Therefore, in this work, the complete composite k_{t} model as derived for methyl methacrylate (MMA) is used instead, taking into account the known significant effect of conversion on the apparent termination rate behaviour.[46,54–56] This assumption is acceptable since it can be expected that as a first approximation BMA and MMA diffuse similarly and the reported apparent rate coefficients at low conversion are similar. The corresponding parameters are taken from Johnston-Hall *et al.*.[44,45,54]

For simplicity, diffusional limitations on (de)activation reactions are neglected as they are only important at very high conversion and for catalysts characterized by a sufficiently high deactivation rate coefficient (> 10^7 L mol^{-1} s^{-1}) and very bulky deactivators.[56–58] From Table 4.2 it follows that the relatively low intrinsic deactivation rate coefficients support this model assumption.

For completeness it is mentioned here that for the calculation of the number average chain length (x_n) and the dispersity ($Đ$), the oligomeric species with a chain length up to 3 are neglected based on SEC column limitations. In practice, this leads mainly to lower simulated $Đ$ values at very low conversion.

4.4 Results and Discussion

4.4.1 Effect of initial Cu^{II} amount and reducing agent loading

Figure 4.1 shows the effect of the initial Cu^{II} amount and reducing agent loading on the conversion profile and change of x_n, $Đ$, initiator efficiency and EGF with conversion in the ARGET ATRP of BMA using $CuBr_2$/TPMA as ATRP catalyst at 70 °C and for a TCL of 35 (reaction conditions: Table 4.1: exp 1-3). For the simulations, the parameters from Table 4.2 are used, while the experimental data are taken from Payne *et al*.[18] In the Supporting Information (Appendix A) a benchmark between the kMC results and the Predici® simulations is provided supporting the accuracy of the kMC method.[57,59]

It follows from Figure 4.1a-c that the kMC model gives a good description of the experimental data, matching in particular the significant decrease in conversion and significant increase in x_n (at a given conversion) with decreasing Cu level (Figure 4.1a and b, respectively; exp 1 vs. exp 2; Table 4.1). In addition, the simulations clearly confirm the low ATRP initiator efficiency (Figure 4.1c), since in each case values much lower than unity are obtained, in agreement with the experimental data. The simulations also demonstrate the increase in $Đ$ with decreasing Cu

level, indicating the existence of a threshold value for the Cu level in cases where the level of control over chain length is important (Figure 4.1b). For the higher Cu level, somewhat higher *Đ* values are simulated, which can be partially attributed to the inability to measure oligomers with the SEC columns used, as explained above.

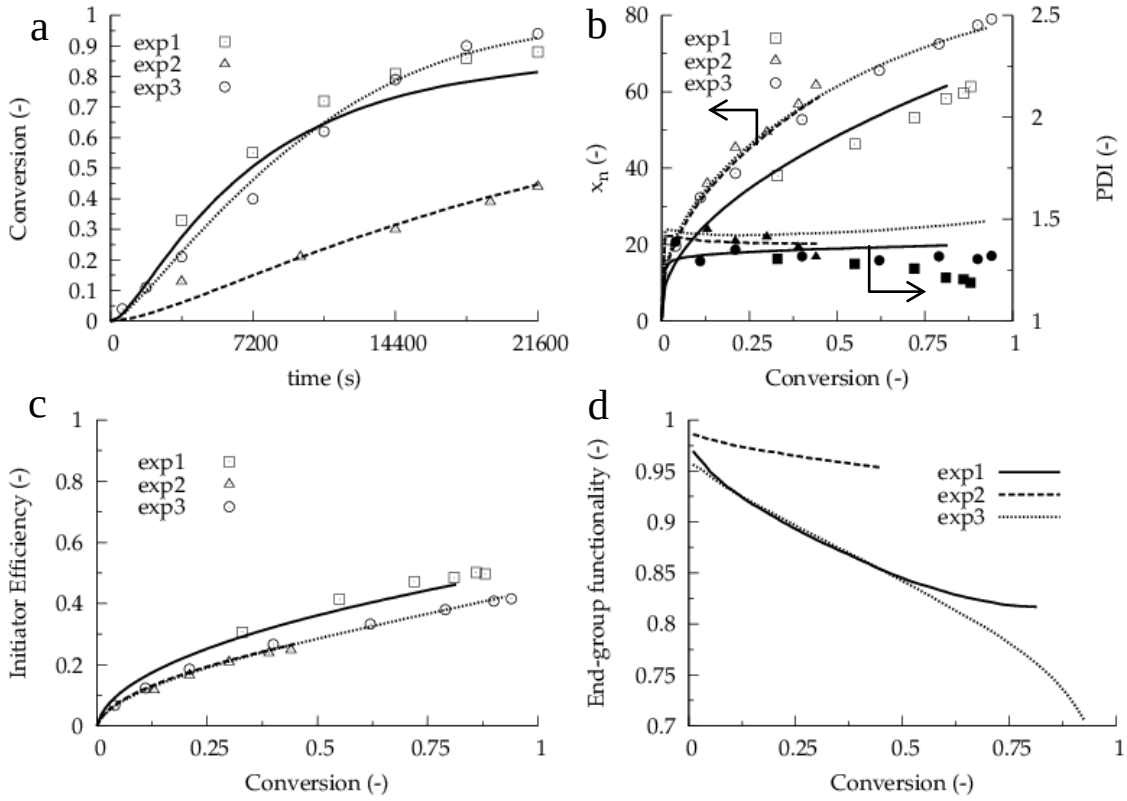

Figure 4.1: **Comparison of experimental (points) and simulation data (lines) at 70 °C using model parameters from Table 4.2. Plot of (a) conversion versus time, (b) number-average chain length (x_n) and dispersity (*Đ*), (c) ATRP initiator efficiency, and (d) end group functionality (EGF) versus conversion; initial conditions given as molar ratios of [BMA]:[EBiB]:[(Cu^{II}TPMABr)Br]: [$Sn(EH)_2$] = 35:1:0.005:0.05 (exp 1); 35:1:0.00125: 0.0125 (exp 2); 35:1:0.00125:0.125 (exp 3).**

Figure 4.1d shows that an increase in EGF is simulated with the decrease in Cu level (exp 1 vs. exp 2; Table 4.1), as has been seen in the literature,[60] with a subsequent increase in reducing

agent loading leading again to a significant decrease in EGF at high conversion (exp 2 vs. 3 (Table 4.1), Figure 4.1d). The latter decrease can be related to the increase in the Cu^{I}/Cu^{II} ratio (exp 2 vs. 3 (Table 4.1), Figure 4.2c) in particular at high conversion. In other words, for a higher reducing agent loading, a higher activator concentration results for which it has been derived that EGF is less preserved and the polymerization rate is increased.[18,19,55,61] Note that experimental EGF values could not be measured reliably for poly(BMA) due to overlapping of the butyl group and initiator group protons in the nuclear magnetic resonance (NMR) spectrum, as has been also reported for the related poly(butyl acrylate).[62,63] The noisiness of the Cu^{I}/Cu^{II} ratio in Figure 4.2c results from the selected sample size for the kMC simulations. Larger sample sizes, which lead to less practical simulation times, are required to reduce the fluctuations for species with very low concentration. However, the trends of the Cu^{I} and Cu^{II} concentration profile are clear, and all other simulated concentrations show much smaller fluctuations relative to mean values. Moreover, as shown in the Supporting Information (Appendix A), the concentration values and resulting polymer CLDs are in good agreement with the Predici® simulations.

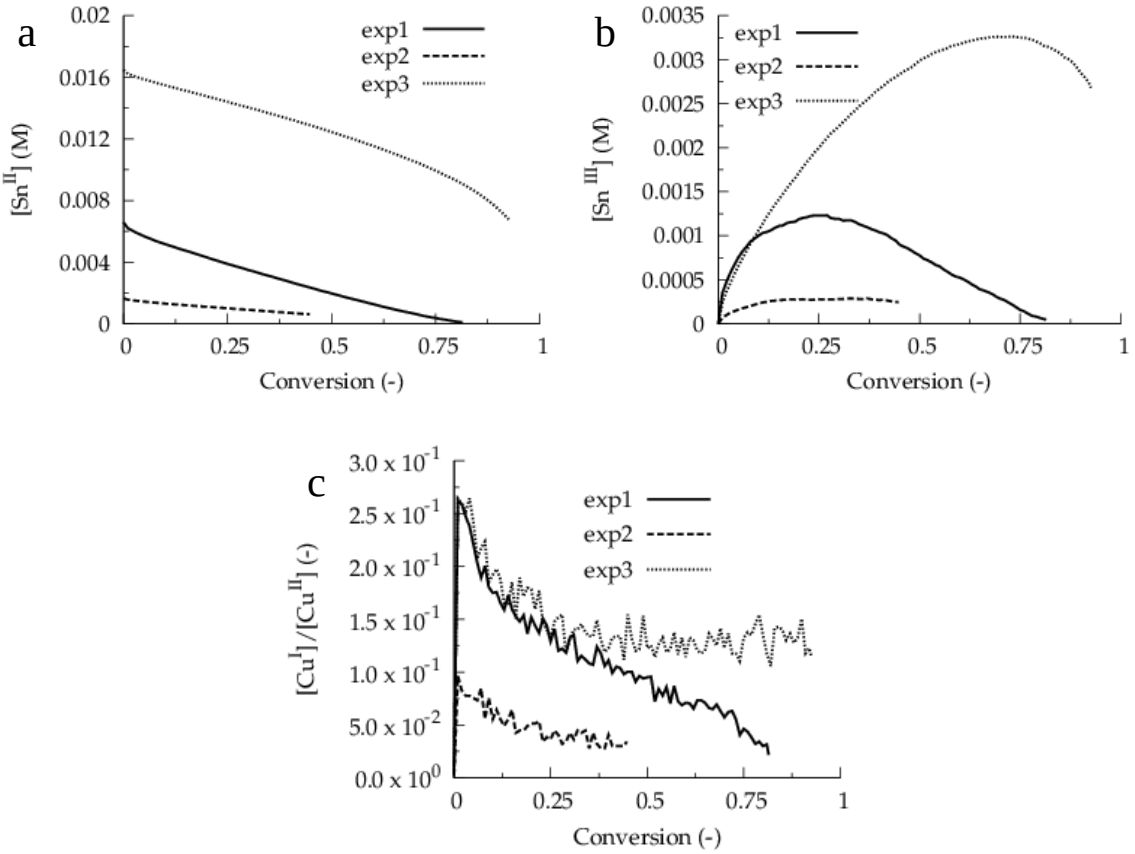

Figure 4.2: Comparison of simulated change in initial Cu^{II} and Sn^{II} loading on (a) $Sn^{II}(EH)_2$ and (b) $Sn^{III}(EH)_2Br$ concentration, and (c) ratio of activator/deactivator (Cu^{I}/Cu^{II}) versus conversion; model parameters in Table 4.2; initial conditions given as molar ratios of [BMA]:[EBiB]: [(Cu^{II}TPMABr)Br]:[$Sn(EH)_2$] = 35:1:0.005:0.05 (exp 1); 35:1:0.00125:0.0125 (exp 2); 35:1:0.00125:0.125 (exp 3).

From the concentration profiles for the Sn species (Figure 4.2a-b), it follows that Sn^{II} is consumed throughout the polymerization, whereas Sn^{III} shows the typical profile of the intermediate species in consecutive reactions, where an increase to a maximum concentration and a subsequent decrease is witnessed. In particular, for the low Cu amount (exp 2 in Table 4.1), reducing agent is no longer present at high conversion, which is directly reflected in the stagnation of the polymerization rate (cf. Figure 4.1a). Hence, in this case higher conversions could be reached

by the extra addition of reducing agent, similar to the addition of conventional radical initiator in initiators for continuous activators regeneration (ICAR) ATRP, a related modified ATRP technique.[64] However, it should be stressed that an experimental measure of the various Sn species would be beneficial both to improve estimates of the associated reduction rate coefficients, and to aid in the optimization of experimental conditions.

4.4.2 Importance of slow ATRP initiation

Table 4.2 shows that the activation intrinsic reactivity of the ATRP initiator at 70 °C is ~80 times lower than for the dormant macrospecies, whereas the deactivation intrinsic reactivity of the ATRP initiator radicals is twice that seen for the macroradicals, both indicative of a very slow ATRP initiation and confirming earlier literature reports[28] of such phenomenon in the ATRP of methacrylates. Indeed, from Figure 4.3, in which the ATRP initiator concentration is plotted as a function of conversion (exp 1-3 in Table 4.1), it follows that in the ARGET ATRP of BMA the ATRP initiator is still present at high conversion, consistent with the extremely low ATRP initiator efficiencies in Figure 4.1c. This can be confirmed by the agreement of experimental and simulation data (exp 3) in Figure 4.3, where the ATRP initiator was detected by GC-FID in significantly large quantities after 6 h of polymerization. It should be stressed that extensive screening revealed that it is not possible to match the reduced ATRP initiator efficiencies observed experimentally by varying other rate coefficients.

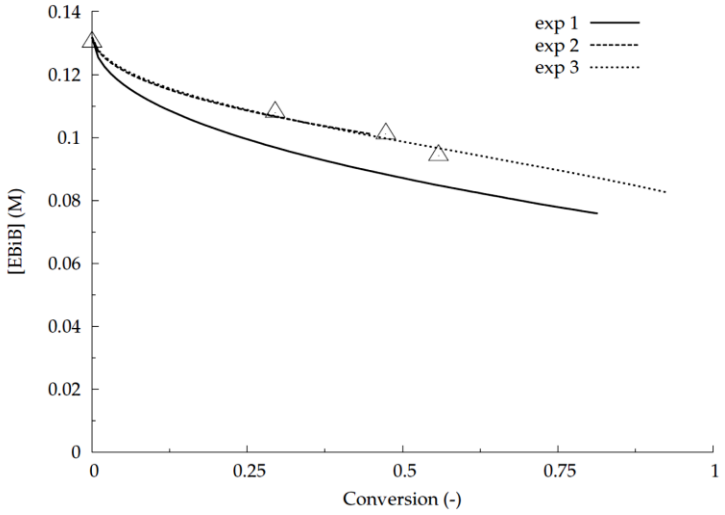

Figure 4.3: Plot of ATRP initiator (EBiB) concentration versus conversion for the ARGET ATRP of BMA at 70 °C; model parameters: Table 4.2; for exp 3 also experimental data (shown); initial conditions given as molar ratios of [BMA]:[EBiB]:[(Cu^{II}TPMABr)Br]: [$Sn(EH)_2$] = 35:1:0.005:0.05 (exp 1); 35:1:0.00125:0.0125 (exp 2); 35:1:0.00125:0.125 (exp 3).

This finding is illustrated in Figure 4.4, in which the simulation results at 35 ppm Cu (exp 3 in Table 4.1) are compared to those obtained assuming the same intrinsic activation/deactivation parameters for the ATRP initiator as for the dormant macrospecies. Clearly, slow ATRP initiation leads to a reduced control over chain length as evidenced by the higher x_n and $Đ$ values (Figure 4.4b). On the other hand, a faster ARGET ATRP polymerization is obtained with slow ATRP initiation at the expense of a reduced control over EGF as a function of conversion (Figure 4.4a and Figure 4.4d, respectively).

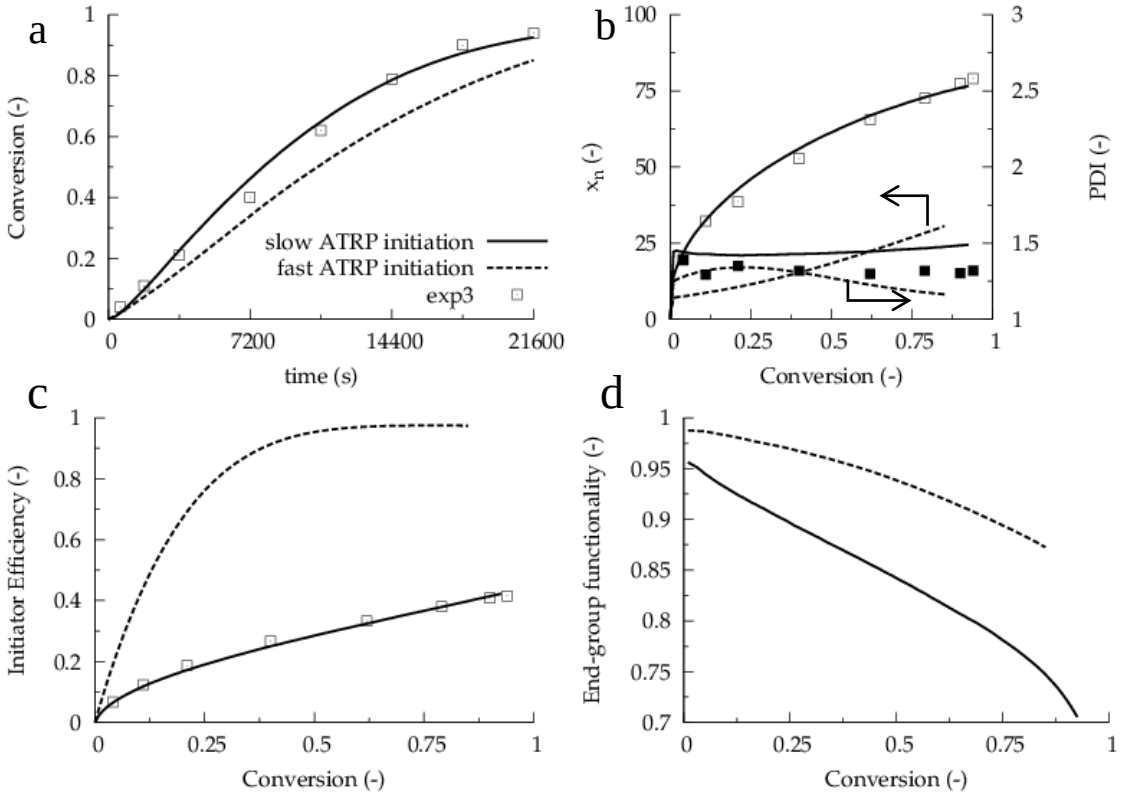

Figure 4.4: Comparison of model results accounting for simulated slow ATRP initiation (solid line; parameters Table 4.2) and assuming an ATRP initiation as fast as the polymeric activation/deactivation process (dotted line; $k_{a,o}=k_a=240$ L mol^{-1} s^{-1} and $k_{da,o}=k_{da}=1.2\times10^7$ L mol^{-1} s^{-1}; other model parameters Table 4.2) for exp 3 ([BMA]:[EBiB]: [(Cu^{II}TPMABr)Br]:[Sn(EH)$_2$] = 35:1:0.00125:0.125, 70 °C) plot of (a) conversion versus time, (b) number-average chain length (x_n), (c) dispersity ($Đ$) and ATRP initiator efficiency, and (d) end group functionality (EGF) versus conversion.

These observations can be understood based on the concentration profile of the activator and deactivator species (Cu^{I} and Cu^{II}, respectively), shown in Figure 4.5 as a function of conversion. With slow ATRP initiation, there is a significant increase in the concentration of activator species. Subsequently, there is a decrease in the deactivator concentration compared with fast ATRP initiation, and thus active chains can propagate and terminate more, explaining the increase in polymerization rate in Figure 4.4a and decrease in EGF in Figure 4.4d. In addition, with

the decrease in deactivator species concentration, there is less demand for reducing agent, allowing the polymerization to proceed to higher conversion (Figure 4.5c and Figure 4.5d).

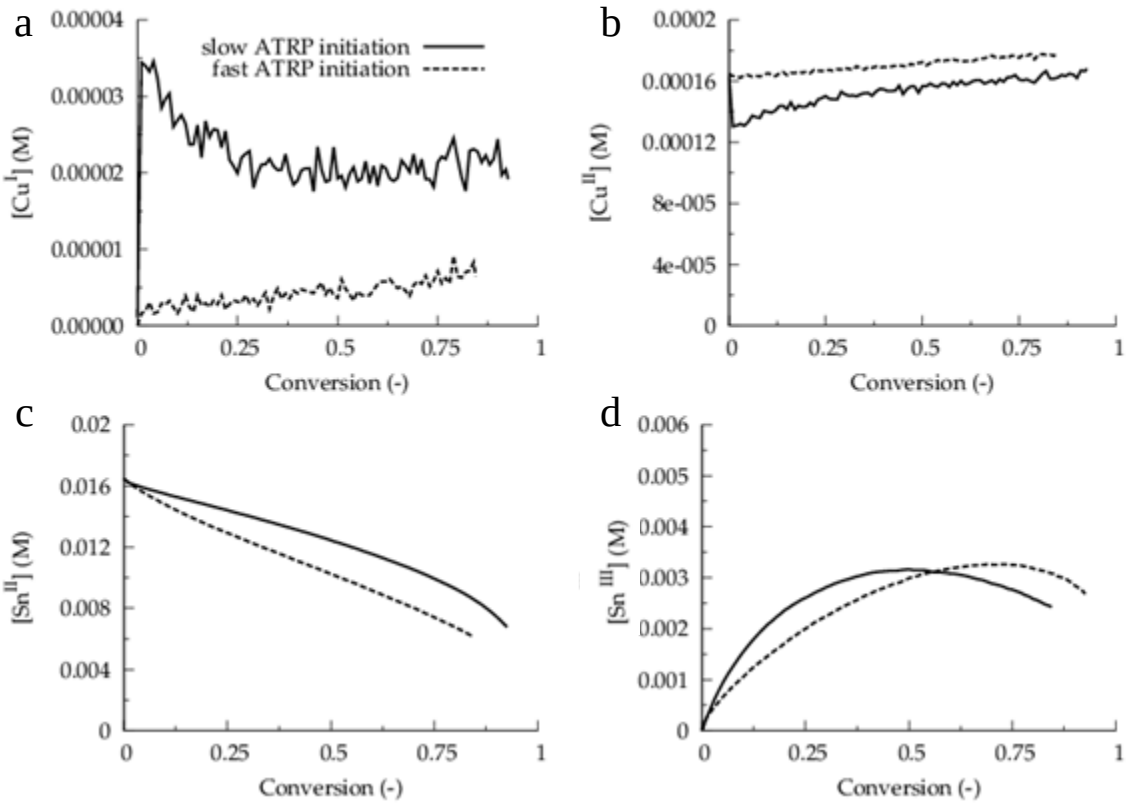

Figure 4.5: Comparison of model results accounting for simulated slow ATRP initiation (solid line; parameters Table 4.2) and assuming an ATRP initiation as fast as the polymeric activation/deactivation process (dotted line; $k_{a,o}=k_a=240$ L mol^{-1} s^{-1} and $k_{da,o}=k_{da}=1.2\times10^7$ L mol^{-1} s^{-1}; other parameters Table 4.2) for exp 3 ([BMA]:[EBiB]:[(Cu^{II}TPMABr)Br]: [Sn(EH)$_2$] = 35:1:0.00125:0.125, 70 °C); model parameters: Table 4.2; plot of (a) concentration of activator species (Cu^{I}), (b) deactivator species (Cu^{II}), (c) Sn^{II}(EH)$_2$ species, and (d) and Sn^{III}(EH)$_2$Br species versus conversion.

In Figure 4.6, for illustration purposes, the CLDs from the kMC simulations with slow initiation are plotted to show the total, dormant, and dead chain number fractions at different conversions (Figure 4.6a, Figure 4.6b, and Figure 4.6c, respectively). The distribution does indeed

shift to higher chain lengths with conversion, with a large number of short chains still present, similar to what is seen in the SEC-derived distributions.[18] It can thus be concluded that the ATRP system under investigation can be improved by identifying a more active initiator to overcome the observed slow initiation, a goal of future work.

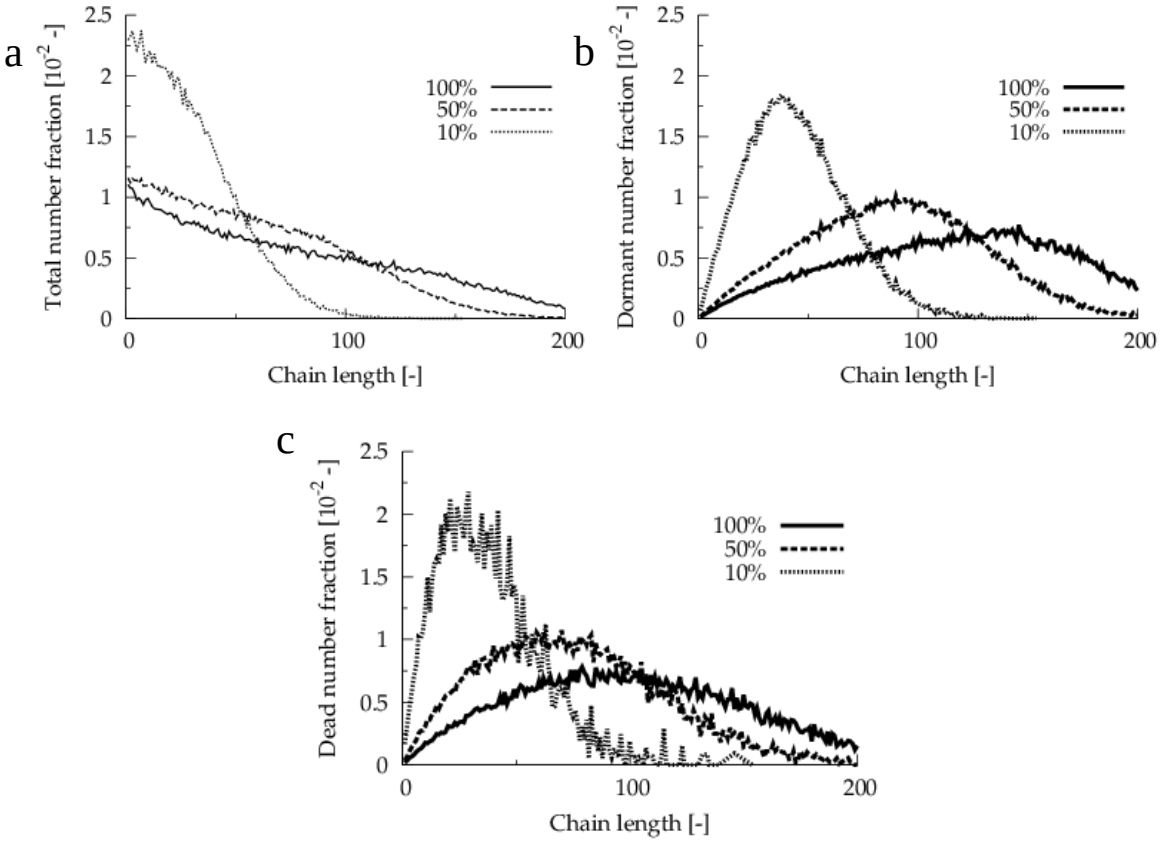

Figure 4.6: Plot of chain length distribution for chain species in the ARGET ATRP of BMA at 70 °C ([BMA]:[EBiB]:[(Cu^{II}TPMABr)Br]:[$Sn(EH)_2$] = 35:1:0.00125:0.125, exp 3) and Table 4.1, respectively. Plot of (a) total, (b) dormant, and (c) dead chain species number fraction versus chain length; model parameters: Table 4.2.

4.4.3 Importance of second reduction reaction

As mentioned above, Jakubowski *et al.*[39] suggested the occurrence of two reduction steps with $Sn(EH)_2$ (Scheme 4.2). In this work, the simulation results presented over a broad range of

polymerization conditions provide evidence supporting the existence of such two steps, as it is found that no adequate description of the conversion data can be obtained with a single reduction step.

For example, Figure 4.7 demonstrates the impact of considering only one reduction step for $Sn(EH)_2$ at a TCL of 35 at 70 °C (exp 3 in Table 4.1). Although there is minimal impact on the x_n and $Đ$ (Figure 4.7b) profile, there is a significant decrease in the simulated conversion (Figure 4.7a). For a single reduction step, an excessive accumulation of deactivator species is simulated, due to the depletion of the reducing agent concentration which is no longer able to regenerate a sufficient amount of activator species. This depletion leads to an overly high rate retardation at high conversion not observed experimentally, an effect even more pronounced with an increased rate of reduction. On the other hand, the inclusion of a second reduction step in the simulations gives an effective doubling of the concentration of reducing groups, thereby preventing a decrease in polymerization rate with the accumulation of deactivator. It should however be emphasized that without any measure of reducing agent concentration during the reaction, it is difficult to estimate the two associated rate coefficients with high precision. Note that there is a significant decrease in EGF with two reduction steps since more reduction implies an increase in activator concentration and a decrease in deactivator concentration (Figure 4.7d).

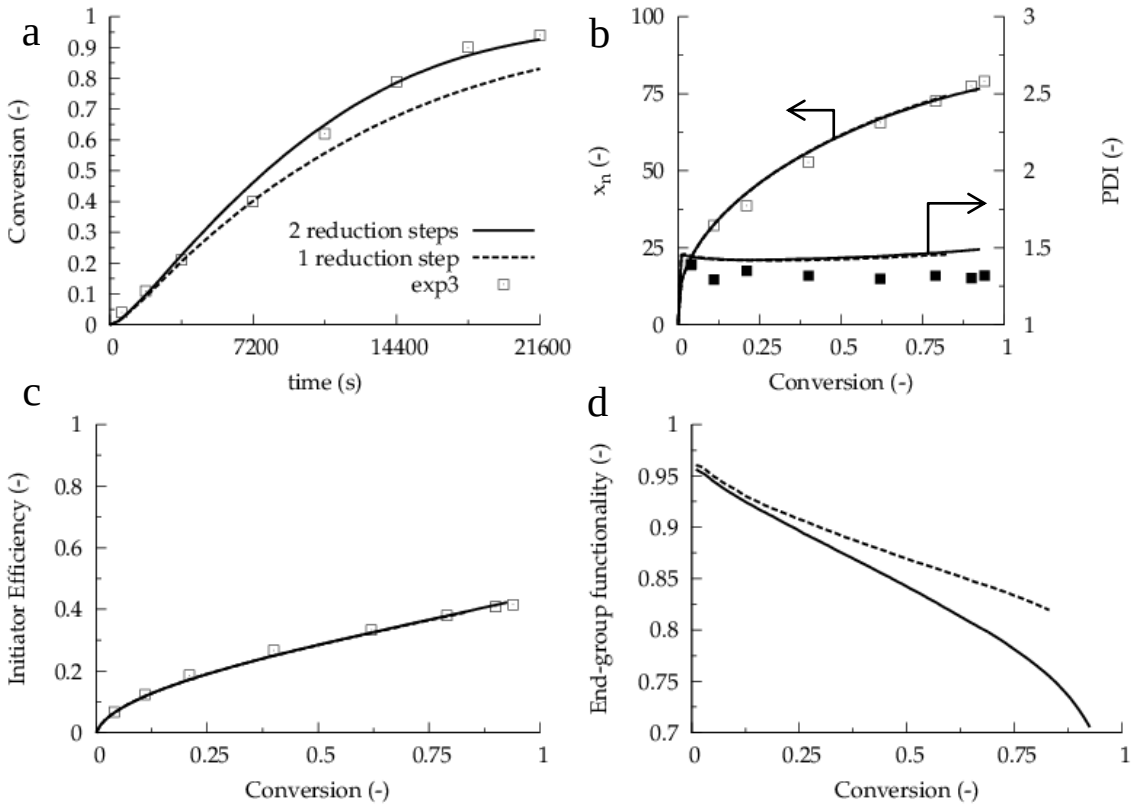

Figure 4.7: Comparison of simulation with two consecutive reduction steps (solid line) and one reduction step (dotted line) at 70 °C using model parameters from Table 4.2. Plot of (a) conversion versus time, (b) number-average chain length (x_n) and dispersity ($Đ$), (c) ATRP initiator efficiency, and (d) end group functionality (EGF) versus conversion; initial conditions [BMA]:[EBiB]:[(Cu^{II}TPMABr)Br]:[$Sn(EH)_2$] = 35:1:0.00125:0.125, exp 3.

From the above results, it is thus clear that for a fixed polymerization temperature of 70 °C a balance between polymerization rate, Cu loading, and EGF will need to be specified for the desired utility of the polymer product. An increased polymerization rate can be achieved at low Cu levels with the addition of excess reducing agent at the expense of EGF.

4.4.4 Effect of Diffusional Limitations on Termination

To determine whether diffusional limitations on termination are a major contributor to the studied ARGET ATRP system, the results for exp 3 (TCL=35; 70 °C) simulated with the composite

k_t model are compared by ignoring chain length dependent apparent termination effects, i.e., assuming an "intrinsic model" with $k_{t,ij}^{app}=k_{t,11}^{app}=1.1\times10^9$ L mol^{-1} s^{-1}.[47] The intrinsic model uses the small molecule limit for termination of all methacrylate macroradicals, while the composite model includes the RAFT-CLD parameters for estimation of the apparent termination rate coefficient as a function of chain length and conversion. The corresponding results for conversion, x_n, $Đ$, ATRP initiator efficiency and EGF are shown in Figure 4.8.

The conversion profile is clearly significantly affected by diffusional limitations on termination. At higher reactions times, the viscosity and chain length of the radicals have increased, leading to a lower apparent termination reactivity and thus to an increase of the polymerization rate (Figure 4.8a). The latter effect is also translated in the EGF profile, which shows significantly higher simulated EGF values at higher conversion (Figure 4.8d). On the other hand, the control over chain length is less affected by diffusional limitations on termination when this control is expressed as a function of conversion (Figure 4.8b). However, it is clear that diffusional limitations on termination are beneficial for the control over chain length as well, since lower $Đ$ values result from intermediate conversions onward.

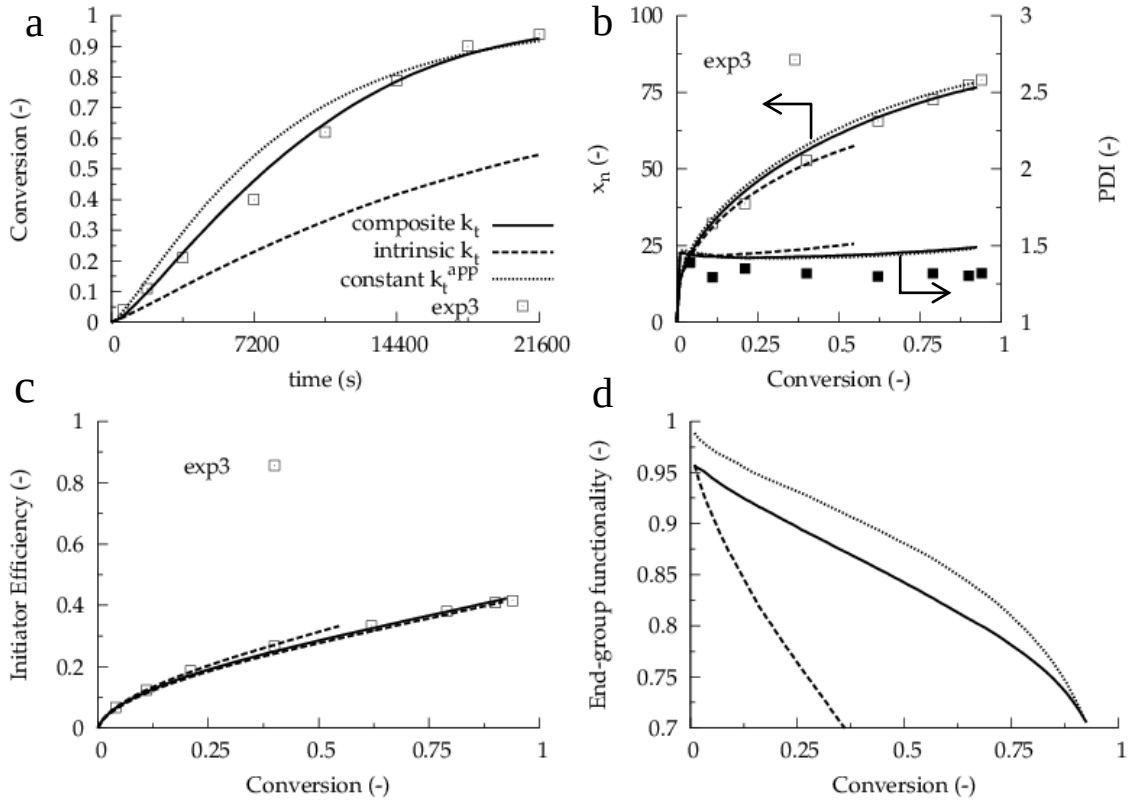

Figure 4.8: Comparison of experimental (see legend) and simulated data without accounting for diffusional limitations on termination (intrinsic model; dotted line; $k_{t,ij}^{app}=k_{t,11}^{app}=1.1\times10^9$ L mol^{-1} s^{-1}), while accounting for diffusional limitations on termination (composite k_t model according to Equation 4-1; solid line), and while assuming a constant k_t^{app}; ($k_t^{app}=9.0\times10^7$ L mol^{-1} s^{-1}; optimized value) at 70 °C (exp 3, [BMA]:[EBiB]:[(Cu^{II}TPMABr)Br]:[Sn(EH)$_2$] = 35:1:0.00125:0.125); plot of (a) conversion versus time, (b) number-average chain length (x_n) and dispersity ($Đ$), (c) ATRP initiator efficiency and (d) end group functionality (EGF) versus conversion; other model parameters Table 4.2.

In addition, in Figure 4.8 the simulation results with the composite k_t model (solid lines) are compared with the case where diffusional limitations are accounted for using a constant apparent termination coefficient (constant k_t^{app} model; dotted lines), with the value estimated based on the experimental data in this figure only. The optimal value of 9.0×10^7 L mol^{-1} s^{-1} is over an

order of magnitude lower than the value used in the intrinsic model. Note that this constant k_t^{app} model underestimates the termination reactivity at low conversion, whereas the opposite is true at high conversion, as directly reflected in the simulated EGF profile. At low conversions with the constant k_t^{app} model higher EGFs are obtained while at high conversions the constant k_t^{app} model and composite k_t model predict similar EGF values.

4.4.5 Effect of targeted chain length

Figure 4.9 (full lines) shows the effect of the decrease of the initial ATRP initiator concentration on the conversion profile and control over chain length and livingness for a temperature of 70 °C and an initial molar ratio of 1:0.00125:0.125 for $[EBiB]_o$: $[CuBr_2/TPMA]_o$: $[Sn(EH)_2]_o$ (TCL = 35 and 50 (exp3 and 4 in Table 4.1)). In the same figure, the results are also presented for a higher TCL = 400 (exp 5 in Table 4.1) with an initial molar ratio of 1:0.01:0.1 for $[EBiB]_o$: $[CuBr_2/TPMA]_o$: [Sn(EH)2]$_o$; a higher Cu loading relative to initiator is selected in order to keep the ppm level relative to monomer the same. Again a good description is obtained with the kinetic parameters in Table 4.2, i.e., over a broad range of polymerization conditions the intrinsic parameters in Table 4.1 can be used at 70 °C. Note in particular that there is a significant increase in the ATRP initiator efficiency for a TCL of 400 (Figure 4.9c), i.e., the number of polymeric chains per Cu complex is more in balance at the higher initial Cu loading. However, the ATRP initiation is still incomplete, while at the same time the polymerization rate (cf. Figure 4.9a) is too slow to obtain an industrially relevant overall polymerization time.

For completeness, in the same figure the simulated profiles are presented for the constant k_t^{app} model (dotted lines). It follows that this model is only valid as a first approximation, as it neglects chain-length dependent termination; in particular higher values of EGF are simulated due to the lower rate of termination at low conversion. Additionally, the simulations indicate that higher EGF values result at higher TCLs. Zhong and Matyjaszewski describe EGF as a function of target

chain length, conversion, and polymerization time;[61] in the present work deviations from this equation can be expected since additional phenomena such as slow initiation and chain-length-dependent apparent termination kinetics have to be accounted for.

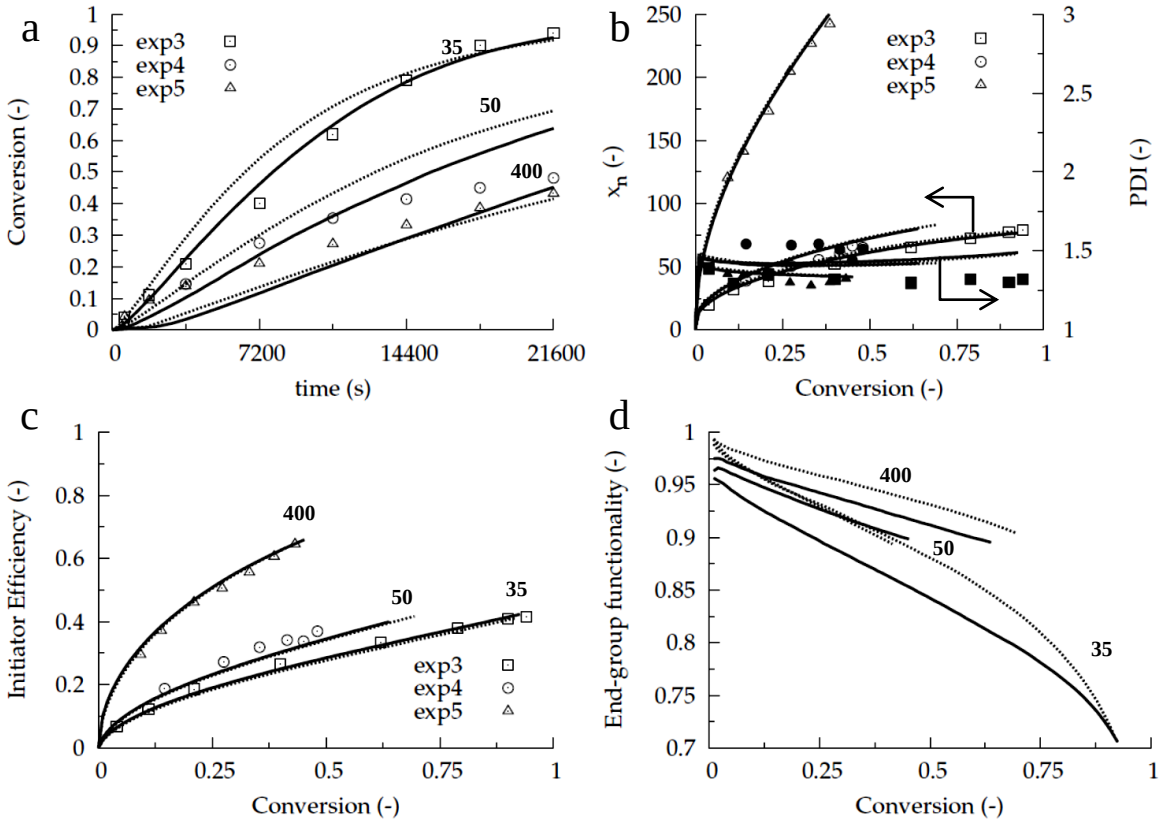

Figure 4.9: Comparison of experimental and simulation data (full lines: composite k_t model (Equation 4-1), dotted lines: constant k_t^{app} model: $k_t^{app}=k_{t,oo}^{app}=9.0\times10^7$ L mol^{-1} s^{-1}) for different TCL (see plot) at 70 °C with other model parameters from Table 4.2. Plot of (a) conversion versus time, and (b) number-average chain length (x_n), dispersity ($Đ$), (c) ATRP initiator efficiency and (d) end group functionality (EGF) versus conversion; initial conditions [BMA]: [EBiB]:[(Cu^{II}TPMABr)Br]:[Sn(EH)$_2$] = 35:1:0.00125:0.125, exp 3; 50:1:0.00125:0.125, exp 4; 400:1:0.01:0.1, exp 5.

4.4.6 Effect of polymerization temperature

To further increase the conversion at the low Cu level (36 ppm), the polymerization was also run at an elevated temperature of 90 °C. Figure 4.10 shows a comparison of the polymerization characteristics for the case when a high initial reducing agent loading is employed (exp 3 and 7 in Table 4.1). The Arrhenius parameters in Table 4.2 clearly show a good capability to simulate the experimental data with the conversion and x_n profiles in excellent agreement (Figure 4.10a and Figure 4.10b, respectively). Note that both reduction steps are characterized by the same activation energy (Table 4.2), i.e., at both temperatures the first reduction rate coefficient is three times lower than the second one. It can be further seen in Figure 4.10 that at 90 °C a higher polymerization rate is obtained with a similar level of control over chain length but with an increased livingness.

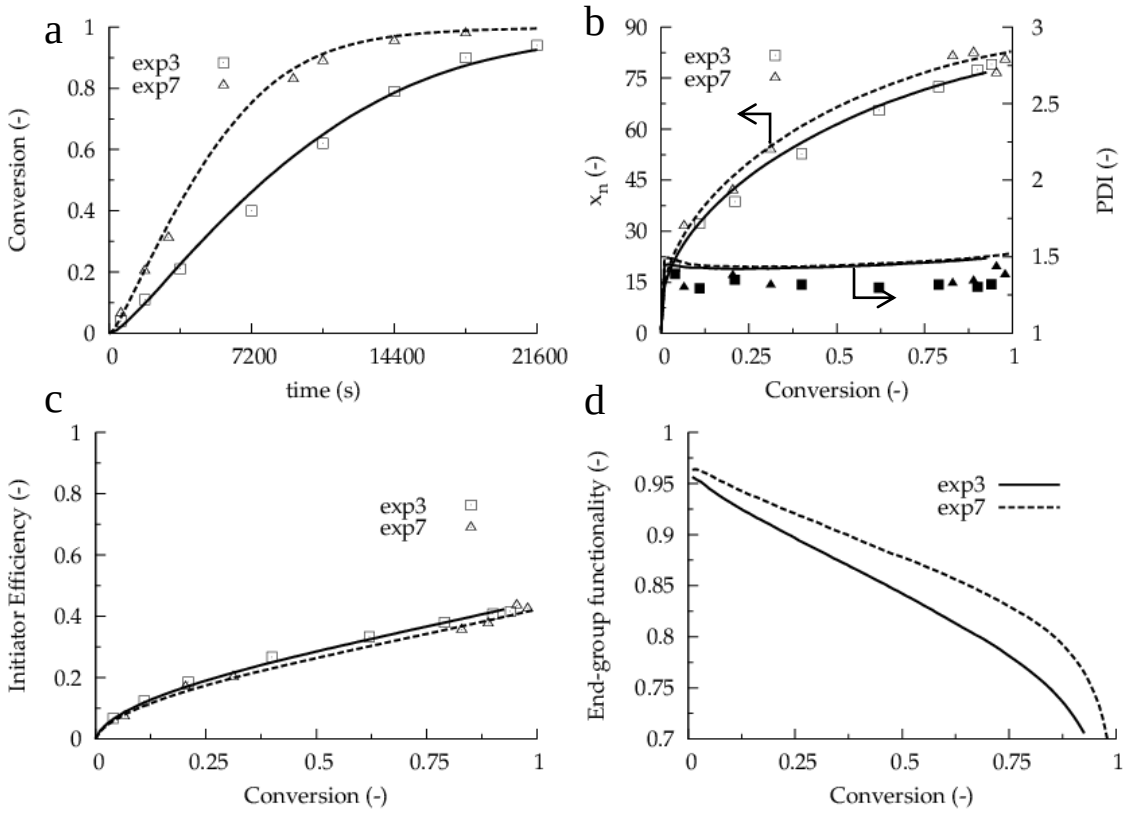

Figure 4.10: Comparison of experimental (see legend) and simulated data at 70 and 90 °C (exp 3 and 7; model parameters Table 4.2). Plot of (a) conversion versus time, (b) number-average chain length (x_n) and dispersity ($Đ$), (c) ATRP initiator efficiency and (d) end group functionality (EGF) versus conversion. Initial conditions [BMA]:[EBiB]: [(Cu^{II}TPMABr)Br]:[Sn(EH)$_2$] = 35:1:0.00125:0.125, exp 3 (70 °C) and exp 7 (90 °C).

Figure 4.11 demonstrates the importance of slow ATRP initiation at 90 °C. The simulation results are similar as at 70 °C (Figure 4.4), with again a significantly higher conversion and x_n due to slow ATRP initiation (Figure 4.11a and Figure 4.11b, respectively). Alternatively, this slow ATRP initiation follows from the change in ATRP initiator concentration, as shown in Figure 4.12, in which the simulation results at 70 °C are also added. In agreement with the similar ATRP initiator efficiency profiles (Figure 4.11c), it follows that the ATRP initiator disappearance is similar at both temperatures.

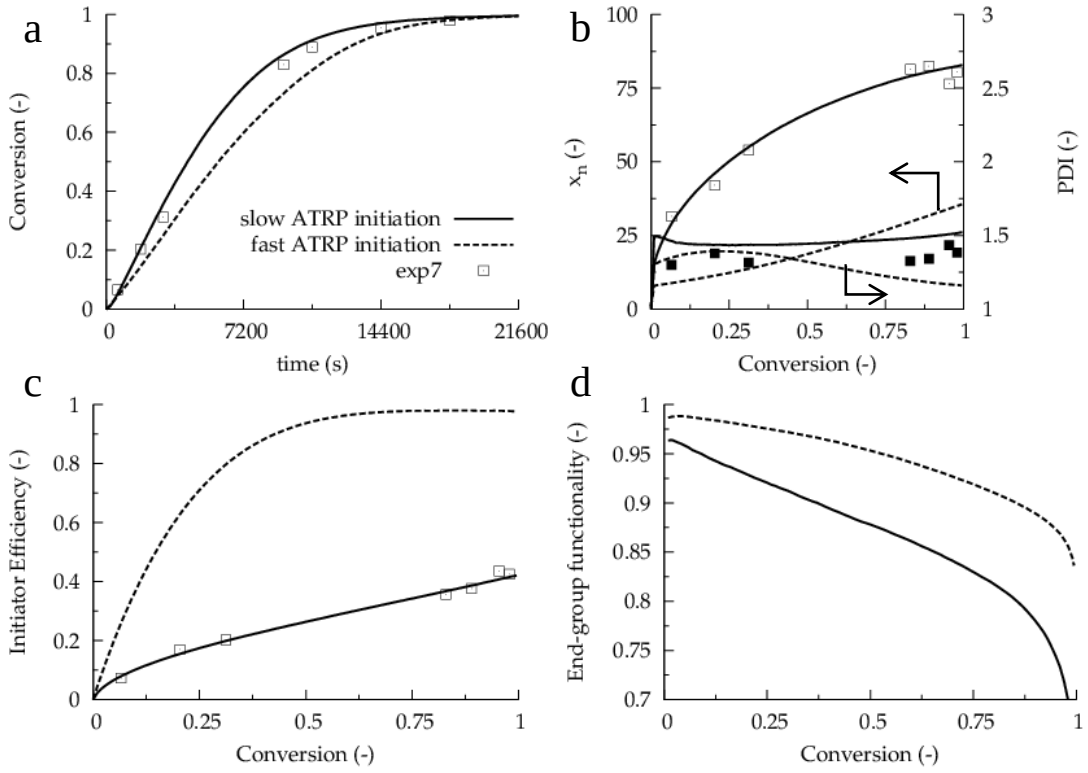

Figure 4.11: Comparison of fast (dashed lines) and slow (solid lines) ATRP initiation at 90 °C using model parameters from Table 4.2. Plot of (a) conversion versus time, (b) number-average chain length (x_n) and dispersity ($Đ$), (c) ATRP initiator efficiency, and (d) end group functionality (EGF) versus conversion; [BMA]:[EBiB]:[(Cu^{II}TPMABr)Br]: [$Sn(EH)_2$] = 35:1:0.00125:0.125, exp 7.

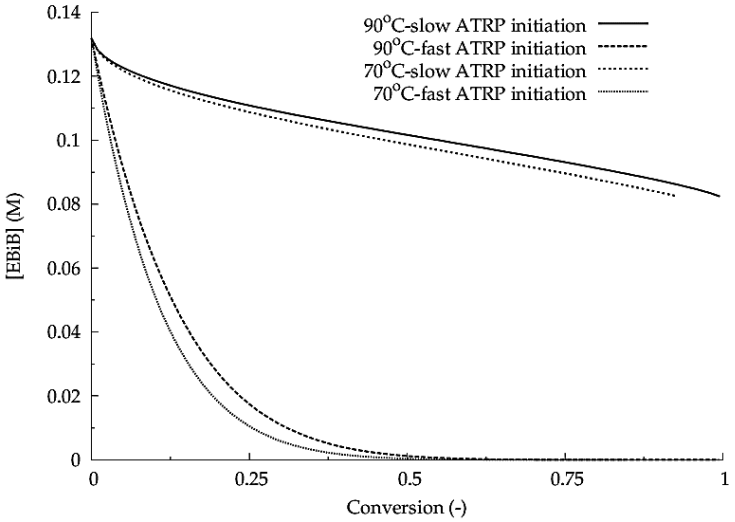

Figure 4.12: Plot of ATRP initiator (EBiB) concentration versus conversion for the ARGET ATRP of BMA at 70 and 90 °C; model parameters: Table 4.2; initial conditions [BMA]:[EBiB]: [(Cu^{II}TPMABr)Br]:[$Sn(EH)_2$] = 35:1:0.00125:0.125, exp 3 (70 °C) and exp 7 (90 °C).

Finally, the simulated evolution of the ATRP initiator efficiency versus conversion is again unaffected by the increase in initial reducing agent concentration (Figure 4.1c and Figure 4.13c, respectively; exp 6 and 7 in Table 4.1), an effect that is also observed experimentally. As before (Figure 4.1d), there is also a high retention of EGF at the low Cu and reducing agent level (Figure 4.13d), while an increase in reducing agent concentration initially results in a large decrease in EGF due to a higher activator concentration (see Supporting Information, Appendix A).

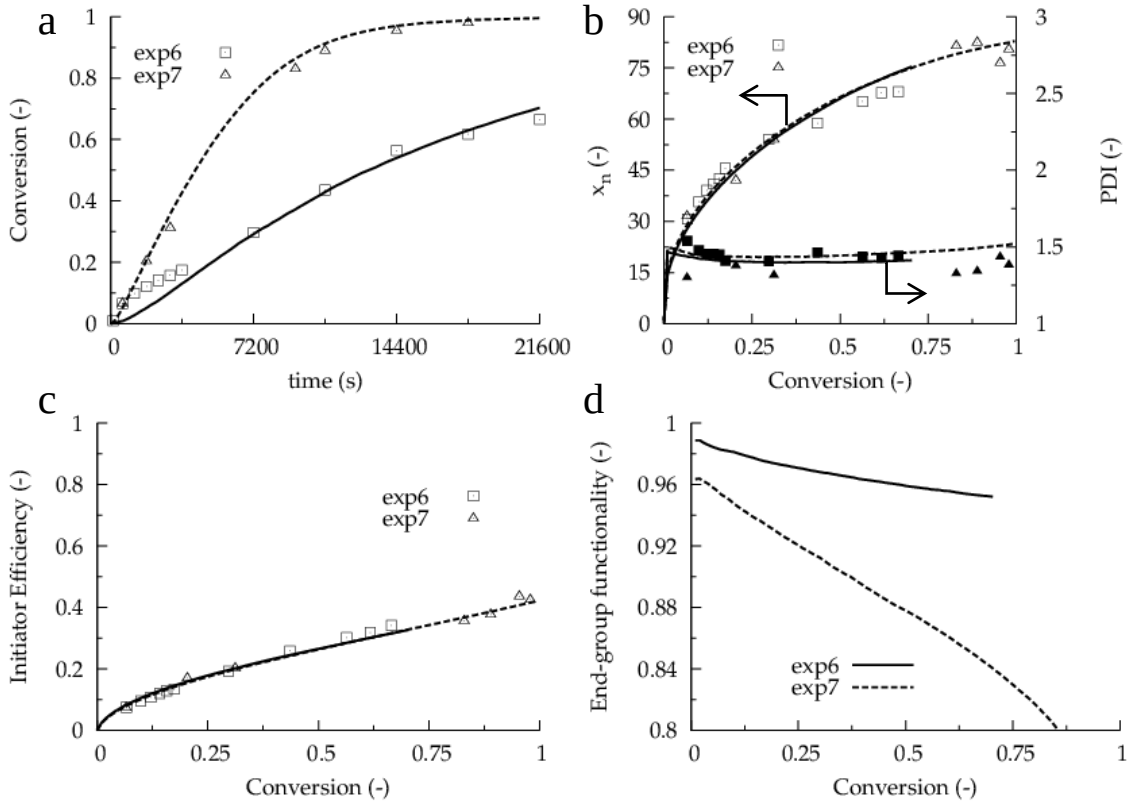

Figure 4.13: Comparison of experimental (see legend) and simulation data (lines) at 90 °C using model parameters from Table 4.2. Plot of (a) conversion versus time, (b) number-average chain length (x_n) and dispersity ($Đ$), (c) ATRP initiator efficiency, and (d) end group functionality (EGF) versus conversion; initial conditions [BMA]:[EBiB]: [(Cu^{II}TPMABr)Br]:[$Sn(EH)_2$] = 35:1:0.00125:0.0125, exp 6; 35:1:0.00125:0.125, exp 7.

4.5 Conclusions

A kMC model is used to successfully describe previously published as well as new experimental data for the ARGET ATRP of BMA using $Sn(EH)_2$ as reducing agent, EBiB as ATRP initiator, and $CuBr_2$/TPMA as deactivator. The model demonstrates the presence of slow ATRP initiation in this system, where distinct initiator and macrospecies activation/deactivation rate coefficients are essential to explain the experimental number-average chain length (x_n) data. Without the distinction between the two species, the ATRP initiator efficiency would approach

100% after a few hours, a result that is inconsistent with the experimental x_n values that significantly exceed the targeted chain length (TCL), indicative of fewer chains being activated than ideally expected. The slow ATRP initiation has the same effect at 70 °C and 90 °C, with the increase in temperature having a negligible impact on the ATRP initiator efficiency. Moreover, due to slow initiation an increased polymerization rate is obtained, which can be explained by a higher activator concentration. The balance between rate and livingness may be improved by the optimization of the ATRP initiator structure, as will be explored in future work.

The model also includes a second reduction step for the reducing agent $Sn(EH)_2$, in accordance with the proposed mechanisms found in the literature. This second reduction step is required in order to accurately describe the conversion profiles witnessed in the experimental data. The use of only one reduction step results in a too low polymerization rate as the reducing agent concentration is depleted too early. A constant ratio of 0.3:1 between the first and second reduction rate coefficient was used at both polymerization temperatures, i.e., both reduction steps are characterized by the same activation energy.

Diffusional limitations on termination are also included in the model, combined with the composite model of chain-length-dependent termination. This model provides a slightly better representation of conversion profiles, with the improved treatment of termination predicted to have a significant effect on end group functionality (EGF).

The initial Cu and $Sn(EH)_2$ loadings have a clear influence on the polymerization rate and EGF. With a reduction in Cu loading, there is an increase in the predicted EGF at the expense of polymerization rate. In industry, the choice between low material costs (low Cu and $Sn(EH)_2$) and low operating costs (fast polymerization rate) should thus be balanced with final product requirements, such as the level of EGF.

4.6 Nomenclature

R_iX	dormant halogen-capped chain with chain length *i* (-)
R_oX	alkyl halide initiator (-)
Cu^IX/L	activator (-)
$Cu^{II}X_2/L$	deactivator (-)
M	monomer (-)
i	chain length (-)
j	chain length (-)
o	initiator (-)
x_n	number-average chain length (-)
X	halogen/end group functionality
L	catalyst complex ligand
L_2	reducing agent complex ligand
$[C]_o$	initial concentration of C ($mol.L^{-1}$)

4.6.1 Subscripts

a	Activation
da	Deactivation
r1	first reduction
r2	second reduction
p	Propagation
t	Termination
tc	termination by combination
td	termination by disproportionation

4.6.2 Superscripts

app	apparent

4.6.3 Abbreviations

ATRP	atom transfer radical polymerization
ARGET	activator regenerated by electron transfer
BMA	butyl methacrylate
bpy	Bipyridine
CLD	chain length distribution
C/LRP	controlled/living radical polymerization
$CuBr_2$	copper (II) bromide
DCM	Dichloromethane
DMF	N,N-dimethylformamide
EBiB	ethyl 2-bromoisobutyrate
EGF	end group functionality
GC-FID	gas chromatography - flame ionization detector
kMC	kinetic Monte Carlo
MMA	methyl methacrylate
Me_6TREN	tris[2-(dimethylamino)ethyl]amine
NMR	nuclear magnetic resonance
PDI (or $Đ$)	polydispersity index (or dispersity)
PMDETA	N,N,N′,N″,N″-Pentamethyldiethylenetriamine
ppm	parts per million
Pr	Predici®
PRE	persistent radical effect
RAFT-CLD-T	reversible addition fragmentation transfer chain length dependent termination
SEC	size exclusion chromatography
$Sn(EH)_2$	tin (II) 2-ethylhexanoate
TCL	target chain length (-)

TPMA tris[(2-peridyl)methyl]amine

4.7 References

(1) Wang, J.-S.; Matyjaszewski, K. *J. Am. Chem. Soc.* **1995**, *117*, 5614–5615.

(2) Matyjaszewski, K.; Xia, J. *Chem. Rev.* **2001**, *101*, 2921–2990.

(3) Wang, J.-S.; Matyjaszewski, K. *Macromolecules* **1995**, *28*, 7901–7910.

(4) Grimaud, T.; Matyjaszewski, K. *Macromolecules* **1997**, *30*, 2216–2218.

(5) Percec, V.; Barboiu, B. *Macromolecules* **1995**, *28*, 7970–7972.

(6) Wang, J.-L.; Grimaud, T.; Matyjaszewski, K. *Macromolecules* **1997**, *30*, 2216–2218.

(7) Fischer, H. *Chem. Rev.* **2001**, *101*, 3581–3610.

(8) Destarac, M. *Macromol. React. Eng.* **2010**, *4*, 165–179.

(9) Matyjaszewski, K.; Jakubowski, W.; Min, K.; Tang, W.; Huang, J.; Braunecker, W. A.; Tsarevsky, N. V. *Proc. Natl. Acad. Sci. U.S.A.* **2006**, *103*, 15309–15314.

(10) Jakubowski, W.; Matyjaszewski, K. *Angew. Chem.* **2006**, *118*, 4594–4598.

(11) Pintauer, T.; Matyjaszewski, K. *Chem. Soc. Rev.* **2008**, *37*, 1087–1097.

(12) Borguet, Y. P.; Tsarevsky, N. V. *Polym. Chem.* **2012**, *3*, 2487-2494.

(13) Magenau, A. J. D.; Strandwitz, N. C.; Gennaro, A.; Matyjaszewski, K. *Science* **2011**, *332*, 81–84.

(14) Nicolaÿ, R.; Kwak, Y.; Matyjaszewski, K. *Angew. Chem., Int. Ed.* **2010**, *49*, 541–544.

(15) Averick, S. E.; Magenau, A. J. D.; Simakova, A.; Woodman, B. F.; Seong, A.; Mehl, R. A.; Matyjaszewski, K. *Polym. Chem.* **2011**, *2*, 1476-1478.

(16) Konkolewicz, D.; Magenau, A. J. D.; Averick, S. E.; Simakova, A.; He, H.; Matyjaszewski, K. *Macromolecules* **2012**, *45*, 4461–4468.

(17) Simakova, A.; Averick, S. E.; Konkolewicz, D.; Matyjaszewski, K. *Macromolecules* **2012**, *45*, 6371–6379.

(18) Payne, K. A.; Cunningham, M. F.; Hutchinson, R. A. In *Progress in Controlled Radical Polymerization: Mechanisms and Techniques*; Matyjaszewski, K.; Sumerlin, B. S.;

Tsarevsky, N. V., Eds.; ACS Symposium Series, American Chemical Society: Washington, DC, 2012; pp. 183–202.

(19) Toloza Porras, C.; D'hooge, D. R.; Reyniers, M.-F.; Marin, G. B. *Macromol. Theory Simul.* **2013**, *22*, 136–149.

(20) Jakubowski, W.; Kirci-Denizli, B.; Gil, R. R.; Matyjaszewski, K. *Macromol. Chem. Phys.* **2008**, *209*, 32–39.

(21) Jakubowski, W.; Matyjaszewski, K. *Angew. Chem.* **2006**, *45*, 4482–4486.

(22) Jakubowski, W.; Min, K.; Matyjaszewski, K. *Macromolecules* **2006**, *39*, 39–45.

(23) Li, X.; Wang, W.-J.; Li, B.-G.; Zhu, S. *Macromol. React. Eng.* **2011**, *5*, 467–478.

(24) Nesvadba, P. In *Encyclopedia of Radicals in Chemistry, Biology and Materials*; Chatgilialoglu, C.; Studer, A., Eds.; John Wiley & Sons, Ltd: Chichester, UK, 2012.

(25) Chan, N.; Cunningham, M. F.; Hutchinson, R. A. *Macromol. Chem. Phys.* **2008**, *209*, 1797–1805.

(26) Min, K.; Gao, H.; Matyjaszewski, K. *Macromolecules* **2007**, *40*, 1789–1791.

(27) Matyjaszewski, K.; Wang, J.-L.; Grimaud, T.; Shipp, D. A. *Macromolecules* **1998**, *31*, 1527–1534.

(28) Nanda, A. K.; Matyjaszewski, K. *Macromolecules* **2003**, *36*, 8222–8224.

(29) Gillies, M. B.; Matyjaszewski, K.; Norrby, P.-O.; Pintauer, T.; Poli, R.; Richard, P. *Macromolecules* **2003**, *36*, 8551–8559.

(30) Guliashvili, T.; Percec, V. *J. Polym. Sci., Part A Polym. Chem.* **2007**, *45*, 1607–1618.

(31) Lin, C. Y.; Coote, M. L.; Petit, A.; Richard, P.; Poli, R.; Matyjaszewski, K. *Macromolecules* **2007**, *40*, 5985–5994.

(32) Van Steenberge, P. H. M.; D'hooge, D. R.; Wang, Y.; Zhong, M.; Reyniers, M.-F.; Konkolewicz, D.; Matyjaszewski, K.; Marin, G. B. *Macromolecules* **2012**, *45*, 8519–8531.

(33) Van Steenberge, P. H. M.; Vandenbergh, J.; D'hooge, D. R.; Reyniers, M.-F.; Adriaensens, P. J.; Lutsen, L.; Vanderzande, D. J. M.; Marin, G. B. *Macromolecules* **2011**, *44*, 8716–8726.

(34) Gillespie, D. T. *J. Phys. Chem* **1977**, *81*, 2340–2361.

(35) Wulkow, M. *Macromol. Theory Simul.* **1996**, *5*, 393–416.

(36) Britovsek, G. J. P.; England, J.; White, A. J. P. *Inorg. Chem.* **2005**, *44*, 8125–8134.

(37) Eckenhoff, W. T.; Garrity, S. T.; Pintauer, T. *Eur. J. Inorg. Chem.* **2008**, *2008*, 563–571.

(38) Tang, W.; Matyjaszewski, K. *Macromol. Theory Simul.* **2008**, *17*, 359–375.

(39) Jakubowski, W.; Matyjaszewski, K. *Macromolecules* **2005**, *38*, 4139–4146.

(40) Tang, W.; Matyjaszewski, K. *Macromolecules* **2007**, *40*, 1858–1863.

(41) Seeliger, F.; Matyjaszewski, K. *Macromolecules* **2009**, *42*, 6050–6055.

(42) Beuermann, S.; Buback, M.; Davis, T. P.; Gilbert, R. G.; Hutchinson, R. A.; Kajiwara, A.; Klumperman, B.; Russell, G. T. *Macromol. Chem. Phys.* **2000**, *201*, 1355–1364.

(43) Wang, W.; Hutchinson, R. A. *AIChE J.* **2011**, *57*, 227–238.

(44) Barth, J.; Buback, M.; Hesse, P.; Sergeeva, T. *Macromolecules* **2009**, *42*, 481–488.

(45) Johnston-Hall, G.; Stenzel, M. H.; Davis, T. P.; Barner-Kowollik, C.; Monteiro, M. J. *Macromolecules* **2007**, *40*, 2730–2736.

(46) Barner-Kowollik, C.; Russell, G. T. *Prog. Polym. Sci.* **2009**, *34*, 1211–1259.

(47) Fischer, H.; Paul, H. *Acc. Chem. Res.* **1987**, *20*, 200–206.

(48) Buback, M.; Morick, J. *Macromol. Chem. Phys.* **2010**, *211*, 2154–2161.

(49) Tang, W.; Tsarevsky, N. V.; Matyjaszewski, K. *J. Am. Chem. Soc.* **2006**, *128*, 1598–1604.

(50) Braunecker, W. A.; Tsarevsky, N. V.; Gennaro, A.; Matyjaszewski, K. *Macromolecules* **2009**, *42*, 6348–6360.

(51) Nanda, A. K.; Matyjaszewski, K. *Macromolecules* **2003**, *36*, 1487–1493.

(52) Johnston-Hall, G.; Monteiro, M. J. *Macromol. Theory Simul.* **2010**, *19*, 387–393.

(53) Bergenudd, H.; Jonsson, M.; Malmström, E. *Macromol. Theory Simul.* **2011**, *20*, 814–825.

(54) Johnston-Hall, G.; Monteiro, M. J. *J. Polym. Sci., Part A Polym. Chem.* **2008**, *46*, 3155–3173.

(55) Achilias, D. S. *Macromol. Theory Simul.* **2007**, *16*, 319–347.

(56) D'hooge, D. R.; Reyniers, M.-F.; Marin, G. B. *Macromol. React. Eng.* **2013**, *7*, 362–379.

(57) D'hooge, D. R.; Reyniers, M.-F.; Marin, G. B. *Macromol. React. Eng.* **2009**, *3*, 185–209.

(58) Zetterlund, P. B. *Macromolecules* **2010**, *43*, 1387–1395.

(59) Konkolewicz, D.; Sosnowski, S.; D'hooge, D. R.; Szymanski, R.; Reyniers, M.-F.; Marin, G. B.; Matyjaszewski, K. *Macromolecules* **2011**, *44*, 8361–8373.

(60) Wang, Y.; Soerensen, N.; Zhong, M.; Schroeder, H.; Buback, M.; Matyjaszewski, K. *Macromolecules* **2013**, *46*, 683–691.

(61) Zhong, M.; Matyjaszewski, K. *Macromolecules* **2011**, *44*, 2668–2677.

(62) Nicolas, J.; Dire, C.; Mueller, L.; Belleney, J.; Charleux, B.; Marque, S. R. A.; Bertin, D.; Magnet, S.; Couvreur, L. *Macromolecules* **2006**, *39*, 8274–8282.

(63) Lligadas, G.; Percec, V. *J. Polym. Sci., Part A Polym. Chem.* **2007**, *45*, 4684–4695.

(64) D'hooge, D. R.; Konkolewicz, D.; Reyniers, M.-F.; Marin, G. B.; Matyjaszewski, K. *Macromol. Theory Simul.* **2012**, *21*, 52–69.

Chapter 5

Controlled Synthesis of poly(BMA-*co*-BA) via ARGET ATRP: Insights and Improvements

Preface

From the kinetic model developed in collaboration with Ghent University for butyl methacrylate (BMA), this was further expanded to include butyl acrylate (BA) as well as a BMA/BA copolymerization system. This model helps to explain the increased initiator efficiency with the BA system witnessed experimentally. To improve the initiator efficiency of the BMA system, varying levels of BA were added, with the model in good agreement with the experimental results. Within the kinetic model, it was found that the reducing agent concentration was depleted during polymerization, leading to a decreased Cu^{I}/Cu^{II} ratio and the resulting polymerization rate. As a result, a "semi-batch" approach was used with an injection of additional reducing agent during the polymerization, leading to an increase in conversion and molar mass, and further consumption of the initiator. If the chemistry is to be adopted industrially, the slow feeding of reducing agent is a suitable means to drive the reaction towards full conversion. However, the tradeoff of reduced copper vs. increased tin (reducing agent) levels would need to be evaluated for industrial implementation. The work in this chapter has been published as a full paper in Polymer International (2014, vol. 63, 848-857).

Abstract

The copolymerization of butyl methacrylate (BMA) and butyl acrylate (BA) initiated by $CuBr_2$/TPMA/EBiB (TPMA: tris[(2-pyridyl)methyl]amine; EBiB: ethyl 2-bromoisobutyrate), with tin (II) 2-ethylhexanoate ($Sn(EH)_2$) as reducing agent, is studied experimentally and by kinetic Monte Carlo simulations at 70 and 90 °C under batch ARGET ATRP conditions in anisole at low Cu levels (down to 35 ppm Cu on a molar basis with respect to monomer). With increasing initial BA content, the initiator efficiency is improved with an accompanying increase in dispersity due to oligomer formation. The addition of reducing agent during the polymerization, i.e. a semi-batch approach, allows an increase in polymerization rate and initiator efficiency, driving the polymerization towards full conversion and allowing for better initiator consumption.

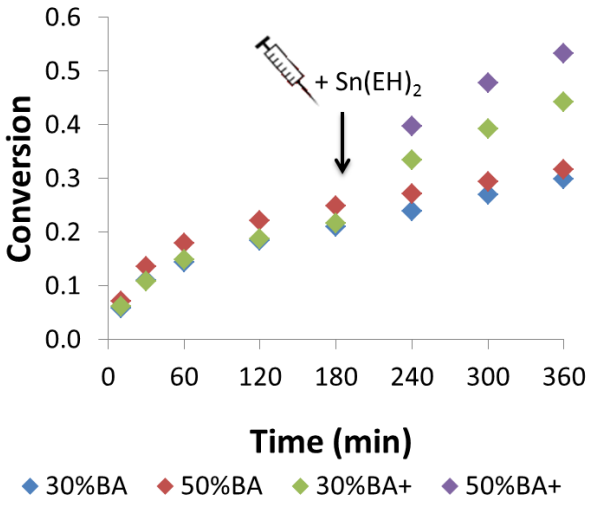

5.1 Introduction

Atom transfer radical polymerization (ATRP; Scheme 5.1a), one important method of reversible-deactivation radical polymerization (RDRP), or controlled radical polymerization (CRP), has witnessed an increasing level of attention since its development in 1995.[1–6] ATRP has been applied for a wide array of (co)monomers under different experimental conditions using various, mostly Cu-based, transition metal complexes which allow alteration of the activation (k_a) and deactivation (k_{da}) behavior. These transition metal complexes, which change oxidation state when activation/deactivation takes place, can be classified as catalysts for polymerization, where the lower and higher oxidation state complex are respectively denoted as activator ($Cu^{I}X/L$) and deactivator ($Cu^{II}X_2/L$).

Scheme 5.1a depicts the main ATRP reactions including termination and propagation as well as the activation-deactivation cycle that, with $k_{da} >> k_a$, results in a low radical (ΣR_i) concentration and a high dormant or "capped" chain ($\Sigma R_i X$) concentration, leading to a low dispersity ($Đ$[6]) for fast ATRP initiation and high end group functionality (EGF; X). In addition, an initial molar ratio of monomer to ATRP initiator ($[M]_o:[R_oX]_o$ = TCL (targeted chain length)) can be selected such that this TCL is ideally achieved as the number-average chain length after full conversion of monomer.

In the last decade, improved ATRP techniques have been developed focusing on low ATRP catalyst amounts, including initiators for continuous activator regeneration (ICAR) ATRP, activator generated by electron transfer (AGET) ATRP, supplemental activator and reducing agent (SARA) ATRP, and activator regenerated by electron transfer (ARGET) ATRP (Scheme 5.1b).[7–10] As a result, the amount of metal (Cu) species required to mediate the ATRP has been reduced to parts per million (ppm) levels (on a molar basis with respect to monomer). With such low Cu levels being sufficient to produce high-quality polymers with controlled topology and composition, there

is potential to make the ATRP process more commercially attractive.[11] Also, these recent ATRP processes are started with the deactivator that is, contrary to the activator, less oxygen sensitive. In particular, ARGET ATRP is well suited, as activator regeneration is performed without creating additional radicals and it does not require a complex synthesis procedure.

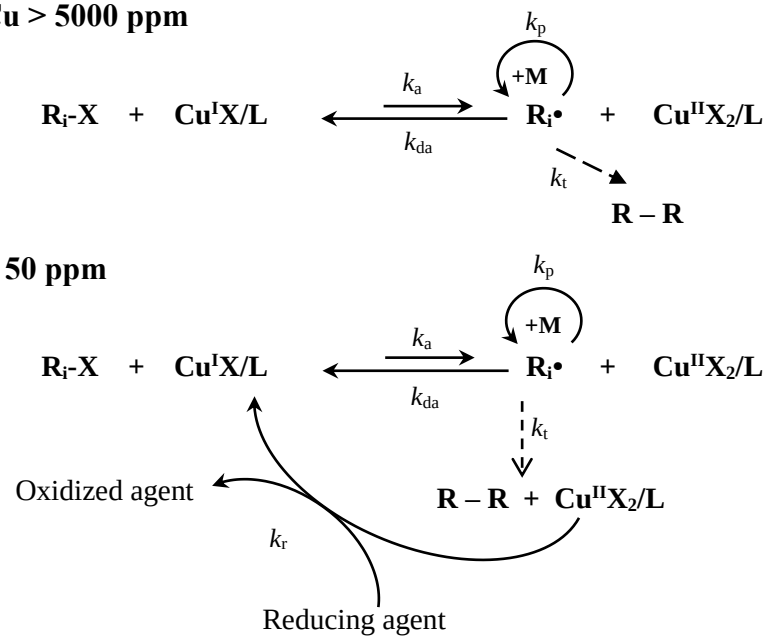

Scheme 5.1: Main reactions in (a) normal Cu-based ATRP and (b) Cu-based ARGET ATRP.[a]

[a]In normal ATRP initially only ATRP initiator (R_oX), monomer (M) and activator (Cu^IX/L) are present (where L = ligand), whereas in ARGET ATRP there is initially only ATRP initiator, monomer and deactivator ($Cu^{II}X_2/L$) with an excess of reducing agent to (re)generate activator; $k_{a,da,p,r,t}$: rate coefficient for activation, deactivation, propagation, reduction, and termination, respectively.

Recently, Payne *et al.*[12] conducted a systematic study of ARGET ATRP of butyl acrylate (BA) at 90 °C and ARGET ATRP of butyl methacrylate (BMA) at 70 °C, in anisole, considering various initial Cu catalyst, reducing agent, and initiator concentrations. For both monomers, the

ATRP was initiated by $CuBr_2$/TPMA/EBiB (TPMA: tris[(2-pyridyl)methyl]amine; EBiB: ethyl 2-bromoisobutyrate) and tin (II) 2-ethylhexanoate ($Sn(EH)_2$) was used as reducing agent. The homopolymerization of BMA was further studied with kinetic Monte Carlo (kMC) simulations to understand the experimentally observed decrease in polymerization rate and initiator efficiency with decreasing Cu loading.[13] It was shown that slow initiation is the main contributor to the low initiator efficiency seen with BMA. The initiator efficiency could be improved with an increase in initial reducing agent concentration leading to an increase in polymerization rate, although, at the expense of EGF. For the ARGET ATRP of BA, the experimental study[12] showed that significantly higher initiator efficiencies but also higher $Đ$ values are obtained compared to the corresponding BMA system. Also, the initiator efficiency was constant, whereas the BMA system exhibited a slowly increasing initiator efficiency throughout the reaction.

In the work reported here, the random copolymerization of BMA with various initial amounts of BA was studied experimentally and via simulations under similar ARGET ATRP conditions as selected for the homopolymerization of BMA (70 °C).[12] Various comonomer solutions are considered to pursue a balance of increased initiator efficiency with increased $Đ$ due to increasing BA content in the monomer feed. Additional homopolymerization experimental data for the ARGET ATRP of BA at 70 °C are reported to allow a better assessment of this approach. Furthermore, we address the question of whether extra addition of reducing agent during the polymerization allows the production of better controlled poly(BMA-*co*-BA).

5.2 Experimental

5.2.1 Materials

BMA (99%, Aldrich), BA (99%, Aldrich), copper (II) bromide ($CuBr_2$; 99%, Aldrich), anisole (99%, Aldrich), EBiB (98%, Aldrich), $Sn(EH)_2$ (95%, Aldrich), and acetone (for HPLC, ≥99%, Aldrich) were used as received. The ligand TPMA was synthesized and complexed with

$CuBr_2$ according to literature.[14,15] Experiments were conducted following the same procedure as specified in Payne *et al*.[12]

5.2.2 Analytical Methods

The analytical methods for the measurement of the conversion by gravimetry and control over chain length by size exclusion chromatography (SEC) are the same as those used in the previous BMA/BA ARGET ATRP study.[12]

In this work reported here, gas chromatography with flame ionization detection (GC-FID) was used for the experimental determination of the ATRP initiator conversion profile. A Waters CP-3800 gas chromatograph with a flame ionization detector was employed to measure the initiator concentration of the samples, with a Chrompack capillary column (CP-Sil 8 CB, 30 m in length and 0.25 mm inside diameter, column oven temperature 300 °C). Acetone was used as solvent to prepare the samples.

5.3 Kinetic model for copolymerization of BMA and BA under ARGET ATRP conditions

The kMC technique was used to simulate the number-average molar mass (M_n), $Đ$, initiator efficiency, and explicit copolymer composition of the individual polymer chains for the ARGET ATRP copolymerization of BA and BMA at 70 °C using EBiB as initiator, $CuBr_2$/TPMA as deactivator and $Sn(EH)_2$ as reducing agent. Further computational details are provided elsewhere.[16–20]

Table 5.1 presents the reactions included in the kMC simulations and the associated kinetic/model parameters for the copolymerization of BA and BMA under ARGET ATRP conditions. As with the kMC study of the homopolymerization of BMA,[13] typical free radical polymerization reactions are included such as propagation and termination, while ATRP-specific activation, deactivation, and reduction reactions are also considered. The two-step reduction

process used in the homopolymerization study is also included in this model. For simplicity, a terminal model is used to describe the copolymerization kinetics.[21] The BMA rate coefficients are taken from the homopolymerization study[13] while the BA coefficients were determined in this work based on the copolymerization data (see the next section for comparison with experimental data).

Chain transfer reactions to monomer and solvent are neglected based on results from previous kinetic modeling studies.[22] Intermolecular chain transfer to polymer and backbiting (with BA), are also neglected based on experimental and simulation data, and as the system contains significant BMA content for most conditions.[23–26] The reversible addition-fragmentation chain transfer chain length-dependent termination (RAFT-CLD-T) parameters to account for diffusional limitations on termination are taken from the literature approximating BA by methyl acrylate (MA) and BMA by methyl methacrylate (MMA).[27–31]

Table 5.1: Reactions and kinetic parameters (70 °C) for the simulation of copolymerization by ARGET ATRP of BMA(1) and BA(2) using EBiB as ATRP initiator, $Cu^{II}X_2$/L as deactivator and $Sn^{II}L_2$ as reducing agent where X=Br, L = TPMA and $L_2 = (EH)_2$; subscript "o" relates to ATRP initiator; terminal model assumed.[21]

ATRP activation/deactivation				Value at 70 °C	Ref.
R_o-X + Cu^IX/L	$\xrightarrow{k_{a,o}}$	R_o• + $Cu^{II}X_2$/L		3.2	[a]
R_iX + Cu^IX/L	$\xrightarrow{k_{a1}}$	R_i• + $Cu^{II}X_2$/L		2.40×10^2	[32,33], [a]
R_iX + Cu^IX/L	$\xrightarrow{k_{a2}}$	R_i• + $Cu^{II}X_2$/L		24.0	[b]
R_o• + $Cu^{II}X_2$/L	$\xrightarrow{k_{da,o}}$	R_o-X + Cu^IX/L		2.40×10^7	[a]
R_i• + $Cu^{II}X_2$/L	$\xrightarrow{k_{da1}}$	R_iX + Cu^IX/L		1.20×10^7	[a]
R_i• + $Cu^{II}X_2$/L	$\xrightarrow{k_{da2}}$	R_iX + Cu^IX/L		1.20×10^7	[b]
Propagation					
R_o• + M_1	$\xrightarrow{k_{p1,o}}$	$R_1{}^1$•		1.23×10^3	[34]
$R_i{}^1$• + M_1	$\xrightarrow{k_{p11}}$	$R_{i+1}{}^1$•		1.23×10^3	[34]
R_o• + M_2	$\xrightarrow{k_{p2,o}}$	$R_1{}^2$•		4.32×10^4	[35]
$R_i{}^2$• + M_2	$\xrightarrow{k_{p22}}$	$R_{i+1}{}^2$•		4.32×10^4	[35]
$R_i{}^1$• + M_2	$\xrightarrow{k_{p12}}$	$R_{i+1}{}^2$•	$k_{p,11}/r_{12}$	$r_{12} = 1.88$	6.54×10^2	[35]
$R_i{}^2$• + M_1	$\xrightarrow{k_{p21}}$	$R_{i+1}{}^1$•	$k_{p,22}/r_{21}$	$r_{21} = 0.3$	1.44×10^5	[35]
Reduction					
$Cu^{II}X_2$/L + $Sn^{II}L_2$	$\xrightarrow{k_{r1}}$	Cu^IX/L + $Sn^{III}L_2X$		0.30	[a]
$Cu^{II}X_2$/L + $Sn^{III}L_2X$	$\xrightarrow{k_{r2}}$	Cu^IX/L + $Sn^{IV}L_2X_2$		1.00	[a]
Irreversible Termination[c]					
R_o• + R_o•	$\xrightarrow{k_{tc,oo}^{app}}$	R-R			
R_i• + R_o•	$\xrightarrow{k_{tc,o}^{app}}$	P_0			
R_i• + R_o•	$\xrightarrow{k_{td,o}^{ap}}$	$P_i + P_0$			
R_i• + R_j•	$\xrightarrow{k_{tc}^{app}}$	P_{i+j}			
R_i+ R_j	$\xrightarrow{k_{td}^{app}}$	P_i + P_j			

[a]From BMA ARGET ATRP homopolymerization study.[13] [b]This work. [c]For termination, apparent termination rate coefficients are used based on RAFT-CLD-T measurements with model parameters taken from MMA radical polymerization for BMA, and MA radical polymerization for

BA (composite k_t model).[35–37,29] For termination between macroradicals with chain length of one and ATRP initiator radicals at zero conversion a value of 1.1×10^9 L mol^{-1} s^{-1} is used (also denoted k_t^{app}) for BMA, and 1.3×10^9 L mol^{-1} s^{-1} is used for BA.[28,38] The cross termination coefficients are calculated based on the geometric mean of the individual apparent termination rate coefficients.

As discussed in the introduction, the focus of this study is the effect of BA addition on the initiation of EBiB at low copper levels. The order of magnitude difference in intrinsic activation rate coefficient between dormant macrospecies with BMA and BA as terminal monomer unit has been seen for similar tertiary and secondary radical structures such as methyl 2-bromoisobutyrate (MBiB, k_a = 2.6 L mol^{-1} s^{-1} at 35 °C) and methyl 2-bromopropionate (MBrP, k_a = 0.33 L mol^{-1} s^{-1} at 35 °C).[32] The significant difference in K_{ATRP} ($=k_a/k_{da}$) values between BMA and BA activation/deactivation has also been seen for MMA and MA at 25 °C with $CuBr_2$/TPMA, where MMA was found to have $K_{ATRP} = 9.4\times10^{-5}$ and MA had an extrapolated value of $K_{ATRP} = 2.0\times10^{-9}$.[39,40]

5.4 Results and Discussion

5.4.1 Effect of copper and reducing agent loading in ARGET ATRP of BA

Figure 5.1 depicts the effect of the initial Cu^{II} and $Sn(EH)_2$ loading on the conversion, number-average molar mass (M_n), dispersity ($Đ$), and initiator efficiency for BA homopolymerization at 70 °C after 6 h using $Cu^{II}Br_2$/TPMA as ATRP catalyst, and for a TCL of 39 (M_{nT} = 5,000 g mol^{-1}; where M_{nT} is the target M_n), similar to the BMA system studied previously.[12] The corresponding profiles can be seen in Figure 5.1. In this work, a polymerization temperature of 70 °C was selected as most experimental data and reliable model parameters for the BMA system are available at this temperature, allowing a direct assessment of the potential use of a certain amount of BA when polymerizing BMA under ARGET ATRP conditions.

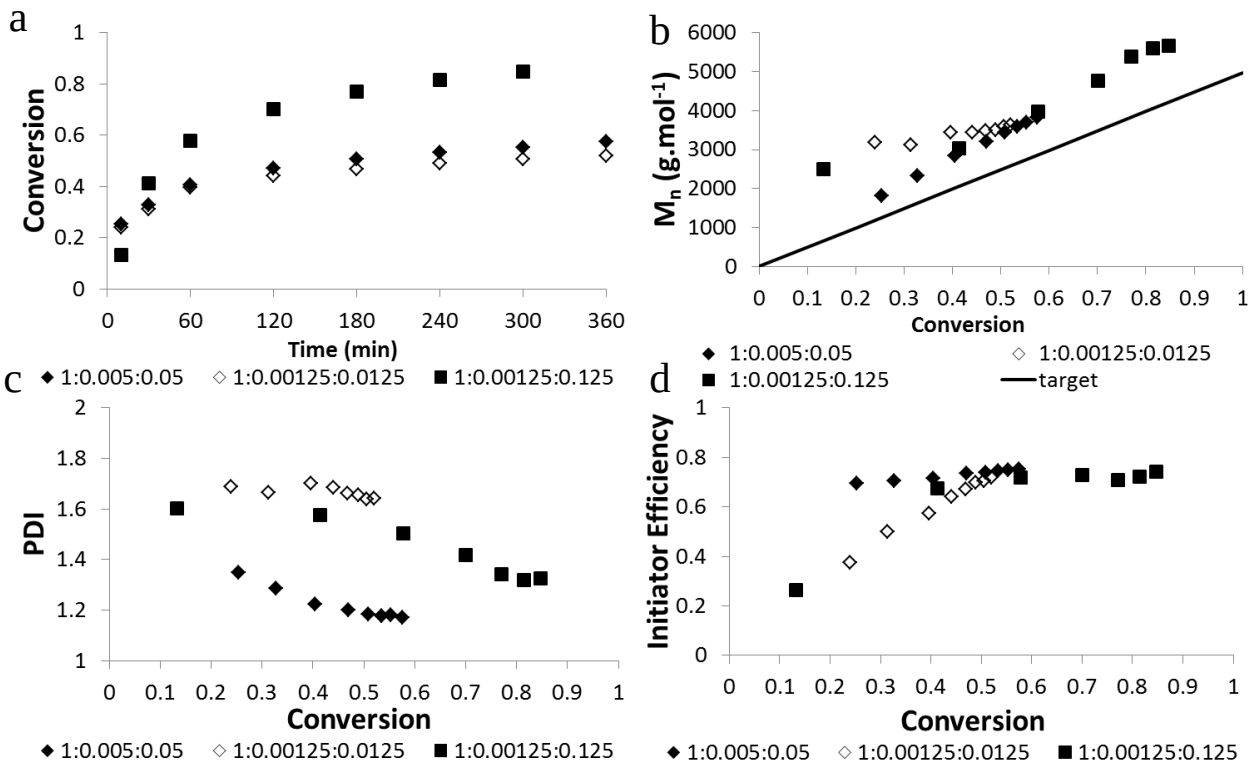

Figure 5.1: Homopolymerization of BA by ARGET ATRP at 70 °C and TCL = 39. Plot of (a) conversion versus time, (b) number-average molar mass (M_n), (c) dispersity ($Đ$), and (d) initiator efficiency versus conversion; initial conditions given as molar ratios of [EBiB]:[(Cu^{II}TPMABr)Br]:[$Sn(EH)_2$] (see also Table 5.2).

Table 5.2: Batch ARGET ATRP of BA at 70 °C with 30 wt% anisole and TCL = 39.

Initial Ratio [M]:[R-X]:[Cu^{II}]:[Sn^{II}]	Cu (ppm)[a]	Time (min)	Conversion	$M_{n,exp}$ (g mol^{-1})	Initiator Efficiency
39:1:0.005:0.05	148	360	0.57	3826	0.75
39:1:0.00125:0.0125	36	360	0.52	3622	0.72
39:1:0.00125:0.125	36	300	0.85	5658	0.74

[a]Molar basis with monomer

With a decrease in the Cu and reducing agent levels (by a factor 4; filled versus open diamond symbols; constant initial ratio of Cu:Sn = 1:10), there is only a slight decrease in the

reaction rate, as seen by examining the BA conversion profiles. This finding suggests that the decrease in the Cu level while maintaining a constant initial ratio of Cu:Sn does not alter the Cu^{I}/Cu^{II} ratio, in agreement with the approximate equation for the polymerization rate (R_p):[41]

$$R_p = k_p[M][R-X]\frac{k_a[Cu^{I}X/L]}{k_{da}[Cu^{II}X_2/L]} \qquad \textbf{Equation 5-1}$$

In this equation, $k_a/k_{da} = K_{ATRP}$ is the ATRP equilibrium coefficient, k_p the propagation rate coefficient, [M] the monomer concentration, [R-X] the concentration of dormant chains, $[Cu^{I}X/L]$ and $[Cu^{II}X_2/L]$ the concentrations of activator and deactivator species. It is found that for the BMA system, on the other hand, the initiator efficiency decreases with a decrease in Cu level,[12] thus altering the value of [R-X] in Equation 5-1. Note that for BA, chain activation is slower for the experiment with the reduced Cu level (open diamond symbols), but the final initiator efficiency reached is the same (Figure 5.1d).

As also observed for BMA,[12] a reduction in the Cu loading (filled versus open diamond symbols) results in an increase in the initial M_n and $Đ$ values of the poly(BA) produced (Figure 5.1b and c, respectively), suggesting the difficulty in mediating the polymer chains at low catalyst levels. A subsequent increase in the reducing agent loading at the low Cu level (open diamond versus square symbols) results in faster activation of EBiB and a significant increase for the conversion profile of BA (Figure 5.1a), as found in the analogous BMA study.[12] Note that the initiator efficiency is limited to ~75% in the BA system at 70 °C regardless of the recipe (Figure 5.1d), as also found with previous experiments conducted at 90 °C.[12]

Table 5.3: Batch ARGET ATRP of BA and BMA at varying temperature with 30 wt% anisole and TCL = 39 and 35, respectively.

Initial Ratio [M]:[R-X]:[Cu^{II}]:[Sn^{II}]	Monomer/ Temperature	Time (min)	Conversion	Mn_{exp} (g mol^{-1})	Initiator Efficiency
39:1:0.00125:0.0125	BA / 70 °C	360	0.52	3622	0.72
	BA / 90 °C	240	0.68	4721	0.72
35:1:0.00125:0.0125	BMA / 70 °C[a]	360	0.44	8778	0.25
	BMA / 90 °C	360	0.66	9668	0.34

[a]Previously published[12]

Table 5.3 summarizes the comparison of the BMA and BA ARGET ATRP homopolymerization at 70 and 90 °C and low Cu and reducing agent loadings at fixed polymerization times, including data from earlier work.[12] The full comparison of conversion versus time and M_n, $Đ$, and initiator efficiency versus conversion can be seen in Figure 5.2. As expected, the polymerization rate is increased for the BA system due to the higher homopropagation rate coefficient (see Table 5.1). M_n decreases and the initiator efficiency significantly increases when the monomer is changed from BMA to BA, as seen in Figure 5.2b and Figure 5.2c, respectively. As seen above, the initiator efficiency for BA increases to a plateau value around 75%, indicating slow initiation at the low Cu levels studied, although still significantly faster than the BMA system (Figure 5.2d).

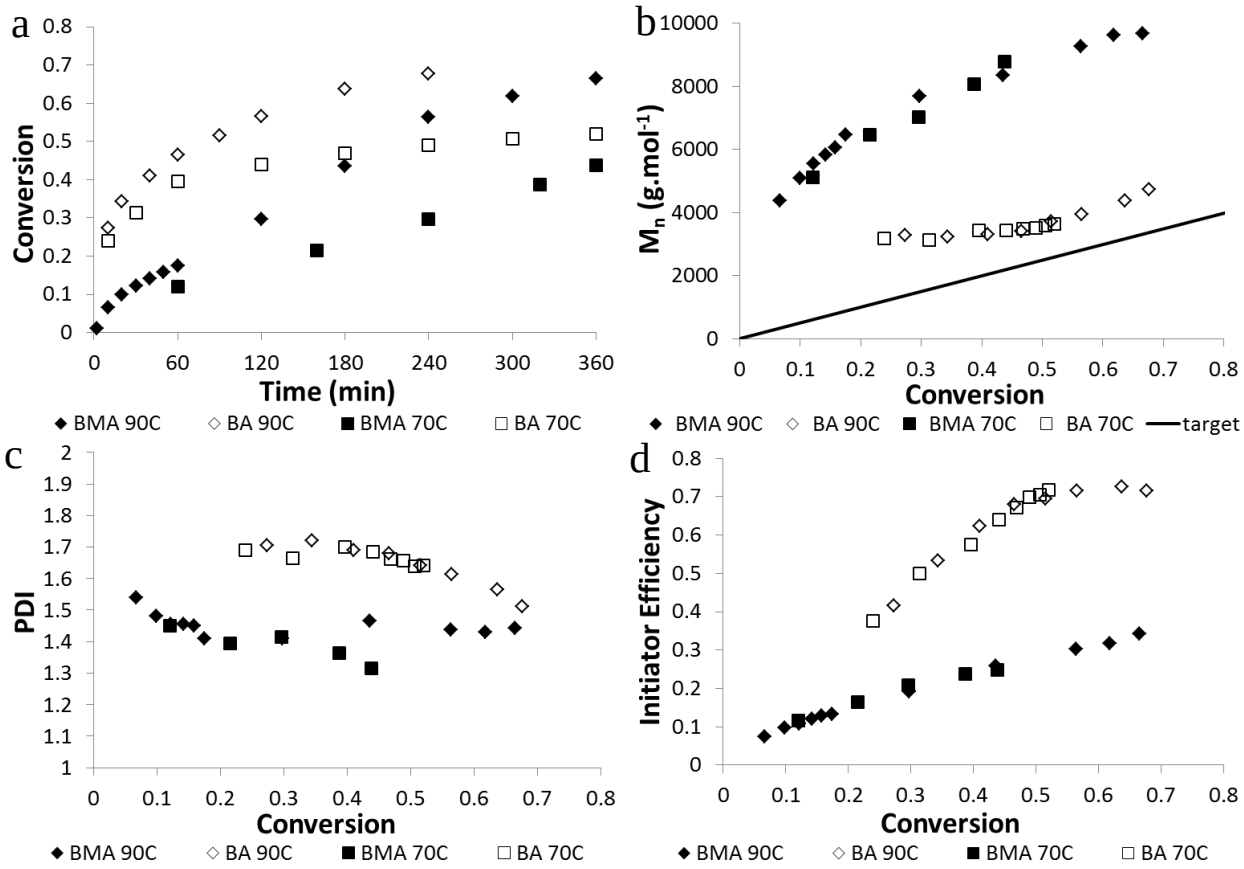

Figure 5.2: Homopolymerization of BMA and BA by ARGET ATRP at 70 °C and 90 °C and TCL = 35(BMA) and 39(BA). Plot of (a) conversion versus time, (b) number-average molar mass (M_n), (c) dispersity ($Đ$), and (d) initiator efficiency versus conversion; initial conditions given as molar ratios of [M]:[EBiB]:[(Cu^{II}TPMABr)Br]:[$Sn(EH)_2$] = 35/39:1:0.00125:0.0125 in all cases for BMA/BA.

5.4.2 Effect of initial comonomer composition in the copolymerization of BMA and BA under ARGET ATRP conditions

To take advantage of the increased initiator efficiency inherently seen in the BA system compared to the BMA system, copolymerizations of the two monomers with different initial monomer compositions were conducted at 70 °C. The results after 6 h of polymerization are summarized in Table 5.4 with the full polymerization profiles presented in Figure 5.3. With

increasing proportions of BA in the comonomer solution, there is a slight increase in the rate of conversion, with only a significant increase observed when a very high amount of 70 wt% BA is used (Figure 5.3a). With up to 50 wt% BA in the comonomer solution there is a small increase in the initiator efficiency (Figure 5.3d). Only with 70 wt% BA does the final sample approach the plateau in initiator efficiency seen for the homopolymerization of BA (see Figure 5.1 and Figure 5.2), indicative of a dominant role of the BMA monomer in the global ARGET ATRP copolymerization kinetics.

Table 5.4: Batch ARGET ATRP of BA and BMA at 70 °C with 30 wt% anisole and TCL = 35.

wt% BA/BMA	Time (min)	Conversion	Mn_{exp} (g mol^{-1})	Initiator Efficiency
0/100[a]	360	0.44	8778	0.25
10/90	360	0.27	7545	0.17
30/70	360	0.30	6225	0.23
50/50	360	0.32	5705	0.26
70/30	360	0.52	4093	0.62

[a]Previously published[12]

Even though the BA addition to BMA has little influence on conversion and initiator efficiency profiles, there is a significant impact on M_n and $Đ$. While adding 10 wt% BA does not create additional chains (M_n profile similar to that for BMA homopolymerization), addition of greater BA levels results in a decrease in the SEC-derived M_n (Figure 5.3b), in agreement with the work of Mueller *et al.*[42] There is also an accompanying increase in $Đ$ with increasing BA content (Figure 5.3c). This phenomenon is also seen in the homopolymerization of BA, but not during BMA homopolymerization,[12] as shown in Figure 5.4. While the distinct oligomeric chains seen in the production of poly(BA) are not seen for the copolymer sample, the low molar mass contribution

is much more evident than for the distribution produced by BMA homopolymerization (same conversion of 0.30).

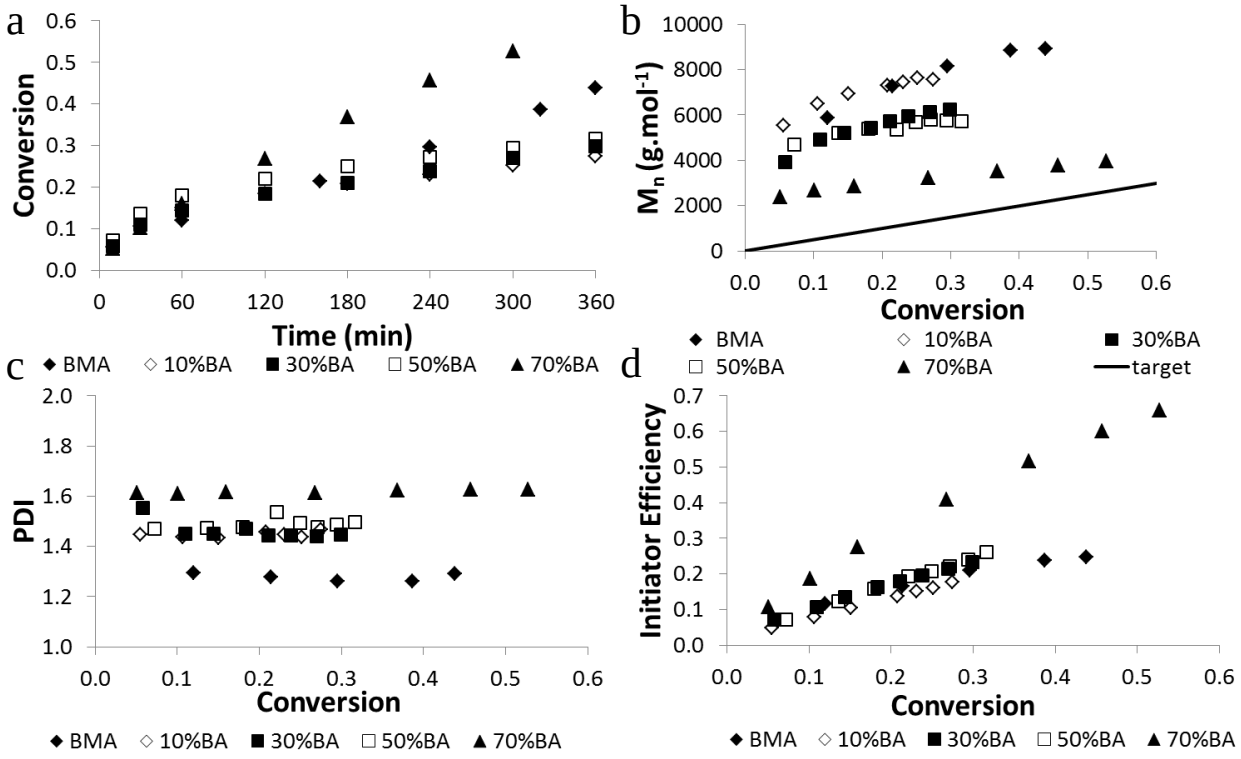

Figure 5.3: Copolymerization of BMA and BA with varying initial comonomer composition (see legend, presented in wt%) by ARGET ATRP at 70 °C and TCL = 35. Plot of (a) conversion versus time, (b) number-average molar mass (M_n), (c) dispersity ($Đ$), and (d) initiator efficiency versus conversion; initial conditions given as molar ratios of [M]:[EBiB]: [(Cu^{II}TPMABr)Br]:[$Sn(EH)_2$] = 35:1:0.00125:0.0125 in all cases.

The GC measurements of residual ATRP initiator (EBiB) for the copolymerization runs are compared to that of BMA homopolymerization in Figure 5.5. It is clear that the consumption is significantly improved with the addition of BA compared to the slow initiation seen in the pure BMA system, although the EBiB consumption rate expressed on a conversion basis is not a function of the initial amount of BA in the system. This increased consumption is reflected in the less

pronounced oligomer formation in the molar mass distributions for the copolymerization experiments (see Figure 5.4c).

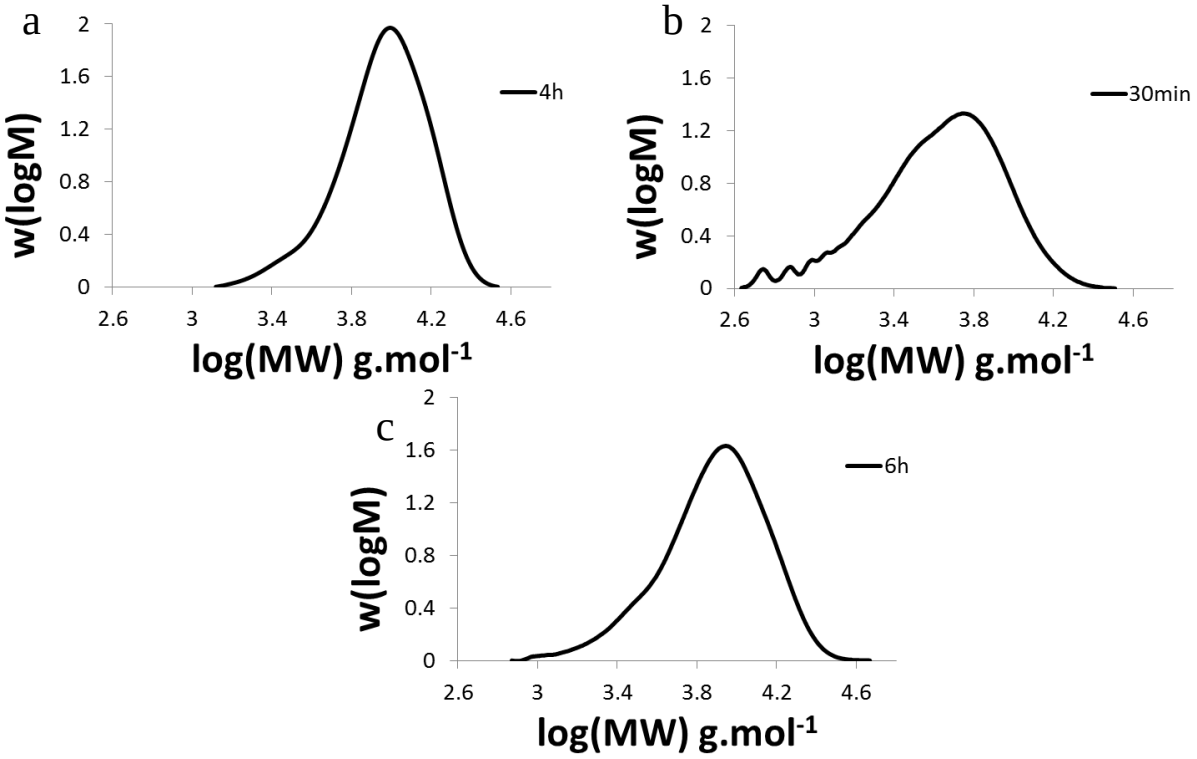

Figure 5.4: Molar mass distribution produced by batch ARGET ATRP at 70 °C and conversion = 0.30: (a) pBMA ; initial [M]:[R-X]:[Cu]:[Sn] = 35:1:0.00125:0.0125 (from Payne *et al.*[12]), (b) pBA; initial [M]:[R-X]:[Cu]:[Sn] = 39:1:0.00125:0.0125, and (c) p(BMA-*co*-BA); initial [M]:[R-X]:[Cu]: [Sn] = 35:1:0.00125:0.0125 with 30 wt% BA in the initial comonomer solution.

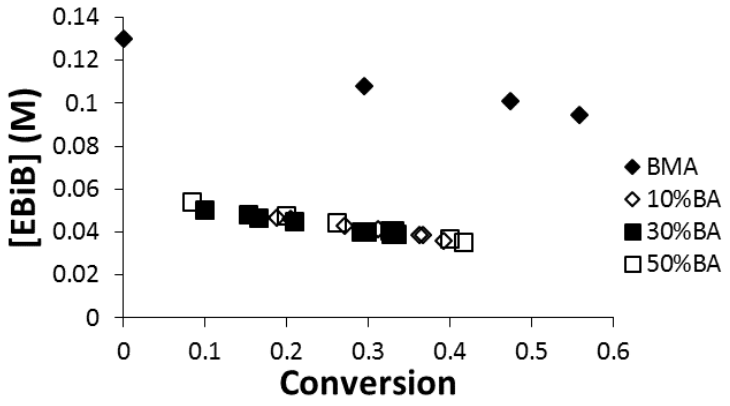

Figure 5.5: Plot of measured ATRP initiator (EBiB) concentration versus conversion for the ARGET ATRP of BMA and BA at 70 °C; see legend for comonomer solution in wt%; initial conditions given as molar ratios of [M]:[EBiB]:[(Cu^{II}TPMABr)Br]:[$Sn(EH)_2$] = 35:1:0.00125:0.0125 in all cases; BMA experiment (35:1:0.00125:0.125) from Payne *et al.*[13]

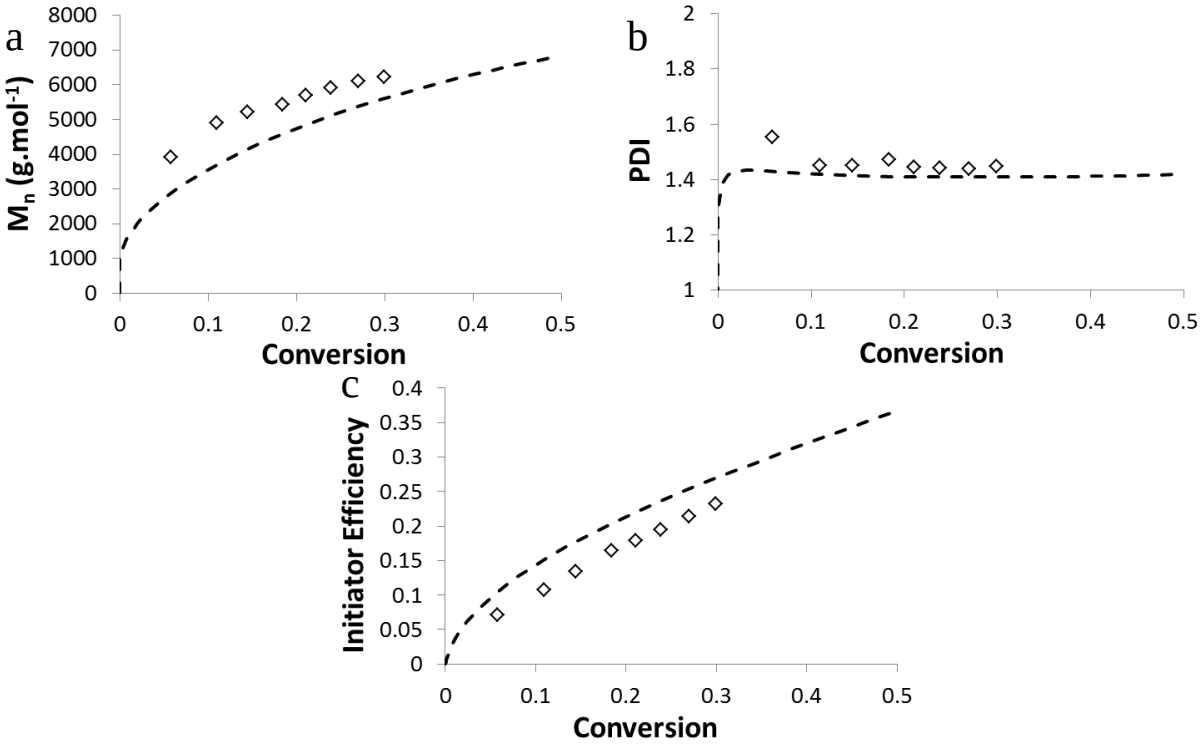

Figure 5.6: Comparison of experimental (points) and simulation data (lines) at 70 °C using model parameters from Table 5.1 for the copolymerization of BMA and BA under ARGET ATRP conditions. Plot of (a) number-average molar mass (M_n), (b) dispersity ($Đ$), and (c) ATRP initiator efficiency versus conversion; initial conditions [M]:[R-X]:[Cu]:[Sn] = 35:1:0.00125:0.0125, 30 wt% BA.

To help analyze these new results, the modeling strategy previously applied to the study of BMA homopolymerization[13] has been extended to the copolymerization system; model details are presented in Table 5.1, as discussed earlier. The focus of the model application is the influence of BA addition on the initiator efficiency. The fit of the kinetic parameters to the experimental copolymerization data is shown in Figure 5.6 to verify the importance of distinct activation/deactivation kinetics for BA and BMA. The effect of slow initiation can be seen in Figure 5.7, in which the simulated explicit copolymer composition is shown for a representative number of polymer chains and different initial feed compositions (10 wt% BA and 50 wt% BA) at an overall

monomer conversion of 0.5 and arranging the dead polymer chains at the top. Note that, as overall monomer conversion is 0.5, the number of monomer units in the polymer chains of the two samples is the same. Hence, for slower initiation (left-hand panel of Figure 5.7), fewer chains result. In both cases still a relatively broad distribution results, in agreement with Figure 5.3c. The effect of this slow initiation on the overall instantaneous incorporation of monomer (Figure 5.8) is, however, limited. Zapata-González *et al*.[43] recently discussed how unequal activation/deactivation kinetics for two monomers may create deviations in CRP from the expected Mayo-Lewis behavior seen in free-radical copolymerization, in particular at low conversions. However, the difference in rate coefficients required is much larger than the BA/BMA coefficients presented in Table 5.1; thus, the simulated composition drift is identical to what is expected from FRP kinetics, as confirmed in Figure 5.8 in which deviations are only occurring at extremely low conversions.

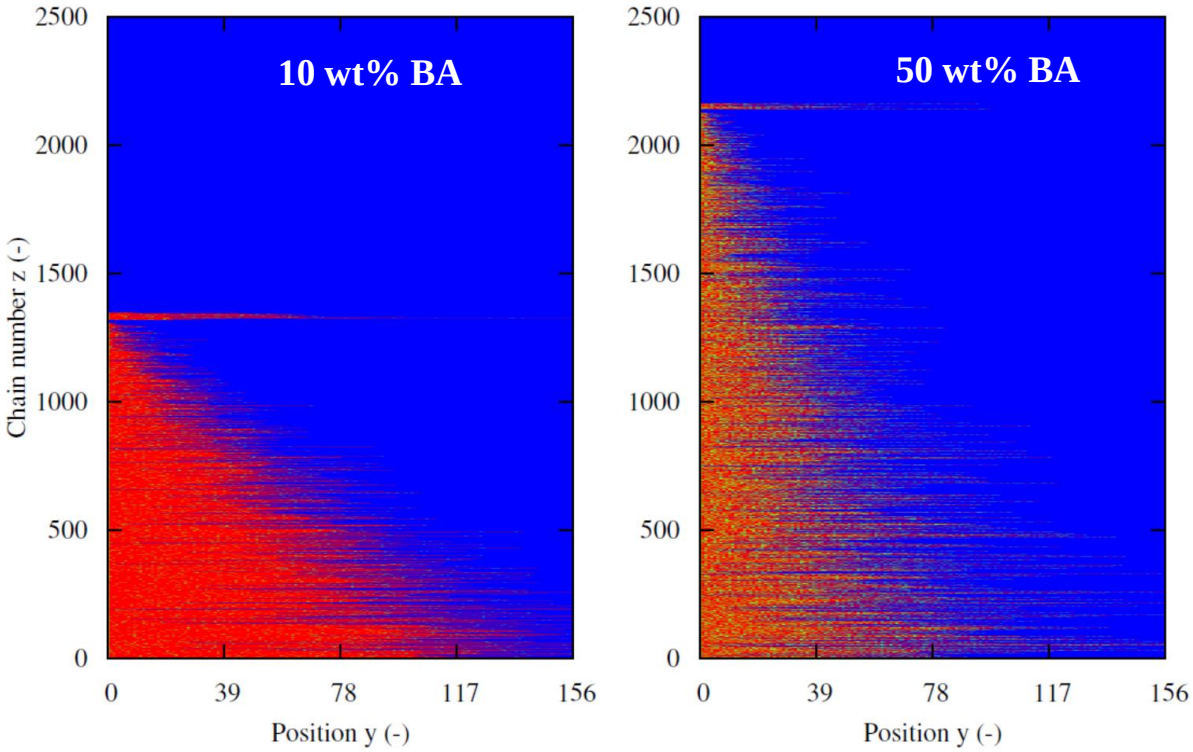

Figure 5.7: Plot of explicit chain composition for a representative number of polymer chains (vertical axis) as a function of position *y* in the chain (horizontal axis) for the ARGET copolymerization of BA and BMA at 70 °C for initial comonomer composition of 10 wt% (left) and 50 wt% (right) BA, respectively. Monomer units are represented as BMA (red) and BA (green); overall conversion: 0.50.

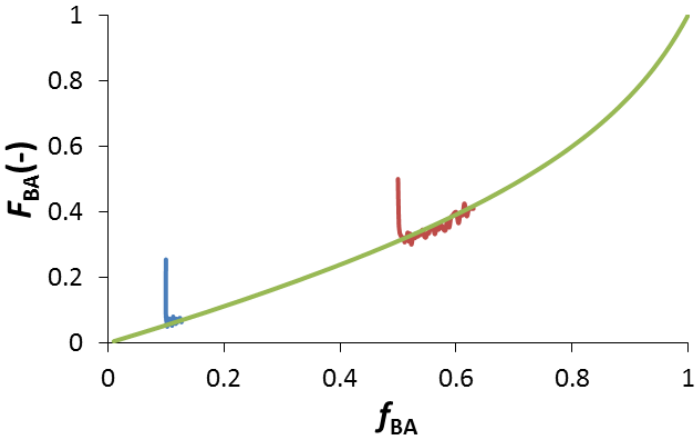

Figure 5.8: Plot of the instantaneous copolymer composition as a function of the initial amount of monomer for the ARGET copolymerization of BA and BMA at 70 °C for initial comonomer composition of 10 wt% (blue) and 50 wt% (red) BA, respectively; green line: Mayo-Lewis equation.

5.4.3 Effect of semi-batch addition of reducing agent in the copolymerization of BMA and BA under ARGET ATRP conditions

To further increase the polymerization rate while improving control over chain length, the copolymerization was conducted with an extra addition of reducing agent in the middle of the polymerization. With an injection of reducing agent, the Cu^{I}/Cu^{II} ratio can be altered by reducing the accumulation of Cu^{II} species. This accumulation of deactivator species was linked to the reduced polymerization rate and initiator efficiency seen in the BMA system by kMC simulations.[13] The final results of the reducing agent injection are presented in Table 5.5, with the full profiles presented in Figure 5.9.

Table 5.5: Batch ARGET ATRP of BA and BMA with additional injection of reducing agent after 3 h of polymerization at 70 °C with 30 wt% anisole and TCL = 39; conditions after reducing agent addition [Cu]:[Sn(EH)$_2$] = 0.00125:0.075.

wt% BA/BMA	Time (min)	Conversion	Mn_{exp} (g mol^{-1})	Initiator Efficiency
30/70	360	0.30	6225	0.23
injection	360	0.44	6707	0.33
50/50	360	0.32	5705	0.26
injection	360	0.53	5701	0.44

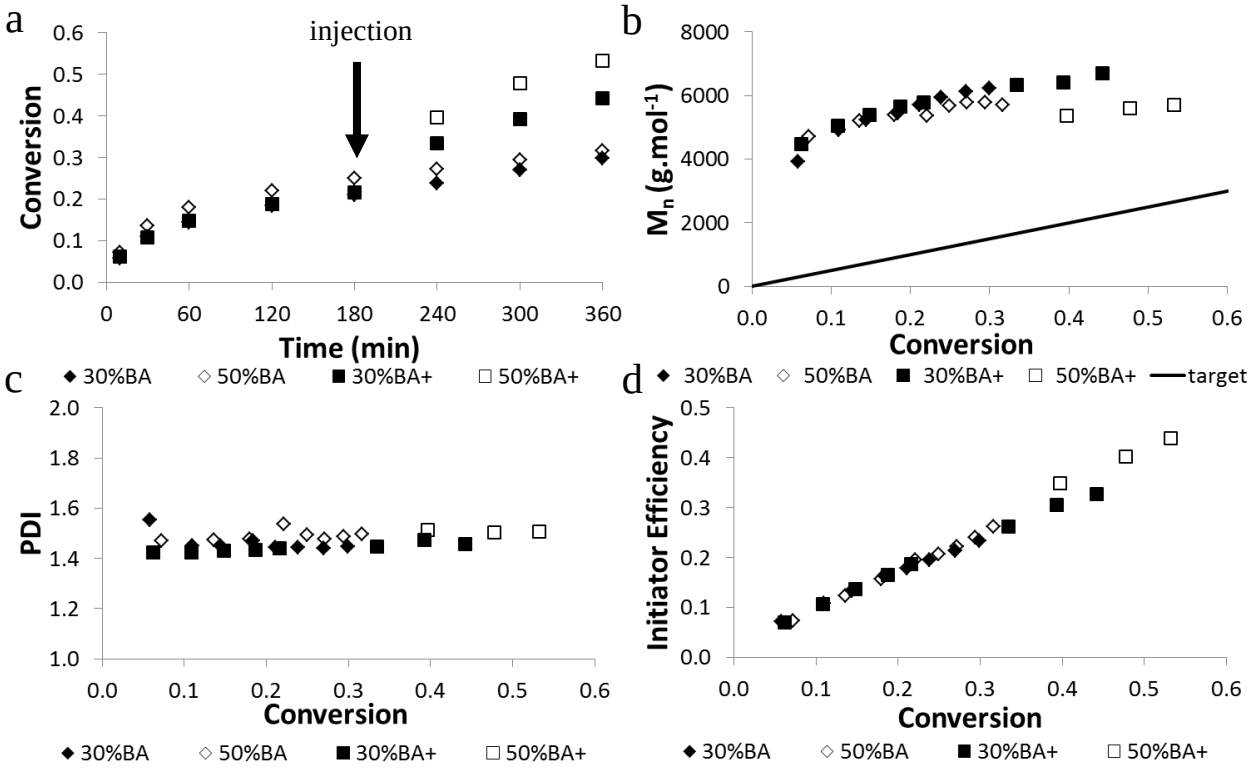

Figure 5.9: Copolymerization of BMA and BA with varying initial comonomer composition and addition of extra reducing agent, denoted as "+", after 3 h (see legend, presented in wt%) by ARGET ATRP at 70 °C and TCL = 35. Plot of (a) conversion versus time, (b) number-average molar mass (M_n), (c) dispersity ($Đ$), and (d) initiator efficiency versus conversion; initial conditions given as molar ratios of [M]:[EBiB]:[(Cu^{II}TPMABr)Br]: [Sn(EH)$_2$] = 35:1:0.00125:0.0125 in all cases (see Table 5.5), conditions after reducing agent addition [Cu]:[Sn(EH)$_2$] = 0.00125:0.075.

From the conversion profile in Figure 5.9a, it is clear that an injection of additional reducing agent results in an increase in polymerization rate. This increase in rate from increased levels of reducing agent is more effective when injected (or added continuously) in small amounts during the polymerization compared to the significant increase in initial reducing agent loading required to achieve an appreciable increase in polymerization rate.[12] The injection of additional reducing agent has negligible impact on the M_n and $Đ$ values (Figure 5.9b and Figure 5.9c, respectively), while the final initiator efficiency is increased due to the polymerization proceeding to higher conversion, allowing further consumption of monomer as well as initiator. Despite the increased polymerization rate, the rate of initiator consumption is not increased as a function of conversion, as shown in Figure 5.10, but follows the rate of decrease seen prior to the injection. Higher EBiB conversions, however, are achieved due to the increased Cu^I levels that result from the addition of the reducing agent.

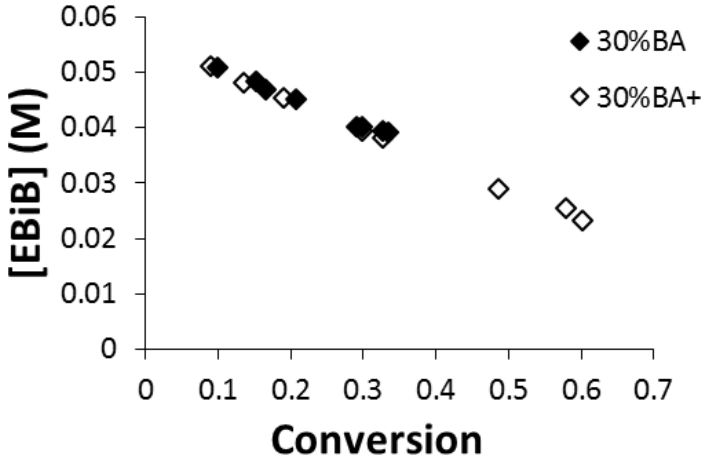

Figure 5.10: Plot of measured ATRP initiator (EBiB) concentration versus conversion for the ARGET ATRP copolymerization of BMA and BA at 70 °C. Injection of additional reducing agent denoted as "+". Initial conditions given as molar ratios of [M]:[EBiB]:[(Cu^{II}TPMABr)Br]: [$Sn(EH)_2$] = 35:1:0.00125:0.0125 in all cases with final conditions after reducing agent addition of [Cu]: [$Sn(EH)_2$] = 0.00125:0.075.

5.5 Conclusions

The homopolymerization of BA under ARGET ATRP conditions shows inherently higher initiator efficiencies and is characterized by higher polymerization rates than the analogous BMA system. Initiator efficiencies reaching a plateau around 75% at low conversion are obtained, in contrast to the slow increase in initiator efficiency throughout the ARGET ATRP when BMA is selected as monomer. Furthermore, reducing the Cu level while maintaining a constant Cu:Sn ratio has negligible impact on the conversion profile, unlike that seen for the BMA system. However, a significant increase in reducing agent loading leads to an increase in the polymerization rate at the low Cu loading for both ARGET ATRP homopolymerizations.

To take advantage of the increased initiator efficiency and polymerization rate with BA, copolymerization with BMA was investigated with the goal of increasing the initiator efficiency with minimal addition of BA. With an increase in initial BA content, M_n was indeed decreased while $Đ$ was increased due to oligomer formation, with negligible impact on the polymerization rate except when very high initial BA amounts (ca. 70 wt%) were considered. With measurements from gas chromatography, the residual ATRP initiator concentration was shown to be significantly lower than seen in the BMA system.

Another strategy for improving the ARGET ATRP is to inject extra reducing agent in the middle of the reaction, i.e. to follow a semi-batch approach. Supplemental addition of a small amount of reducing agent during the reaction leads to a significant increase in conversion while maintaining control over M_n, and $Đ$, and higher initiator efficiency is obtained during the same polymerization time. As a result, the ARGET ATRP process can be tailored to generate the desired process or polymer quality objectives while minimizing the use of excess materials. Further optimization with modeling of continuous processes will be the focus of future work to aid in the potential adoption of ARGET ATRP in an industrially relevant process.

5.6 References

(1) Wang, J.-S.; Matyjaszewski, K. *J. Am. Chem. Soc.* **1995**, *117*, 5614–5615.

(2) Wang, J.-S.; Matyjaszewski, K. *Macromolecules* **1995**, *28*, 7901–7910.

(3) Grimaud, T.; Matyjaszewski, K. *Macromolecules* **1997**, *30*, 2216–2218.

(4) Wang, J.-L.; Grimaud, T.; Matyjaszewski, K. *Macromolecules* **1997**, *30*, 2216–2218.

(5) Matyjaszewski, K. *Macromolecules* **2012**, *45*, 4015–4039.

(6) Stepto, R. F. T. *Pure Appl. Chem.* **2009**, *81*, 351–353.

(7) Jakubowski, W.; Matyjaszewski, K. *Macromolecules* **2005**, *38*, 4139–4146.

(8) Jakubowski, W.; Min, K.; Matyjaszewski, K. *Macromolecules* **2006**, *39*, 39–45.

(9) D'hooge, D. R.; Konkolewicz, D.; Reyniers, M.-F.; Marin, G. B.; Matyjaszewski, K. *Macromol. Theory Simul.* **2012**, *21*, 52–69.

(10) Zhang, Y.; Wang, Y.; Peng, C.; Zhong, M.; Zhu, W.; Konkolewicz, D.; Matyjaszewski, K. *Macromolecules* **2012**, *45*, 78–86.

(11) Destarac, M. *Macromol. React. Eng.* **2010**, *4*, 165–179.

(12) Payne, K. A.; Cunningham, M. F.; Hutchinson, R. A. In *Progress in Controlled Radical Polymerization: Mechanisms and Techniques*; Matyjaszewski, K.; Sumerlin, B. S.; Tsarevsky, N. V., Eds.; ACS Symposium Series, American Chemical Society: Washington, DC, 2012; pp. 183–202.

(13) Payne, K. A.; D'hooge, D. R.; Van Steenberge, P. H. M.; Reyniers, M.-F.; Cunningham, M. F.; Hutchinson, R. A.; Marin, G. B. *Macromolecules* **2013**, *46*, 3828–3840.

(14) Britovsek, G. J. P.; England, J.; White, A. J. P. *Inorg. Chem.* **2005**, *44*, 8125–8134.

(15) Eckenhoff, W. T.; Garrity, S. T.; Pintauer, T. *Eur. J. Inorg. Chem.* **2008**, *2008*, 563–571.

(16) Van Steenberge, P. H. M.; D'hooge, D. R.; Wang, Y.; Zhong, M.; Reyniers, M.-F.; Konkolewicz, D.; Matyjaszewski, K.; Marin, G. B. *Macromolecules* **2012**, *45*, 8519–8531.

(17) Van Steenberge, P. H. M.; Vandenbergh, J.; D'hooge, D. R.; Reyniers, M.-F.; Adriaensens, P. J.; Lutsen, L.; Vanderzande, D. J. M.; Marin, G. B. *Macromolecules* **2011**, *44*, 8716–8726.

(18) Toloza Porras, C.; D'hooge, D. R.; Reyniers, M.-F.; Marin, G. B. *Macromol. Theory Simul.* **2013**, *22*, 136–149.

(19) Van Steenberge, P. H. M.; D'hooge, D. R.; Vandenbergh, J.; Reyniers, M.-F.; Adriaensens, P. J.; Vanderzande, D. J. M.; Marin, G. B. *Macromol. Theory Simul.* **2013**, *22*, 246–255.

(20) Toloza Porras, C.; D'hooge, D. R.; Van Steenberge, P. H. M.; Reyniers, M.-F.; Marin, G. B. *Macromol. React. Eng.* **2013**, *7*, 311–326.

(21) Asua, J. M. *Polymer Reaction Engineering*; Blackwell Publishing, 2007.

(22) Tang, W.; Matyjaszewski, K. *Macromol. Theory Simul.* **2008**, *17*, 359–375.

(23) D'hooge, D. R.; Reyniers, M.-F.; Stadler, F. J.; Dervaux, B.; Bailly, C.; Du Prez, F. E.; Marin, G. B. *Macromolecules* **2010**, *43*, 8766–8781.

(24) Ahmad, N. M.; Charleux, B.; Farcet, C.; Ferguson, C. J.; Gaynor, S. G.; Hawkett, B. S.; Heatley, F.; Klumperman, B.; Konkolewicz, D.; Lovell, P. A.; Matyjaszewski, K.; Venkatesh, R. *Macromol. Rapid Commun.* **2009**, *30*, 2002–2021.

(25) Reyes, Y.; Asua, J. M. *Macromol. Rapid Commun.* **2011**, *32*, 63–67.

(26) Hlalele, L.; Klumperman, B. *Macromolecules* **2011**, *44*, 5554–5557.

(27) Theis, A.; Davis, T. P.; Stenzel, M. H.; Barner-Kowollik, C. *Macromolecules* **2005**, *38*, 10323–10327.

(28) Johnston-Hall, G.; Monteiro, M. J. *J. Polym. Sci., Part A Polym. Chem.* **2008**, *46*, 3155–3173.

(29) Barner-Kowollik, C.; Russell, G. T. *Prog. Polym. Sci.* **2009**, *34*, 1211–1259.

(30) D'hooge, D. R.; Reyniers, M.-F.; Marin, G. B. *Macromol. React. Eng.* **2013**, *7*, 362–379.

(31) Achilias, D. S. *Macromol. Theory Simul.* **2007**, *16*, 319–347.

(32) Tang, W.; Matyjaszewski, K. *Macromolecules* **2007**, *40*, 1858–1863.

(33) Seeliger, F.; Matyjaszewski, K. *Macromolecules* **2009**, *42*, 6050–6055.

(34) Beuermann, S.; Buback, M.; Davis, T. P.; Gilbert, R. G.; Hutchinson, R. A.; Kajiwara, A.; Klumperman, B.; Russell, G. T. *Macromol. Chem. Phys.* **2000**, *201*, 1355–1364.

(35) Wang, W.; Hutchinson, R. A. *AIChE J.* **2011**, *57*, 227–238.

(36) Barth, J.; Buback, M.; Hesse, P.; Sergeeva, T. *Macromolecules* **2009**, *42*, 481–488.

(37) Johnston-Hall, G.; Stenzel, M. H.; Davis, T. P.; Barner-Kowollik, C.; Monteiro, M. J. *Macromolecules* **2007**, *40*, 2730–2736.

(38) Fischer, H.; Paul, H. *Acc. Chem. Res.* **1987**, *20*, 200–206.

(39) Wang, Y.; Kwak, Y.; Buback, J.; Buback, M.; Matyjaszewski, K. *ACS Macro Lett.* **2012**, *1*, 1367–1370.

(40) Buback, M.; Morick, J. *Macromol. Chem. Phys.* **2010**, *211*, 2154–2161.

(41) *Handbook of Radical Polymerization*; Matyjaszewski, K.; Davis, T. P., Eds.; John Wiley & Sons, Inc., Hoboken, 2002; Vol. 125.

(42) Mueller, L.; Jakubowski, W.; Tang, W.; Matyjaszewski, K. *Macromolecules* **2007**, *40*, 6464–6472.

(43) Zapata-González, I.; Hutchinson, R. A.; Matyjaszewski, K.; Saldívar-Guerra, E.; Ortiz-Cisneros, J. *Macromol. Theory Simul.* **2014**, *23*, 245–265.

Chapter 6

Nitroxide-Mediated Polymerization at Elevated Temperatures

Preface

ATRP uses a metal catalyst to control the polymerization, with residual metal needing to be removed from the polymer for most applications. This can further increase the cost of this polymerization if applied to an industrial process. As described in the previous chapters, copper levels can be reduced only by adding larger amounts of reducing agent to the system, with the reduced copper levels also decreasing the efficiency of the ATRP initiator. Another reversible deactivation radical polymerization (RDRP) technique, nitroxide-mediated polymerization (NMP), uses a stable free radical nitroxide species to mediate the polymerization. This nitroxide is incorporated into the polymer, thereby eliminating the need for any post-polymerization processing. For industrial polymerization processes, reaction time and reactor volume play a large role in the economics of the process. As such, it is essential that any RDRP process exhibits a fast polymerization rate. With continuous processes, elevated temperatures can increase polymerization rates, requiring smaller reactor volumes for high throughput. However, nitroxides in the literature have typically moved towards lower temperatures to limit side reactions with monomers other than styrene. It was thus of interest to evaluate the effectiveness of the commercially available nitroxide 2,2,6,6-tetramethyl-1-piperidinyloxy (TEMPO) at temperatures above those previously reported (>140 °C). An experimental method was developed using Low Pressure/Vacuum (LPV) NMR tubes, which facilitated the study of the impact of nitroxide concentration on the thermal polymerization of styrene at elevated temperatures. As summarized as Appendix B, the stability of the nitroxide and an analogue 4-oxo-TEMPO at these elevated temperatures was shown to be limited by a UV-Vis analysis. As a potential solution, a thermal initiator was added to increase the rate of polymerization and maintain control during the short lifetime of the nitroxides. Ultimately,

it was determined that the current nitroxides available are not effective mediating agents at elevated temperatures due to their insufficient stability. A full description of this investigation is summarized in Appendix B.

From the study of TEMPO and 4-oxo-TEMPO as mediating agents for the thermal polymerization of styrene, it was determined that the nitroxides currently available are not effective at elevated temperatures above 140 °C due to increased decomposition of the nitroxide. These elevated temperatures allow an increased polymerization rate while obtaining the unique products of RDRP, an attractive combination for a continuous industrial process, where the increased polymerization rates lead to high throughput in smaller reactor volumes. In collaboration with Dr. Jon Debling (BASF Corp.) and Dr. Peter Nesvadba (BASF Schweiz AG), a novel nitroxide that is thermally stable to above 200 °C (provided by BASF) was evaluated to assess its effectiveness as a mediating agent in NMP. The corresponding alkoxyamine was used to effectively polymerize styrene and butyl acrylate up to 200 °C. The target chain length was altered with varying concentrations of alkoxyamine in both systems, with polymerization rate independent of alkoxyamine concentration. The results in this section are published as a communication in ACS Macro Letters (2015, vol.4, 280-283). The introduction from the publication is expanded for this chapter to include an introduction to NMP with TEMPO in addition to the novel alkoxyamine. Supporting Information can be found in Appendix C.

Abstract

A new alkoxyamine based on a highly thermally stable nitroxide is used for the controlled polymerization of styrene and butyl acrylate at temperatures up to 200 °C. High monomer conversions are reached in a few minutes with a linear increase in polymer chain-length with conversion, a final dispersity (Đ) of ~1.2, and successful chain-extension of the resulting material. The alkoxyamine concentration was altered to target various chain lengths, with autopolymerization dictating the polymerization rate of styrene regardless of alkoxyamine concentration. Controlled polymerization of methacrylate monomers and acrylic acid was successful with the addition of styrene. The new material opens the possibility to increase the range of specialty products made for applications in coatings, inks, overprint varnishes and adhesives.

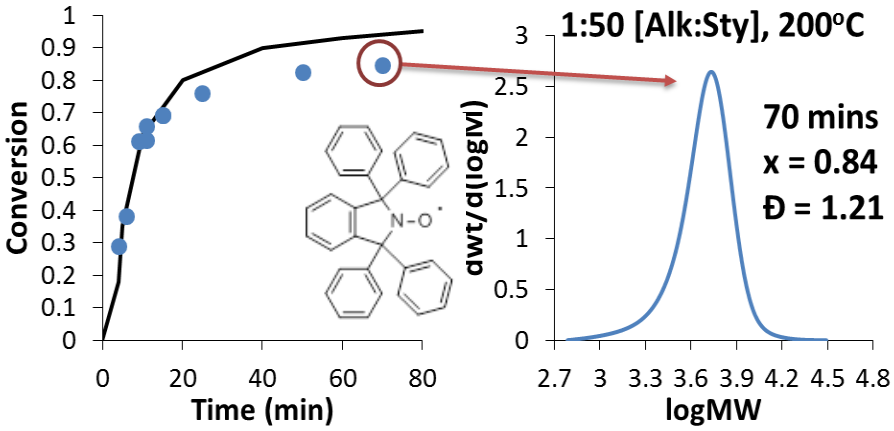

6.1 Introduction

The first mention of nitroxide-mediated polymerization (NMP) was by the group of Solomon and coworkers, whose seminal work with the use of 2,2,6,6-tetramethylpiperidinyl-1-oxy (TEMPO) as a radical trap led to further development by Georges *et al.* to produce polystyrene (PS) resins with low dispersities.[1–4] As with other RDRP (reversible-deactivation radical polymerization) methods, the mechanism involves the reversible trapping of the propagating radical (R•) by the stable free nitroxide (Y•) to produce the dormant species or (macro)alkoxyamine (R_n-Y). The forward activation (decomposition) reaction is significantly slower than the reverse deactivation (cross-coupling) reaction such that the radical species concentration is lowered, facilitating control over the polymerization due to the suppression of termination and other side reactions. However, some bimolecular termination is unavoidable, leading (in the absence of newly generated radicals) to an excess of the persistent radical (Y•) as described by the persistent radical effect.[5]

Unlike atom transfer radical polymerization (ATRP) or reverse addition-fragmentation chain transfer (RAFT), NMP does not require removal of a transition metal from the final polymer or the use of undesirable thio-based mediating agents. NMP is particularly appealing as the nitroxide is a stable free radical species that is reversibly incorporated in the polymer. Additionally, the polymerization can be initiated by a thermal initiator and nitroxide (bimolecular initiation) or an alkoxyamine (unimolecular initiation). A variety of nitroxide/initiator and alkoxyamine systems have been studied to improve the polymerization rate or control the polymerization of other monomers, with a nice summary by Nicolas *et al.*.[6] The nitroxide to initiator ratio in a bimolecular system is crucial in determining the kinetics of the polymerization after the initiation step, as an increase in excess nitroxide leads to the activation-deactivation equilibrium shifting towards dormant species and reducing the polymerization rate. A consequence of using thermal initiators is that the precise number of chains that are generated in the system is not known, leading to less than

ideal end group functionality and difficulty reproducing polymerization kinetics. This led to the development of alkoxyamines, which decompose to generate one initiating alkyl fragment and one stable free nitroxide species. As a result, improved control over the molar mass and the molar mass distribution (MMD) was achieved compared to the bimolecular system.[7] For the styrene system, early NMP work used only a nitroxide and thermal initiator such as benzoyl peroxide (BPO) to generate an alkoxyamine *in-situ* which would mediate the radicals that are continually produced by thermal initiation. In this system, with an excess of nitroxide, an induction period is expected until sufficient thermal initiation has occurred to consume the excess nitroxide, and the polymerization can proceed. The induction period can then be tuned based on the level of nitroxide added and the polymerization temperature.[8–10]

The inability for TEMPO to effectively mediate monomers other than styrene was circumvented with the development of other nitroxides such as 2,2,5-trimethyl-4-phenyl-3-azahexane-3-oxyl (TIPNO)[11] and N-*tert*-butyl-N-[1-diethylphosphono-(2,2-dimethylpropyl)] nitroxide (DEPN or SG1).[12,13] This inspired a diversity of nitroxides and alkoxyamines (as summarized in the review paper of Nicolas *et al*.[6]), allowing the successful NMP of methyl methacrylate (MMA),[14,15] *n*-butyl acrylate (BA),[16] and acrylic acid (AA),[17] among other monomers. The need to minimize H-transfer to the nitroxide during the polymerization of methacrylates[14,18,19] has been achieved through copolymerization with styrene or acrylonitrile and by the synthesis of alkoxyamines that have a low dissociation temperature due to long-range polar effects.[14,15,20,21]

While promising developments have been witnessed, the widespread industrial application of NMP has remained elusive due to the need to tailor the alkoxyamine/nitroxide to the reaction conditions.[22] Typical polymerization temperatures for NMP of styrene with TEMPO have not exceeded 125-145 °C due to the elevated rate of alkoxyamine homolysis.[23] Nitroxides in the literature trend towards lower temperatures as a means to limit competitive side reactions and operate under emulsion polymerization conditions.[24–26] To the best of our knowledge, no one has

pursued NMP for application at the elevated temperature conditions (>150 °C) used to produce commercial low molecular weight (MW) materials. In particular, continuous processes at elevated temperatures facilitate better temperature control, with high reaction rates allowing the use of small reactors for high output.[27] Providing tailored MW acrylic resins with low viscosity arising from low dispersities, as well as novel materials such as macromers and block copolymers, will extend the range of commercial products with applications in coatings, inks, varnishes, and adhesives. Herein, we describe the development and application of alkoxyamines **1** and **2** based on a nitroxide **3** (Scheme 6.1) to control polymerizations at higher temperatures.

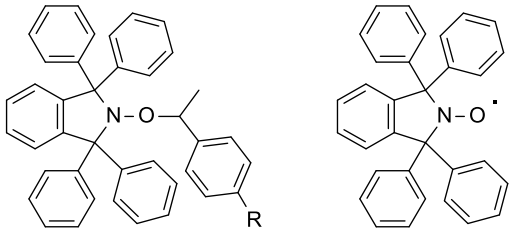

1, R = H
2, R = *tert*-Butyl

3

Scheme 6.1: Alkoxyamines 1, 2 and the nitroxide 3

6.2 Results

6.2.1 High Temperature NMP of Bulk Styrene

A range of alkoxyamine concentrations were used to generate polystyrene (PS) of target chain lengths (TCL) between 25 and 300 from bulk monomer at 160 °C. Figure 6.1 plots the monomer conversion profiles and evolution of polymer chain length and dispersity for Alkoxyamine-**2**; as shown in Supporting Information (Appendix C), results for Alkoxyamine-**1** were similar. There is no appreciable effect of alkoxyamine concentration on the conversion profiles, which closely follow that expected from styrene thermal polymerization in the absence of controlling agent.[28] The control of reaction rate by thermal polymerization is expected from previous literature, where an increase in initiator (alkoxyamine) concentration increases rate only

slightly even at high concentrations.[29,30] The measured polymer number-average molar masses (M_n) are in excellent agreement with target values for experiments with TCL of 100 or lower, with final polymer dispersities ($Đ$) of less than 1.2 (Figure 6.1b).

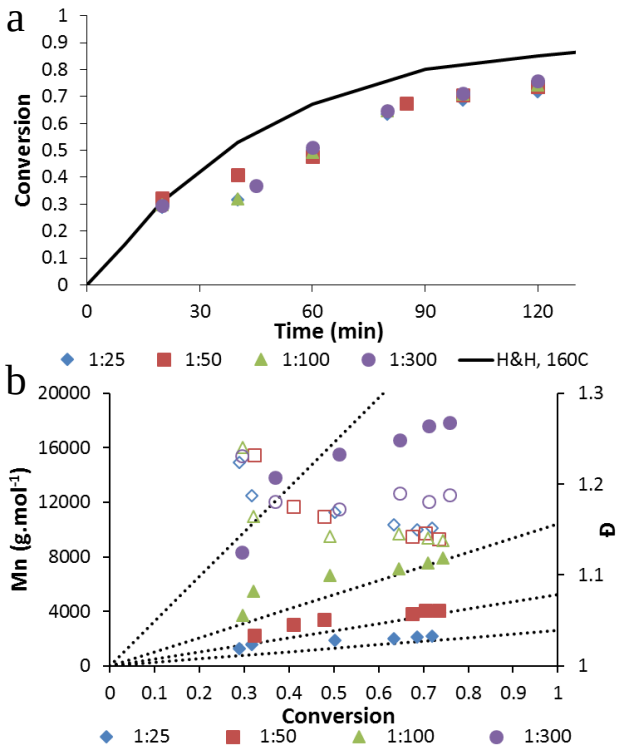

Figure 6.1: Batch NMP of bulk styrene at 160 °C, with initial alkoxyamine-2/styrene molar ratios presented in the legend: (a) conversion versus time and (b) number-average molar mass (M_n, closed symbols) and dispersity ($Đ$, open symbols) versus conversion. Thermal polymerization profile ("H&H" line) included for comparison.[28]

The efficacy of alkoxyamine-**2** for NMP at elevated temperatures was studied between 140 °C and 200 °C for a TCL of 50. The polymerization rate is greatly accelerated with increasing temperature, with 70% conversion achieved in 15 min (Figure 6.2a), still in agreement with the thermal polymerization profiles reproduced from the experimental data of Hui and Hamielec (H&H).[28] The M_n profiles with conversion remain linear with $Đ$ values at 1.2 (Figure 6.2b), indicating that good control is maintained even at 200 °C. Indeed, this unprecedented combination

of fast reaction rate and excellent control strongly suggests that this family of alkoxyamines can be used at even higher temperatures, beyond our current experimental capabilities. The unusual thermostability of nitroxide **3** can be explained by its cyclic structure and the presence of the strong aromatic C-H bonds.

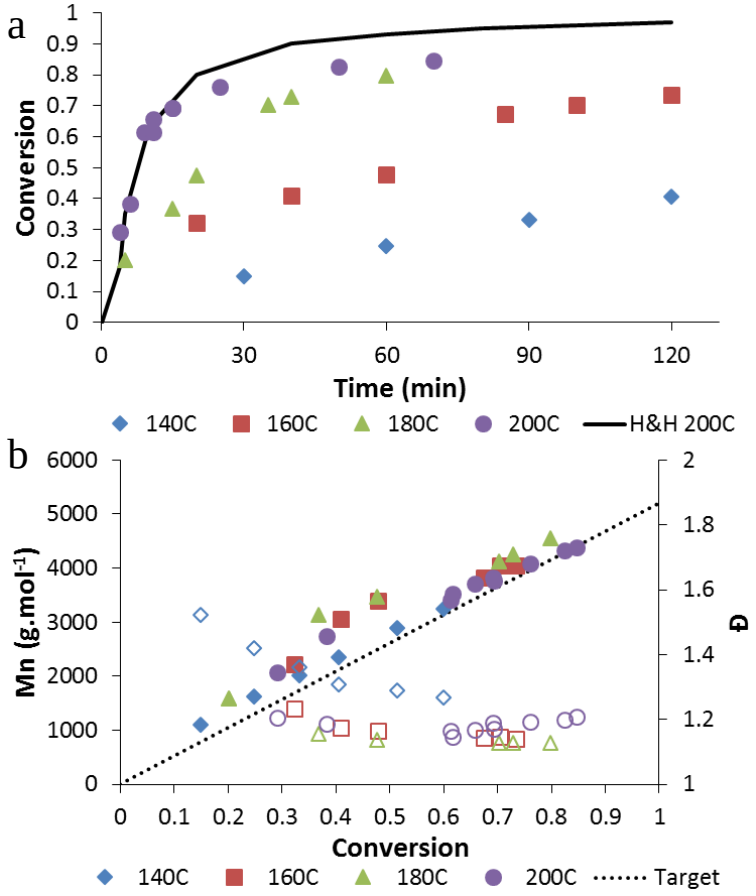

Figure 6.2: Batch NMP of bulk styrene at various reaction temperatures (see legend), with initial alkoxyamine-2/styrene molar ratio of 1:50: (a) conversion versus time and (b) number-average molar mass (M_n, closed symbols) and dispersity ($Đ$, open symbols) versus conversion. Thermal polymerization profile at 200 °C ("H&H" line) included for comparison.[28]

6.2.2 Butyl Acrylate

The ability of the **3**-based alkoxyamines to mediate *n*-butyl acrylate (BA) has also been investigated. The experiments with alkoxyamine-**1** were conducted in the presence of 50 vol% DMF to overcome the poor solubility of the material in monomer at room temperature (see Supporting Information, Appendix C). However, alkoxyamine-**2** was entirely soluble at room temperature, enabling the study of BA bulk homopolymerization over the same range of conditions examined for styrene. Results at varying temperatures for a constant TCL = 55 are presented in Figure 6.3, with further results for the variation of TCL included as Supporting Information (Appendix C).

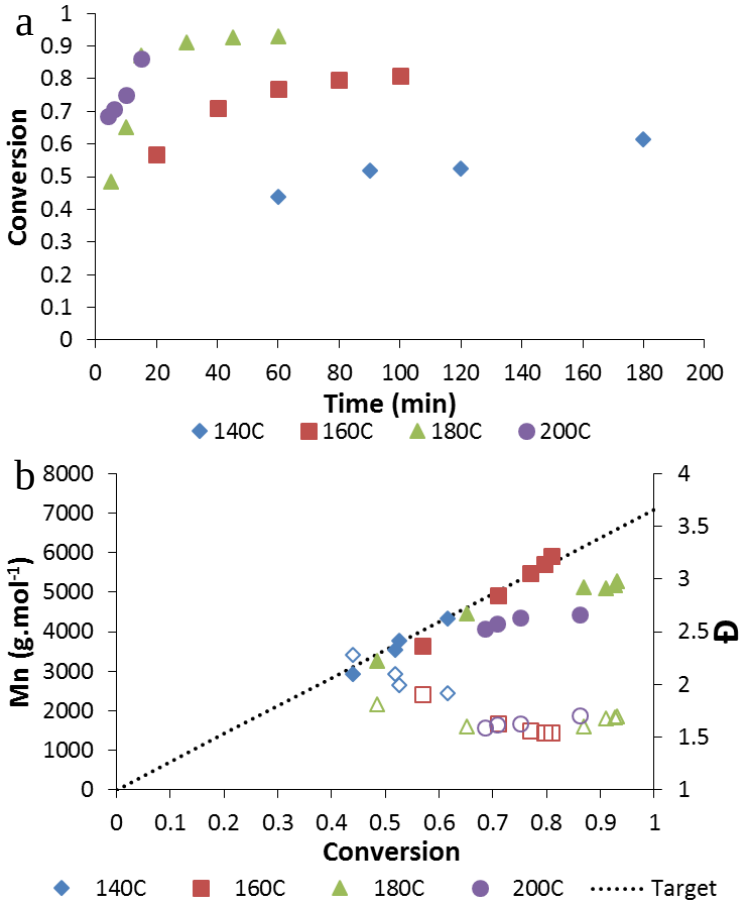

Figure 6.3: Batch NMP of bulk BA at various reaction temperatures (see legend), with initial alkoxyamine-2/BA molar ratio of 1:55: (a) conversion versus time and (b) number-average molar mass (M_n, closed symbols) and dispersity ($Đ$, open symbols) versus conversion.

The BA results are very promising, with reaction rates even faster than those of styrene; as shown in Figure 6.3a, monomer conversion of almost 90% is achieved in 15 min at 200 °C. MW control remains good, with the highest dispersity found at 140 °C (Figure 6.3b), suggesting the alkoxyamine activation/deactivation kinetics are more favourable for control at higher temperatures, as also seen for styrene. However, final $Đ$ values were 1.5-1.6, a result seen in the broader molar mass distributions (MMDs) of poly(BA) compared to PS in Figure 6.4. This result is likely related to the significantly faster propagation kinetics of BA compared to styrene; in

addition, the MMD is broadened by the slower alkoxyamine initiation in the acrylate system, as seen by the slowly disappearing peak at log(MW) = 2.8. Interestingly, no evidence of branching could be detected by ^{13}C NMR, even for the poly(BA) produced at 200 °C (see Supporting Information, Appendix C), a result consistent with other reversible deactivation radical polymerization (RDRP) processes,[31] for which it is hypothesized that fast deactivation suppresses the backbiting mechanism compared with conventional free radical polymerization.[32,33]

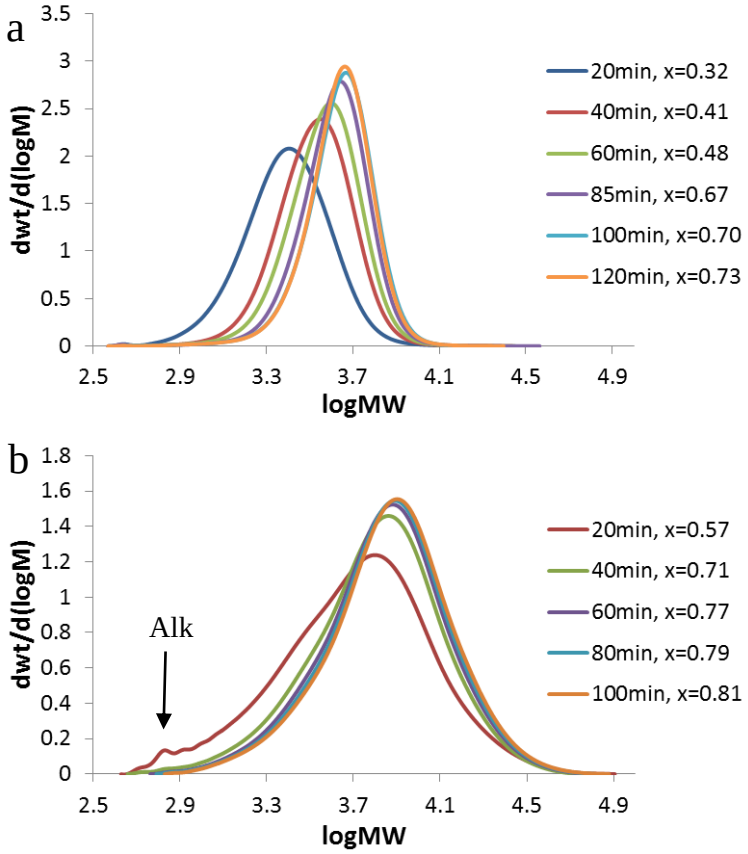

Figure 6.4: Molar mass distribution resulting from bulk NMP at 160 °C of (a) styrene and (b) butyl acrylate with initial alkoxyamine-2/monomer molar ratios of 1:50 (styrene) and 1:55 (butyl acrylate); polymerization time and conversion presented in the legend.

In addition, first experiments have been conducted with other monomers of interest. As detailed in the Supporting Information (Appendix C), excellent control is achieved for

copolymerization of acrylic acid with styrene ($Đ$ = 1.3 produced with 90% conversion in 60 min at 160 °C), and even some measure of control is achieved at 160 °C for bulk *n*-butyl methacrylate polymerized with 10 mol% styrene.

A chain extension experiment of PS of chain length 39 (produced at 160 °C) extended to 370 was run in order to demonstrate livingness with alkoxyamine-**1**. As shown in Figure 6.5, over an order-of-magnitude increase in MW was achieved with no obvious low MW tail observed and a $Đ$ value of 1.4, thus demonstrating the high end group functionality of the polystyrene macromer.

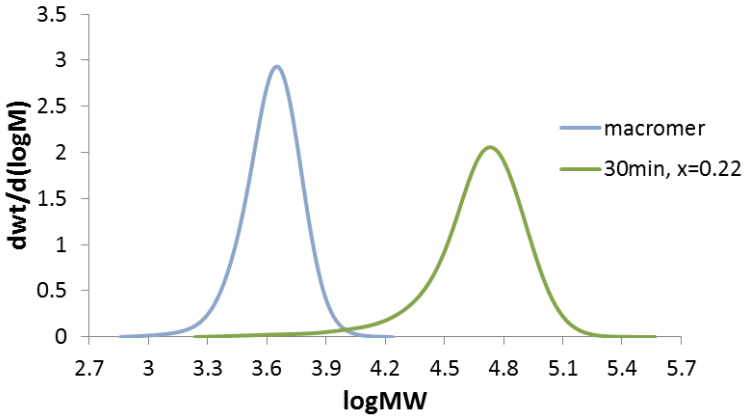

Figure 6.5: Molar mass distribution resulting from chain extension of PS by bulk NMP at 160 °C of styrene; polymerization time and conversion presented in the legend.

6.3 Conclusions

Herein we report the ability of alkoxyamines **1** and **2** based on a highly thermally stable nitroxide **3** to mediate polymerizations at high temperature, providing excellent control of both styrene and BA bulk homopolymerization over a range of TCLs and up to 200 °C, with polymer dispersities of 1.2 for styrene and 1.5 for butyl acrylate. The results indicate that the alkoxyamine should exhibit good control at even higher temperatures, which will further decrease the time required (less than 15 min at 200 °C) to achieve high conversions. Livingness has been verified by

chain extension experiments, demonstrating the potential to produce block copolymers in continuous reactors under high temperature conditions.

6.4 Experimental

6.4.1 Synthesis of the alkoxyamines

Alkoxyamine-**1** was prepared as described by Hafner *et al*..[34] The novel alkoxyamine-**2** was made by CuBr promoted radical coupling of the nitroxide **3** with 1-(1-bromoethyl)-4-*tert*-butylbenzene (See Supporting Information in Appendix C).[35,36]

The nitroxide 1,1,3,3-tetraphenylisoindoline-*N*-oxyl **3** was prepared by oxidation of 1,1,3,3-tetraphenylisoindoline with *m*-chloroperbenzoic acid.[34] Alternatively, **3** can be made via oxidation of *N*-benzyl-1,1,3,3-tetraphenylisoindoline with *m*-chloroperbenzoic acid.[37] The nitroxide **3,** a red solid, mp 250-253 °C, is remarkably thermally stable, a sample of **3** remaining unchanged (TLC and HPLC) after being heated for 7 h at 200 °C under air.

6.4.2 Polymerization

Styrene (Sigma Aldrich) was passed through a prepacked column (Aldrich) to remove the 4-*tert*-butylcatechol inhibitor and stored in the freezer prior to reaction. Stock solutions were prepared under nitrogen by adding uninhibited styrene to the alkoxyamine in a ChemGlass AirFree 50mL round-bottom flask. 0.2 mL of stock solution was added to Low Pressure/Vacuum (LPV) NMR tubes (Wilmad-LabGlass) using a 1 mL glass syringe. For alkoxyamine-**1**, it was necessary to heat the stock solution to 70 °C in a water bath to ensure solubility; no polymerization occurred, as confirmed by ^{1}H NMR. The LPV NMR tubes were subjected to 4 freeze-pump-thaw cycles and sealed under nitrogen (<1 atm) using a Schlenk line and liquid nitrogen, to prevent monomer boiling during reaction at elevated temperature. The tubes were kept refrigerated until use and were suspended in a silicone oil bath to start the polymerization. The reaction was stopped at designated times by removing the tube and immersing in an ice bath for 30 s, with each tube used as an

individual sample to reconstruct a complete polymerization profile. Monomer conversions were determined by ^{1}H NMR analysis using a Bruker Avance-400 (400 MHz) instrument after adding deuterated chloroform (Aldrich). Size exclusion chromatography (SEC) was performed as described in the Supporting Information (Appendix C).

6.5 References

(1) Solomon, D. H.; Rizzardo, E.; Cacioli, P. Polymerization Process and Polymers Produced Thereby. US 4581429, 1986.

(2) Moad, G.; Solomon, D. H. *The Chemistry of Free Radical Polymerization*; Elsevier Science: Oxford, 1995; Vol. 42.

(3) Solomon, D. H. *J. Polym. Sci., Part A Polym. Chem.* **2005**, *43*, 5748–5764.

(4) Georges, M. K.; Veregin, R. P. N.; Kazmaier, P. M.; Hamer, G. K. *Macromolecules* **1993**, *26*, 2987–2988.

(5) Fischer, H. *Chem. Rev.* **2001**, *101*, 3581–3610.

(6) Nicolas, J.; Guillaneuf, Y.; Lefay, C.; Bertin, D.; Gigmes, D.; Charleux, B. *Prog. Polym. Sci.* **2013**, *38*, 63–235.

(7) Hawker, C. J.; Barclay, G. G.; Orellana, A.; Dao, J.; Devonport, W. *Macromolecules* **1996**, *29*, 5245–5254.

(8) Veregin, R. P. N.; Odell, P. G.; Michalak, L. M.; Georges, M. K. *Macromolecules* **1996**, *29*, 3346–3352.

(9) Veregin, R. P. N.; Odell, P. G.; Michalak, L. M.; Georges, M. K. *Macromolecules* **1996**, *29*, 2746–2754.

(10) Zhang, M.; Ray, W. H. *J. Appl. Polym. Sci.* **2002**, *86*, 1630–1662.

(11) Benoit, D.; Chaplinski, V.; Braslau, R.; Hawker, C. J. *J. Am. Chem. Soc.* **1999**, *121*, 3904–3920.

(12) Le Mercier, C.; Lutz, J.-F.; Marque, S. R. A.; Le Moigne, F.; Tordo, P.; Lacroix-Desmazes, P.; Boutevin, B.; Couturier, J.-L.; Guerret, O.; Martschke, R.; Sobek, J.; Fischer, H. In *Controlled/Living Radical Polymerization*; ACS Symposium Series, American Chemical Society: Washington, DC, 2000; pp. 108–122.

(13) Benoit, D.; Grimaldi, S.; Robin, S.; Finet, J.-P.; Tordo, P.; Gnanou, Y. *J. Am. Chem. Soc.* **2000**, *122*, 5929–5939.

(14) Guillaneuf, Y.; Gigmes, D.; Marque, S. R. A.; Astolfi, P.; Greci, L.; Tordo, P.; Bertin, D. *Macromolecules* **2007**, *40*, 3108–3114.

(15) Greene, A. C.; Grubbs, R. B. *Macromolecules* **2009**, *42*, 4388–4390.

(16) Studer, A.; Harms, K.; Knoop, C. A.; Müller, C.; Schulte, T. *Macromolecules* **2004**, *37*, 27–34.

(17) Couvreur, L.; Lefay, C.; Belleney, J.; Charleux, B.; Guerret, O.; Magnet, S. *Macromolecules* **2003**, *36*, 8260–8267.

(18) Georges, M. K.; Lukkarila, J. L.; Szkurhan, A. R. *Macromolecules* **2004**, *37*, 1297–1303.

(19) Chauvin, F.; Dufils, P.-E.; Gigmes, D.; Guillaneuf, Y.; Marque, S. R. A.; Tordo, P.; Bertin, D. *Macromolecules* **2006**, *39*, 5238–5250.

(20) Charleux, B.; Nicolas, J.; Guerret, O. *Macromolecules* **2005**, *38*, 5485–5492.

(21) Nicolas, J.; Brusseau, S.; Charleux, B. *J. Polym. Sci., Part A Polym. Chem.* **2010**, *48*, 34–47.

(22) Destarac, M. *Macromol. React. Eng.* **2010**, *4*, 165–179.

(23) Goto, A.; Kwak, Y.; Yoshikawa, C.; Tsujii, Y.; Sugiura, Y.; Fukuda, T. *Macromolecules* **2002**, *35*, 3520–3525.

(24) Jing, Y.; Mardyukov, A.; Bergander, K.; Daniliuc, C. G.; Studer, A. *Macromolecules* **2014**, *47*, 3595–3602.

(25) Edeleva, M. V.; Parkhomenko, D. A.; Morozov, D. A.; Dobrynin, S. A.; Trofimov, D. G.; Kanagatov, B.; Kirilyuk, I. A.; Bagryanskaya, E. G. *J. Polym. Sci., Part A Polym. Chem.* **2014**, *52*, 929–943.

(26) Guo, Y.; Zetterlund, P. B. *ACS Macro Lett.* **2012**, *1*, 748–752.

(27) Campbell, J. D.; Kaai, M.; Mori, Y.; Pekarik, A. J.; Srisiri-Sisson, W.; Villalobos, M. A. Process for the continuous production of gel free polymers, and powder and liquid coating applications containing gel free polymers. US 6552144, 2003.

(28) Hui, A. W.; Hamielec, A. E. *J. Appl. Polym. Sci.* **1972**, *16*, 749–769.

(29) Schulte, T.; Knoop, C. A.; Studer, A. *J. Polym. Sci., Part A Polym. Chem.* **2004**, *42*, 3342–3351.

(30) Catala, J.-M.; Bubel, F.; Hammouch, S. O. *Macromolecules* **1995**, *28*, 8441–8443.

(31) Ahmad, N. M.; Charleux, B.; Farcet, C.; Ferguson, C. J.; Gaynor, S. G.; Hawkett, B. S.; Heatley, F.; Klumperman, B.; Konkolewicz, D.; Lovell, P. A.; Matyjaszewski, K.; Venkatesh, R. *Macromol. Rapid Commun.* **2009**, *30*, 2002–2021.

(32) Reyes, Y.; Asua, J. M. *Macromol. Rapid Commun.* **2011**, *32*, 63–67.

(33) Ballard, N.; Rusconi, S.; Akhmatskaya, E.; Sokolovski, D.; de la Cal, J. C.; Asua, J. M. *Macromolecules* **2014**, *47*, 6580–6590.

(34) Hafner, A.; Kirner, Hans, J.; Schwarzenbach, F.; Van Der Schaaf, P. A.; Nesvadba, P. Process for the Synthesis of Amine Ethers from Secondary Amino Oxides. WO/2001/092228, 2001.

(35) Matyjaszewski, K.; Woodworth, B. E.; Zhang, X.; Gaynor, S. G.; Metzner, Z. *Macromolecules* **1998**, *31*, 5955–5957.

(36) Kitano, Y.; Manoda, T.; Miura, T.; Chiba, K.; Tada, M. *Synthesis* **2006**, 405–410.

(37) Chan, K. S.; Li, X. Z.; Lee, S. Y. *Organometallics* **2010**, *29*, 2850–2856.

Chapter 7

NMP of Styrene in Batch and CSTR at Elevated Temperatures: Modeling Experimental Trends

Preface

In order to better understand the batch NMP of styrene at elevated temperatures with the thermally stable nitroxide-based alkoxyamine, a kinetic model was developed and implemented in the commercially available Predici© software package. The model, based on a previous model developed for another alkoxyamine and different experimental conditions, was used to estimate the activation/deactivation kinetics of the novel alkoxyamine. The model successfully captures the experimental behavior witnessed from the batch study of styrene, where polymerization rate is independent of alkoxyamine concentration. The model also gives insight into the end group functionality of the polymer throughout the polymerization.

The model reactor configuration was converted from batch to continuous stirred-tank (CSTR) and applied to analysis of the experimental data that was acquired at BASF Corp. in Wyandotte, Michigan using the same parameters from the batch study. This is the first known implementation of NMP in a CSTR. Supporting Information can be found in Appendix D.

7.1 Introduction

Nitroxide-mediated polymerization (NMP) is one method of reversible deactivation radical polymerization (RDRP) that has been studied extensively in the literature, with a comprehensive summary provided by Nicolas *et al.*.[1] The polymerization is initiated by a thermal initiator and mediated by a stable free nitroxide (bimolecular initiation) or by an alkoxyamine (unimolecular initiation). Use of alkoxyamine allows for good control over the number of chains in the system, with a 1:1 ratio of initiating alkyl fragment and nitroxide generated from the homolysis that occurs at increased temperature. Typically, nitroxides and alkoxyamines in the literature have trended towards lower reaction temperatures in order to minimize side reactions and to help mitigate the higher propagation rate coefficients of certain monomers.[2–6] In the coatings industry, increased environmental regulations have required lower solvent content, which is achieved through increased polymerization temperatures in the production of short chain polymers. The increased polymerization temperature also facilitates smaller reaction volumes for continuous production of polymers with high throughput. It would therefore be of interest to industry if an alkoxyamine (and corresponding nitroxide) can be synthesized that is able to effectively mediate polymerizations at elevated temperatures. Payne *et al.* recently demonstrated the successful mediation of styrene and butyl acrylate polymerizations up to 200 °C using a novel alkoxyamine based on a thermally stable nitroxide.[7] The conversion profile was found to be independent of alkoxyamine concentration, suggesting that the polymerization rate is driven by thermal initiation of styrene. Good control of the molecular weight (MW) was obtained up to a target chain length (TCL) of 100, at which point the decreased alkoxyamine concentration is unable to provide enough nitroxide to mediate the increased contribution from thermally generated chains.

Kinetic modeling is a useful tool to help the interpretation of RDRP systems, in addition to predicting polymer properties which may be unavailable experimentally. NMP has been modelled extensively in the literature for batch, semi-batch, and continuous tubular reactor

configurations,[8–16] with limited theoretical work done considering a continuous stirred-tank reactor (CSTR).[8,17–19] Theoretical and experimental CSTR studies have been conducted with atom transfer radical polymerization (ATRP) and reversible addition-fragmentation chain transfer (RAFT) systems,[20–27] but no known work has been done with NMP experimentally. It is therefore of interest to develop a model to represent the batch polymerization kinetics of NMP at elevated temperatures and then apply it to CSTR operation in an effort to successfully implement NMP in an industrially relevant process.

7.2 Experimental

Batch NMP was conducted as described by Payne *et al*..[7] Studies of continuous polymerization were conducted in a 100 mL stainless steel CSTR manufactured by Parr (model 4655).[28] The feed to the reactor was controlled by a Scientific Systems, Series II pump (240SFP01). Product from the reactor was evaporated in a flash unit operating under vacuum at 635mmHg. Conversion was measured using GC using a Waters 2695 Separations Module equipped with a Waters 2487 Dual Absorbance Detector and Waters 2414 Refractive Index Detector. Molecular weight data were obtained from a Waters 2695 instrument coupled with a Waters 2410 Refractive Index Detector. One pair of PLGEL MIXED B columns with one guard column were used. Millennium software was used to determine the number-average molar mass (M_n), and weight-average molar mass (M_w) of the polymer obtained from the CSTR.

7.3 Kinetic Model

Using known parameters from the literature for radical styrene polymerization, the RDRP activation-deactivation rate coefficients were estimated using the commercially available Predici® software package. A kinetic model developed for MAMA-SG1 and styrene was used as a basis for the development.[13] Preliminary values were chosen to give the closest fit to the experimental data using the parameter estimation features available in the Predici® package. Next, a box search was

conducted within reasonable limits of the activation-deactivation rate coefficients from parameter estimation, considering values previously estimated for the styrene/TEMPO system[29] and choosing estimated values of deactivation that were below the small-molecule termination limit of $k_{t,11}$ = 1.1 × 10^9 L mol^{-1} s^{-1} from Fischer *et al.*.[30] From this box search it was determined that the activation-deactivation kinetics of the alkoxyamine had minimal impact on the simulation results once an adequate set of dormant polymeric species activation-deactivation rate coefficients had been found (see Appendix D). Finally, fine tuning of the parameters was conducted by refitting the data at each temperature with fixed alkoxyamine activation/deactivation parameters to generate an Arrhenius plot. This parameter estimation was conducted with experimental data ranging from 140 °C to 200 °C with a constant alkoxyamine/styrene loading of 1:50, and a range of alkoxyamine concentrations at 160 °C, as presented by Payne *et al.*.[7] The final parameters used in the model are presented in Table 7.1, with conventional free radical mechanisms from the literature, and the estimated activation-deactivation rate coefficients and corresponding Arrhenius estimates.

Table 7.1: Reactions and Arrhenius parameters for the simulation of NMP of styrene; subscript "o" relates to alkoxyamine/alkyl fragment.

			A ($L\ mol^{-1}\ s^{-1}$)	E_a ($J\ mol^{-1}$)	Value at 160 °C	Ref.
NMP activation/deactivation						
R_o-Y	$\xrightarrow{k_{a,o}}$	$R_o\bullet$ + $Y\bullet$	9.60×10^{6}	7.93×10^{4}	2.58×10^{-3}	*a*
R_i-Y	$\xrightarrow{k_{a}}$	$R_i\bullet$ + $Y\bullet$	8.10×10^{8}	9.13×10^{4}	7.97×10^{-3}	*a*
$R_o\bullet$ + $Y\bullet$	$\xrightarrow{k_{da,o}}$	R_o-Y	7.20×10^{8}	0	7.20×10^{8}	*a*
$R_i\bullet$ + $Y\bullet$	$\xrightarrow{k_{da}}$	R_i-Y	2.31×10^{7}	0	2.31×10^{7}	*a*
Thermal Initiation						
M + M	$\xrightarrow{k_{1}}$	DA	4.74×10^{5}	9.35×10^{4}	2.51×10^{-6}	12,31,b
DA	$\xrightarrow{k_{-1}}$	M + M	1.05×10^{2}	4.43×10^{4}	4.77×10^{-4}	12,31
DA + M	$\xrightarrow{k_{i}}$	$ST_1\bullet$ + $ST_2\bullet$	1.51×10^{6}	9.95×10^{4}	2.58×10^{-3}	12,31
$ST_1\bullet$ + M	$\xrightarrow{k_{p}}$	$P_2\bullet$	4.27×10^{6}	3.25×10^{4}	5.14×10^{3}	32
$ST_2\bullet$ + M	$\xrightarrow{k_{p}}$	$P_3\bullet$	4.27×10^{6}	3.25×10^{4}	5.14×10^{3}	32
Propagation						
$R_o\bullet$ + M	$\xrightarrow{k_{p,o}}$	$R_1\bullet$	6.70×10^{6}	1.65×10^{4}	6.86×10^{4}	33,34
$R_i\bullet$ + M	$\xrightarrow{k_{p}}$	$R_{i+1}\bullet$	4.27×10^{6}	3.25×10^{4}	5.14×10^{3}	32
Chain Transfer						
$R_i\bullet$ + M	$\xrightarrow{k_{trm}}$	Dead + M$\bullet$	2.31×10^{6}	5.30×10^{4}	9.33×10^{-1}	35
$R_i\bullet$ + DA	$\xrightarrow{k_{trDA}}$	P_i + $P_2\bullet$	6.76×10^{5}	2.75×10^{4}	3.27×10^{2}	36,37
Irreversible Termination[c]						
$R_o\bullet$ + $R_o\bullet$	$\xrightarrow{k_{t,11}^{app}}$	R_o-R_o				
$R_i\bullet$ + $R_o\bullet$	$\xrightarrow{k_{t,i1}^{app}}$	P_i + P_0				
$R_i\bullet$ + $R_j\bullet$	$\xrightarrow{k_{tc,ij}^{app}}$	P_{i+j}				
$R_i\bullet$ + $R_j\bullet$	$\xrightarrow{k_{td,ij}^{app}}$	P_i + P_j				

[a]This work. [b]DA = Diels-Alder adduct. [c]For termination: fraction of termination by combination is 0.99; apparent termination rate coefficients are used based on RAFT-CLD-T measurements with styrene (composite k_t model; Equation 7-1 to Equation 7-7, where $\alpha_s = 0.51$, $\alpha_l = 0.16$, and $i_{SL} = 30$);[38–41] for termination between macroradicals with chain length of one and alkyl fragment radicals at zero conversion a value of 1.1×10^{9} L mol^{-1} s^{-1} is used (also denoted $k_{t,11}^{app}$).[30]

In the kinetic Monte Carlo procedure used by Van Steenberge *et al.*,[42] the termination behavior is described through a population-weighted apparent rate coefficient in which the terminating radicals are randomly selected taking into account their individual concentration and apparent termination reactivity. The individual (chain length dependent) apparent termination rate coefficients ($k_{t,ij}^{app}$; i, j: chain length) are calculated as a function of conversion (x) via a composite k_t model:[43,44]

$$\text{for } i < i_{gel} \text{ and } i < i_{SL}: k_{t,ii}^{app} = k_{t,11}^{app} i^{-\alpha_s} \quad \textbf{Equation 7-1}$$

$$\text{for } i < i_{gel} \text{ and } i \geq i_{SL}: k_{t,ii}^{app} = k_{t,11}^{app} i_{SL}^{\alpha_l - \alpha_s} i^{-\alpha_l} \quad \textbf{Equation 7-2}$$

$$\text{for } i \geq i_{gel} \text{ and } i < i_{SL}: k_{t,ii}^{app} = k_{t,11}^{app} i_{gel}^{\alpha_{gel} - \alpha_s} i^{-\alpha_{gel}} \quad \textbf{Equation 7-3}$$

$$\text{for } i \geq i_{gel} \text{ and } i < i_{SL}: k_{t,ii}^{app} = k_{t,11}^{app} i_{SL}^{\alpha_l - \alpha_s} i_{gel}^{\alpha_{gel} - \alpha_l} i^{-\alpha_{gel}} \quad \textbf{Equation 7-4}$$

$$k_{t,ij}^{app} = \sqrt{k_{t,ii}^{app} k_{t,jj}^{app}} \quad \textbf{Equation 7-5}$$

$$i_{gel} = 3.3 x_p^{-2.13} \quad \textbf{Equation 7-6}$$

$$\alpha_{gel} = 1.22 x_p - 0.11 \quad \textbf{Equation 7-7}$$

where x is the conversion, i_{gel} the characteristic chain length at the onset of the gel regime, α_s the short chain power law exponent in dilute solution, α_l the long chain power law exponent in dilute solution, i_{SL} the dilute solution crossover chain length when power laws for termination change from short to long chains, and α_{gel} the power law exponent for termination in the gel regime.[43,44] This formulation has been implemented in the Predici® model using the parameter values from Fierens *et al.*,[13] and will be compared to the case where a constant value of k_t^{app} is assumed (4.18×10^8 L mol^{-1} s^{-1} at 160 °C[38]).

7.4 Results

7.4.1 Batch NMP of styrene

Figure 7.1 compares the simulation fits to experimental data at varying polymerization temperatures where a constant termination rate coefficient (k_t^{app}) is considered and diffusional limitations are neglected. The model is able to capture the expected change in polymerization rate with temperature with a minimal impact on number-average molar mass (M_n) and dispersity ($Đ$), as found experimentally. The model predicts that an increased polymerization rate leads to a decrease in the end group functionality (EGF), as is expected from Zhong *et al.*.[45]

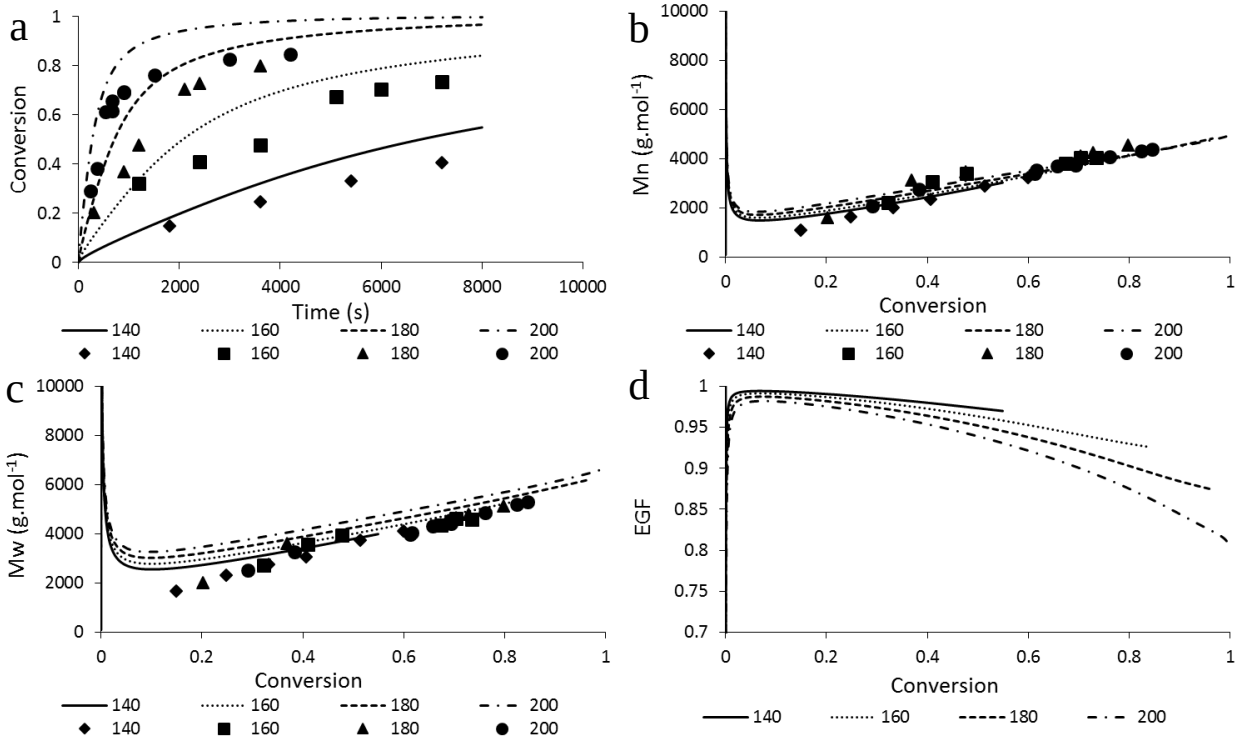

Figure 7.1: Comparison of experimental (symbols) and simulation data (lines) for batch NMP of styrene with a constant ratio of alkoxyamine/styrene of 1:50 and varying temperature (see legend). Plot of (a) conversion versus time, (b) number-average molar mass (M_n), (c) weight-average molar mass (M_w), and (d) end group functionality versus conversion. Model parameters from Table 7.1 using constant k_t^{app};[38] experimental data from Payne *et al.*.[7]

The comparison of simulation and experimental data across a range of temperatures while considering diffusional limitations is presented in Figure 7.2. It can be seen that chain length dependent (CLD) termination is not required to represent the data, and that neglecting the diffusional limitations in the model (Figure 7.1) even results in closer agreement between the simulated and the experimental conversion data.

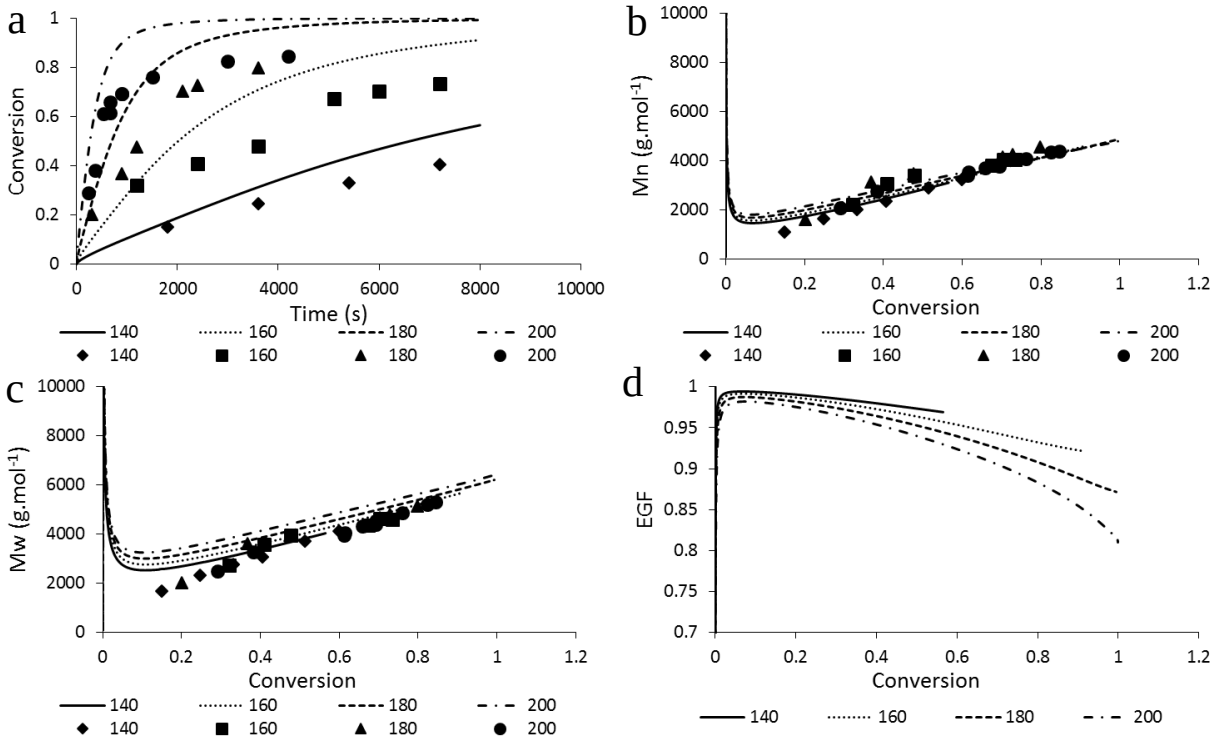

Figure 7.2: Comparison of experimental (symbols) and simulation data (lines) for batch NMP of styrene at 160 °C with varying temperature (see legend). Plot of (a) conversion versus time, (b) number-average molar mass (M_n), (c) weight-average molar mass (M_w), and (d) end group functionality versus conversion. Model parameters from Table 7.1 while accounting for diffusional limitations (composite k_t according to Equation 7-1 to Equation 7-7); experimental data from Payne *et al.*.[7]

The model was also used to predict the effect of varying alkoxyamine concentration or target chain length (TCL) at 160 °C. The results are presented in Figure 7.3 with a constant k_t^{app} and Figure 7.4 with consideration of diffusional limitations (CLD termination).

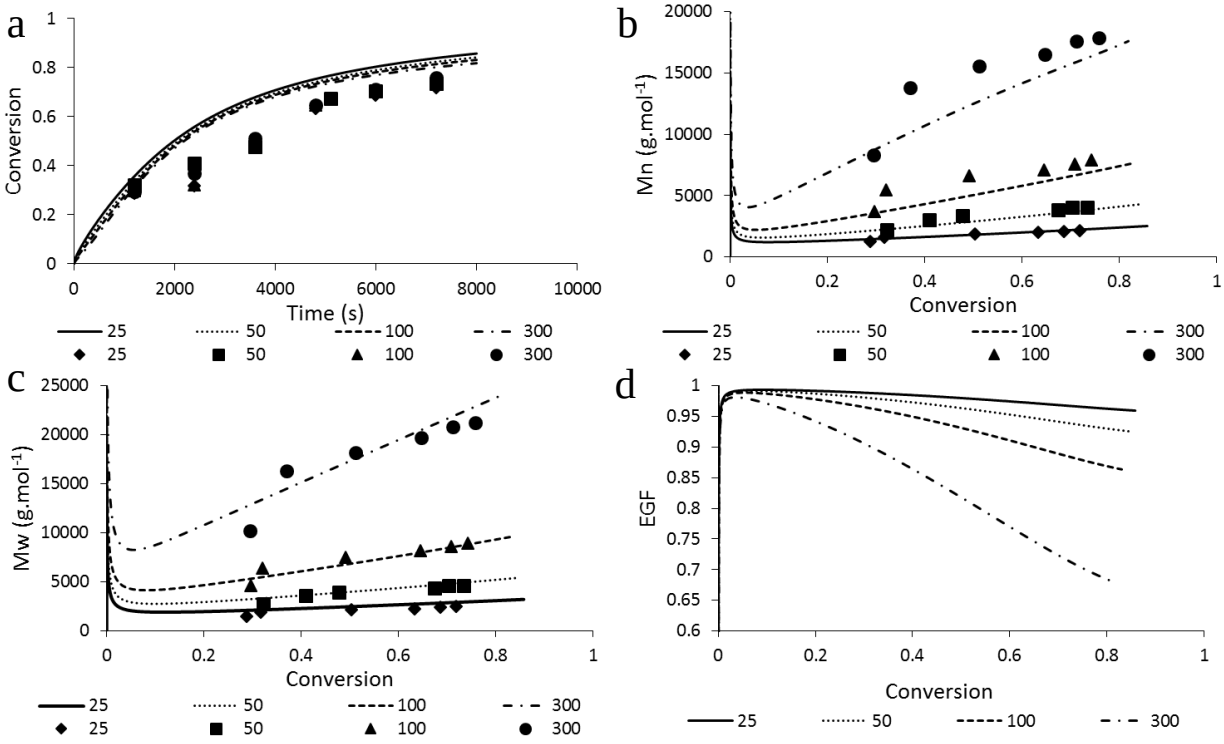

Figure 7.3: Comparison of experimental (symbols) and simulation data (lines) for batch NMP of styrene at 160 °C with varying ratios of alkoxyamine/styrene (or TCL, see legend). Plot of (a) conversion versus time, (b) number-average molar mass (M_n), (c) weight-average molar mass (M_w), and (d) end group functionality versus conversion. Model parameters from Table 7.1 using constant k_t^{app};[38] experimental data from Payne *et al.*.[7]

The model is able to effectively simulate the change in TCL with various alkoxyamine concentrations at 160 °C (Figure 7.3b). The model also depicts negligible change in polymerization rate with alkoxyamine concentration, as witnessed experimentally (Figure 7.3a), and predicts a decrease in EGF with increasing TCL, consistent with literature findings.[45]

When considering diffusional limitations, the model is able to effectively predict the change in M_n with varying alkoxyamine concentrations (Figure 7.4b), while simulating an expected decrease in EGF with increasing TCL (Figure 7.4d). However, the conversion profile is predicted to change with alkoxyamine concentration, inconsistent with experimental findings (Figure 7.4a). As a result, diffusional limitations are not considered for further modeling results. To verify that diffusional limitations can be neglected, a box search was conducted with diffusional limitations and compared to a box search neglecting chain length dependent termination (see Appendix D).

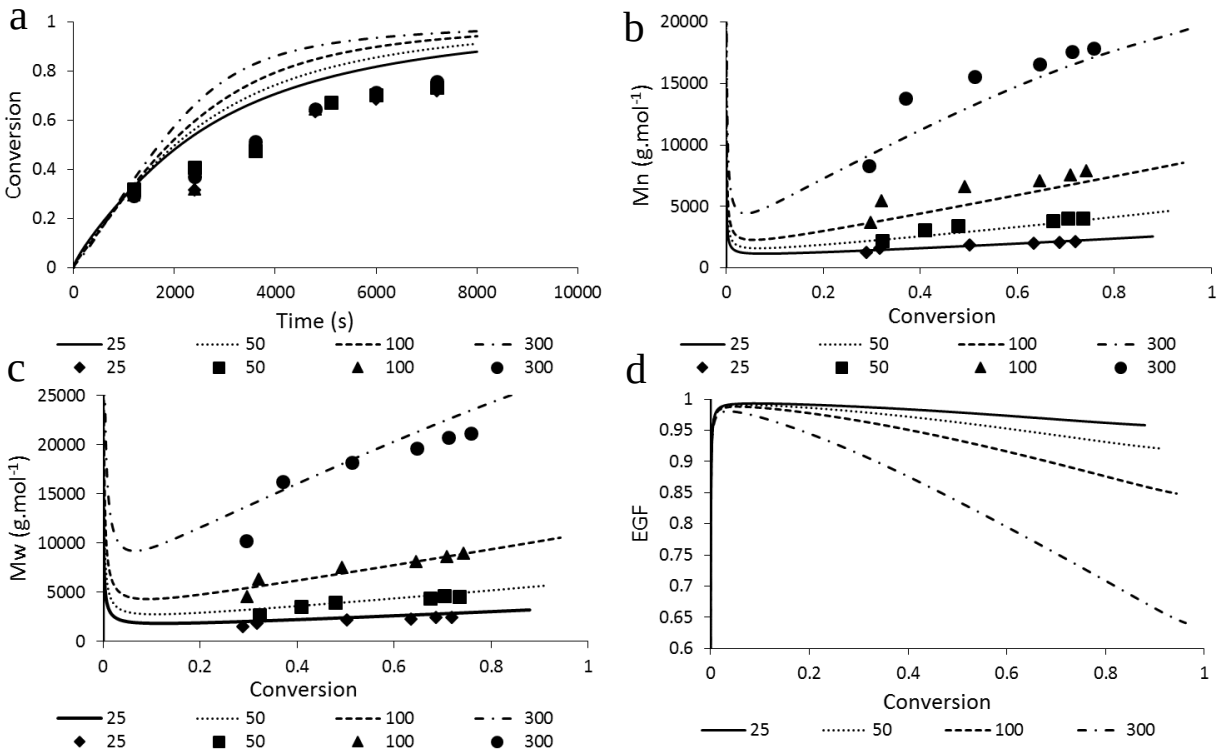

Figure 7.4: Comparison of experimental (symbols) and simulation data (lines) for batch NMP of styrene at 160 °C with varying ratios of alkoxyamine/styrene (or TCL, see legend). Plot of (a) conversion versus time, (b) number-average molar mass (M_n), (c) weight-average molar mass (M_w), and (d) end group functionality versus conversion. Model parameters from Table 7.1 while accounting for diffusional limitations (composite k_t according to Equation 7-1 to Equation 7-7); experimental data from Payne *et al.*.[7]

7.4.2 Sensitivity of k_a/k_{da} for alkoxyamine and polymer

From Table 7.1, it can be seen that the alkoxyamine activation/deactivation coefficients ($k_{a,o}/k_{da,o}$) are distinct from the polymeric activation/deactivation coefficients (k_a/k_{da}), as has been shown in other NMP models that represent experimental data with alkoxyamine as the initiator.[11,13] To demonstrate the sensitivity of the distinct rate activation rate coefficients for the alkoxyamine and polymer species, Figure 7.5 depicts varying the effects of different alkoxyamine activation rate coefficients.

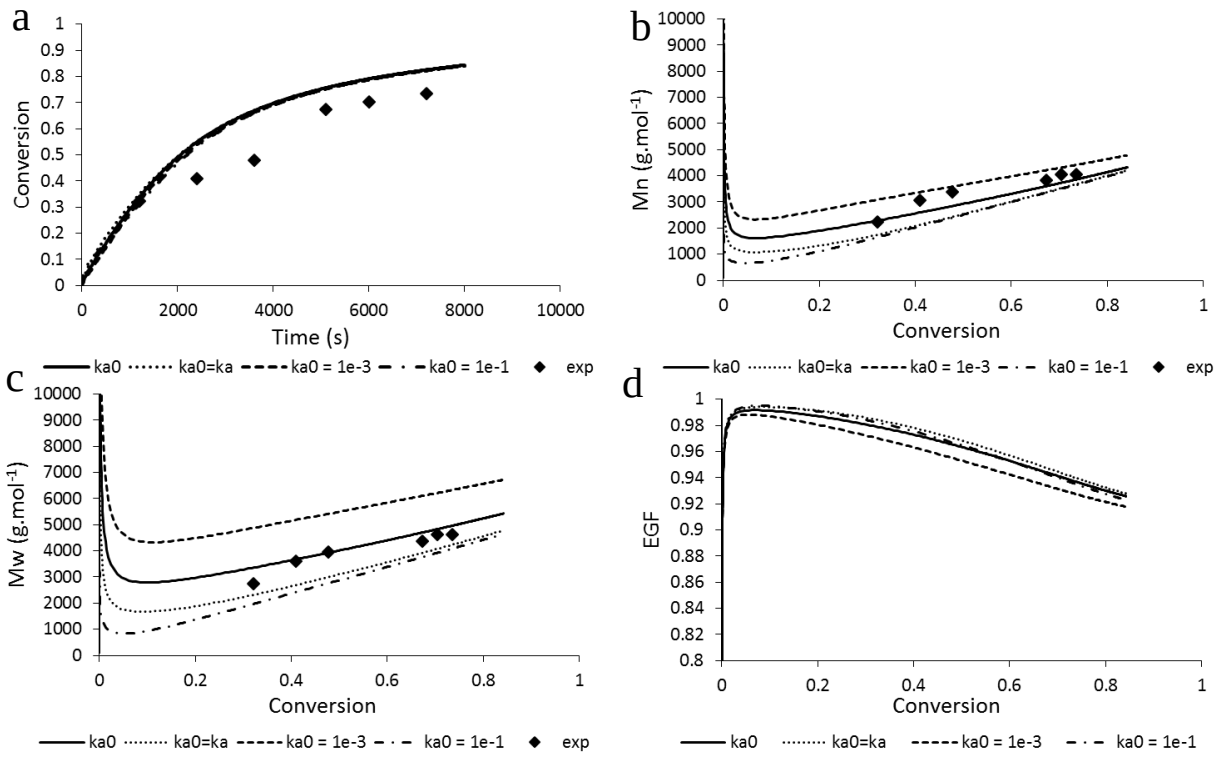

Figure 7.5: Comparison of model results accounting for distinct alkoxyamine activation ($k_{a,o}$ = 2.58x10^{-3} L mol^{-1} s^{-1}, solid line; parameters Table 7.1) and varying alkoxyamine initiation for TCL = 50 at 160 °C (experimental data from Payne *et al.*[7]). Plot of (a) conversion versus time, (b) number-average molar mass (M_n), (c) weight-average molar mass (M_w), and (d) end group functionality versus conversion.

Although the change in activation rate coefficient has a negligible impact on the conversion profile (Figure 7.5a), there is a clear effect on the MW and EGF (Figure 7.5b, c, and d, respectively). It is also clear that the alkoxyamine activation must be slower than the polymeric activation in order to accurately represent the experimental data, as setting $k_{a,o} = k_a = 7.97\text{x}10^{-3}$ L mol^{-1} s^{-1} leads to the M_n and M_w being underestimated (dotted line ⋯, Figure 7.5b and c).

Similarly, distinct deactivation rate coefficients are necessary to accurately represent the experimental data, as presented in Figure 7.6. As with activation, the change in deactivation rate coefficient has negligible impact on the conversion profile (Figure 7.6a), but an appreciable difference in M_n and M_w is witnessed when $k_{da,o} = k_{da}$ (Figure 7.6b and c, respectively). However, the deactivation rate coefficients appear to be less important for the accurate prediction of MW relative to the activation rate coefficients, as is also demonstrated by the box search results in Appendix D.

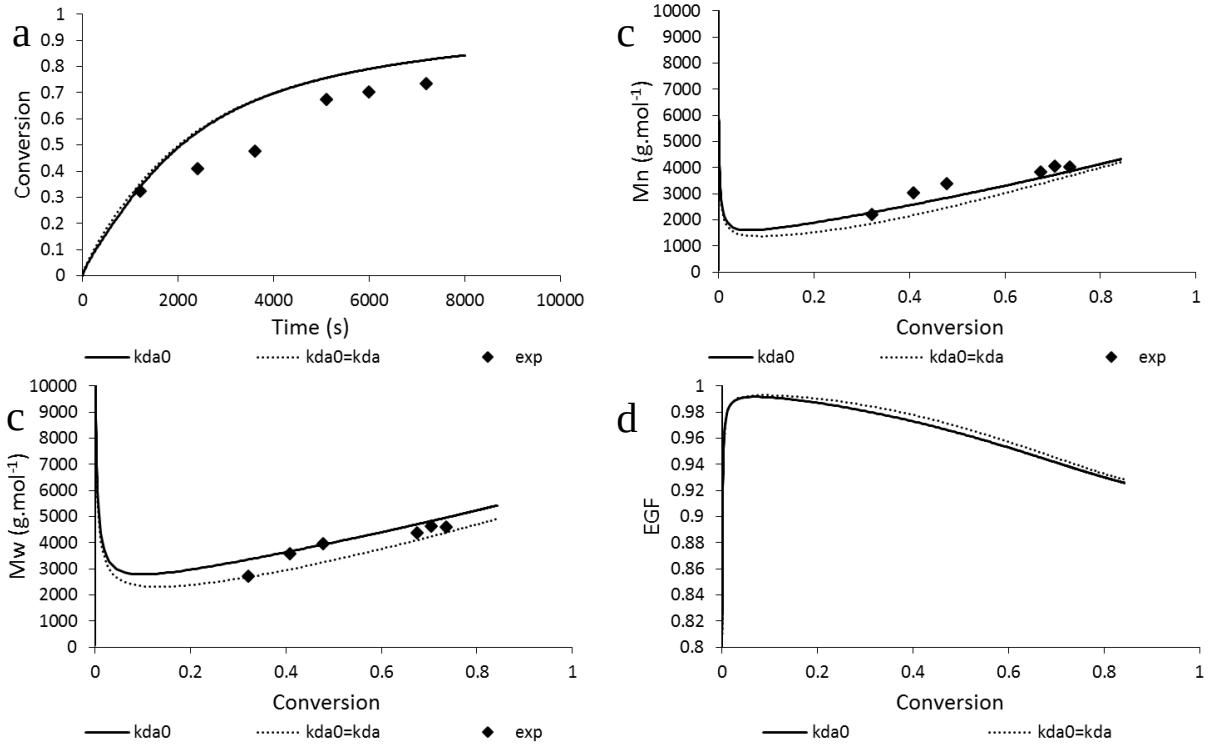

Figure 7.6: Comparison of model results accounting for distinct alkoxyamine deactivation (solid line; parameters Table 7.1) and equal alkoxyamine and polymeric deactivation ($k_{da,o}$ = k_{da} = 2.31x10^7 L mol^{-1} s^{-1}) for TCL = 50 at 160 °C (experimental data from Payne *et al.*[7]). Plot of (a) conversion versus time, (b) number-average molar mass (M_n), (c) weight-average molar mass (M_w), and (d) end group functionality versus conversion.

7.4.3 NMP of styrene in a CSTR

The kinetic model developed for the batch polymerization of styrene is able to represent the experimental results over a range of alkoxyamine concentrations and temperatures. The model reactor configuration was then altered to CSTR constant volume operation in order to compare model predictions with the experimental data presented in Table 7.2. The comparison of model and experimental data at 160 °C with varying TCL and residence time (τ) is shown in Figure 7.7.

Table 7.2: NMP of styrene in a CSTR with varying temperature, target chain length (TCL), and residence time (τ) with 30 wt% xylenes. Experimental results are reported at steady state.

Experiment	Temperature (°C)	τ (min)	TCL ([M]/[Alk])	Conversion	M_n (g mol^{-1})	M_w (g mol^{-1})
1	160	15	200	0.23	4459	8838
2	160	30	200	0.31	5603	12227
3	160	15	300	0.26	6621	13423
4	160	30	300	0.26	8362	18274
5	200	15	100	0.54	4326	8438
6	200	30	100	0.55	4460	8802
7	200	15	200	0.53	6999	14442
8*	200	15	200	0.40	6089	12310

*50 wt% xylenes

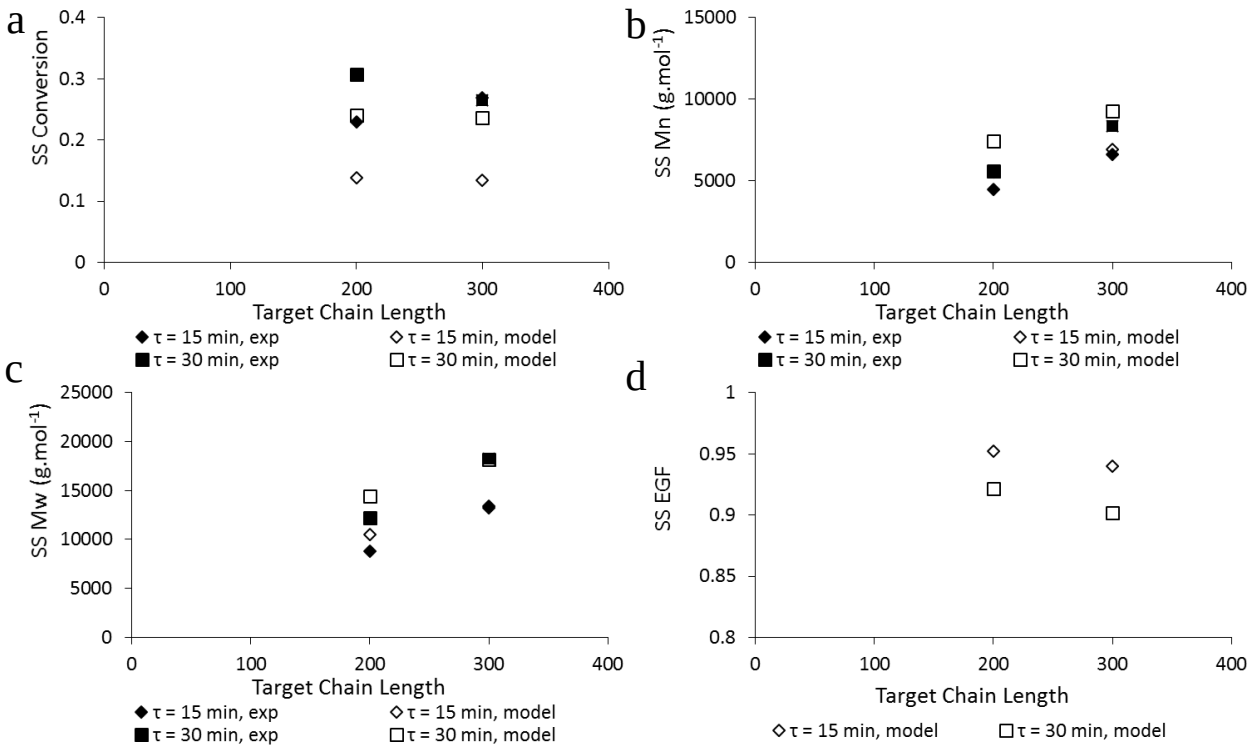

Figure 7.7: Comparison of experimental (closed symbols) and simulation data (open symbols) at steady state for NMP of styrene with 30 wt% xylenes in a CSTR at 160 °C with varying TCL and residence time, τ (see legend). Plot of (a) conversion, (b) number-average molar mass (M_n), (c) weight-average molar mass (M_w), and (d) end group functionality versus target chain length. Model parameters from Table 7.1 using constant k_t^{app};[38] experimental data from Table 7.2.

The kinetic model is able to predict the significant decrease in the conversion witnessed in the CSTR compared to batch conditions (Figure 7.7a). The model also effectively captures the measured M_n and M_w of the polymer resin that is collected from the CSTR (Figure 7.7b and c, respectively), and how the values increase with increasing average residence time (30 vs. 15 min). The final polymer dispersity approaches ~2, which is larger than the batch system due to the residence time distribution in the CSTR.[27] However, the observed dispersity is close to the theoretical limit for an ideal homogeneous RDRP in a single CSTR.[46] In addition, the alkoxyamine

loading in the feed is shown to effectively influence the polymer chain length. It is important to note that polymer was collected after 4 turnovers (4τ) from the start of the alkoxyamine feed to ensure steady state behavior, as is confirmed by the leveling off of the simulated profiles after 4τ (not shown). The predicted end group functionality also follows from the batch study, where an increase in target chain length and temperature results in decreased end group functionality (Figure 7.7d). The relatively high EGF (>90%) predicted for the final polymer is promising for the potential to produce block copolymers with further chain extension.

As seen above, the steady state monomer conversion is quite low at 160 °C. From the batch study, the increased reaction temperature resulted in an increase in polymerization rate with negligible impact on polymer dispersity and MW control. Therefore, an increase in the CSTR temperature was first evaluated at TCL = 200, as this resulted in higher end group functionality at 160 °C. This was accompanied by an increase in alkoxyamine loading (TCL = 100) for two different residence times, as shown in Figure 7.8.

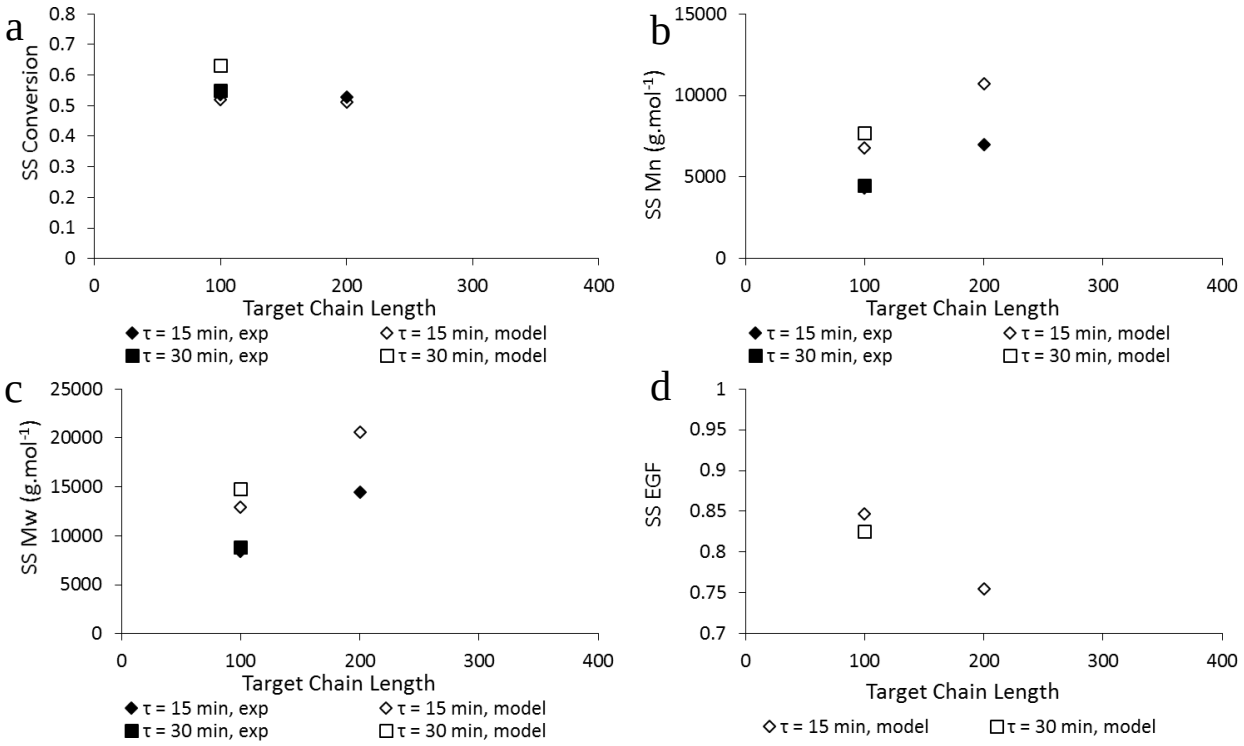

Figure 7.8: Comparison of experimental (symbols) and simulation data (lines) at steady state for NMP of styrene with 30 wt% xylenes in a CSTR at 200 °C with varying TCL and residence time, τ (see legend). Plot of (a) conversion, (b) number-average molar mass (M_n), (c) weight-average molar mass (M_w), and (d) end group functionality versus target chain length. Model parameters from Table 7.1 using constant k_t^{app};[38] experimental data from Table 7.2.

As seen at 160 °C, polymer conversion is independent of TCL, and increases with residence time (Figure 7.8a). Polymer conversion in the CSTR is shown to significantly increase relative to 160 °C, but is appreciably reduced compared to the batch conversion observed at 200 °C (~53% for τ = 15 min in the CSTR versus 69% for a 15 min batch reaction). M_n and M_w are also shown to increase slightly with residence time, and significantly increase with a reduction in alkoxyamine feed (Figure 7.8b and c, respectively). However, while the model provides a good estimate of steady state conversions at 200 °C, the MW values are over predicted, the opposite to what was found at

160 °C. Finally, the model predicts EGF to decrease with increased residence time and TCL, as expected (Figure 7.8d).

The SEC-derived molar mass distributions for the polystyrene produced at 160 °C and 200 °C under steady state conditions can be seen in Figure 7.9. It is clear that with increased residence time and TCL (reduced alkoxyamine feed), there is a decrease in the low MW peak attributed to the alkoxyamine species seen at log(MW) ~ 2.6. The occurrence of this low MW peak makes accurate determination of M_n difficult. This experimental observation is in qualitative agreement with the model predictions of the steady state concentrations of nitroxide and alkoxyamine species relative to the feed concentration of alkoxyamine, shown in Figure 7.10.

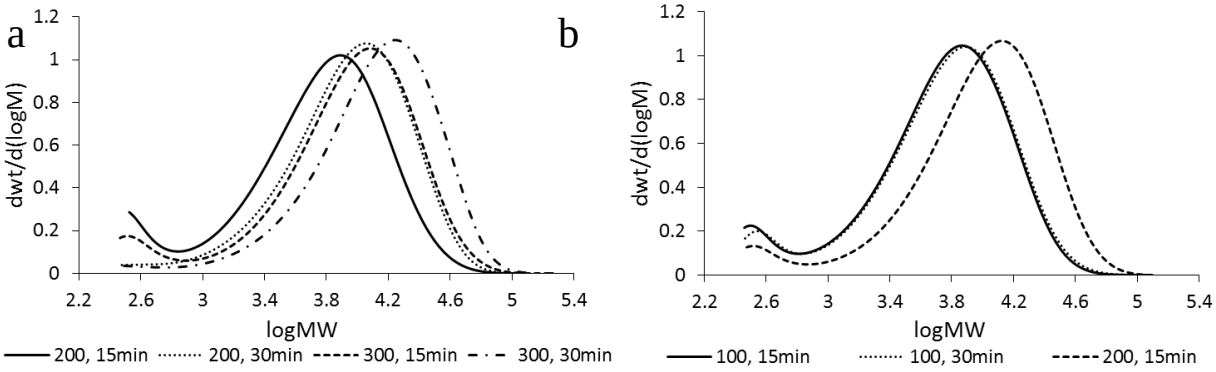

Figure 7.9: Molar mass distribution of final polymer samples from NMP of styrene with 30 wt% xylenes at (a) 160 °C and (b) 200 °C in a CSTR; TCL and residence time presented in the legend.

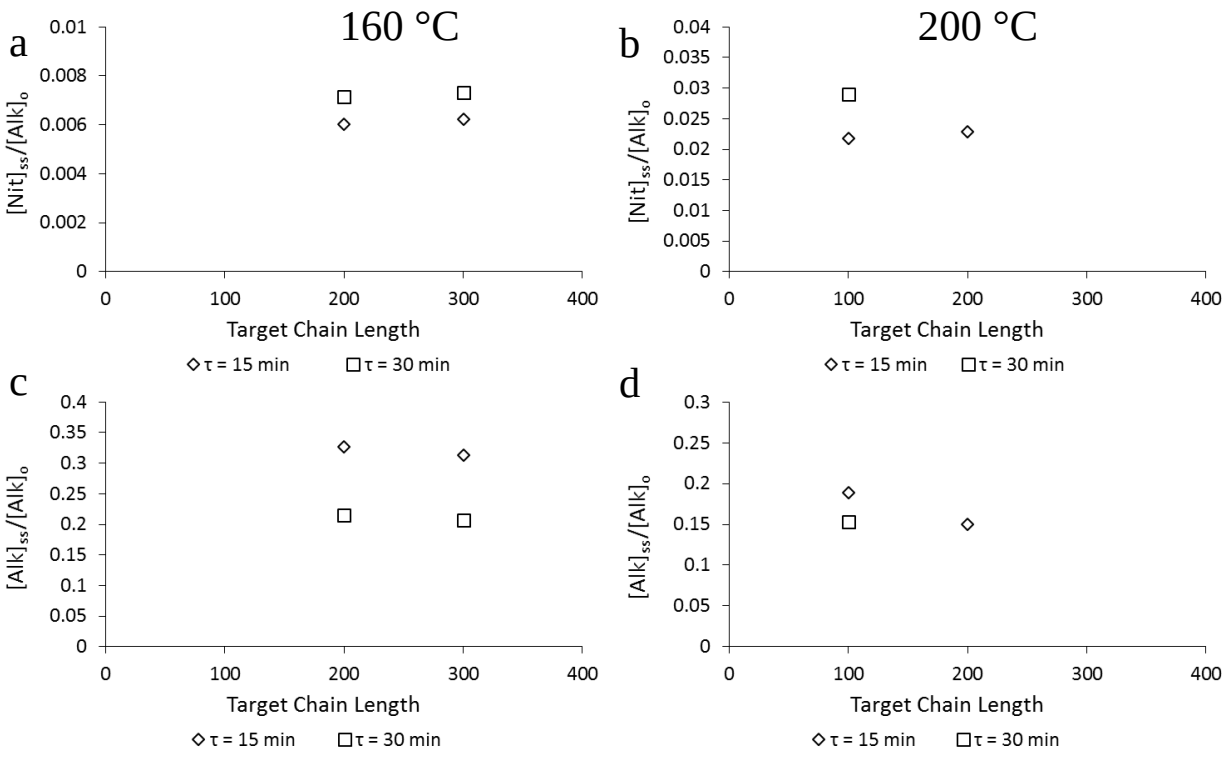

Figure 7.10: Plot of ratio of steady state concentration to alkoxyamine feed concentration of (a, b) nitroxide and (c, d) alkoxyamine versus target chain length for the NMP of styrene with 30 wt% xylenes at (a, c) 160 °C and (b, d) 200 °C. Residence time presented in the legend.

The presence of a significant concentration of alkoxyamine species can be seen at both 160 °C and 200 °C, with an increase in temperature for TCL = 200 and τ = 15 min leading to a significantly lower predicted steady state concentration of alkoxyamine (Figure 7.10c and d); for 160 °C and τ = 15 min, over 30% of the alkoxyamine exits the reactor without initiating polymerization, with the fraction decreasing to 15% at 200 °C. The predicted decrease in steady state alkoxyamine concentration with increased residence time, temperature, and TCL supports the observed decrease in the alkoxyamine peak in the experimental MMDs (Figure 7.9a). This prediction suggests that it would be beneficial to conduct the reaction in a series of CSTRs (also good for production of block copolymers), or using a plug flow reactor configuration for improved

utilization of the alkoxyamine. Operation at an even higher temperature would also be beneficial, although perhaps at the expense of reduced EGF.

To ensure that the polymer has preserved end group functionality, the polymer resin obtained from the CSTR was further extended with additional styrene monomer under batch conditions, as shown in Figure 7.11.

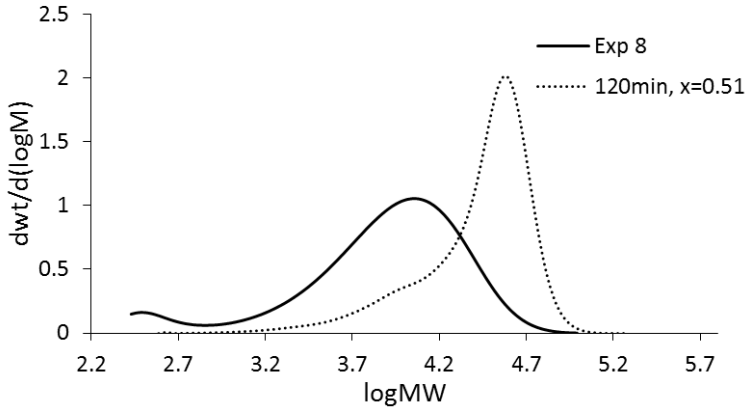

Figure 7.11: Molar mass distribution resulting from chain extension of PS obtained from CSTR (Exp 8, Table 7.2) by batch NMP in bulk at 160 °C of styrene (TCL = 300); polymerization time and conversion presented in the legend.

It can be seen that the entire MMD shifts to higher MW, with a small shoulder around logMW ~ 4. This lower MW shoulder may correspond to the residual alkoxyamine present in the resin from the CSTR being initiated, resulting in a second growing chain population, or may be the contribution from the dead chain population in the polymer obtained from the CSTR, as the kinetic model predicts a steady state EGF ~ 0.75 under the same operating conditions and 30 wt% xylenes (Figure 7.8d). Due to the broad residence time distribution in the CSTR, there will be a broader chain distribution which will continue during the batch chain extension, as all chains undergo the same residence time in the batch system, which could lead to the bimodal MMD witnessed after

chain extension. Future work will help to elucidate the chain populations and EGF of the polymer obtained from the CSTR.

7.5 Conclusion

A kinetic model has been developed to represent the NMP of styrene at temperatures up to 200 °C under batch and CSTR conditions. Using previously published data from the batch NMP of styrene, a set of activation/deactivation rate coefficients was estimated using the parameter estimation tools within the Predici software package. The model is able to successfully predict the experimental behavior witnessed in the batch study, with styrene polymerization rate independent of alkoxyamine concentration (TCL) and an increase in polymerization rate with temperature without any loss of control of the MW.

The model was then converted to CSTR operation in order to better understand the experimental results acquired from a high temperature CSTR setup. The model was able to predict the observed increase in final polymer conversion with residence time and temperature. The increase in M_n and M_w with increased residence time and decreased alkoxyamine feed is also represented by the kinetic model. Finally, the low MW peak witnessed in the experimental MMD obtained by SEC was explained by the presence of a significant steady state alkoxyamine concentration. The experimentally observed decrease in the low MW peak intensity with an increase in TCL and residence time is accompanied by a similar decrease in alkoxyamine concentration under the same conditions.

This work demonstrates the first known implementation of NMP in a CSTR, allowing the production of well-controlled polymers with a high degree of end group functionality in a continuous process.

7.6 References

(1) Nicolas, J.; Guillaneuf, Y.; Lefay, C.; Bertin, D.; Gigmes, D.; Charleux, B. *Prog. Polym. Sci.* **2013**, *38*, 63–235.

(2) Marchand, J.; Autissier, L.; Guillaneuf, Y.; Couturier, J.-L.; Gigmes, D.; Bertin, D. *Aust. J. Chem.* **2010**, *63*, 1237–1244.

(3) Gigmes, D.; Vinas, J.; Chagneux, N.; Lefay, C.; Phan, T. N. T.; Trimaille, T.; Dufils, P.-E.; Guillaneuf, Y.; Carrot, G.; Boué, F.; Bertin, D. In *Controlled/Living Radical Polymerization: Progress in RAFT, DT, NMP & OMRP*; ACS Symposium Series, American Chemical Society: Washington, DC, 2009; pp. 245–262.

(4) Couvreur, L.; Lefay, C.; Belleney, J.; Charleux, B.; Guerret, O.; Magnet, S. *Macromolecules* **2003**, *36*, 8260–8267.

(5) Le Mercier, C.; Lutz, J.-F.; Marque, S. R. A.; Le Moigne, F.; Tordo, P.; Lacroix-Desmazes, P.; Boutevin, B.; Couturier, J.-L.; Guerret, O.; Martschke, R.; Sobek, J.; Fischer, H. In *Controlled/Living Radical Polymerization*; ACS Symposium Series, American Chemical Society: Washington, DC, 2000; pp. 108–122.

(6) Farcet, C.; Charleux, B.; Pirri, R. *Macromol. Symp.* **2002**, *182*, 249–260.

(7) Payne, K. A.; Nesvadba, P.; Debling, J.; Cunningham, M. F.; Hutchinson, R. A. *ACS Macro Lett.* **2015**, *4*, 280–283.

(8) Zhang, M.; Ray, W. H. *J. Appl. Polym. Sci.* **2002**, *86*, 1047–1056.

(9) Enright, T. E.; Cunningham, M. F.; Keoshkerian, B. *Macromol. React. Eng.* **2010**, *4*, 186–196.

(10) Wang, Y.; Hutchinson, R. A.; Cunningham, M. F. *Macromol. Mater. Eng.* **2005**, *290*, 230–241.

(11) Nicolas, J.; Mueller, L.; Dire, C.; Matyjaszewski, K.; Charleux, B. *Macromolecules* **2009**, *42*, 4470–4478.

(12) Bentein, L.; D'hooge, D. R.; Reyniers, M.-F.; Marin, G. B. *Macromol. Theory Simul.* **2011**, *20*, 238–265.

(13) Fierens, S. K.; D'hooge, D. R.; Van Steenberge, P. H. M.; Reyniers, M.-F.; Marin, G. B. *Chem. Eng. J.* **2015**, *278*, 407-420.

(14) Fu, Y.; Cunningham, M. F.; Hutchinson, R. A. *Macromol. React. Eng.* **2007**, *1*, 243–252.

(15) Enright, T. E.; Cunningham, M. F.; Keoshkerian, B. *Macromol. Rapid Commun.* **2005**, *26*, 221–225.

(16) Fortunatti, C.; Sarmoria, C.; Brandolin, A.; Asteasuain, M. *Macromol. React. Eng.* **2014**, *8*, 260–281.

(17) Farkas, E.; Meszéna, Z. G. *Period. Polytech. Chem.* **2010**, *54*, 15-25.

(18) Lemoine-Nava, R.; Flores-Tlacuahuac, A.; Saldívar-Guerra, E. *Chem. Eng. Sci.* **2006**, *61*, 370–387.

(19) Lemos, T.; Melo, P. A.; Pinto, J. C. *Macromol. React. Eng.* **2015**, *9*, 259-270.

(20) Smulders, W. W.; Jones, C. W.; Schork, F. J. *Macromolecules* **2004**, *37*, 9345–9354.

(21) Smulders, W. W.; Jones, C. W.; Schork, F. J. *AIChE J.* **2005**, *51*, 1009–1021.

(22) Wang, W.; Zhou, Y.-N.; Luo, Z.-H. *Macromol. React. Eng.* **2015**, n/a – n/a.

(23) Chan, N.; Meuldijk, J.; Cunningham, M. F.; Hutchinson, R. A. *Ind. Eng. Chem. Res.* **2013**, *52*, 11931–11942.

(24) Burns, J. A.; Houben, C.; Anastasaki, A.; Waldron, C.; Lapkin, A. A.; Haddleton, D. M. *Polym. Chem.* **2013**, *4*, 4809-4813.

(25) Chan, N.; Cunningham, M. F.; Hutchinson, R. A. *Macromol. React. Eng.* **2010**, *4*, 369–380.

(26) Chan, N.; Boutti, S.; Cunningham, M. F.; Hutchinson, R. A. *Macromol. React. Eng.* **2009**, *3*, 222–231.

(27) Zhang, M.; Ray, W. H. *J. Appl. Polym. Sci.* **2002**, *86*, 1630–1662.

(28) Campbell, J. D.; Kaai, M.; Mori, Y.; Pekarik, A. J.; Srisiri-Sisson, W.; Villalobos, M. A. Process for the continuous production of gel free polymers, and powder and liquid coating applications containing gel free polymers. US 6552144, 2003.

(29) Greszta, D.; Matyjaszewski, K. *Macromolecules* **1996**, *29*, 7661–7670.

(30) Fischer, H.; Paul, H. *Acc. Chem. Res.* **1987**, *20*, 200–206.

(31) Woloszyn, J. D.; McAuley, K. B. *Macromol. React. Eng.* **2011**, *5*, 453–466.

(32) Buback, M.; Gilbert, R. G.; Hutchinson, R. A.; Klumperman, B.; Kuchta, F.-D.; Manders, B. G.; O'Driscoll, K. F.; Russell, G. T.; Schweer, J. *Macromol. Chem. Phys.* **1995**, *196*, 3267–3280.

(33) Chauvin, F.; Dufils, P.-E.; Gigmes, D.; Guillaneuf, Y.; Marque, S. R. A.; Tordo, P.; Bertin, D. *Macromolecules* **2006**, *39*, 5238–5250.

(34) Zytowski, T.; Knühl, B.; Fischer, H. *Helv. Chim. Acta* **2000**, *83*, 658–675.

(35) Hui, A. W.; Hamielec, A. E. *J. Appl. Polym. Sci.* **1972**, *16*, 749–769.

(36) Fu, Y.; Cunningham, M. F.; Hutchinson, R. A. *Macromol. Symp.* **2007**, *259*, 151–163.

(37) Pryor, W. A.; Coco, J. H. *Macromolecules* **1970**, *3*, 500–508.

(38) Buback, M.; Kuchta, F.-D. *Macromol. Chem. Phys.* **1997**, *198*, 1455–1480.

(39) Johnston-Hall, G.; Monteiro, M. J. *Macromolecules* **2008**, *41*, 727–736.

(40) Kattner, H.; Buback, M. *Macromolecules* **2015**, *48*, 309–315.

(41) Chen, C.-Y.; Wu, Z.-Z.; Kuo, J.-F. *Polym. Eng. Sci.* **1987**, *27*, 553–557.

(42) Van Steenberge, P. H. M.; Vandenbergh, J.; D'hooge, D. R.; Reyniers, M.-F.; Adriaensens, P. J.; Lutsen, L.; Vanderzande, D. J. M.; Marin, G. B. *Macromolecules* **2011**, *44*, 8716–8726.

(43) Johnston-Hall, G.; Monteiro, M. J. *Macromol. Theory Simul.* **2010**, *19*, 387–393.

(44) Bergenudd, H.; Jonsson, M.; Malmström, E. *Macromol. Theory Simul.* **2011**, *20*, 814–825.

(45) Zhong, M.; Matyjaszewski, K. *Macromolecules* **2011**, *44*, 2668–2677.

(46) Schork, F. J.; Smulders, W. W. *J. Appl. Polym. Sci.* **2004**, *92*, 539–542.

Chapter 8

Conclusions and Recommendations

8.1 Concluding Remarks

Reversible deactivation radical polymerization (RDRP) has witnessed an exponential growth in the number of publications in the open literature since the first major developments in the early 1990s. RDRP chemistries have led to the facile synthesis of a wide variety of unique polymers with a plethora of applications. Despite this, RDRP has not been widely developed towards commercial production. The main deterrent is the cost of the required mediating agents, with most of these not available at commercial scale. Another factor is the toxicity of the mediating agents, thus requiring post polymerization processing, particularly for the copper used in atom transfer radical polymerization (ATRP). In the case of reversible addition-fragmentation chain transfer (RAFT), thio-based mediators are less desirable in commercial products, and there is difficulty in obtaining RAFT agents in commercial quantities. In addition, end group removal can be a challenge, which must be overcome to prevent degradation to smelly and toxic volatile sulfur compounds. However, select nitroxides are currently produced at the pilot scale, a positive step towards the potential industrial adoption of nitroxide-mediated polymerization (NMP) at an appreciable level.

Recent advances in ATRP have led to low copper variants as a means to limit the barriers to commercial application. Activator regenerated by electron transfer (ARGET) ATRP is a promising alternative to normal ATRP, and was implemented in a lab-scale continuous process with moderate success, thus providing the initial motivation of this thesis to further understand the factors influencing the ARGET ATRP system. The influence of the initiator concentration (or target chain length), monomer choice, temperature, copper loading and reducing agent loading on the batch ARGET ATRP system were studied. Decreasing the copper loading to 35 ppm on a molar

basis relative to monomer was accompanied by a significant decrease in the initiator efficiency and polymerization rate, the latter of which was only recovered with a significant excess of reducing agent.

The systematic study of the ARGET ATRP of BMA was then represented with a kinetic model developed using the commercially available Predici software. The model showed that the significant reduction in polymerization rate with a reduction in copper loading can be attributed to the decrease in the ratio of activator to deactivator species (Cu^{I}/Cu^{II}) with conversion. The model suggests that the significant excess of reducing agent necessary to recover the polymerization rate is capable of restoring the Cu^{I}/Cu^{II} ratio that dictates the polymerization rate. The model was then applied to the copolymerization of BMA and BA. As BMA exhibited low initiator efficiencies leading to higher MW polymer than expected, varying amounts of BA were added to increase the polymerization rate and initiator efficiency. The knowledge of the ARGET ATRP system gained from the modeling study led to an alternate feed strategy for the reducing agent, with a semi-batch approach resulting in a lowered amount of reducing agent needed to improve the monomer conversion relative to the batch system. As the study indicated that a reduction in toxic copper loading must be offset by an increase in reducing agent in order to achieve appreciable conversion, it is clear that ARGET ATRP still presents challenges to becoming an economically viable process due to the inevitable need to remove metal from the final polymer.

The research focus was then turned toward another method of RDRP that does not require any post polymerization processing other than residual monomer removal. Nitroxide-mediated polymerization (NMP) incorporates the initiating alkoxyamine into the polymer, providing effective control of the polymer structure and the possibility for block copolymers. A batch experimental study was conducted with a commercially available nitroxide 2,2,6,6-tetramethyl-1-piperidinyloxy (TEMPO) and styrene at elevated temperatures. Ultimately, the nitroxide was unable to successfully control the polymerization of styrene above 140 °C, the maximum

temperature studied in the literature, due to decomposition of TEMPO. As a result, a novel alkoxyamine was evaluated as a mediating agent. The alkoxyamine was shown to successfully control the MW of styrene and BA up to 200 °C. The polymer was shown to maintain high levels of end group functionality, with chain extension to higher MW showing a clear shift of the entire molar mass distribution (MMD), demonstrating the potential to synthesize block copolymers. The alkoxyamine was then utilized in a continuous stirred-tank reactor (CSTR) in the first experimental implementation of NMP in a CSTR at elevated temperatures. The alkoxyamine was able to control the polymer MW, with an increase in steady state conversion and MW with increased temperature and residence time, consistent with the trends observed in the batch study. A kinetic model developed was able to represent the experimental trends, with the conversion profile independent of alkoxyamine concentration while controlling the polymer chain length. The model also helps to explain the experimentally observed low MW peak seen in the MMD of the steady state polymer product obtained from the CSTR, attributable to a significant concentration of residual alkoxyamine exiting the reactor. A high level of end group functionality is predicted for CSTR operation, suggesting that higher value block copolymers may be produced in a continuous process with the addition of additional monomer in a second CSTR. The research in this thesis has demonstrated that RDRP, particularly NMP with a novel alkoxyamine, can be successfully adapted to an existing industrial process.

8.2 Summary of Original Contributions

Despite the abundance of literature related to RDRP, comprehensive kinetic studies rarely include experimental data to support the findings of theoretical studies. Further, continuous operation is modelled with little implementation in a laboratory setting. This research represents the first time NMP has been applied to industrially relevant conditions in a continuous process. Original contributions include:

- Improved understanding of ARGET ATRP and the limitations to reducing copper levels while maintaining good control and rate in the production of short chain polymers. Copper levels can be reduced down to 35 ppm, however a significant excess of reducing agent is required to recover the significantly reduced polymerization rate, and in many cases the initiator has reduced efficiency under these conditions.
- The first comprehensive experimental study which is accompanied by a kinetic model to represent ARGET ATRP of butyl methacrylate at various temperatures, copper loadings, and initiator loadings (target chain lengths). The modeling suggests the polymerization is adversely affected by slow activation of the ATRP initiator, which is confirmed with experimental evidence.
- Initiator efficiency and polymerization rate of this ARGET ATRP system is improved by copolymerizing butyl acrylate with butyl methacrylate, as demonstrated both experimentally and through modeling. Reducing agent feed strategy is improved through semi-batch addition, leading to a decrease in the amount of reducing agent needed to increase polymerization rate at low copper levels.
- The first successful batch NMP of styrene and butyl acrylate at elevated temperatures (>140 °C) is demonstrated, mediated by a novel alkoxyamine. The conversion profile is independent of alkoxyamine concentration, suggesting the polymerization rate is dictated by thermal initiation. Low polymer dispersities and successful chain extensions demonstrate good control of the polymerization and the possibility to produce block copolymers.

- The first experimental implementation of NMP in a CSTR, demonstrating the ability to adapt NMP to an existing industrial process. The alkoxyamine is shown to effectively control the MW at elevated temperatures, with a kinetic model developed to represent the experimental trends witnessed in the CSTR with changes in temperature, residence time, and alkoxyamine concentration, as well as successfully representing the range of conditions studied in batch. The high end group functionality predicted by the model suggests that block copolymers may be produced under these conditions.

8.3 Current State of RDRP

Alternate ATRP chemistries were developed in the past decade in the pursuit of lowering copper levels, including initiators for continuous activator regeneration (ICAR) ATRP and ARGET ATRP. Since this thesis was undertaken, there have been relatively few studies undertaken that strive to further improve the ATRP system. The monomer conversion for an ICAR ATRP system in bulk was driven to higher conversion with the optimization of a temperature ramp towards the end of the reaction.[1] Meanwhile, theoretical studies have been conducted to provide guidance for optimal synthesis of homopolymers and block copolymers.[2–5] The recent focus on ARGET ATRP has not been on process optimization, but the generation of polymers for specific applications where low Cu levels are preferred and its removal is not a significant barrier, as in higher value polymers used for biomedical applications produced in both non-aqueous[6,7] and aqueous media.[8,9]

Research interest in these chemistries has significantly diminished, largely due to the appearance of other low copper variants of ATRP, single electron transfer living radical polymerization (SET-LRP) or supplemental activator and reducing agent (SARA) ATRP,[10,11] electrochemically mediated ATRP (eATRP), and photochemically mediated RDRP (photoRDRP).[12–14] The abundance of recent publications related to these chemistries revolve

around reducing copper levels while producing a wide range of controlled polymers, typically in aqueous media.[15–18] The wide range of products being synthesized as of late are typically targeted towards bioapplications which can be highly sequence specific so as to mimic natural polymers such as peptides and proteins or encapsulate certain drugs for targeted release. Recent patent activity for RAFT polymerization has seen applications such as contact lenses or controlled release of therapeutics, with a summary of recently issued patents in the update from Moad *et al.*.[19] Further examples are included in recent reviews for Cu(0)-mediated polymerization and RAFT.[20,21]

However, there are still limited efforts to adapt the chemistry to a continuous process, with only a few examples of ATRP in continuous tubular reactors.[22-25] A few attempts to develop a continuous process for RDRP can be seen across the literature, as discussed in Chapter 2, with little recent progress outside of ATRP. The latest theoretical studies of NMP in continuous processes suggest there is a sustained interest in adapting this particular chemistry to industrially relevant conditions.[26,27] However, it would appear that the majority of the current research efforts in RDRP are working towards niche applications which can support the higher costs of the mediators necessary for polymer production.

8.4 Recommendations for Future Work

From the investigations into the ARGET ATRP system presented in this thesis, it is clear that an alternate chemistry is necessary to reduce copper levels further while maintaining good control and kinetics. In contrast, the successful implementation of NMP of styrene at elevated temperatures under batch and CSTR operation provides ample opportunity for further study of this system.

8.4.1 Continuous ATRP

With the previous developments in the literature and in our laboratory regarding continuous SET-LRP or SARA ATRP,[24,28] it is of interest to conduct a similar systematic investigation of this

system as has been conducted in this thesis for ARGET ATRP. Work is currently underway to further develop an understanding of the Cu(0)-mediated polymerization system in aqueous media.[29] The knowledge gained can help to further build upon previous developments in a CSTR and tubular reactor.

ARGET ATRP has also been modified for aqueous systems by employing water-soluble reducing agents such as ascorbic acid, to develop a more environmentally benign system that is free of organic solvents and metallic reducing agents. This has been demonstrated in the literature,[8,30,31] and could be an interesting system to optimize towards continuous production of industrial coatings, for example, as environmental regulations become increasingly stringent. Using different water-soluble monomers could also provide motivation to develop a continuous process for production of block copolymers for applications such as drug encapsulation, as mentioned above.

8.4.2 NMP of different monomers

Nitroxides and their corresponding alkoxyamines are typically tailored to the reaction conditions in order to effectively mediate the polymerization of a variety of monomer types. Therefore, it would be of interest to pursue the polymerization of other monomers besides styrene and butyl acrylate with the novel alkoxyamine studied in this thesis. An alkoxyamine that is capable of mediating the polymerization of a variety of monomers will be more attractive than synthesizing derivatives for different systems, as evidenced by other successful nitroxides developed for application at lower temperatures such as 2,2,5-trimethyl-4-phenyl-3-azahexane-3-oxyl (TIPNO) and N-*tert*-butyl-N-[1-diethylphosphono-(2,2-dimethylpropyl)] nitroxide (DEPN or SG1), with SG1 being produced at pilot scale.

Expanding the kinetic model to represent butyl acrylate is a focus of future work to accompany the experimental study conducted in this thesis.

8.4.3 NMP in a CSTR

Chain extension has been demonstrated in the batch NMP system, with a clear shift in the entire molar mass distribution (MMD) indicating a high level of end group functionality. Further study of the polymer end groups is desirable using matrix-assisted laser desorption/ionization time of flight (MALDI-TOF), electrospray ionization mass spectrometry (ESI-MS) or size exclusion chromatography (SEC) coupled with a UV-Vis detector. The kinetic model developed in this thesis predicts a high level of end group functionality, suggesting that block copolymers could be produced in a continuous process by using multiple CSTRs with monomer addition or different monomer feed points in a tubular reactor. The impact of monomer sequence and monomer type should be investigated, as this has a significant effect on the quality of the block copolymers produced. The industrial adoption of NMP will be encouraged by the capability to produce higher value block copolymers in a continuous process in order to offset the cost of the alkoxyamine synthesis.

8.5 References

(1) Mohammad Rabea, A.; Zhu, S. *Macromol. React. Eng.* **2014**, *8*, 771–776.

(2) D'hooge, D. R.; Konkolewicz, D.; Reyniers, M.-F.; Marin, G. B.; Matyjaszewski, K. *Macromol. Theory Simul.* **2012**, *21*, 52–69.

(3) Toloza Porras, C.; D'hooge, D. R.; Van Steenberge, P. H. M.; Reyniers, M.-F.; Marin, G. B. *Macromol. React. Eng.* **2013**, *7*, 311–326.

(4) Toloza Porras, C.; D'hooge, D. R.; Reyniers, M.-F.; Marin, G. B. *Macromol. Theory Simul.* **2013**, *22*, 136–149.

(5) Zhong, M.; Matyjaszewski, K. *Macromolecules* **2011**, *44*, 2668–2677.

(6) Popescu, D.-L.; Tsarevsky, N. V. *Macromol. Rapid Commun.* **2012**, 1–7.

(7) Siegwart, D. J.; Leiendecker, M.; Langer, R.; Anderson, D. G. *Macromolecules* **2012**, *45*, 1254-1261.

(8) Simakova, A.; Averick, S. E.; Konkolewicz, D.; Matyjaszewski, K. *Macromolecules* **2012**, *45*, 6371–6379.

(9) Averick, S.; Simakova, A.; Park, S.; Konkolewicz, D.; Magenau, A. J. D.; Mehl, R. A.; Matyjaszewski, K. *ACS Macro Lett.* **2012**, *1*, 6–10.

(10) Percec, V.; Popov, A. V.; Ramirez-Castillo, E.; Monteiro, M. J.; Barboiu, B.; Weichold, O.; Asandei, A. D.; Mitchell, C. M. *J. Am. Chem. Soc.* **2002**, *124*, 4940–4941.

(11) Konkolewicz, D.; Wang, Y.; Zhong, M.; Krys, P.; Isse, A. A.; Gennaro, A.; Matyjaszewski, K. *Macromolecules* **2013**, *46*, 8749–8772.

(12) Bortolamei, N.; Isse, A. A.; Magenau, A. J. D.; Gennaro, A.; Matyjaszewski, K. *Angew. Chem., Int. Ed.* **2011**, *50*, 11391–11394.

(13) Treat, N. J.; Sprafke, H.; Kramer, J. W.; Clark, P. G.; Barton, B. E.; Read de Alaniz, J.; Fors, B. P.; Hawker, C. J. *J. Am. Chem. Soc.* **2014**, *136*, 16096–16101.

(14) Xiao, P.; Zhang, J.; Campolo, D.; Dumur, F.; Gigmes, D.; Fouassier, J. P.; Lalevée, J. *J. Polym. Sci., Part A Polym. Chem.* **2015**, n/a – n/a.

(15) Chmielarz, P.; Krys, P.; Park, S.; Matyjaszewski, K. *Polymer* **2015**, *71*, 143–147.

(16) Chmielarz, P.; Park, S.; Simakova, A.; Matyjaszewski, K. *Polymer* **2015**, *60*, 302–307.

(17) Pester, C. W.; Poelma, J. E.; Narupai, B.; Patel, S. N.; Su, G. M.; Mates, T. E.; Luo, Y.; Ober, C. K.; Hawker, C. J.; Kramer, E. J. *J. Polym. Sci., Part A Polym. Chem.* **2015**, n/a – n/a.

(18) Nicol, E.; Nzé, R. *Macromol. Chem. Phys.* **2015**, *216*, 1405–1414.

(19) Moad, G.; Rizzardo, E.; Thang, S. H. *Aust. J. Chem.* **2012**, *65*, 985-1076.

(20) Anastasaki, A.; Nikolaou, V.; Nurumbetov, G.; Wilson, P.; Kempe, K.; Quinn, J. F.; Davis, T. P.; Whittaker, M. R.; Haddleton, D. M. *Chem. Rev.* **2015**, *48*, 5140-5147.

(21) Hill, M. R.; Carmean, R. N.; Sumerlin, B. S. *Macromolecules* **2015**, *48*, 5459-5469.

(22) Parida, D.; Serra, C. A.; Garg, D. K.; Hoarau, Y.; Muller, R.; Bouquey, M. *Macromol. React. Eng.* **2014**, *8*, 597–603.

(23) Burns, J. A.; Houben, C.; Anastasaki, A.; Waldron, C.; Lapkin, A. A.; Haddleton, D. M. *Polym. Chem.* **2013**, *4*, 4809-4813.

(24) Chan, N.; Cunningham, M. F.; Hutchinson, R. A. *J. Polym. Sci., Part A Polym. Chem.* **2013**, *51*, 3081-3096.

(25) Wang, W.; Zhou, Y.-N.; Luo, Z.-H. *Macromol. React. Eng.* **2015**, n/a – n/a.

(26) Fortunatti, C.; Sarmoria, C.; Brandolin, A.; Asteasuain, M. *Macromol. React. Eng.* **2014**, *8*, 260–281.

(27) Lemos, T.; Melo, P. A.; Pinto, J. C. *Macromol. React. Eng.* **2015**, *9*, 259-270.

(28) Chan, N.; Meuldijk, J.; Cunningham, M. F.; Hutchinson, R. A. *Ind. Eng. Chem. Res.* **2013**, *52*, 11931–11942.

(29) Zhang, M.; Cunningham, M. F.; Hutchinson, R. A. *Polym. Chem.* **2015**, *6*, 6509-6518.

(30) Matyjaszewski, K.; Dong, H.; Jakubowski, W.; Pietrasik, J.; Kusumo, A. *Langmuir* **2007**, *23*, 4528–4531.

(31) Min, K.; Gao, H.; Matyjaszewski, K. *Macromolecules* **2007**, *40*, 1789–1791.

Appendix A

Supporting Information: ARGET ATRP of Butyl Methacrylate: Utilizing Kinetic Modeling to Understand Experimental Trends

A.1 Model Comparison

Using the rate coefficients presented in Table 4.2, a benchmark simulation was run with the commercially available Predici® (Pr) software package and with a kinetic Monte Carlo (kMC) approach.[1] The results for exp 1 (see Table 4.1) at 70 °C may be found in Figure A.1 and Figure A.2 with a constant k_t^{app} of 9.0×10^7 L mol^{-1} s^{-1}.

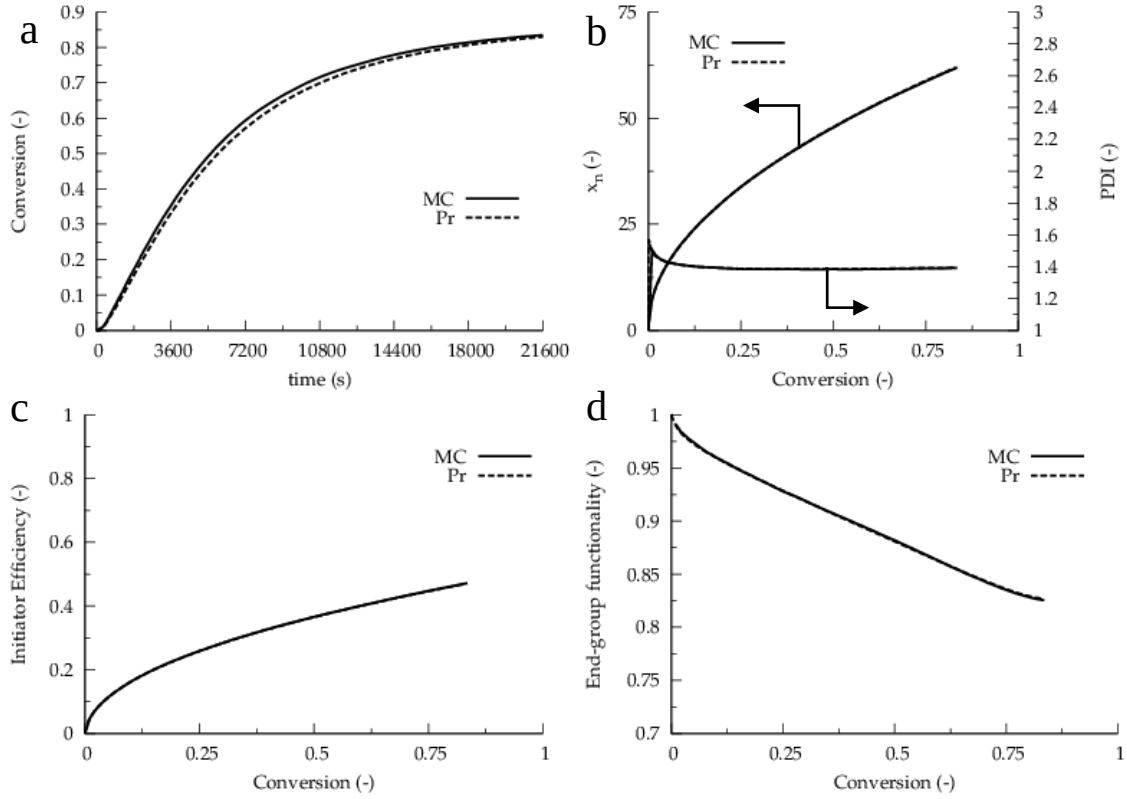

Figure A.1: Comparison of intrinsic simulation data from Predici® (Pr, dashed line) and kinetic Monte Carlo (kMC, solid line) at 70 °C using model parameters in Table 4.2 but with a constant k_t^{app} of 9.0×10^7 L mol^{-1} s^{-1}. Plot of (a) conversion versus time, (b) number-average chain length (x_n) and polydispersity index (PDI), (c) ATRP initiator efficiency, and (d) end group functionality versus conversion; initial conditions given as molar ratios of [BMA]:[EBiB]:[(Cu^{II}TPMABr)Br]: [Sn(EH)$_2$] = 35:1:0.005:0.05 (exp 1).

There is good agreement between the intrinsic Predici® and kinetic Monte Carlo simulations, as has been seen before.[2] Note that the end group functionality is predicted to be around 83% at full conversion for this system (Figure A.1d). The equivalency of both modeling approaches also follows from a comparison of the concentration profiles, as shown in Figure A.2.

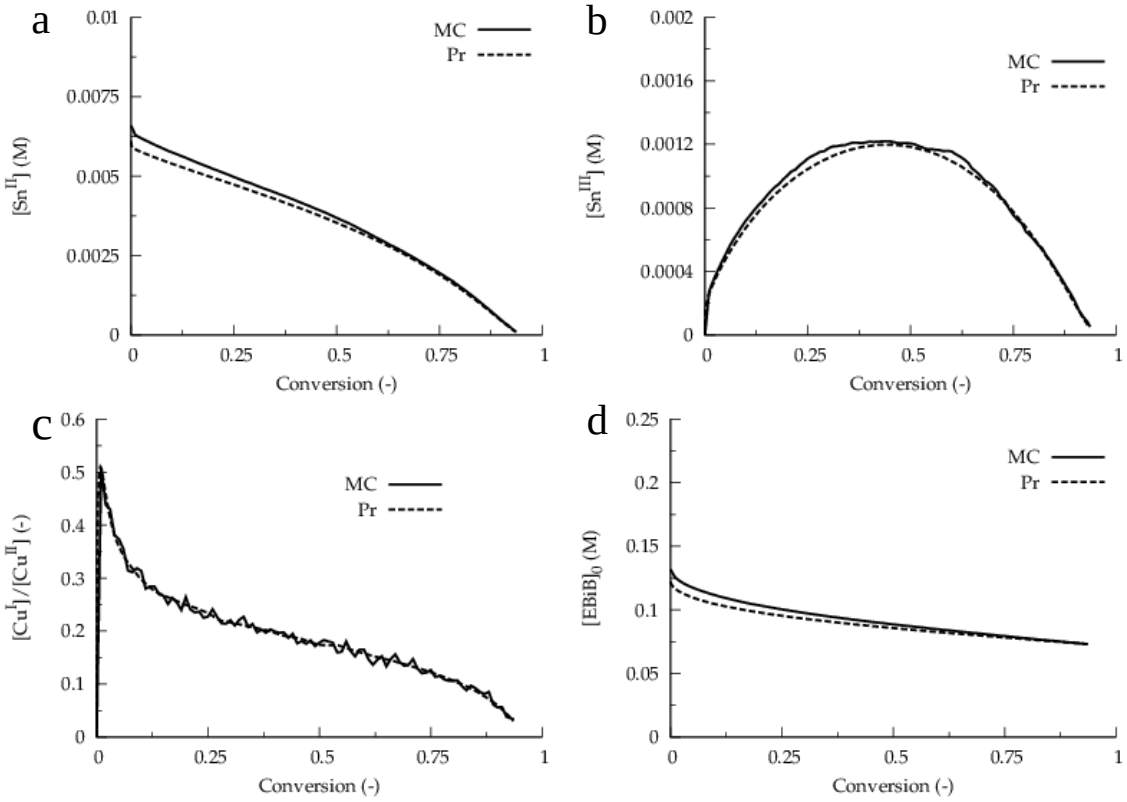

Figure A.2: Comparison of simulation data at 70 °C from Predici® (Pr, dashed lines) and kinetic Monte Carlo (kMC, solid lines) using model parameters in Table 4.2 but with a constant k_t^{app} of 9.0×10^7 L mol^{-1} s^{-1}. Plot of (a) $Sn^{II}(EH)_2$ concentration, (b) $Sn^{III}(EH)_2Br$ concentration, (c) ratio of activator/deactivator (Cu^I/Cu^{II}) and (d) initiator concentration versus conversion; initial conditions given as molar ratios of [BMA]:[EBiB]: [(Cu^{II}TPMABr)Br]:[$Sn(EH)_2$] = 35:1:0.005:0.05 (exp 1).

It can be seen that there are only minor deviations initially in the concentration profiles of the tin species (Figure A.2a and b), the copper species (Figure A.2c), and the initiator (Figure A.2d) concentrations. The ratio of Cu^I/Cu^{II} is in good agreement throughout the reaction for both simulations (Figure A.2c), indicating the negligible difference in the two approaches.

Similarly, when including RAFT-CLD parameters for estimation of the apparent termination rate coefficient, there is good agreement between the kMC and Predici® simulations for exp 3 (see Table 4.1), notably in the small concentration profiles (Figure A.3 and Figure A.4).

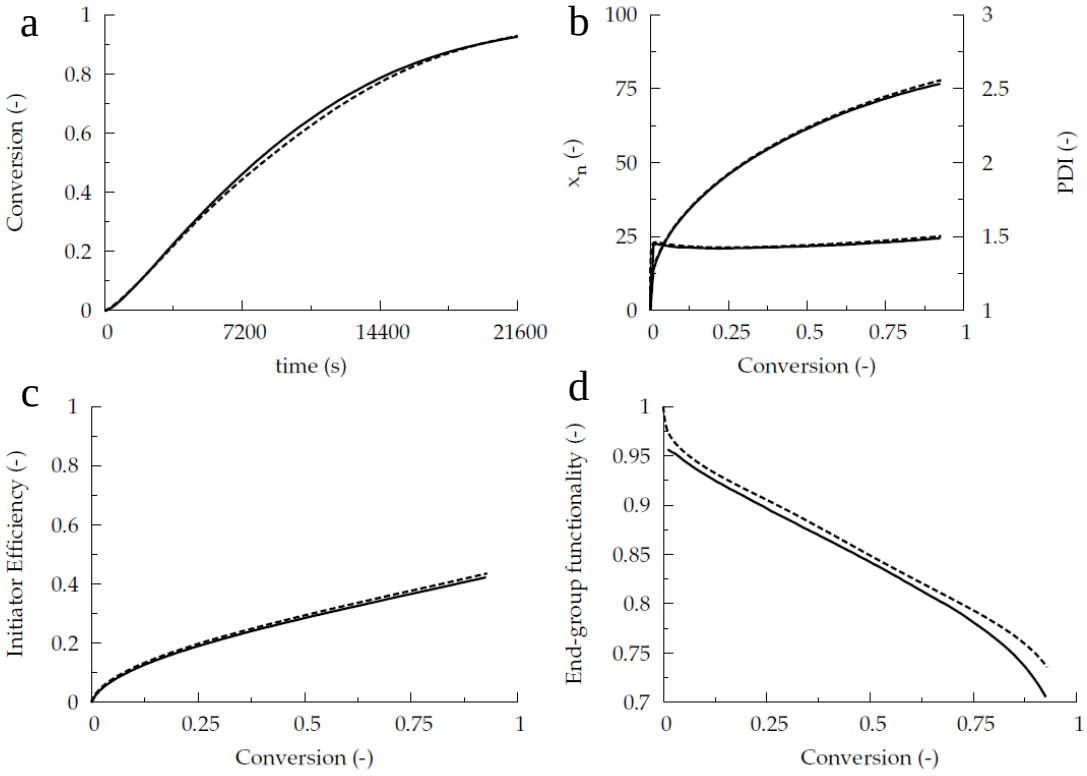

Figure A.3: Comparison of intrinsic simulation data from Predici® (Pr, dashed line) and kinetic Monte Carlo (kMC, solid line) at 70 °C using model parameters in Table 4.2 and composite k_t. Plot of (a) conversion versus time, (b) number-average chain length (x_n) and polydispersity index (PDI), (c) ATRP initiator efficiency, and (d) end group functionality versus conversion; initial conditions given as molar ratios of [BMA]:[EBiB]: [(Cu^{II}TPMABr)Br]:[$Sn(EH)_2$] = 35:1:0.00125:0.125 (exp 3).

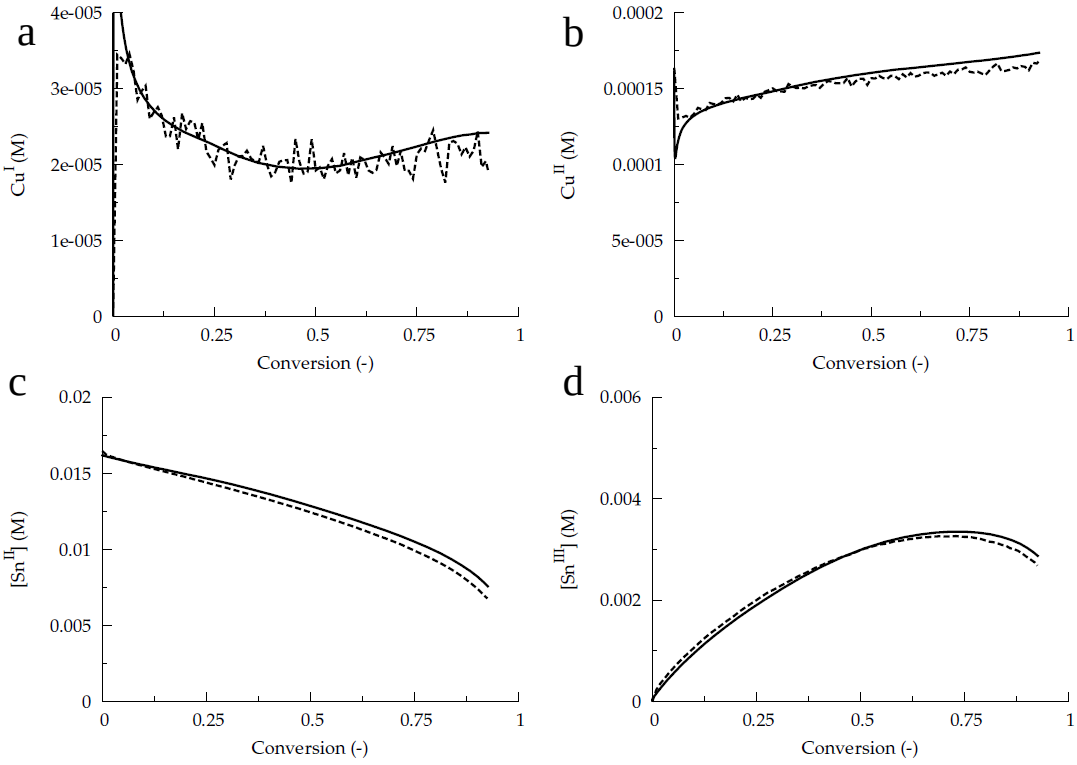

Figure A.4: Comparison of simulation data at 70 °C from Predici® (Pr, dashed lines) and kinetic Monte Carlo (kMC, solid lines) using model parameters in Table 4.2 and composite k_t. Plot of (a) activator (Cu^{I}) concentration, (b) deactivator (Cu^{II}) concentration, (c) $Sn^{II}(EH)_2$ concentration, and (d) $Sn^{III}(EH)_2Br$ concentration versus conversion; initial conditions given as molar ratios of [BMA]:[EBiB]:[(Cu^{II}TPMABr)Br]:[$Sn(EH)_2$] = 35:1:0.00125:0.125 (exp 3).

A.2 Elevated Temperatures

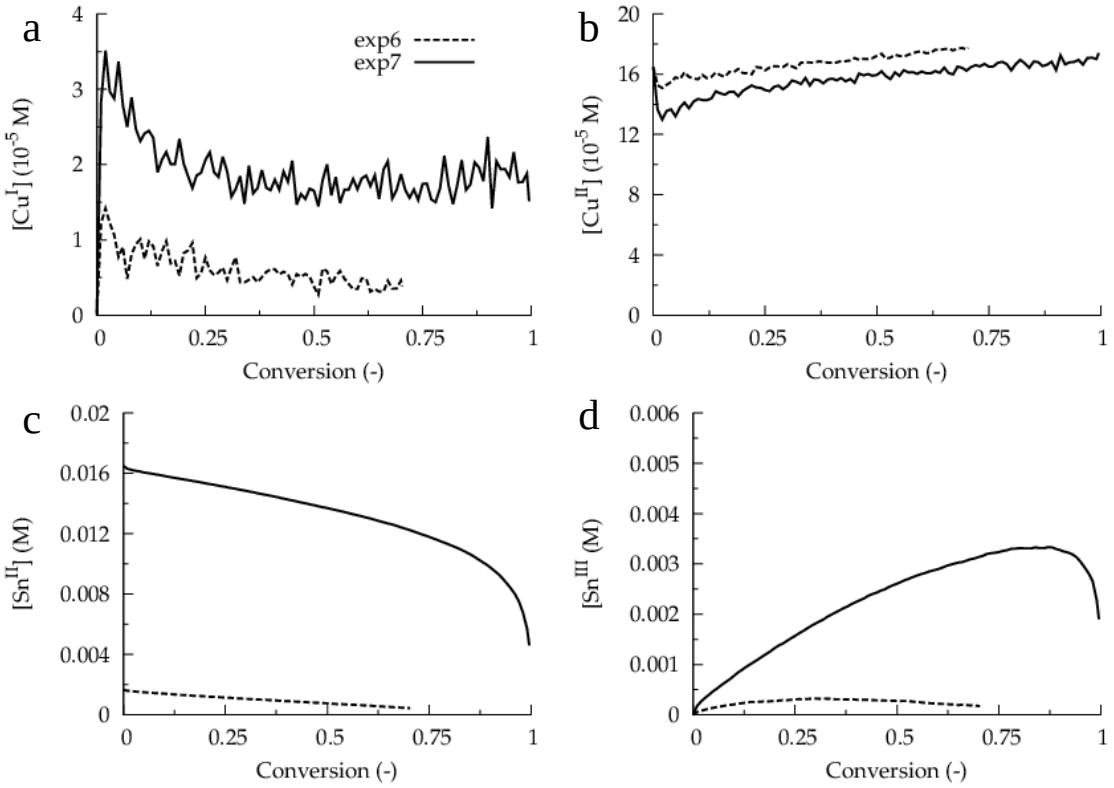

Figure A.5: Comparison of kMC simulation data at 90 °C using model parameters from Table 4.2. Plot of (a) concentration of activator species (Cu^{I}), (b) deactivator species (Cu^{II}), (c) $Sn^{II}(EH)_2$ species, and (d) and $Sn^{III}(EH)_2Br$ species versus conversion; initial conditions given as molar ratios of [BMA]:[EBiB]:[(Cu^{II}TPMABr)Br]:[$Sn(EH)_2$] = 35:1:0.00125:0.0125 (exp 6), 35:1:0.00125:0.125 (exp 7).

A.3 References

(1) D'hooge, D. R.; Reyniers, M.-F.; Marin, G. B. *Macromol. React. Eng.* **2009**, *3*, 185–209.

(2) Konkolewicz, D.; Sosnowski, S.; D'hooge, D. R.; Szymanski, R.; Reyniers, M.-F.; Marin, G. B.; Matyjaszewski, K. *Macromolecules* **2011**, *44*, 8361–8373.

Appendix B

Efficacy of TEMPO-Mediated Polymerization at Elevated Temperatures

B.1 Experimental

Styrene (Sigma Aldrich) was vacuum distilled to remove inhibitor prior to reaction. In preparation of stock solutions, while under nitrogen (UHP, 99.999%), distilled styrene was added to 2,2,6,6-tetramethyl-1-piperidinyloxy (TEMPO)/4-oxo-TEMPO and dicumyl peroxide (DCP) (Sigma Aldrich), as needed. 0.2 mL of stock solution was added to the Low Pressure/Vacuum (LPV) NMR tubes (Wilmad LabGlass) using a glass syringe while under nitrogen. Each LPV NMR tube was subjected to 4 freeze-pump-thaw cycles and sealed under nitrogen using a Schlenk line and liquid nitrogen. The tubes were kept in the refrigerator at 4-6 °C until use, then the tubes were suspended in a silicone oil bath (no smoke until >200 °C) to start the polymerization. The reaction was stopped by removing the tube and immersing in an ice bath for 20 s. Each tube was used as a sample point for a polymerization. Tubes were then opened to add deuterated chloroform and submitted for ^{1}H NMR analysis using a Bruker Avance-400 (400 MHz) instrument. Size exclusion chromatography (SEC) was performed using a Waters 2960 GPC separation module with Styragel packed columns HR 0.5, HR 1, HR 3, HR4, HR 5E (Waters Division Millipore). Using THF as eluent at 1 mL min^{-1}, the detection was provided by a Waters 410 Differential Refractometer, and Wyatt Instruments Dawn EOS 690 nm laser photometer multiangle light scattering (LS) unit. UV-Vis was performed using a Varian Cary 100 Spectrophotometer.

B.2 Results

B.2.1 Autopolymerization of styrene

In order to minimize the volume of monomer and amount of nitroxide/initiator used at elevated temperatures, LPV NMR tubes were used to study the polymerization. To validate the

experimental procedure, the autopolymerization of styrene conducted by Hui and Hamielec was reproduced at 140 °C and 160 °C.[1] The conversion measured in the LPV NMR tubes is compared to the experimental data of Hui and Hamielec (presented as a solid line in Figure B.1 and Figure B.2).

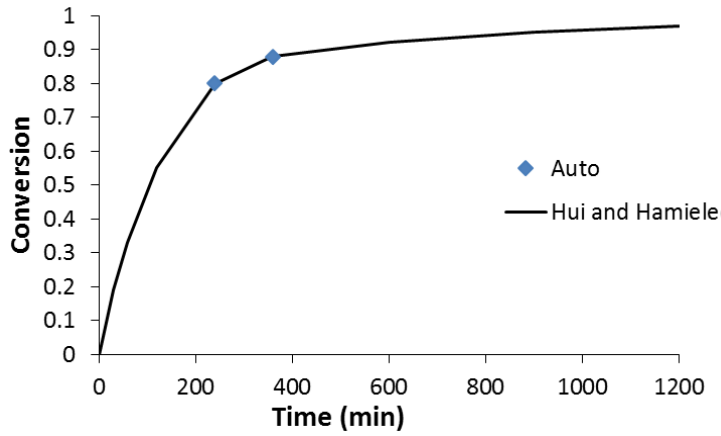

Figure B.1: Plot of conversion for the autopolymerization of styrene in an LPV NMR tube at 140 °C. Thermal polymerization profile ("Hui and Hamielec" line) included for comparison.[1]

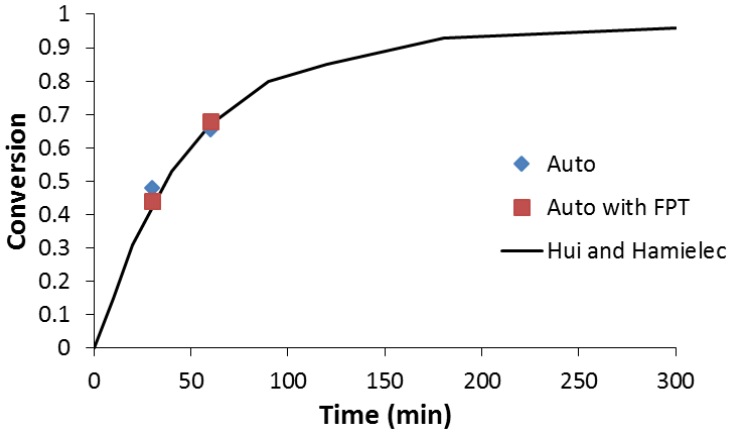

Figure B.2: Plot of conversion for the autopolymerization of styrene in an LPV NMR tube at 160 °C. The freeze-pump-thaw (FPT) technique was used to degas the tube. Thermal polymerization profile ("Hui and Hamielec" line) included for comparison.[1]

The autopolymerization follows closely the previously reported data (Figure B.1 and Figure B.2), whether conducted under atmospheric conditions or under vacuum following the freeze-pump-thaw (FPT) degassing technique. The LPV NMR tube technique was thus deemed a suitable method for polymerization. The freeze-pump-thaw technique is included in the experimental procedure when using the oxygen-sensitive initiator and nitroxide.

B.2.2 Addition of TEMPO

To investigate whether the addition of nitroxide to the polymerization of styrene would reduce the molecular weight relative to autopolymerization, TEMPO was added. The polymerization of bulk styrene and TEMPO was performed at 160 °C and 180 °C with a molar ratio of TEMPO:styrene 1:50, or a target chain length of 50 (M_n = 5,208 g mol^{-1}). 4-oxo-TEMPO (denoted by *) was run at 160 °C, as it is known to be stable at higher temperatures than TEMPO. The stability of the TEMPO and 4-oxo-TEMPO will be examined in the next section. The results of the TEMPO experiments are shown in Figure B.3 and Figure B.4.

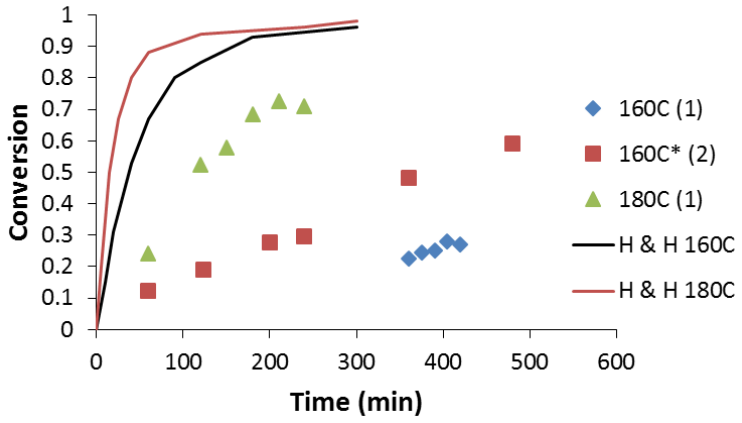

Figure B.3: Plot of conversion for the NMP of styrene using TEMPO and 4-oxo-TEMPO (denoted by *) at 160 °C and 180 °C under vacuum. Thermal polymerization profiles ("H & H" lines) included for comparison.[1]

Interestingly, the conversion profile for 4-oxo-TEMPO depicts a faster rate than with TEMPO (Figure B.3) at 160 °C. It should be noted that the actual molar ratio of 4-oxo-TEMPO:styrene = 1:41 at 160 °C (denoted by *). Regardless, the induction period that is expected with the addition of nitroxide was not witnessed to a significant extent. Meanwhile, Hawker *et al.* saw an induction period of 17-19 hours at 125 °C.[2]

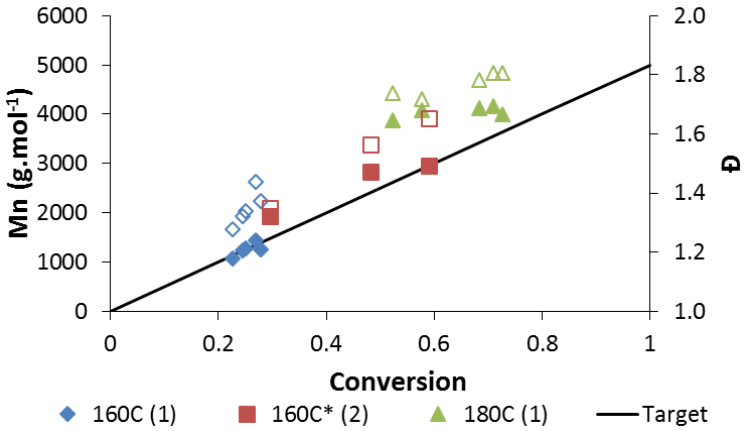

Figure B.4: Plot of number-average molar mass (M_n) and polymer dispersity ($Đ$) versus conversion for the NMP of styrene using TEMPO and 4-oxo-TEMPO (denoted as *) under vacuum at 160 °C and 180 °C.

The M_n profile seemed to follow near 100% initiator efficiency at 160 °C for both the TEMPO and 4-oxo-TEMPO experiments, while the 180 °C experiment with TEMPO witnessed almost no change in the M_n from ~4,000 g mol^{-1} (Figure B.4). Between the experiments, it appears that increased conversion is accompanied by an increase in the polymer dispersity, shown by the broadening of the MMDs in Figure B.5. However, it is clear TEMPO is having a significant impact on molecular weight (MW), as Hui & Hamielec found an M_n of 91,000 g mol^{-1} at 46.3% conversion in the absence of TEMPO (thermal polymerization), with $Đ$ = 1.75.

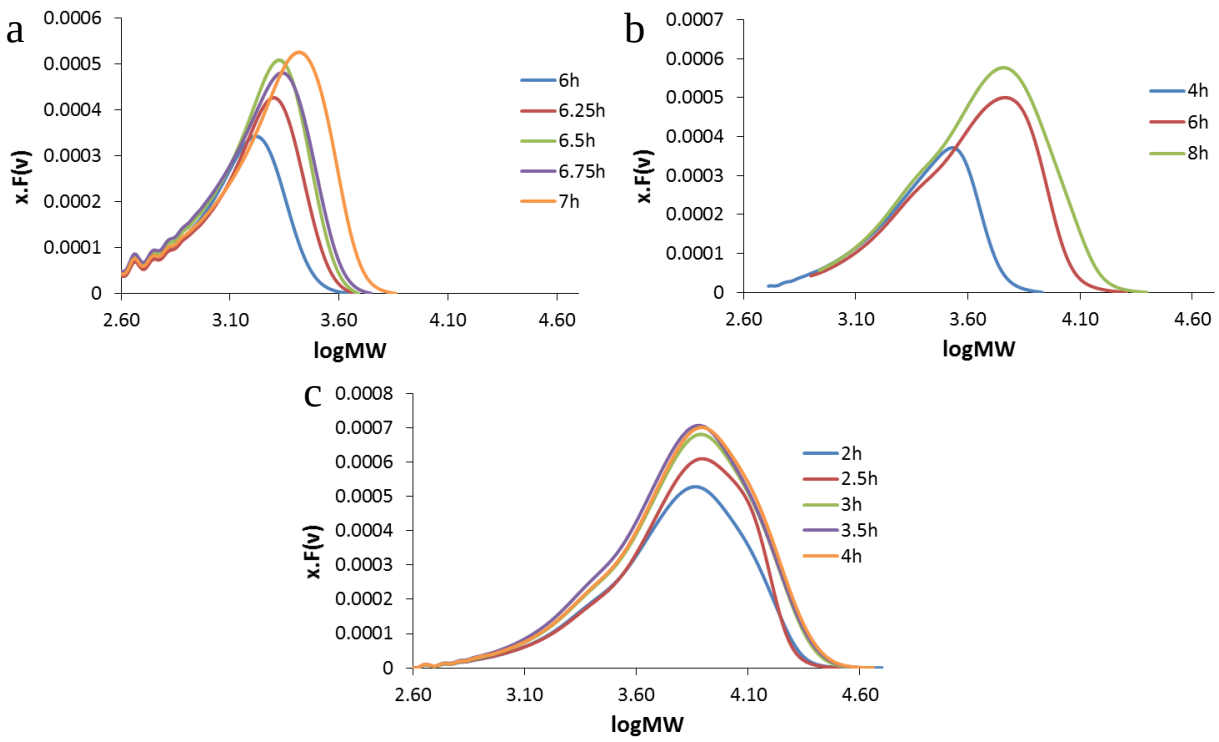

Figure B.5: MMD normalized with conversion for NMP of styrene with TEMPO at (a) 160 °C and (c) 180 °C, and (b) 4-oxo-TEMPO at 160 °C. Molar ratio of TEMPO:styrene = 1:50, 4-oxo-TEMPO:styrene = 1:41.

B.2.3 Stability of Nitroxide at Elevated Temperatures

The deviation from the target M_n and increasing polymer dispersity with temperature may be due to the poor stability of the nitroxide at the temperatures being studied in this research (>140 °C). To investigate the stability of the nitroxides, UV-Vis spectroscopy was utilized. Samples were taken from a solution of TEMPO and ethylbenzene, which was purged with nitrogen, heated, and stirred at 160 °C. The ethylbenzene acts as an inert analogue to styrene, with the solution made to match the 1:50 recipe used for TEMPO:styrene. Using a Cary 100 UV Spectrophotometer, the absorbance of TEMPO in styrene should be λ_{max} = ~447 nm[3] or 463 nm in acetonitrile[4] with a molar absorptivity of ε = 10 L mol^{-1} cm^{-1}. The transmittance was monitored between 300 and 800 nm,

with the λ_{max} monitored for samples taken over time. The UV-Vis spectra for TEMPO and 4-oxo-TEMPO can be seen in Figure B.6 and Figure B.7, respectively.

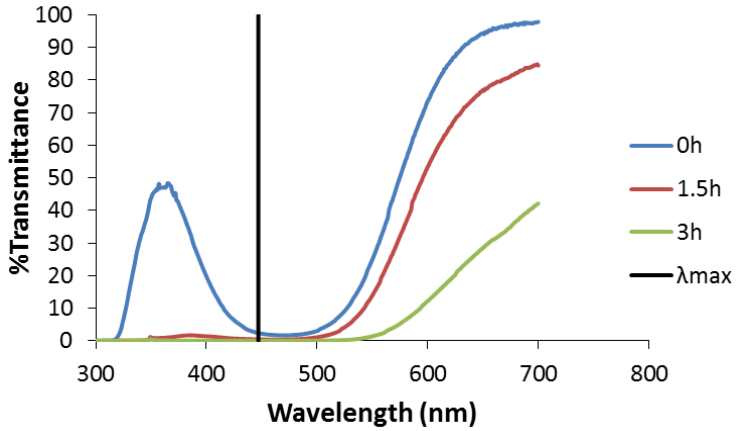

Figure B.6: UV-Vis spectra depicting the transmittance of a TEMPO and ethylbenzene solution over time at 160 °C. The estimated λ_{max} is shown at 447 nm.[3]

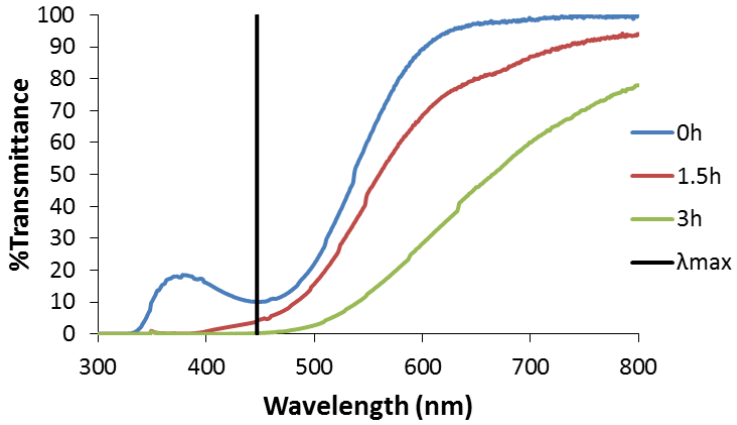

Figure B.7: UV-Vis spectra depicting the transmittance of a 4-oxo-TEMPO and ethylbenzene solution over time at 160 °C. The estimated λ_{max} is shown at 447 nm.[3]

For both TEMPO and 4-oxo-TEMPO, the peak was seen to broaden within the first hour, with significant broadening after 90 min of heating at 160 °C. This indicates the lack of stability at the elevated temperatures in this study (>140 °C), which has been attributed to disproportionation and decomposition of the nitroxide.[5,6]

B.2.4 NMP with Initiator

To counter the low stability of TEMPO and 4-oxo-TEMPO at 160 °C, dicumyl peroxide initiator was added to increase the polymerization rate. At this temperature, the initiator has a half-life of approximately 3.4 min. The initiator was used at two different levels for 4-oxo-TEMPO. The results are presented in Figure B.8 and Figure B.9.

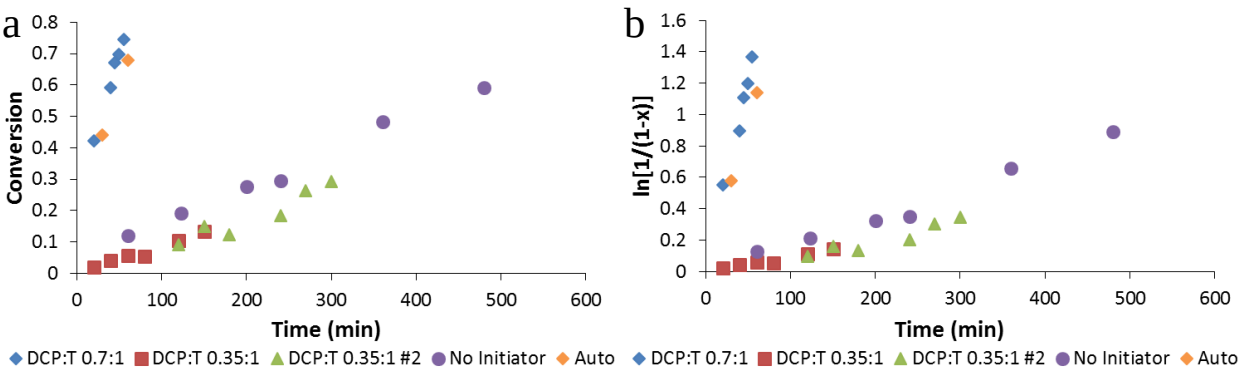

Figure B.8: (a) Plot of conversion and (b) kinetic plot for the NMP of styrene with 4-oxo-TEMPO and varying initiator loadings at 160 °C under vacuum. Dicumyl peroxide loading presented as a molar ratio with 4-oxo-TEMPO (see legend). Profiles for runs with autopolymerization and absence of initiator are also presented.

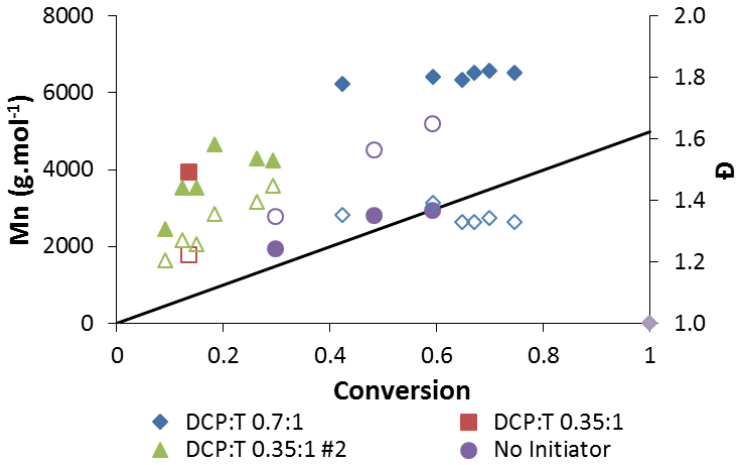

Figure B.9: Plot of number-average molar mass (M_n) and polymer dispersity ($Đ$) with conversion for the NMP of styrene with 4-oxo-TEMPO and varying initiator loadings at 160 °C under vacuum. Dicumyl peroxide loading presented as a molar ratio with 4-oxo-TEMPO (see legend). A run with absence of initiator is also presented.

As before, no induction period was seen with 4-oxo-TEMPO, with the addition of initiator having a slightly negative impact on rate when added at a molar ratio of 0.35 relative to the nitroxide. The higher level of initiator loading (0.7) resulted in a similar conversion profile as the autopolymerization system (Figure B.8). The M_n profiles of the initiator-added experiments appear to reach a plateau with increasing conversion at values well above the theoretical MW; almost no change in MW is seen at the higher initiator loading (M_n of 6,000 g mol^{-1}). The polymer dispersity steadily increased up to 1.4-1.5 with the lower initiator loading, while the higher initiator loading exhibited a $Đ$ of 1.3-1.4 throughout the reaction. The MMDs of the low and high initiator loadings normalized with conversion (Figure B.10 and Figure B.11, respectively) depict the growth of the chains with good control, with the number of chains increasing when the distribution ceases to shift to higher MW.

These data show with the addition of lower amounts of initiator, the rate is unexpectedly and slightly decreased with a loss of livingness earlier in the reaction than seen with no initiator.

M_n is also significantly increased when initiator is added. This would suggest there is an increase in the amount of termination with the addition of initiator, leading to a loss of radicals and number of growing chains compared to the initiator-free experiment. In the literature, the addition of an initiator while maintaining a constant ratio of nitroxide to monomer leads to an increase in polymerization rate with negligible change in the M_n profile and an increase in $Đ$.[7–10] This behavior is explained by the increase in radical concentration caused by the increased rate of initiation, as explained by the stationary rate of polymerization for NMP of styrene:

$$R_p = k_p[R\cdot][M] = \left(\frac{k_p}{k_t^{1/2}}\right) R_i^{1/2}[M] \qquad \textbf{Equation B-1}$$

where R_p is the rate of polymerization, k_p is the propagation rate coefficient, [R•] is the radical concentration, [M] is the monomer concentration, k_t is the termination rate coefficient, and R_i is the rate of initiation (here described as thermal initiation of styrene).[8] At this stationary state, it is assumed an equilibrium between the activation-deactivation process is obtained, leading to equilibrium concentrations of radical [R•] and nitroxide [Y•] species. However, the current system exhibits the opposite behavior, with no increase in polymerization rate with added initiator and an increase in the M_n witnessed. This would suggest that there is no significant change in the stationary radical concentration when initiator is added, but a decrease in the concentration of growing chains in the system is inferred from the increase in M_n. This may occur if there is an initial termination event, leading to a loss of initiator and nitroxide before the polymerization reaches a stationary state. Then, the increase in M_n and $Đ$ with conversion can be explained by the dead population of chains appearing as a low MW shoulder in the MMD as the growing chains continue to higher MW (see Figure B.10). When further initiator is added, there is an increase in polymerization rate, suggesting an increase in the radical concentration. Meanwhile, there is negligible change in M_n or $Đ$ with increasing conversion, which indicates an increasing number of chains in the system similar to a conventional free radical polymerization (or an absence of nitroxide). Nitroxide decomposition

may also be a factor, with the increased contribution of radicals from added DCP leading to further decomposition of TEMPO to TEMPOH, which has been shown to be significant at 120 °C.[6,11]

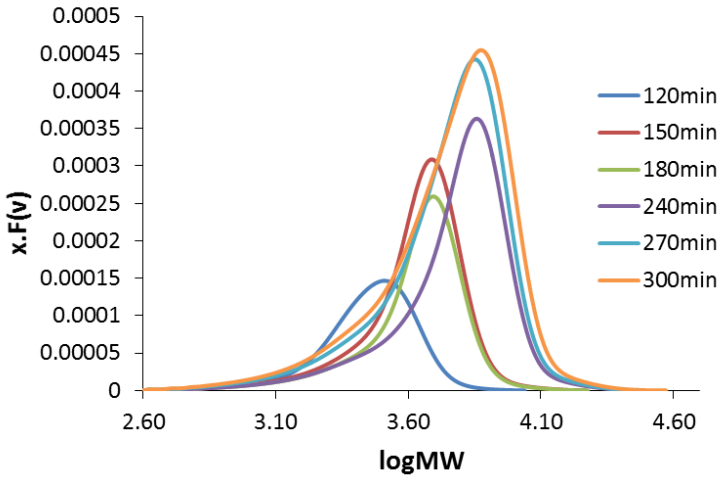

Figure B.10: MMD normalized with conversion for NMP of styrene at 160 °C. Molar ratio of dicumyl peroxide:4-oxo-TEMPO:styrene = 0.35:1:50.

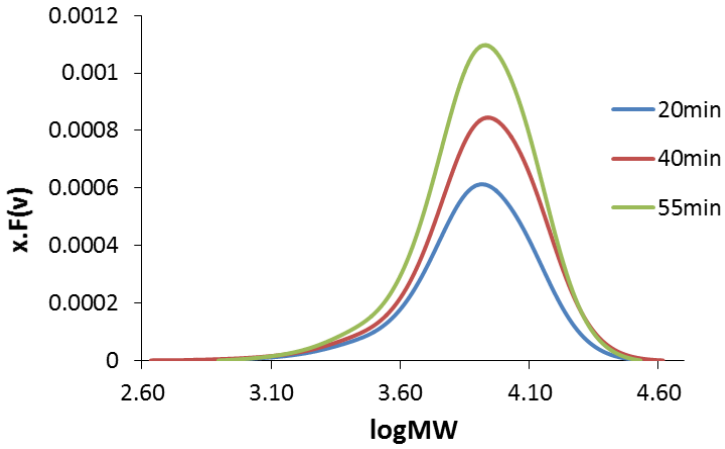

Figure B.11: MMD normalized with conversion for NMP of styrene at 160 °C. Molar ratio of dicumyl peroxide:4-oxo-TEMPO:styrene = 0.7:1:50.

The addition of initiator to the 4-oxo-TEMPO and styrene polymerization was replicated with TEMPO for comparison. The results are presented in Figure B.12 and Figure B.13.

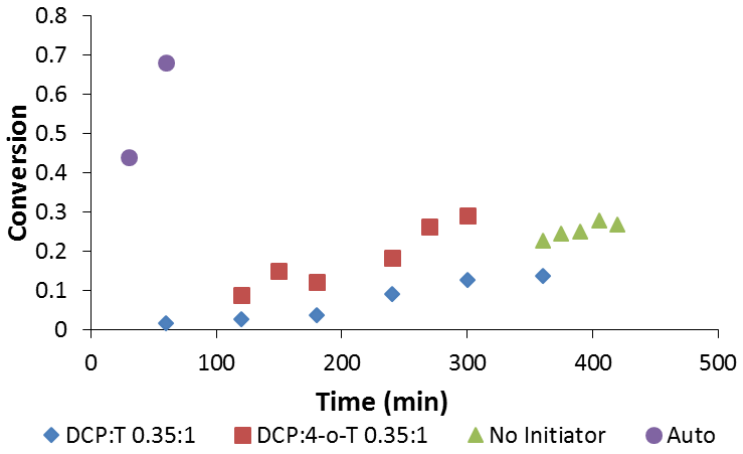

Figure B.12: Plot of conversion for the NMP of styrene with TEMPO/4-oxo-TEMPO and initiator at 160 °C under vacuum. Dicumyl peroxide loading presented as a molar ratio with TEMPO/4-oxo-TEMPO. The absence of initiator and autopolymerization profiles are also shown.

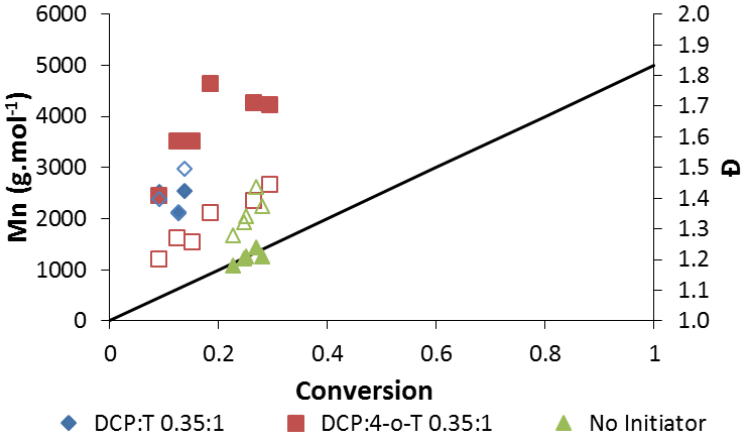

Figure B.13: Plot of number-average molar mass (M_n) and polymer dispersity ($Đ$) with conversion for the NMP of styrene with TEMPO/4-oxo-TEMPO with initiator at 160 °C under vacuum. Dicumyl peroxide loading presented as a molar ratio with TEMPO/4-oxo-TEMPO. The absence of initiator is also shown.

As seen previously with 4-oxo-TEMPO, the addition of a small amount of initiator leads to a small decrease in the polymerization rate relative to having no initiator in the system (Figure

B.8 and Figure B.12). The 4-oxo-TEMPO with initiator conversion profile is shown for comparison, depicting a slightly higher conversion than TEMPO and DCP. The M_n profile again shows a deviation from the expected molecular weight, as the initiator contributes to a lower chain concentration, likely due to initial termination (Figure B.13). In all experiments $Đ$ increases to 1.4-1.5. As before, there is a shift in the MMD, but there is also a low MW shoulder seen in the MMD (Figure B.14), indicating a significant population of dead chains for the TEMPO system.

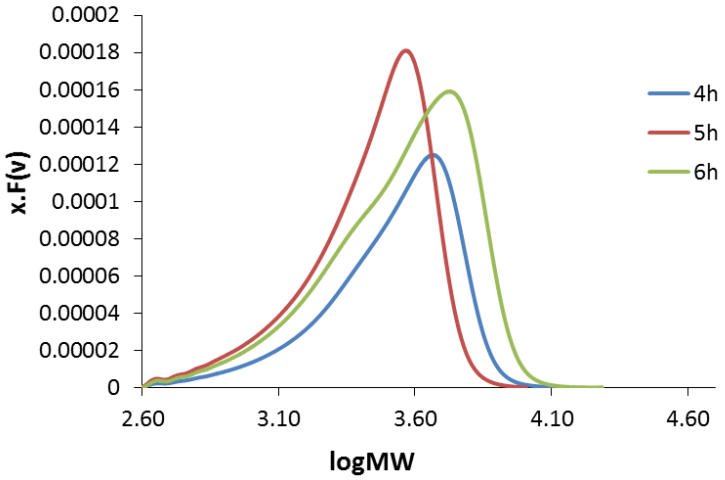

Figure B.14: MMD normalized with conversion for NMP of styrene at 160 °C. Molar ratio of dicumyl peroxide:TEMPO:styrene = 0.35:1:50.

There is also a similar profile to the 4-oxo-TEMPO experiment, where there is some growth and then an increase in the number of chains. 4-oxo-TEMPO is a less commonly used alternative to TEMPO, and there is not comparable experimental data in the literature for these temperatures. However, a literature study done at 135 °C using TEMPO, 4-oxo-TEMPO, and 4-acetamido-TEMPO with BPO also found an increase in conversion from TEMPO to 4-oxo-TEMPO, attributing this difference to the lower bond dissociation energy of the polystyrene-alkoxyamine-adducts based on calculated reaction enthalpies.[12] The M_n profile was also seen to be higher with 4-oxo-TEMPO compared to TEMPO, which was attributed to the reduction of the polymer chain

concentration due to thermal decomposition of 4-oxo-TEMPO. At elevated temperatures, it can be assumed that both TEMPO and 4-oxo-TEMPO are thermally decomposed, leading to the increased polydispersity.

B.3 Conclusion

In order to investigate the nitroxide-mediated polymerization of styrene at elevated temperatures, an experimental method was developed using LPV NMR tubes. The method was validated by comparison with the thermal polymerization of styrene study conducted by Hui and Hamielec.[1] Using the developed experimental procedure, TEMPO and 4-oxo-TEMPO were investigated as nitroxides for mediating the thermal polymerization of styrene at 160 °C and 180 °C. The nitroxides were found to be unstable at the elevated temperatures, as evidenced by the poor control of MW and *Đ*, which was confirmed by the disappearance of the nitroxide peak seen by UV-Vis. To utilize the short lifetime of the nitroxide at these elevated temperatures, a thermal initiator was added to the system at two different loadings. It was found that a low initiator loading resulted in a slightly decreased polymerization rate and decreased number of chains in the system. With an increased initiator loading, the polymerization rate is comparable to thermal polymerization of styrene, accompanied by a plateau in the MW profile.

To continue this work at elevated temperatures, another alkoxyamine must be selected that decomposes at a slow enough rate to allow the free nitroxide to mediate the polymerization over the 6 hour period required to reach high conversion at 160 °C. The decomposition reaction needs to be minimized, which may be done with bulky substituents on nitroxides, which are more effective in preventing decomposition. Indeed, it has been shown that steric factors play a more important role in the decomposition reaction than polar interactions at 140 °C.[6] The decomposition reaction was also shown to be more likely to occur during the deactivation process rather than the activation process, indicating the ratio of k_{act}/k_{deact} should not be too large. Therefore, minimizing

the amount of free nitroxide by a fast deactivation step would be beneficial in maintaining the nitroxide species, allowing successful control over the polymerization. Activation is maximized by bulky, electron-donating substituents, so the opposite strategy must be pursued to achieve a stable nitroxide at elevated temperatures.

B.4 References

(1) Hui, A. W.; Hamielec, A. E. *J. Appl. Polym. Sci.* **1972**, *16*, 749–769.

(2) Devonport, W.; Michalak, L. M.; Malmström, E.; Mate, M.; Kurdi, B.; Hawker, C. J.; Barclay, G. G.; Sinta, R. *Macromolecules* **1997**, *30*, 1929–1934.

(3) Ma, J. W.; Cunningham, M. F.; McAuley, K. B.; Keoshkerian, B.; Georges, M. K. *J. Polym. Sci., Part A Polym. Chem.* **2001**, *39*, 1081–1089.

(4) Nakahara, K.; Iwasa, S.; Iriyama, J.; Morioka, Y.; Suguro, M.; Satoh, M.; Cairns, E. *Electrochim. Acta* **2006**, *52*, 921–927.

(5) Ananchenko, G. S.; Fischer, H. *J. Polym. Sci., Part A Polym. Chem.* **2001**, *39*, 3604–3621.

(6) Goto, A.; Kwak, Y.; Yoshikawa, C.; Tsujii, Y.; Sugiura, Y.; Fukuda, T. *Macromolecules* **2002**, *35*, 3520–3525.

(7) Greszta, D.; Matyjaszewski, K. *J. Polym. Sci., Part A Polym. Chem.* **1997**, *35*, 1857–1861.

(8) Goto, A.; Fukuda, T. *Macromolecules* **1997**, *30*, 4272–4277.

(9) Veregin, R. P. N.; Odell, P. G.; Michalak, L. M.; Georges, M. K. *Macromolecules* **1996**, *29*, 2746–2754.

(10) Veregin, R. P. N.; Odell, P. G.; Michalak, L. M.; Georges, M. K. *Macromolecules* **1996**, *29*, 3346–3352.

(11) Nilsen, A.; Braslau, R. *J. Polym. Sci., Part A Polym. Chem.* **2006**, *44*, 697–717.

(12) Han, C. H.; Drache, M.; Baethge, H.; Schmidt-Naake, G. *Macromol. Chem. Phys.* **1999**, *200*, 1779–1783.

Appendix C

Supporting Information: Nitroxide-Mediated Polymerization at Elevated Temperatures

C.1 Styrene

Alkoxyamine-**1** was used to polymerize styrene across a range of target chain lengths (TCL) and temperatures. The results can be seen in Figure C.1 and Figure C.2, respectively.

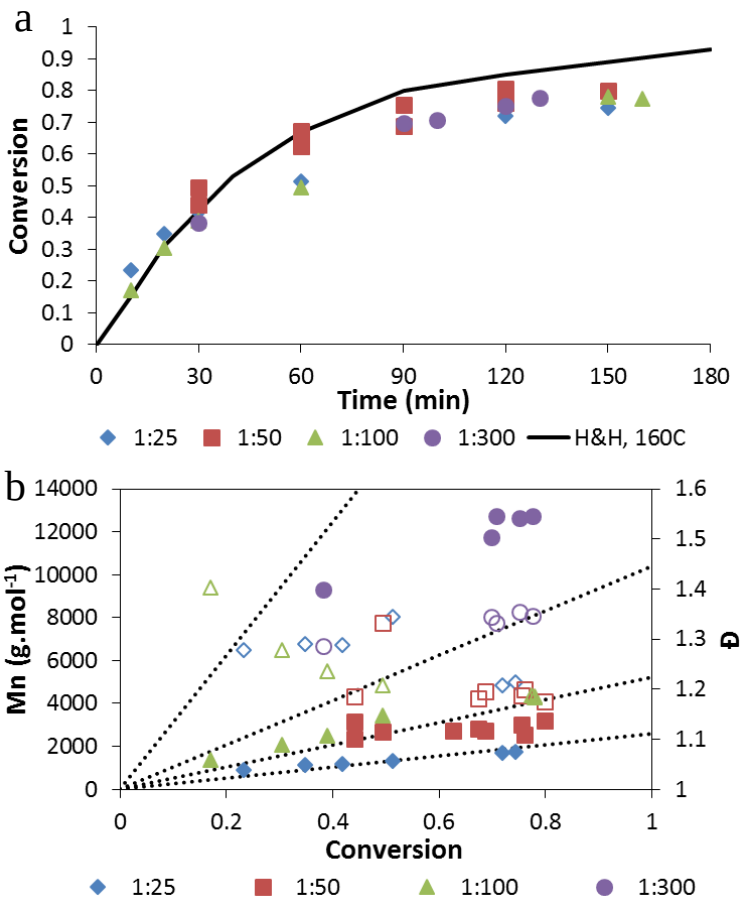

Figure C.1: NMP of bulk styrene at 160 °C, with initial alkoxyamine-1:styrene molar ratios presented in the legend: (a) conversion versus time and (b) number-average molar mass (M_n, closed symbols) and dispersity ($Đ$, open symbols) versus conversion. Thermal polymerization profile (line) included for comparison.[1]

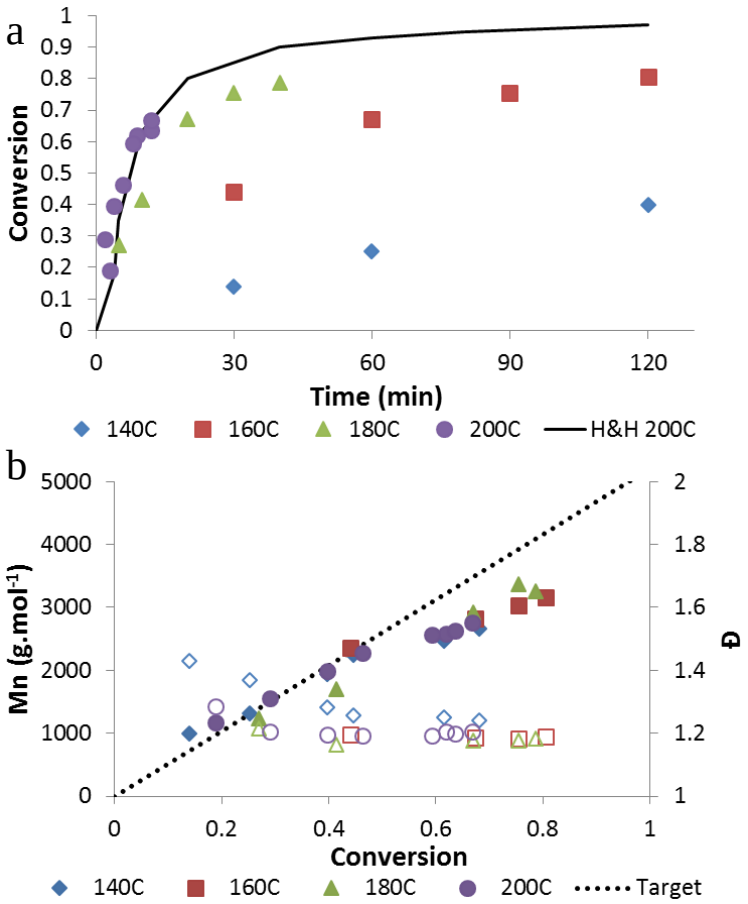

Figure C.2: Batch NMP of bulk styrene at various reaction temperatures (see legend), with initial alkoxyamine-1:styrene molar ratio of 1:50: (a) conversion versus time and (b) number-average molar mass (M_n, closed symbols) and dispersity ($Đ$, open symbols) versus conversion. Thermal polymerization profile at 200 °C (line) included for comparison.[1]

C.2 Butyl Acrylate

In order to improve the solubility of alkoxyamine-**1** in the stock solution with butyl acrylate, and therefore the reproducibility of the experiments, dimethylformamide (DMF) was used as solvent at a loading of 50 %v/v. The results from the improved solubility of the stock solution can be seen in Figure C.3.

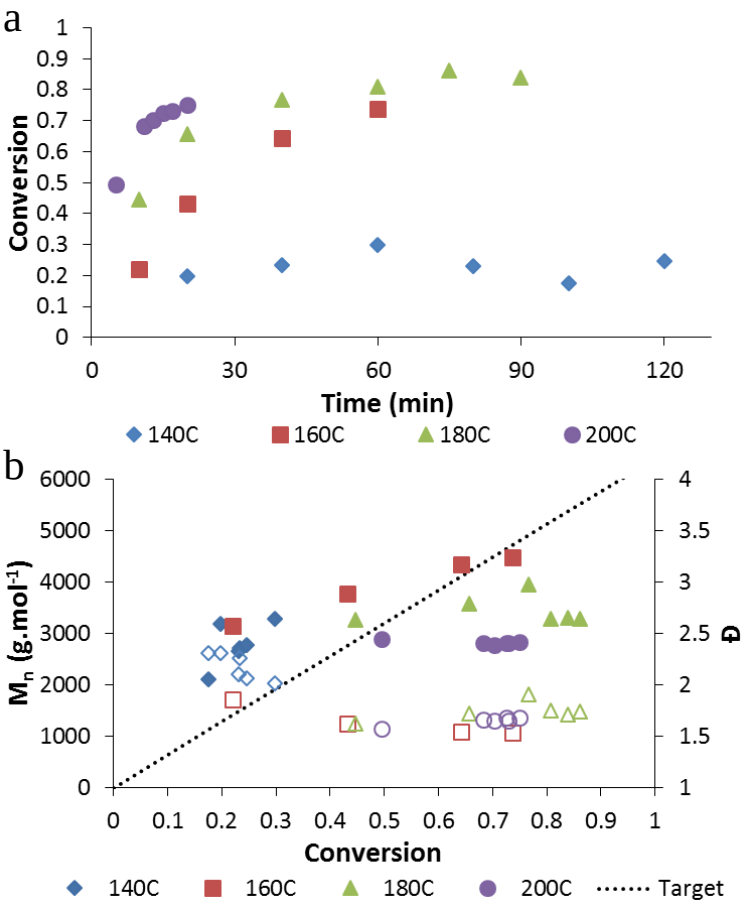

Figure C.3: Batch NMP of butyl acrylate in 50 %v/v DMF with alkoxyamine-1 at various reaction temperatures (see legend), with initial alkoxyamine:butyl acrylate ratio of 1:55: (a) conversion versus time and (b) number-average molar mass (M_n, closed symbols), and dispersity ($Đ$, open symbols) versus conversion.

With the decreased monomer content and the improved solubility of the stock solution, there is an improved dispersity at higher conversion, with final values around 1.6 at 200 °C (Figure C.3b). In addition, polymer M_n values decrease to below the target value, suggesting thermal initiation of the monomer is a significant contribution to the total number of chains.

Interestingly, ^{13}C NMR does not show any evidence of significant branching in bulk BA at 140 °C and 200 °C (see Figure C.4), consistent with literature studies of reversible deactivation radical polymerizations.[2–4]

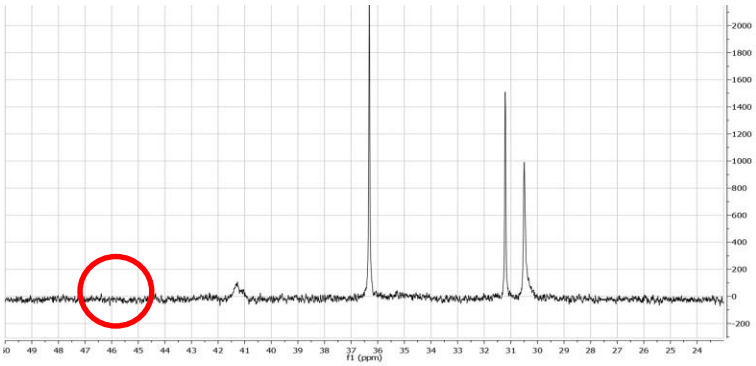

Figure C.4: ^{13}C NMR spectrum of final polymer produced from batch NMP of BA with 50 %v/v DMF at 200 °C. Final polymer conversion: 75% after 20 min of reaction. Note the absence of a quaternary carbon peak at ~48 ppm.[2]

The TCL of butyl acrylate polymerizations in bulk were varied at 160 °C with alkoxyamine-**2**, as shown in Figure C.5. As seen for styrene, the change in alkoxyamine concentration does not influence the rate of polymerization for the butyl acrylate system (Figure C.5a). There is adequate control of the polymerization with final *Đ* values around 1.5 (Figure C.5b), except for the highest TCL of 300; at the lowest concentration of alkoxyamine (TCL = 300) there is an insufficient amount of nitroxide available to effectively mediate the polymerization.

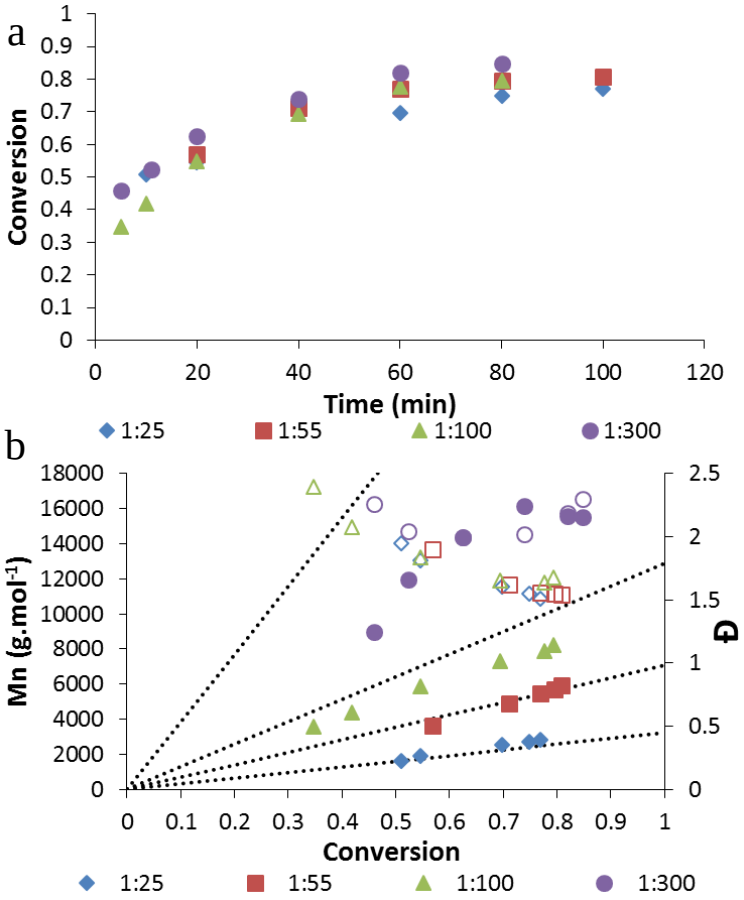

Figure C.5: Batch NMP of bulk butyl acrylate at 160 °C, with initial alkoxyamine-2:BA molar ratios presented in the legend: (a) conversion versus time and (b) number-average molar mass (M_n, closed symbols) and dispersity ($Đ$, open symbols) versus conversion.

C.3 Additional Monomers

Other monomers were also used to test the range of monomer families that may be controlled with these alkoxyamines. Using alkoxyamine-**2** with butyl methacrylate (BMA) and acrylic acid (AA) with 50 mol% styrene, the results in Figure C.6 were produced. The polymerization of BMA with 10 mol% styrene depicts reasonable control, with a linear increase in MW and dispersities around 1.5 (Figure C.6b). Interestingly, the polymerization of acrylic acid with 50 mol% styrene exhibited the increased rate of polymerization due to the high propagation

rate coefficient of acrylic acid (Figure C.6a) while maintaining good control of MW, with a final *Đ* of <1.3 (Figure C.6b).

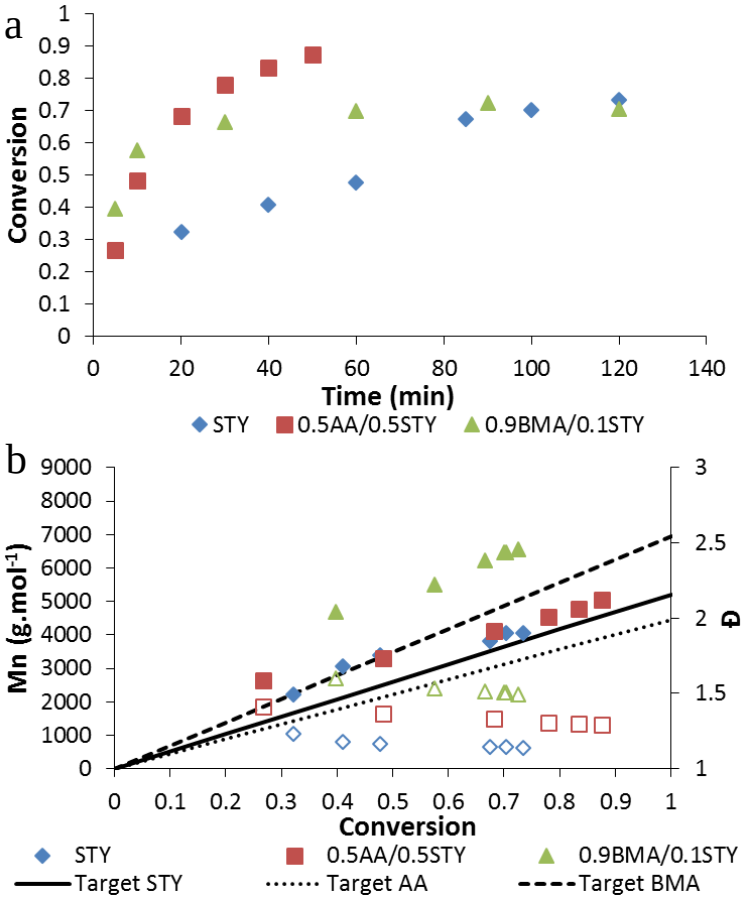

Figure C.6: Batch NMP of various monomers in bulk at 160 °C, with initial alkoxyamine-2:monomer molar ratio of 1:50: (a) conversion versus time and (b) number-average molar mass (M_n, closed symbols) and dispersity (*Đ*, open symbols) versus conversion. Molar ratios of monomers presented in the legend.

C.4 Experimental Methods

C.4.1 Synthesis of 2-[1-(4-*tert*-butylphenyl)ethoxy]-1,1,3,3-tetra-phenyl-isoindoline 2

A 100 mL flask was filled with argon and charged with dichloromethane (30 mL), 1,1,3,3-tetraphenylisoindoline-N-oxyl **3** (4.39 g, 10 mmol, 1-(1-bromoethyl)-4-*tert*-butylbenzene (2.89 g,

12 mmol) and copper (I) bromide (2.87 g, 20 mmol). A solution of N,N,N′,N′,N″-pentamethyl diethylenetriamine (3.47 g, 20 mmol, Aldrich 99%) in absolute ethanol (10 mL) was added to the stirred suspension at room temperature (RT) within 15 min. The resulting green suspension was stirred 3 h under argon and then additional (1-bromoethyl)-4-*tert*-butylbenzene (0.7 g, 2.9 mmol) was added. The green mixture was stirred at RT for 16 h, then diluted with water (50 mL) and extracted with dichloromethane (3 x 30 mL). The combined extracts are washed with water (20 mL), 1M-HCl (2 x 20 mL), 1M-NH_3 (20 mL) and water (20 mL) and dried over $MgSO_4$. The residue after evaporation of the solvent was chromatographed on silica gel with heptane-ethyl acetate (50:1) and the pure fractions were crystallized from dichloromethane-methanol to afford 5.6 g (93%) of **2** as white crystals, mp. 125-130 °C. ^{1}H-NMR (400 MHz, $CDCl_3$, δ ppm): 7.6-6.7 (m, 28 ArH), 4.74-4.69 (q, J=4.8 Hz, -**CH**CH_3), 1.31 (s, C(**CH$_3$**)$_3$, 1.02-1.01 (d, J=4.8 Hz, -CH**CH$_3$**)

Size exclusion chromatography (SEC) was performed using a Waters 2960 GPC separation module with Styragel packed columns HR 0.5, HR 1, HR 3, HR4, and HR 5E (Waters Division Millipore). Using distilled tetrahydrofuran (THF) as eluent at 0.3 mL min^{-1}, the detection was provided by a Waters 410 Differential Refractometer, and Wyatt Instruments Dawn EOS 690 nm laser photometer multiangle light scattering (LS) unit. The detector was calibrated with eight narrow polystyrene standards, ranging from 374 to 355000 g mol^{-1}. The molecular weights of poly(BA), poly(BMA), and poly(AA) samples were obtained by universal calibration using known Mark-Houwink parameters for polystyrene (K = 11.4x10^{-5} dL g^{-1}, a = 0.716)[5], poly(BMA) (K = 14.8x10^{-5} dL g^{-1}, a = 0.664)[5], poly(BA) (K = 7.4x10^{-5} dL g^{-1}, a = 0.750),[6] and poly(MA) (K = 9.5x10^{-5} dL g^{-1}, a = 0.719).[6,7]

Poly(acrylic acid) samples were methylated before SEC analysis to ensure solubility in THF. Poly(AA) was first solubilized in a mixture of methanol and THF at room temperature. The methylating agent trimethylsilyldiazomethane (Sigma Aldrich) was added dropwise to the polymer

solution until no bubbling is witnessed and the solution remains yellow in colour, indicating full conversion to the methyl ester with excess methylating agent.[7]

C.5 References

(1) Hui, A. W.; Hamielec, A. E. *J. Appl. Polym. Sci.* **1972**, *16*, 749–769.

(2) Ahmad, N. M.; Charleux, B.; Farcet, C.; Ferguson, C. J.; Gaynor, S. G.; Hawkett, B. S.; Heatley, F.; Klumperman, B.; Konkolewicz, D.; Lovell, P. A.; Matyjaszewski, K.; Venkatesh, R. *Macromol. Rapid Commun.* **2009**, *30*, 2002–2021.

(3) Reyes, Y.; Asua, J. M. *Macromol. Rapid Commun.* **2011**, *32*, 63–67.

(4) Ballard, N.; Rusconi, S.; Akhmatskaya, E.; Sokolovski, D.; de la Cal, J. C.; Asua, J. M. *Macromolecules* **2014**, *47*, 6580–6590.

(5) Hutchinson, R. A.; Beuermann, S.; Paquet, D. A.; McMinn, J. H. *Macromolecules* **1997**, *30*, 3490–3493.

(6) Penzel, E.; Goetz, N. *Die Angew. Makromol. Chem.* **1990**, *178*, 191–200.

(7) Couvreur, L.; Lefay, C.; Belleney, J.; Charleux, B.; Guerret, O.; Magnet, S. *Macromolecules* **2003**, *36*, 8260–8267.

Appendix D
Supporting Information: Kinetic Modeling of NMP in batch and CSTR

D.1 Box search

Table D.1: Box search of activation/deactivation rate coefficients using constant k_t^{app} with residual from comparison with experimental data from Payne *et al.*[1] ([alkoxyamine]:[styrene] = 1:50 @ 160 °C).

steps	$k_{a,o}$	$k_{da,o}$	k_a	k_{da}	*z:residual*
1	**0.001**	**1e+07**	**0.001**	**1e+07**	**0.240566**
2	**0.001**	**1e+07**	**0.001**	**1e+08**	**0.202674**
3	**0.001**	**1e+07**	**0.001**	**1e+09**	**0.200739**
4	0.001	1e+07	0.01	1e+07	0.370388
5	0.001	1e+07	0.01	1e+08	0.113262
6	0.001	1e+07	0.01	1e+09	0.0740184
7	0.001	1e+07	0.1	1e+07	1.12979
8	0.001	1e+07	0.1	1e+08	0.324461
9	0.001	1e+07	0.1	1e+09	0.0871742
10	0.001	1e+08	0.001	1e+07	0.25742
11	0.001	1e+08	0.001	1e+08	0.203954
12	0.001	1e+08	0.001	1e+09	0.200889
13	0.001	1e+08	0.01	1e+07	0.450243
14	0.001	1e+08	0.01	1e+08	0.121267
15	0.001	1e+08	0.01	1e+09	0.0747075
16	0.001	1e+08	0.1	1e+07	1.62455
17	0.001	1e+08	0.1	1e+08	0.394998
18	0.001	1e+08	0.1	1e+09	0.093723
19	0.001	1e+09	0.001	1e+07	0.413151
20	0.001	1e+09	0.001	1e+08	0.219473
21	0.001	1e+09	0.001	1e+09	0.202394
22	0.001	1e+09	0.01	1e+07	0.99107
23	0.001	1e+09	0.01	1e+08	0.202651
24	0.001	1e+09	0.01	1e+09	0.0819879
25	0.001	1e+09	0.1	1e+07	3.67008
26	0.001	1e+09	0.1	1e+08	0.89002
27	0.001	1e+09	0.1	1e+09	0.163979
28	0.01	1e+07	0.001	1e+07	0.15953
29	0.01	1e+07	0.001	1e+08	0.18147
30	0.01	1e+07	0.001	1e+09	0.187459
31	0.01	1e+07	0.01	1e+07	0.0355422
32	0.01	1e+07	0.01	1e+08	0.129398
33	0.01	1e+07	0.01	1e+09	0.141593
34	0.01	1e+07	0.1	1e+07	0.37612
35	0.01	1e+07	0.1	1e+08	0.044453
36	0.01	1e+07	0.1	1e+09	0.145857
37	0.01	1e+08	0.001	1e+07	0.154776

38	0.01	1e+08	0.001	1e+08	0.180605
39	0.01	1e+08	0.001	1e+09	0.187208
40*	**0.01**	**1e+08**	**0.01**	**1e+07**	**0.0344722**
41	0.01	1e+08	0.01	1e+08	0.128636
42	0.01	1e+08	0.01	1e+09	0.141582
43	0.01	1e+08	0.1	1e+07	0.42323
44	0.01	1e+08	0.1	1e+08	0.0419512
45	0.01	1e+08	0.1	1e+09	0.146974
46	0.01	1e+09	0.001	1e+07	0.138107
47	0.01	1e+09	0.001	1e+08	0.172934
48	0.01	1e+09	0.001	1e+09	0.185552
49	0.01	1e+09	0.01	1e+07	0.0849957
50	0.01	1e+09	0.01	1e+08	0.127374
51	0.01	1e+09	0.01	1e+09	0.141458
52	0.01	1e+09	0.1	1e+07	1.02283
53	0.01	1e+09	0.1	1e+08	0.049465
54	0.01	1e+09	0.1	1e+09	0.14285
55	0.1	1e+07	0.001	1e+07	0.285644
56	0.1	1e+07	0.001	1e+08	0.215601
57	0.1	1e+07	0.001	1e+09	0.22839
58	0.1	1e+07	0.01	1e+07	0.104105
59	0.1	1e+07	0.01	1e+08	0.1587
60	0.1	1e+07	0.01	1e+09	0.149336
61	0.1	1e+07	0.1	1e+07	0.320611
62	0.1	1e+07	0.1	1e+08	0.0690441
63	0.1	1e+07	0.1	1e+09	0.15448
64	0.1	1e+08	0.001	1e+07	0.274876
65	0.1	1e+08	0.001	1e+08	0.214991
66	0.1	1e+08	0.001	1e+09	0.228226
67	0.1	1e+08	0.01	1e+07	0.0939007
68	0.1	1e+08	0.01	1e+08	0.156848
69	0.1	1e+08	0.01	1e+09	0.148715
70	0.1	1e+08	0.1	1e+07	0.323535
71	0.1	1e+08	0.1	1e+08	0.070086
72	0.1	1e+08	0.1	1e+09	0.154748
73	0.1	1e+09	0.001	1e+07	0.219441
74	0.1	1e+09	0.001	1e+08	0.210101
75	0.1	1e+09	0.001	1e+09	0.227096
76	0.1	1e+09	0.01	1e+07	0.06401
77	0.1	1e+09	0.01	1e+08	0.15046
78	0.1	1e+09	0.01	1e+09	0.147973
79	0.1	1e+09	0.1	1e+07	0.357493
80	0.1	1e+09	0.1	1e+08	0.0651424
81	0.1	1e+09	0.1	1e+09	0.154799

*Minimum in 40

Table D.2: Box search of activation/deactivation rate coefficients using composite k_t with residual from comparison with experimental data from Payne *et al.* ([alkoxyamine]:[styrene] = 1:50 @ 160 °C).[1]

steps	$k_{a,o}$	$k_{da,o}$	k_a	k_{da}	*z:residual*
1	**0.001**	**1e+07**	**0.001**	**1e+07**	**0.285549**
2	**0.001**	**1e+07**	**0.001**	**1e+08**	**0.247327**
3	**0.001**	**1e+07**	**0.001**	**1e+09**	**0.246416**
4	0.001	1e+07	0.01	1e+07	0.407201
5	0.001	1e+07	0.01	1e+08	0.131243
6	0.001	1e+07	0.01	1e+09	0.0949778
7	0.001	1e+07	0.1	1e+07	1.19892
8	0.001	1e+07	0.1	1e+08	0.347883
9	0.001	1e+07	0.1	1e+09	0.0926075
10	0.001	1e+08	0.001	1e+07	0.303018
11	0.001	1e+08	0.001	1e+08	0.249003
12	0.001	1e+08	0.001	1e+09	0.246348
13	0.001	1e+08	0.01	1e+07	0.495065
14	0.001	1e+08	0.01	1e+08	0.140499
15	0.001	1e+08	0.01	1e+09	0.0960204
16	0.001	1e+08	0.1	1e+07	1.68937
17	0.001	1e+08	0.1	1e+08	0.42616
18	0.001	1e+08	0.1	1e+09	0.111504
19	0.001	1e+09	0.001	1e+07	0.471604
20	0.001	1e+09	0.001	1e+08	0.264672
21	0.001	1e+09	0.001	1e+09	0.247749
22	0.001	1e+09	0.01	1e+07	1.09846
23	0.001	1e+09	0.01	1e+08	0.234192
24	0.001	1e+09	0.01	1e+09	0.104356
25	0.001	1e+09	0.1	1e+07	3.90574
26	0.001	1e+09	0.1	1e+08	0.971818
27	0.001	1e+09	0.1	1e+09	0.19373
28	0.01	1e+07	0.001	1e+07	0.225326
29	0.01	1e+07	0.001	1e+08	0.245015
30	0.01	1e+07	0.001	1e+09	0.248433
31	0.01	1e+07	0.01	1e+07	0.0737174
32	0.01	1e+07	0.01	1e+08	0.146075
33	0.01	1e+07	0.01	1e+09	0.151074
34	0.01	1e+07	0.1	1e+07	0.37482
35	0.01	1e+07	0.1	1e+08	0.0785065
36	0.01	1e+07	0.1	1e+09	0.157851
37	0.01	1e+08	0.001	1e+07	0.218957
38	0.01	1e+08	0.001	1e+08	0.243933
39	0.01	1e+08	0.001	1e+09	0.248484
40*	**0.01**	**1e+08**	**0.01**	**1e+07**	**0.0719764**
41	0.01	1e+08	0.01	1e+08	0.145637

42	0.01	1e+08	0.01	1e+09	0.151138
43	0.01	1e+08	0.1	1e+07	0.424788
44	0.01	1e+08	0.1	1e+08	0.0774097
45	0.01	1e+08	0.1	1e+09	0.157767
46	0.01	1e+09	0.001	1e+07	0.19693
47	0.01	1e+09	0.001	1e+08	0.235778
48	0.01	1e+09	0.001	1e+09	0.246432
49	0.01	1e+09	0.01	1e+07	0.106004
50	0.01	1e+09	0.01	1e+08	0.141231
51	0.01	1e+09	0.01	1e+09	0.151055
52	0.01	1e+09	0.1	1e+07	1.04542
53	0.01	1e+09	0.1	1e+08	0.0796129
54	0.01	1e+09	0.1	1e+09	0.155523
55	0.1	1e+07	0.001	1e+07	0.333168
56	0.1	1e+07	0.001	1e+08	0.271412
57	0.1	1e+07	0.001	1e+09	0.279349
58	0.1	1e+07	0.01	1e+07	0.149493
59	0.1	1e+07	0.01	1e+08	0.181975
60	0.1	1e+07	0.01	1e+09	0.160704
61	0.1	1e+07	0.1	1e+07	0.31089
62	0.1	1e+07	0.1	1e+08	0.101698
63	0.1	1e+07	0.1	1e+09	0.167827
64	0.1	1e+08	0.001	1e+07	0.324931
65	0.1	1e+08	0.001	1e+08	0.27059
66	0.1	1e+08	0.001	1e+09	0.279191
67	0.1	1e+08	0.01	1e+07	0.136107
68	0.1	1e+08	0.01	1e+08	0.180883
69	0.1	1e+08	0.01	1e+09	0.161224
70	0.1	1e+08	0.1	1e+07	0.316501
71	0.1	1e+08	0.1	1e+08	0.101018
72	0.1	1e+08	0.1	1e+09	0.168911
73	0.1	1e+09	0.001	1e+07	0.284354
74	0.1	1e+09	0.001	1e+08	0.266599
75	0.1	1e+09	0.001	1e+09	0.278069
76	0.1	1e+09	0.01	1e+07	0.100147
77	0.1	1e+09	0.01	1e+08	0.170481
78	0.1	1e+09	0.01	1e+09	0.159553
79	0.1	1e+09	0.1	1e+07	0.356583
80	0.1	1e+09	0.1	1e+08	0.0955238
81	0.1	1e+09	0.1	1e+09	0.167118

*Minimum in 40

The final RDRP activation/deactivation parameter estimates are presented for each temperature in Table D.3 and are depicted as an Arrhenius plot in Figure D.1.

Table D.3: Final parameter estimates for RDRP activation/deactivation for simulation of NMP of styrene at various temperatures and TCL = 50.

Temp. (°C)	*1/T* (K^{-1})	$k_{a,o}$	$\ln(k_{a,o})$	$k_{da,o}$	$\ln(k_{da,o})$	k_a	$\ln(k_a)$	k_{da}	$\ln(k_{da})$
140	0.00242	9.00E-04	-7.01	7.2E+08	20.39	2.31E-03	-6.07	2.31E+07	16.95
160	0.00231	2.62E-03	-5.94	7.2E+08	20.39	7.92E-03	-4.84	2.31E+07	16.95
180	0.00221	6.94E-03	-4.97	7.2E+08	20.39	2.41E-02	-3.73	2.31E+07	16.95
200	0.00211	1.68E-02	-4.09	7.2E+08	20.39	6.74E-02	-2.70	2.31E+07	16.95

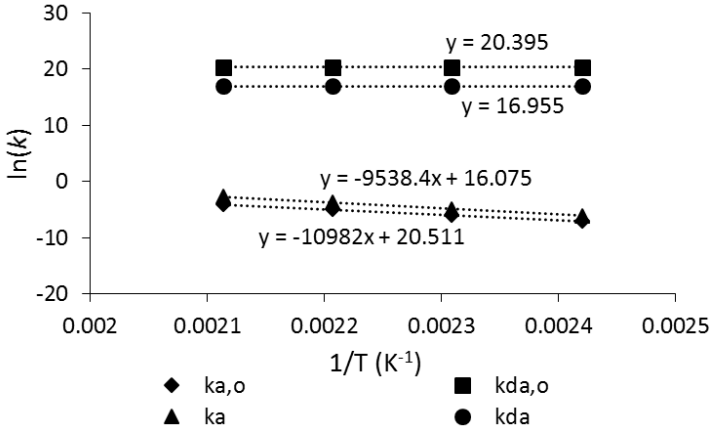

Figure D.1: Arrhenius plot of final activation/deactivation parameter estimates for simulation of NMP of styrene at various temperatures and TCL = 50.

D.2 References

(1) Payne, K. A.; Nesvadba, P.; Debling, J.; Cunningham, M. F.; Hutchinson, R. A. *ACS Macro Lett.* **2015**, *4*, 280–283.

Appendix E Copyright Permissions

ROYAL SOCIETY OF CHEMISTRY LICENSE
TERMS AND CONDITIONS

Aug 05, 2015

This is a License Agreement between Kevin Payne ("You") and Royal Society of Chemistry ("Royal Society of Chemistry") provided by Copyright Clearance Center ("CCC"). The license consists of your order details, the terms and conditions provided by Royal Society of Chemistry, and the payment terms and conditions.

All payments must be made in full to CCC. For payment instructions, please see information listed at the bottom of this form.

License Number	3682571381928
License date	Aug 05, 2015
Licensed content publisher	Royal Society of Chemistry
Licensed content publication	Chemical Society Reviews
Licensed content title	Kinetic subtleties of nitroxide mediated polymerization
Licensed content author	Denis Bertin,Didier Gigmes,Sylvain R. A. Marque,Paul Tordo
Licensed content date	Jan 13, 2011
Volume number	40
Issue number	5
Type of Use	Thesis/Dissertation
Requestor type	academic/educational
Portion	figures/tables/images
Number of figures/tables/images	1
Format	print
Distribution quantity	6
Will you be translating?	no
Order reference number	None
Title of the thesis/dissertation	Controlled radical polymerization towards industrially relevant conditions
Expected completion date	Sep 2015
Estimated size	200
Total	0.00 CAD

Terms and Conditions

This License Agreement is between {Requestor Name} (“You”) and The Royal Society of Chemistry (“RSC”) provided by the Copyright Clearance Center (“CCC”). The license consists of your order details, the terms and conditions provided by the Royal Society of Chemistry, and the payment terms and conditions.

RSC / TERMS AND CONDITIONS

INTRODUCTION

The publisher for this copyrighted material is The Royal Society of Chemistry. By clicking “accept” in connection with completing this licensing transaction, you agree that the following terms and conditions apply to this transaction (along with the Billing and Payment terms and conditions established by CCC, at the time that you opened your RightsLink account and that are available at any time at .

LICENSE GRANTED

The RSC hereby grants you a non-exclusive license to use the aforementioned material anywhere in the world subject to the terms and conditions indicated herein. Reproduction of the material is confined to the purpose and/or media for which permission is hereby given.

RESERVATION OF RIGHTS

The RSC reserves all rights not specifically granted in the combination of (i) the license details provided by your and accepted in the course of this licensing transaction; (ii) these terms and conditions; and (iii) CCC’s Billing and Payment terms and conditions.

REVOCATION

The RSC reserves the right to revoke this license for any reason, including, but not limited to, advertising and promotional uses of RSC content, third party usage, and incorrect source figure attribution.

THIRD-PARTY MATERIAL DISCLAIMER

If part of the material to be used (for example, a figure) has appeared in the RSC publication with credit to another source, permission must also be sought from that source. If the other source is another RSC publication these details should be included in your RightsLink request. If the other source is a third party, permission must be obtained from the third party. The RSC disclaims any responsibility for the reproduction you make of items owned by a third party.

PAYMENT OF FEE

If the permission fee for the requested material is waived in this instance, please be advised that any future requests for the reproduction of RSC materials may attract a fee.

ACKNOWLEDGEMENT

The reproduction of the licensed material must be accompanied by the following acknowledgement:

Reproduced (“Adapted” or “in part”) from {Reference Citation} (or Ref XX) with permission of The Royal Society of Chemistry.

If the licensed material is being reproduced from New Journal of Chemistry (NJC), Photochemical & Photobiological Sciences (PPS) or Physical Chemistry Chemical Physics (PCCP) you must include one of the following acknowledgements:

For figures originally published in NJC:

Reproduced (“Adapted” or “in part”) from {Reference Citation} (or Ref XX) with permission of The Royal Society of Chemistry (RSC) on behalf of the European Society for Photobiology, the European Photochemistry Association and the RSC.

For figures originally published in PPS:

Reproduced (“Adapted” or “in part”) from {Reference Citation} (or Ref XX) with permission of The Royal Society of Chemistry (RSC) on behalf of the Centre National de la Recherche Scientifique (CNRS) and the RSC.

For figures originally published in PCCP:

Reproduced (“Adapted” or “in part”) from {Reference Citation} (or Ref XX) with permission of the PCCP Owner Societies.

HYPERTEXT LINKS

With any material which is being reproduced in electronic form, you must include a hypertext link to the original RSC article on the RSC’s website. The recommended form for the hyperlink is http://dx.doi.org/10.1039/DOI suffix, for example in the link

http://dx.doi.org/10.1039/b110420a the DOI suffix is ‘b110420a’. To find the relevant DOI suffix for the RSC article in question, go to the Journals section of the website and locate the article in the list of papers for the volume and issue of your specific journal. You will find the DOI suffix quoted there.

LICENSE CONTINGENT ON PAYMENT

While you may exercise the rights licensed immediately upon issuance of the license at the end of the licensing process for the transaction, provided that you have disclosed complete and accurate details of your proposed use, no license is finally effective unless and until full payment is received from you (by CCC) as provided in CCC's Billing and Payment terms and conditions. If full payment is not received on a timely basis, then any license preliminarily granted shall be deemed automatically revoked and shall be void as if never granted. Further, in the event that you breach any of these terms and conditions or any of CCC's Billing and Payment terms and conditions, the license is automatically revoked and shall be void as if never granted. Use of materials as described in a revoked license, as well as any use of the materials beyond the scope of an unrevoked license, may constitute copyright infringement and the RSC reserves the right to take any and all action to protect its copyright in the materials.

WARRANTIES The RSC makes no representations or warranties with respect to the licensed material.

INDEMNITY

You hereby indemnify and agree to hold harmless the RSC and the CCC, and their respective officers, directors, trustees, employees and agents, from and against any and all claims arising out of your use of the licensed material other than as specifically authorized pursuant to this licence.

NO TRANSFER OF LICENSE

This license is personal to you or your publisher and may not be sublicensed, assigned, or transferred by you to any other person without the RSC's written permission.

NO AMENDMENT EXCEPT IN WRITING

This license may not be amended except in a writing signed by both parties (or, in the case of "Other Conditions, v1.2", by CCC on the RSC's behalf).

OBJECTION TO CONTRARY TERMS

You hereby acknowledge and agree that these terms and conditions, together with CCC's Billing and Payment terms and conditions (which are incorporated herein), comprise the entire agreement between you and the RSC (and CCC) concerning this licensing transaction, to the exclusion of all other terms and conditions, written or verbal, express or implied (including any terms contained in any purchase order, acknowledgment, check endorsement or other writing prepared by you). In the event of any conflict between your obligations established by these terms and conditions and those established by CCC's Billing and Payment terms and conditions, these terms and conditions shall control.

JURISDICTION

This license transaction shall be governed by and construed in accordance with the laws of the District of Columbia. You hereby agree to submit to the jurisdiction of the courts located in the District of Columbia for purposes of resolving any disputes that may arise in connection with this licensing transaction.

LIMITED LICENSE

The following terms and conditions apply to specific license types:

Translation

This permission is granted for non-exclusive world English rights only unless your license was granted for translation rights. If you licensed translation rights you may only translate this content into the languages you requested. A professional translator must perform all translations and reproduce the content word for word preserving the integrity of the article.

Intranet

If the licensed material is being posted on an Intranet, the Intranet is to be passwordprotected and made available only to bona fide students or employees only. All content posted to the Intranet must maintain the copyright information line on the bottom of each image. You must also fully reference the material and include a hypertext link as specified above.

Copies of Whole Articles

All copies of whole articles must maintain, if available, the copyright information line on the bottom of each page.

Other Conditions v1.2

Gratis licenses (referencing $0 in the Total field) are free. Please retain this printable license for your reference. No payment is required.

If you would like to pay for this license now, please remit this license along with

yourpayment made payable to "COPYRIGHT CLEARANCE CENTER" otherwise you will be invoiced within 48 hours of the license date. Payment should be in the form of a check or money order referencing your account number and this invoice number {Invoice Number}.

Once you receive your invoice for this order, you may pay your invoice by credit card.

Please follow instructions provided at that time.

Make Payment To:

Copyright Clearance Center

Dept 001

P.O. Box 843006

Boston, MA 02284-3006

For suggestions or comments regarding this order, contact Rightslink Customer Support: customercare@copyright.com or +1-855-239-3415 (toll free in the US) or +1-978-646-2777.

Questions? customercare@copyright.com or +1-855-239-3415 (toll free in the US) or +1-978-646-2777.